INAUGURALDISSERTATION

zur Erlangung des Grades eines Doktors der Naturwissenschaften (Dr. rer. Nat.)

vorgelegt dem Fachbereich Chemie der Universität-GH Essen

Ruthenium Nanoparticles:

Synthesis, Characterisation and Organisation in Alumina Membranes and Mesoporous Materials; Applications in Catalysis

THESE

Présentée en vue de l'obtention du Doctorat de l'Université Paul Sabatier

Spécialité : Chimie et Physico-Chimie des Eléments de Transition

Katrin Pelzer

Toulouse, 13. October 2003

JURY:

M. A. Lattes	Professeur à l'Université Paul Sabatier, Toulouse	President
R. A. Fischer	Professor at the Ruhr-Universität Bochum	Referee
J.-P. Candy	Directeur de Recherche CNRS, CPE, Lyon	Referee
H.-H. Limbach	Professor at the Freie Universiät Berlin	Member of the Jury
G. Schmid	Professor at the Universität GH Essen	Supervisor
B. Chaudret	Directeur de Recherche CNRS, LCC, Toulouse	Supervisor
Mme K. Philippot	Chargée de Recherche CNRS, LCC, Toulouse	Invited Member

Jeder Tag, an dem Du nicht lächelst, ist ein verlorener Tag.

(Charlie Chaplin)

Für meine Eltern

Mein größter Dank gilt Prof. Dr. Schmid, der mir ermöglicht hat, diese „außergewöhnliche“ Promotion durchzuführen. Vielen Dank für Ihr Vertrauen, den gegebenen Freiraum und ganz besonders Ihren ausgeglichen Charakter, der dazu führt, dass man sich nach jedem Gespräch mit Ihnen einfach wohlfühlen muss.

Bruno, je te remercie tout particulièrement pour avoir dirigé mes travaux de recherche et d’avoir accepté une thèse “en cotutelle“. Merci pour l’accueil dans ton équipe et pour la liberté que tu m’as accordée. Merci de m'avoir fait profiter de tes compétences nombreuses.

Karine, merci pour ta disponibilité et ta gentillesse pendant ces trois années de thèse à Toulouse. Merci également pour ton aide et ton soutien.

Sylvianne, Catherine et André, je vous remercie pour m’avoir soutenue et écoutée.

Ce travail n’aurait jamais pu être réalisé sans les collaborations : avec François Senoq concernant les études de diffraction des rayons X; Pierre Lecante pour le WAXS, Olivier Balmes pour la Cryo-TEM, Yannick Coppel pour la RMN et Yannick Guari pour les matériaux mésoporeux.

Many thanks to the group of Jan-Olov Bovin at Lund University for accepting to teach me TEM, HREM and Cryo-TEM in Sweden.

Monserrat, gracias por tu apoyo, por la oportunidad de trabajar juntas y por tu hospitalidad en Barcelona.

Prof. H.-H. Limbach, ich danke Ihnen für die vielen fruchtbaren Gespräche und die nette Betreuung in ihrer Gruppe in Berlin. Vielen Dank für die Bereitschaft, das Amt eines Jurymitgliedes zu übernehmen. Ich hoffe auf weitere Zusammenarbeit...

Tal, einfach nur danke für alles.

Martine, merci pour ton sourire.

Cathy, Susanna, Steph, Pascal – merci pour les pauses café-détente.

Vincent, merci beaucoup pour la microscopie et pour t’avoir abîmé tes yeux sur mes échantillons.

Je n’oublierai jamais toute l’équipe L pour son agréable compagnie. Ces trois années ont passé très vite et ont été exceptionnelles grâce à l’ambiance très sympathique. Merci pour tous les bons moments que nous avons partagés.

Seb, merci pour R.

Ich danke allen meinen Lieben, ohne die diese Zeit nur halb so lustig gewesen wäre.

Merci mes Toulousains!!!

Meine Essener, auf euch kann man sich verlassen!!!

Meiner Familie danke ich für die viele „Trostschokolade“ und die Seelenpflege während dieser Zeit.

Bzzz, danke, dass du da warst. Never forget who you are…

Introduction

There is presently a considerable interest for the study and the use of metal nanoparticles because of their novel and attractive physical and chemical properties.[1,2] For example, transition metal particles are studied as catalysts in organic and inorganic transformations,[3] electro catalysts in fuel cells[4] or materials with novel electronic,[5] optical,[6] and magnetic properties.[7] The catalytic and electronic properties are strongly influenced by the size of the particles, especially in the range 1-6 nm evidencing the need for size-selective synthesis techniques. The synthesis of nanoparticles is mainly achieved by chemical reduction of transition metal salts using various reagents such as alcohols,[8] borohydrides[9] or dihydrogen.[10] The drawback of these methods may be the presence of surface contaminants resulting from the reaction conditions, such as water, salts, organic residues, or even an oxide shell, which can alter the physical properties of the particles or limit access to their surface.

The particles are usually stabilised by the addition of a surfactant, a polymer or a ligand to the reaction mixture for preventing undesired agglomeration and metal precipitation. Presently, a large interest is also devoted to various applications of ligand protected particles for their physical properties.[11,12,13]

The preparation of metal nanoparticles was therefore achieved following an organometallic approach since this way does not employ drastic reaction conditions and avoids surface contamination. In addition, the size, the shape and the surface state of the particles can be controlled using various stabilizing agents. Besides catalysis, such work can find applications in different areas such as chemical sensors[14] or magnetic properties.[15]

This work concerns more particularly the preparation of Ru nanoparticles, their characterisation and their application in catalysis. The method used for this study is based on the spontaneous decomposition of a precursor in an organic solvent and under a reactive gas. The organometallic precursor Ru(COD)(COT) has been chosen as a starting material for the synthesis of Ru nanoparticles since this complex is easily decomposed under dihydrogen atmosphere giving then only cyclooctane as by-product. This precursor is very interesting for the elaboration of Ru nanoparticles with controlled size, dispersion and morphology of the particles. This technique allowed to produce ruthenium particles in a reproducible manner. IR, NMR, TEM, HRTEM, WAXS and microanalysis were used as characterisation methods.

Alcohols and simple organic ligands such as thiols and amines have been used as stabilisers. Chiral aminoalcohols and oxazolines were also employed for their interest in enantioselective catalysis. The behaviour of stabilising ligands at the surface of the particles has been investigated in particular by solution, solid state and gas phase NMR experiments. In addition, the organisation of the Ru particles has been accomplished in nanometric dimensions in pre-organised templates such as alumina membranes and mesoporous silica. Finally, catalytic tests have been performed with some of these new materials.

This work was performed in collaboration between the group of Professor G. Schmid at the Department of Inorganic Chemistry at the University of Essen in Germany and the group of Dr. B. Chaudret at the Laboratoire de Chimie de Coordination of the CNRS in France.

In chapter 2, ruthenium nanoparticles only stabilised by alcohols are described. New stabilisation methods to prepare some particles of "clean" surface state usable in catalysis are investigated. In these systems, the metal nanoparticles are not truly bare: they are stabilised by solvents adsorbed on their surface.

Ruthenium nanoparticles stabilised by a mixture containing methanol and THF are described in chapter 3. The size of these materials can be controlled simply be the solvent mixture composition. A highly porous surface has been created which is suitable for catalytic application.

Chapter 4 is dedicated to the synthesis of ruthenium nanoparticles solely stabilised by heptanol. The characterisation of their surface state by NMR spectroscopy in solution will be investigated.

In chapter 5, the preparation of ligand protected ruthenium nanoparticles, the study of the influence of the ligands on the size and shape of the nanoparticles and their characterisation both by techniques of material characterisation (electron microscopy, X-ray scattering) and by techniques of the molecular chemistry as solution NMR studies are described. The use of various long chain alkylthiols and alkylamines as stabilisers leads to Ru particles dispersed in solution displaying an hcp structure. The size and the organisation of the particles fluctuate with the nature and the quantity of the ligand and an organisation in superstructures is provoked in some cases.

Chiral aminoalcohols and oxazoline ligands were also selected for the stabilisation of the particles for further application in asymmetric catalysis.

Chapter 6 illustrates ruthenium nanoparticles included in alumina membranes of various pore sizes and in mesoporous silica materials which have been functionalised to favour the organisation of the particles.

Chapter 7 is devoted to the catalytic applications of the ruthenium particles previously prepared. At first, the ruthenium particles inside the pores of alumina membranes were tested in the hydrogenation of 1,3-butadiene and CO oxidation in the gas phase. Secondly, enantioselective activities of chiral aminoalcohols and oxazoline stabilised ruthenium particles in asymmetric hydrogen transfer reaction are reported.

The last chapter corresponds to the exact description of the experimental part.

1 Generals

1.1 Metal nanoparticles

1.1.1 Interest of metal nanoparticles

Nanometer size materials have attracted a remarkable academic and industrial interest of research due to their fundamental properties and their potential application ranging from fundamental studies to catalysis.[11,13,16,17,18,19] A precise control of size and chemical behaviour (stability *and* reactivity) by means of the synthesis itself is a major aim due to the direct correlation of intriguing new properties with particle size, bridging the gap between molecules and bulk materials.

There is currently a considerable interest in controlling the structure of a material at the microscopic level as this influences its physical and chemical properties and as well as its reactivity. The change in chemical behaviour is due to the electronic change of the nano-sized materials. The three-dimensional size reduction of metal particles down to the range of the de Broglie wavelength changes their properties. The limited size reduces the mobility of the electrons and leads to the formation of discrete energy levels that result in quantum size effects (QSE).

In many ways the most successful model in order to understand the electronic structures of metals, and later of nanoparticles, is an extended form of the molecular orbital theory that deals with physical properties such as electrical conductivity. The theory is known as the band theory of metals. The overlapping of orbitals on adjacent atoms leads to bonding, non-bonding and anti-bonding orbitals. Within limits, the larger the overlap between atom orbitals, the greater the energy gap between bonding and anti-bonding orbitals. The band of the orbital energies for the valence electrons of metal atoms approaches a continuum. When the number of atoms increases, an energy band develops. Because the band width for any particular type of atomic orbital depends on orbital overlap at the normal metal-metal distances of metallic lattices, the inner orbitals form fairly narrow bands separated from each other by appreciable energy gaps and together constitute the valence orbital bands (Figure 1-1).

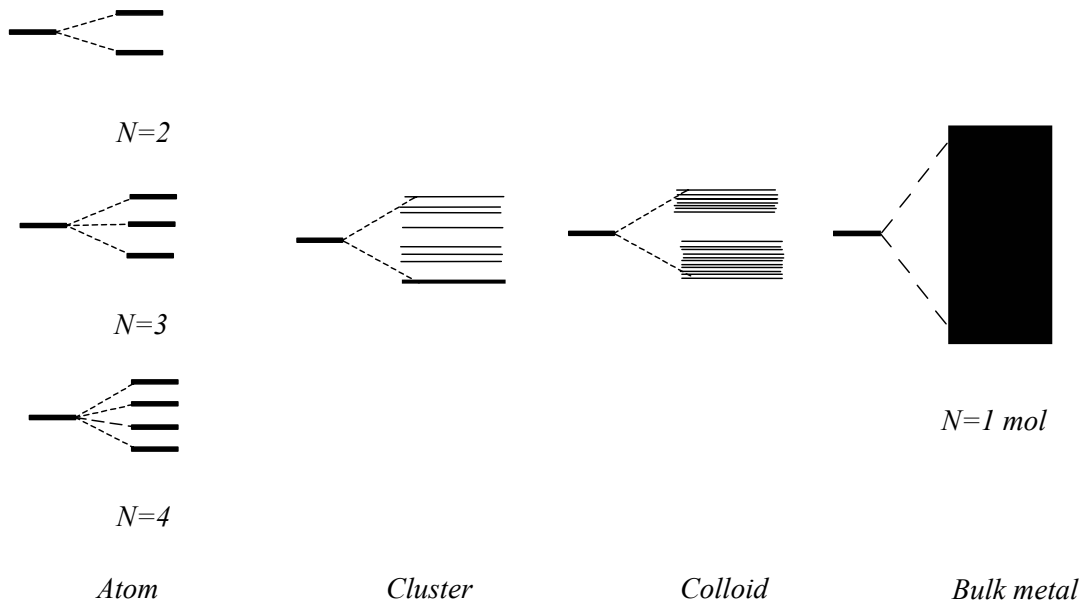

Figure 1-1 : Electron levels of atom, cluster, colloid and bulk metal

All the lattice orbitals arising from core atomic orbitals are filled with electrons. Unoccupied lattice orbitals must be available for the transport of valence electrons throughout the crystal. An insulator is represented as a case in which completely filled bands are separated by a considerable energy gap from unoccupied bands. Conductors are identified as cases in which a particular valence band in only partially filled. The gap between the bands increases when the size of the material decreases by up to several electron volts. In this case the orbital energies do not form a continuum but they remain as discrete energy levels. The presence of these well separated energy levels lead to different quantum size effects which show themselves in changed optical, electronic and catalytic properties. These properties are not only different from the bulk metal but from molecular structures as well. The continuous reduction in size of a material finally leads to a state where the solid state properties can only be partially observed or are even completely lost. Further size reduction finally leads to the typical molecular behaviour. When a metal is reduced to a size of a few thousand atoms we enter the world of nanoparticles or colloids. Smaller units of a few hundred atoms can be described as nanoclusters. An interesting question concerns the size required for a cluster to exhibit the same typical properties as observed for the bulk metal, when do we have use the methods of the quantum chemistry which are valuable for the molecular range instead of the laws of classical physics. Metal clusters between 1-10 nm are the most interesting because they correspond to the intermediate state connecting metals and non-metallic compounds. In this range they show characteristics depending on their size which can be explained by

quantum mechanics. The difference between the physical properties of metals and nanoparticles is due to the loss of the continuum of the electronic bands. When a material is reduced to nanometer size and the de Broglie wavelength of the valence electrons is equal to its thickness, the freely mobile electrons are very limited in the reduced dimension. If a three-dimensional material is reduced to a layer of atoms, the original electrons, which had unrestricted motion in the three dimensions, can now only move in two dimensions within a quantum wall. Further reduction of the size leads to a quantum wire where the electrons can only move in one dimension. In a zero dimensional quantum dots the last "metallic" electrons are fenced and can not move freely as in the bulk material (Figure 1-2). Such a miniaturization affects the properties of the material because these electrons determine the physical and chemical characteristics of the nanoparticles. The effect which leads to this change in properties is called "Size Induced Metal-Insulator Transition".

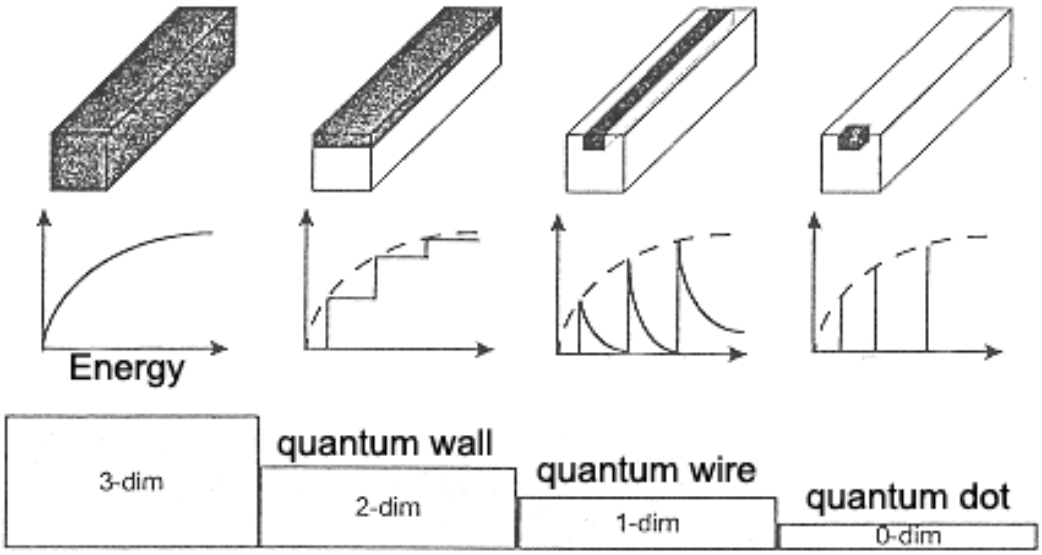

Figure 1-2 : Change of the electronic properties on the way from the bulk to nanosized species by reducing the dimension from three dimensions via a quantum wall and a quantum wire to a quantum dot[20]

Elements like Au, Pt, Pd, Rh and Ru from the I. and VIII. Group form clusters with a part of the bulk metal in the hexagonal closed packed (hcp) or the cubic closed packed (ccp) structure. The central atom can be surrounded by 12 other metal atoms, which is the maximum possible co-ordination for a full-shell cluster. The number of atoms for the cluster follows from the equation of the magic number, as shown below. Stable clusters are clusters with 13, 55, 147, 309, 561 or 1415 atoms (Figure 1-3).

$$N = 10n^2 + 2$$

with

N = magic number

n = number of atom layers

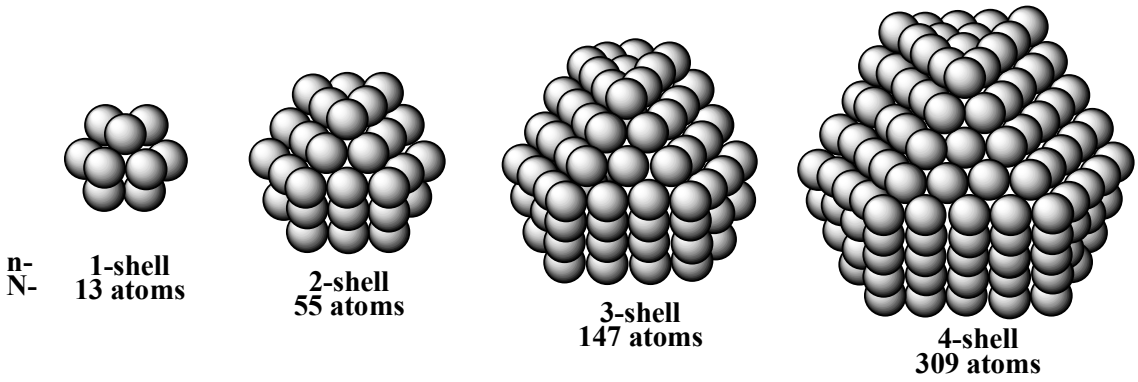

Figure 1-3 : Examples of full-shell clusters with the magic number of atoms

An example is the cluster $Au_{55}[P(C_6H_5)_3]_{12}Cl_6$.[2] This cluster consists of two layers and is protected by its ligand shell. One can observe the changing behaviour between bulk and molecule of this cluster since it has only two free moving electrons.

Such particles with a well defined size and structure are generally called clusters. Therefore the particles in this work will be named colloids or nanoparticles. There are basically two methods for the synthesis of nanosized materials (Figure 1-4): the top-down method starts with the bulk material whose size is reduced using physical tools. On the other hand the bottom-up method forms nanostructures from molecular structures via chemical reactions. The bottom-up method provides better results for the synthesis of nano materials with good reproducibility and yields.

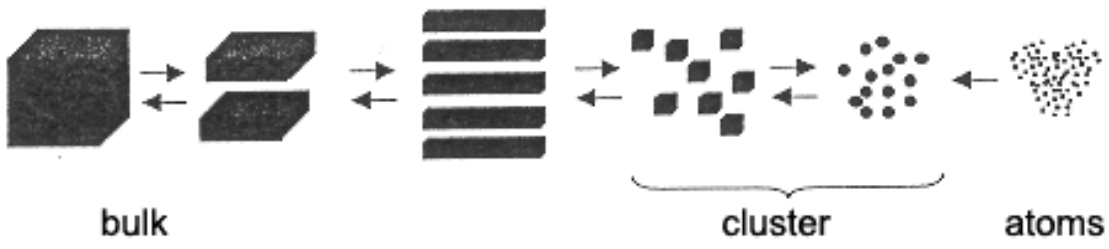

Figure 1-4 : top-down and bottom-up methods to synthesise nanomaterials[21]

1.1.2 Nucleation, growth and stabilisation of metal nanoparticles in solution

To obtain nanoparticles with a surface/volume ratio as large as possible solutions are used as a reaction mediums, since for catalysis a large surface is important.[22] A colloidal solution is characterised by the size distribution of the nanoparticles contained within it, which depends on the mechanism of the nucleation and the subsequent growth of the particles. A homogeneous nucleation is the spontaneous condensation between the metal atoms to form particles as shown in Figure 1-5.

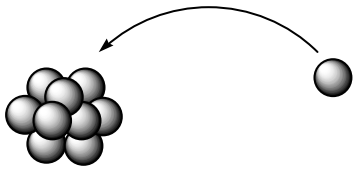

Figure 1-5 : Homogeneous nucleation of nanoparticles

A heterogeneous nucleation (Figure 1-6) is introduced by impurities in the reaction mixture. The growth of the particles is then determined by the adsorption of atoms to the pre-formed core due to the attraction between particles caused by van der Waals forces. The dispersion of the particles is determined by the Brownian movements.[23]

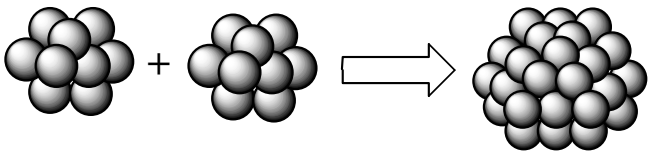

Figure 1-6 : Heterogeneous nucleation of nanoparticles

The aim is to control the dispersion of the particles in solution. Their stability depends on the energy between them in the system, which is a product of both the attractive (van der Waals) and the repulsive forces (Figure 1-7).[2]

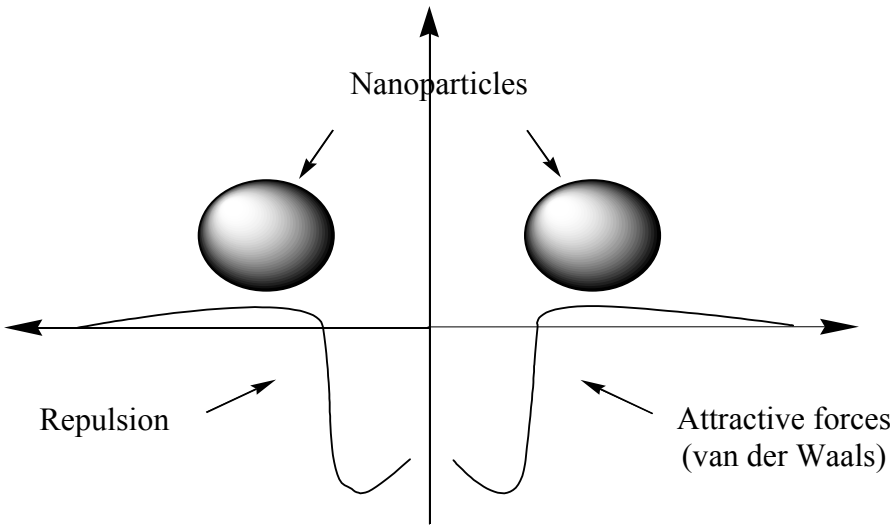

Figure 1-7 : Electrostatic stabilisation of nanoparticles

In general, the formation of the particles follows the two mechanisms simultaneously: the clusters which have been formed by the adsorption of atoms begin to coalesce due to the Brownian movements and form nanoparticles. Figure 1-8 illustrates the phenomenon of the nucleation of the particles and underlines the importance of their stabilisation in solution in order to control their size and morphology efficiently to avoid a precipitation of the bulk metal.

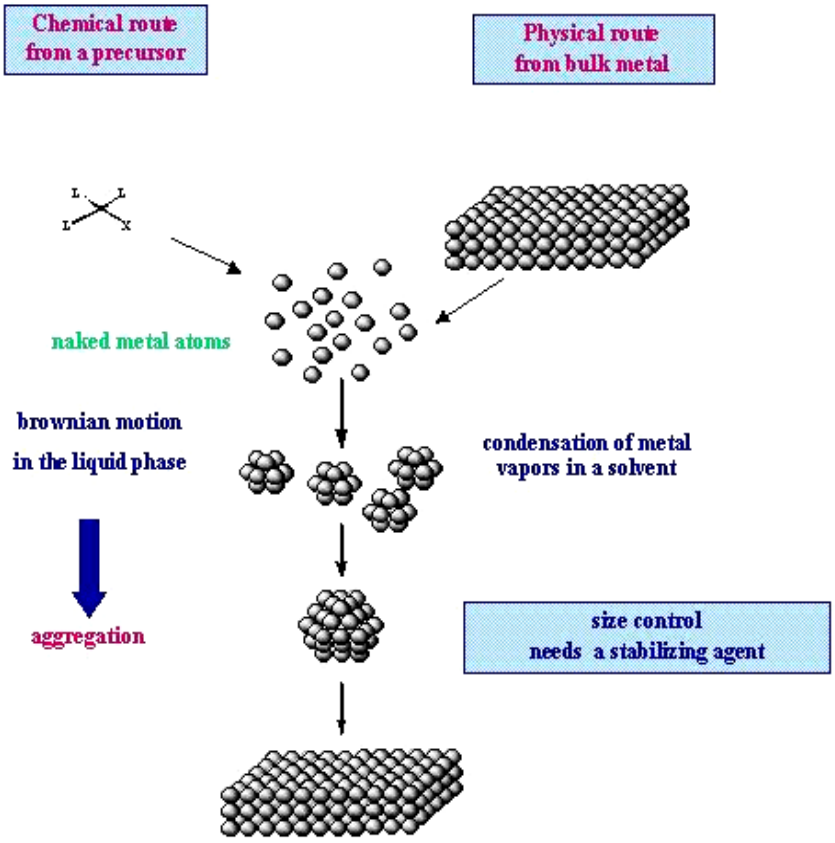

Figure 1-8 : Synthesis of colloidal solutions of metal nanoparticles

1.1.3 Synthesis methods of metal nanoparticles

Colloidal solutions of nanoparticles can be prepared via different methods such as:

- Radiation induced synthesis of colloids
- Electrochemical synthesis of colloids
- Ultrasound-assisted electrochemical synthesis
- Salt reduction
- Organometallic synthesis (thermal decomposition, ligand reduction or ligand displacement)

The radiation method was described by Rogninski and Schalnikoff for the first time and is based on the condensation of the metal atoms after collision.[24] Reetz et al. prepared nanoparticles via electrochemical synthesis.[25,26] The use of ultra sounds for the synthesis of nanoparticles was discovered by Schubert in 1981 and further developed.[27,28] Salt reduction was developed by Bönnemann to obtain mono- and bi-metallic nanoparticles in solution.[10,29] Salt reduction is the most widely practised method for the synthesis of colloidal metal suspensions. Faraday synthesised gold particles by reduction of $HAuCl_4$.[30]

Colloidal solutions of nanoparticles can also be synthesised via an organometallic approach, organometallic derivatives providing a general route for the synthesis of monodisperse nanoparticles, as exemplified in Figure 1-9 for Ruthenium nanoparticles synthesis. Using this approach, the particles are prepared via the bottom-up method.

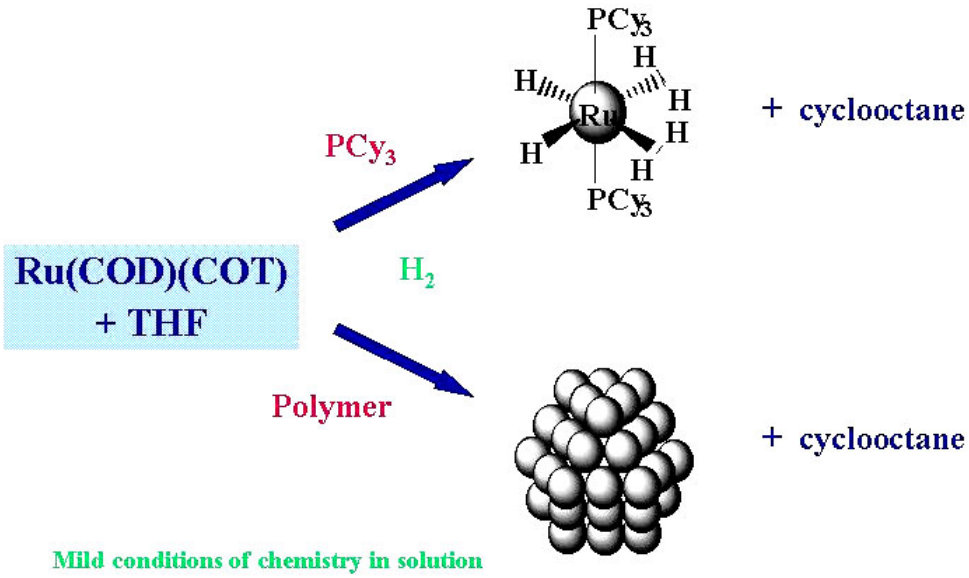

Figure 1-9 : An organometallic route towards colloids

We have to distinguish between almost naked particles surfaces and ligand protected particles. In fact, most of the particles are protected by a shell of ligand molecules in order to stabilise them and to separate them from each other to prevent agglomeration. In the absence of any stabiliser to assure their dispersion in solution, thermodynamically, the particles will agglomerate and finally precipitate. Therefore, the nanoparticles have to be stabilised from conglomeration.

1.1.4 Stabilisation modes

In general, there are two different methods to achieve this stabilisation:

- Stabilisation by amplification of the repulsive forces by ionic additivs
- Sterical stabilisation by ligands or polymers

For the amplification of the repulsive forces an additive is added to the solution to fortify the electrostatic stabilisation. Bönnemann et al. used ammonium salts (NR_4X) for the in-situ decomposition of the precursor.[10] Another method to prevent the coalescence of the particles is the steric stabilisation which can be achieved by the adsorption of molecules with

long chain like organic ligands or polymers. Napper[31] was the first to study the adsorption of polymers and since then different types of polymers like vinyl polymers with polar side groups such as poly(vinyl)pyrrolidine (PVP) and poly(vinyl)alcohol (PVA) have been applied.[32,33] The use of poly(vinyl)pyrrolidine) (PVP) as a polymer matrix has been studied previously and showed the formation of regularly dispersed nanoparticles of uniform size.[34,35] For example, the reaction of Ru(COD)(COT) in THF in the presence of PVP ([Ru] / polymer; 5 wt%) with 3 bar dihydrogen at 193K for 15 hours leads to an homogeneous brown solution. Addition of pentane leads to the precipitation of a brown powder which can then be dissolved in methanol and precipitated with pentane. High resolution electron micrographs show particles homogeneously dispersed in the PVP matrix. They display uniform size centred around 1.2 nm and the hcp structure of bulk ruthenium. This study demonstrates that the decomposition of the precursor Ru(COD)(COT), in a medium which has a weak electronic interaction with the surface of the particles but which is able to provide a good steric protection of the surface, yields crystalline nanoparticles of spherical appearance, small size and narrow size distribution.

The most common tools used for stabilising nanoparticles have so far been polymers but they may not be usable in certain chemical or physical applications. For this reason, the use of ligands coordinated at the surface of the particles has been considerably developed in the past few years.[36,37,38,39,40,41,42,43] The presence of ligands prevents the particles from coalescing and can allow their self-assembly onto various surfaces. The main difference between the stabilisation with polymers and organic ligands is the interaction of the stabilising agent with the particle surface. The nature, number and arrangement of the protecting ligands may effect the electronic properties of the particles. It follows that ligand stabilised particles may differ considerably from quasi-naked clusters or polyemer stabilised ones in their electronic properties. The interactions of ligands with the particles surface makes the access to the particles surface difficult. There is a wide variety of ligands used for the stabilisation of nanoparticles. These organic ligands can introduce true chemical metal-ligand bonds which ensures their electronic stability as well, while polymers are only absorbed at the particles surface. The presence of ligands at the surface of the particles can then modulate their properties. In addition, when the ligand has a long alkyl chain a steric protection is also guaranteed.

1.1.5 Organisation of nanoparticles in templates

Metal nanoparticles can be organised in templates in order to synthesise nanowires. The syntheses of nanostructured materials by the means of templates or matrices are widely applied and provide the possibility of access to materials of exact dimensions.[21,44,45] Matrix materials polycarbonat-[46] and other polymers[47]-membranes have been applied. Porous silica[48] and zeolithes[49] are used for the organisation as well. However, mesoporous alumina membranes present the advantages of easy preparation, stability in air and at high temperatures and variable pore diameter.[50] Therefore, Al_2O_3 membranes may be used for the organisation of nanoparticles.[21] These membranes, which are prepared by anodic oxidation possess high pore densities, a narrow mean pore diameter and hexagonal array of the pores.

Supported nanoparticles can be induced in mesoporous silica.[51] Highly ordered and hydrothermally stable mesoporous silica with unique pore sizes and a huge internal surface are suitable supports.[52]

1.1.6 Application of metal nanoparticles

Metal clusters may find applications in catalysis. The smaller the particles' size, the higher is the number of their surface atoms.[53,54] This makes the particles interesting candidates for catalytic applications. Crooks used palladium clusters for hydrogenation and could show an elevated reactivity with the particles depending on the particle' size.[55] Nanoparticles are also known as sensitve layer in selective gas detectors.[56]

The investigation of the synthesis of ruthenium nanoparticles has been since it is a metal of choice for numerous applications in catalysis (selective hydrogenation of carbonyl groups, partial hydrogenation of aromatic compounds...).

1.2 Ruthenium nanoparticles

1.2.1 Ruthenium[57,58]

Ruthenium with a mass of 101.07 g/mol was discovered in 1843 by the Russian G. Klaus. A member of the platinum group, ruthenium occurs natively with other members of the group in ores found in the Ural mountains and in North and South America. The metal is isolated commercially by a complex chemical process, the final stage of which is the hydrogen reduction of ammonium ruthenium chloride, which yields a powder. Ruthenium is a hard, white metal and has four crystal modifications. Ruthenium is largely immune to atmospheric attack. It does not tarnish at room temperature, but oxidizes explosively on heating with oxygen: ruthenium metal gives ruthenium (IV) oxide, RuO_2 (Equation 1-1).

$$Ru(s) + O_2(g) \rightarrow RuO_2(s)$$

Equation 1-2 : Oxidation of Ruthenium with oxygen

It is attacked by halogens, hydroxides, etc. Ruthenium can be plated by electro deposition or thermal decomposition methods. This metal is one of the most effective hardeners for platinum and palladium, and is alloyed with these metals to make electrical contacts with severe wear resistance. The crystal structure of ruthenium is hexagonal closed-packed (hcp) as shown in Figure 1-10.

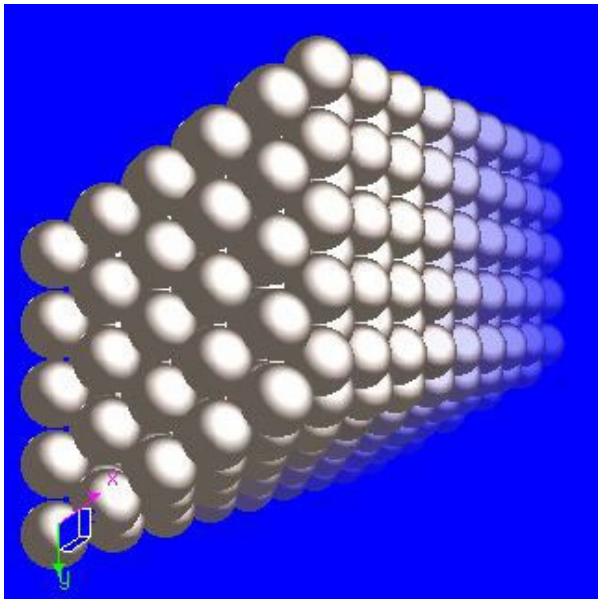

Figure 1-10 : Hexagonal closed-packed (hcp) ruthenium structure[59]

1.2.2 Ruthenium nanoparticles and their application

Ruthenium is widely applied for catalysis. Ruthenium demand in 2004 is forecast to rebound by more than 22 %. The recovery is due to excess inventories largely having been eliminated from the electronics industry, and to growing demand for ruthenium-based catalysts. Production of ruthenium-based products such as resistors has therefore increased. This includes a small contribution from a new application for ruthenium in computer hard disks, as leading manufacturers adopt the new technology. The chemical industry uses ruthenium in process catalysts employed in the manufacture of acetic acid, ammonia and speciality chemicals.

Due to their reduced size (1-100 nm), ruthenium nanoparticles possess different chemical and physical properties from the bulk metal, which make their study of great interest. For small particles, the majority of the atoms are situated at the surface. The smaller the particles, the higher is the number of atoms situated at their surfaces. Surface atoms are responsible for an elevated reactivity and this makes ruthenium particles interesting for future application in catalysis.

1.3 Synthesis of ruthenium nanoparticles through an organometallic approach

There are a number of ways to synthesise metal particles with diameters between 1 and 20 nm. This includes precipitation,[60] organometallic preparation and deposition,[61] sonochemical methods[62] and via microemulsions created using organic stabilising agents.[63] Most routes mentioned include nucleation, growth and stabilisation of the particles, which results in a range of particle sizes. For monodisperse size control, the use of organic stabilising agents is regarded as one of the most promising routes.[64,65]

Organometallic derivatives may provide a general route for the synthesis of monodisperse nanoparticles as has been recently illustrated.[66] The bottom-up method together with the tools of organometallic chemistry is used to synthesise nanoparticles.[67,68,69,70,71,72,7374,75,76]

Suslick reported that metallic nanoparticles can be obtained by the decomposition of organometallic complexes by ultra sounds.[77] The effect of ultra sounds to decompose

precursors in solution is very efficient. Usually this method leads to the formation of highly porous materials which have an enhanced catalytic activity in comparison with the conventional catalysts.[78] With this method zinc,[79] iron,[80] palladium[81] and molybdenum[78] nanoparticles have been synthesised. Iron nanoparticles have then been prepared by the decomposition of the precursor $Fe(CO)_5$ by ultra sounds. This complex dissociates due to the local developed heat and forms at first the intermediate $Fe_3(CO)_{12}$ which is not stable and gives a fine powder of amorphous Fe.[82]

De Caro et al. decomposed the same complex by ultra sounds and obtained various sizes of particles depending on the stabilising agent between 3 and 10 nm.[83]

Also using ultra sounds, Gedanken et al. synthesised iron[84,85] and palladium[86] nanoparticles which are stabilised by a carbon layer at the surface of the particles which assures their stabilisation. The advantages of this method are the high yield and the high surface areas of the obtained particles. Colloidal nanoparticles can be attained with reasonable size distributions. But the presence of solvents and of ligands lead to the presence of contaminants like C and O at the surface of the particles.

The exposure of organometallic precursors under reactiv gases atmospheres like CO and H_2, undergo the displacement of the ligands and their reduction through breaking of carbon-metal bonds.[87] The decomposition is carried out under mild conditions of temperature and pressure. This synthesis avoids the use of strong reduction agents (e.g. $NaBH_4$, $NaBEt_3H$,…) and therefore the presence of impurities which could be adsorbed to the particles' surface.[88] The control of the growth of the particles requests a stabilising agent like polymers or organic ligands. With this technique several metal nanoparticles like palladium, platinum and ruthenium have been prepared.[36,89,90]

Bradley et al. decomposed the complex $Ni(COD)_2$ at room temperature and in the presence of PVP as stabiliser simply using dichloromethane as solvent.[32] When they changed the ratio Ni/PVP, they observed a small variation of the particles size from 2-3 nm.

To our knowledge, only a few studies concerning the synthesis of ruthenium particles have been published in the literature,[91] most of them reporting the use of $RuCl_3$ as metal precursor. For example, stable colloidal solutions of monodisperse Ru particles can be obtained by reduction of $RuCl_3$ in polyols. The stabilisation is then achieved by addition of PVP (steric stabilisation) or of sodium acetate (electrostatic stabilisation).[92]

For this work ruthenium has been chosen for being a metal of catalytic interest and a precursor for semi-conducting oxides but for which the literature remains very limited.[93,94,95]

A method which is based on the decomposition of an organometallic precursor by a reactive gas was optimised. An interesting possibility to obtain ruthenium particles is the decomposition of the organometallic ruthenium precursor Ru(COD)(COT) (COD: 1,5 cyclooctadiene; COT: 1,3,5, cyclooctatriene) which is prepared according to a published procedure (Scheme 1-1).[96] Yellow crystals of this complex are obtained with a yield of 70 % and can be characterised by NMR spectroscopy and microanalysis.

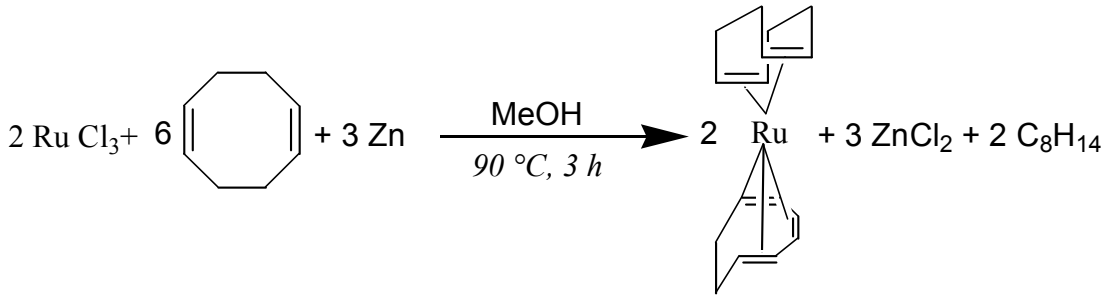

Scheme 1-1: Synthesis of the organometallic precursor Ru(COD)(COT)

The decomposition of the organometallic precursor Ru(COD)(COT) under mild conditions (room temperature, 3 bar H_2) leads easily to ruthenium nanoparticles.[35,67,97] A central metal atom of a low oxidation state (0) is linked to organic ligands which are easily displaced via chemical activation, hydrogenated and finally eliminated from the co-ordination sphere of the metal. This method was optimised in our laboratory. The stabilisation of the particles by polymers has previously been studied by Chaudret et al..[98,99] Following these results, the objective was the preparation of Ruthenium nanoparticles without a polymer matrix to facilitate the approach of molecules to the surface and in order to obtain clean and reactive surfaces. Therefore an efficient method for the control of size, surface state and morphology of ruthenium nanoparticles as catalysts had to be developed.

The stabilisation of the ruthenium nanoparticles can be accomplished with pure alcohols, mixtures of methanol/tetrahydrofurane, long chain amines and thiols and chiral aminoalcohols and oxazoline ligands.

In this work, the synthesis of Ru nanoparticles in the presence of an alcohol or a ligand will be described. Another point concerning the organisation of Ru particles in nanoporous

alumina membranes and silica will be developed. Finally their reactivity in catalytic application will be evaluated.

2 Stabilisation of ruthenium nanoparticles by pure alcohols

2.1 Introduction

First of all, the ruthenium nanoparticles have been prepared in the absence of further stabiliser to obtain "naked" nanoparticles with a rather clean and reactive surface. The decomposition of Ru(COD)(COT) under 3 bar H_2 in pure solvents such as THF, cyclooctane or pentane leads at room temperature to a black precipitate after approximately 15 min exposure.[100] The reaction solution is colourless and the precipitate is easily separated from the clear solution by simple settling giving then a fine powder after drying under vacuum. TEM analysis of the precipitate reveals the presence of strongly agglomerated large ruthenium particles. Agglomerates of approx. 100 nm are observed in which the size of the individual particles could not be determined exactly. THF, cyclooctane and pentane are then not able to maintain the ruthenium particles stable in solution. In these solvents, the stabilisation of the particles could not be achieved and they eventually coalesce and precipitate due to the formation of large agglomerates.

The objective of this work was to prepare in a reproducible way ruthenium nanoparticles with a clean surface, a controlled size and stable in solution. The properties of small naked nanoparticles are dominated by their different average atomic co-ordination compared to that in the bulk. It has become quite apparent that naked nano-size particles present a very good catalytic reactivity. Small particles can be used for heterogeneous or homogenous catalysis, their activity and selectivity depending on their size. This chapter investigates the aspects of naked nanoparticles which are stable in an organic solvent or an organic solvent mixture without any further common stabiliser. Pure alcohols have been chosen for the synthesis since alcohols seem to have weak interactions with the metal surface.

Methanol was chosen to try to obtain more stable particles, since methanol is more polar than, for example, THF. In addition, interactions through the OH-group with the metal surface may happen and allow the stabilisation of the particles.

Ruthenium nanoparticles stabilised by pure solvents were prepared by decomposition of the organometallic precursor Ru(COD)(COT) (COD = 1,5-cyclooctadiene, COT = 1,3,5-cyclooctatriene) under an H_2 atmosphere in a pure alcohol as solvent and without other

stabilisers like organic ligands (e.g. amines, thiols). The particles were characterised by electron microscopy (TEM, HREM), X-ray diffraction (XRD) and wide-angle X-ray scattering (WAXS). The colloidal solutions are stable for long periods of time, over a year in some cases. The TEM micrographs reveal in some cases the presence of sponge like agglomerates of regular spherical shape and homogeneous size inside which individual crystallites are chemically linked to one another or, in other cases, the presence of isolated and well dispersed monocrystalline particles depending upon the alcohol alkyl chain. In all cases, the size distributions are relatively narrow. WAXS and XRD analyses indicate the exclusive presence of hcp ruthenium in these materials.

2.2 Stabilisation of ruthenium nanoparticles by pure methanol

In contrast to the coalescence of the nanoparticles observed in the three previously mentioned solvents, the particles are stable in the colloidal solution when the decomposition is performed in pure methanol under the same conditions (Scheme 2-1): room temperature, 45 minutes under 3 bar H_2.

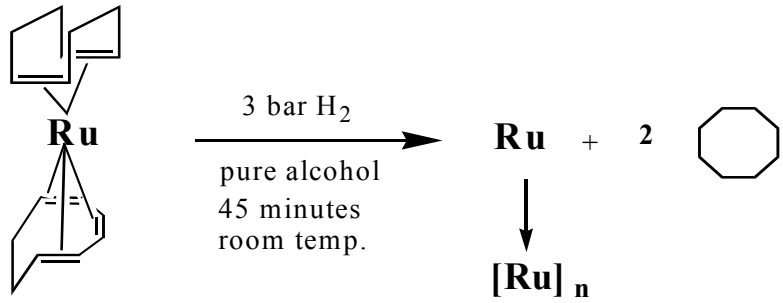

Scheme 2-1: Decomposition of Ru(COD)(COT) under 3 bar H_2 in a pure alcohol

A dark brown colloidal solution is rapidly formed after exposure to a dihydrogen atmosphere. The solution can be stored under argon and is stable for at least two weeks. After that period of time, a gradual decantation is observed. Therefore, a drop of the freshly prepared colloidal solution was deposited under argon on a carbon covered copper grid and the particles were visualised by electron microscopy after complete evaporation of the solvent. Large, but well-dispersed sponge-like particles of homogeneous size (mean diameter = 76 nm) are observed by TEM and HREM (Figure 2-1 a and b). They display a porous and polycrystalline aspect and under larger amplification (Figure 2-1 b) the size of the individual

crystallites can be estimated in the order of a few nanometers.[67] Due to their porous aspect, these particles are called “cauliflower”.

a) b)

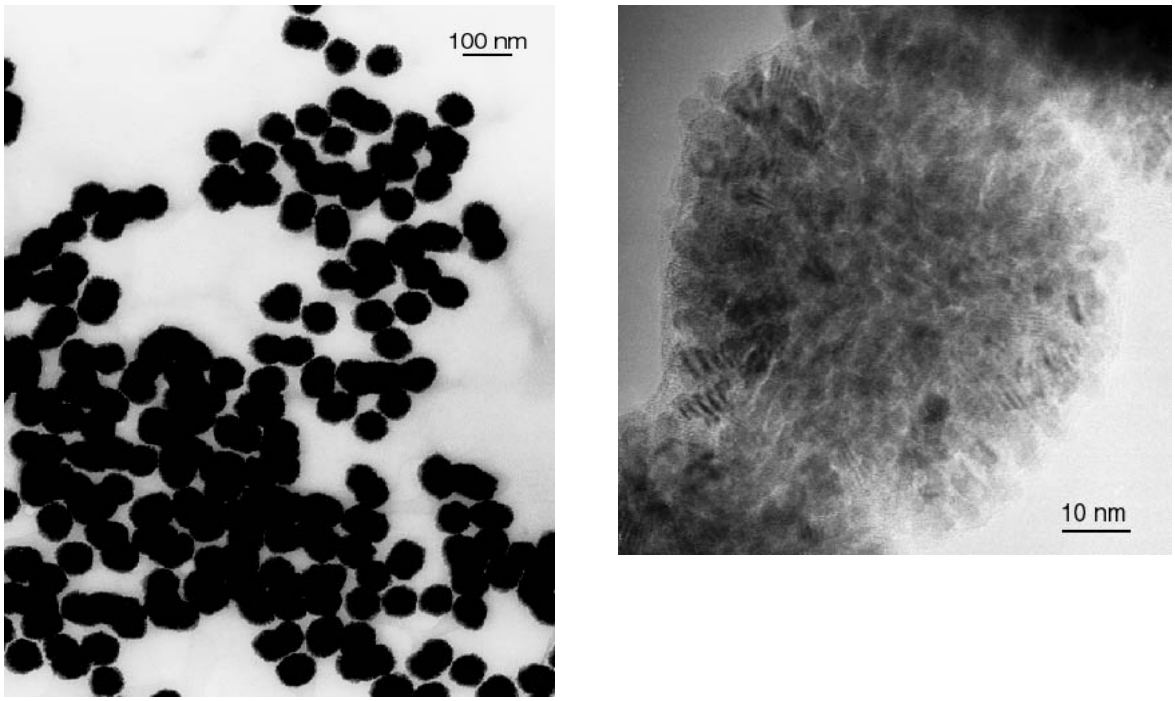

Figure 2-1: TEM (a) and HREM (b) micrographs of Ru nanoparticles synthesised in pure methanol

These particles can be isolated as a fine shiny powder by evaporation to dryness or precipitation of the reaction solution after cyclooctane or pentane addition, but they cannot be dissolved again in methanol. The particles are very air sensitive and burn in the open air. XRD experiments showed that the particles consist of hexagonal close packed (hcp) ruthenium. When WAXS experiments were carried out in an air-free Lindemann capillary only peaks corresponding to well-crystallised hcp ruthenium particles were observed.

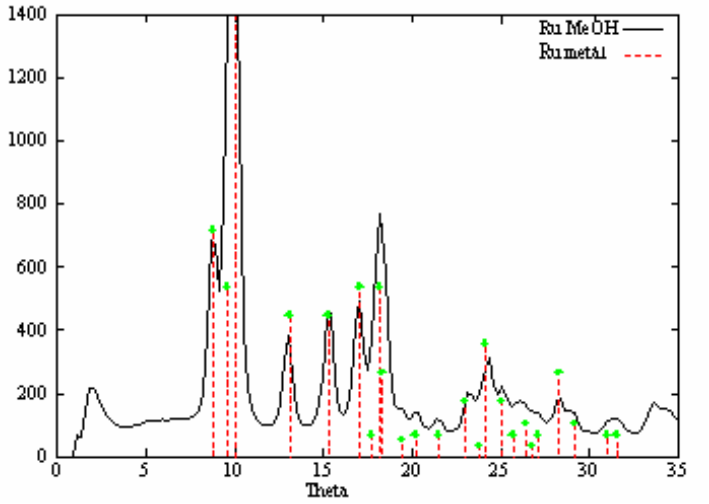

Figure 2-2: Comparison of XRD diagrams of Ru/MeOH nanoparticles and Ru bulk metal

Then, in pure methanol, it was possible to obtain size controlled ruthenium nanoparticles in an efficient and reproducible manner. Nevertheless, the particles obtained are large. Therefore, the stabilisation of ruthenium nanoparticles was attempted with long chain alcohols, since a good dispersion of the particles in pure methanol was assured in a reproducible way.

2.3 Stabilisation of Ru nanoparticles by various long chain alcohols

In order to determine the influence of pure alcohols on the stability, dispersion and morphology of the particles, the decomposition was carried out in solutions of n-propanol, isopropanol, pentanol, heptanol, dodecanol and oleylalcohol. The different alcohols used in this study were tested with the main objective of studying the influence of the alkyl chain length on the particles size and their dispersion. In all cases, the decomposition proceeded quickly, indicated by a rapid colour change from yellow to brown after two minutes. More or less stable colloidal solutions of ruthenium particles are obtained.

2.3.1 Stabilisation of Ru nanoparticles by pure n-propanol

When the decomposition is performed in pure n-propanol under the same conditions as with methanol, the colour of the colloidal reaction solution is lighter than that observed using methanol, which seems to indicate a smaller particle size. The colloidal solution is also more stable than the methanol one (3-4 months). TEM analysis, realised immediately after synthesis, reveals the presence of much smaller particles (mean diameter: 4 nm), which are well dispersed on the microscopy grid and display a spherical shape (Figure 2-3). The size distribution is narrow (between 3.9 and 4.05 nm) and 53% of the particles have a mean size of 4 nm. The structure of the particles could be analysed by HREM (acceleration voltage: 300kV): a polycrystalline aspect is observed. These particles again appear to be composed of small chemically linked crystallites.

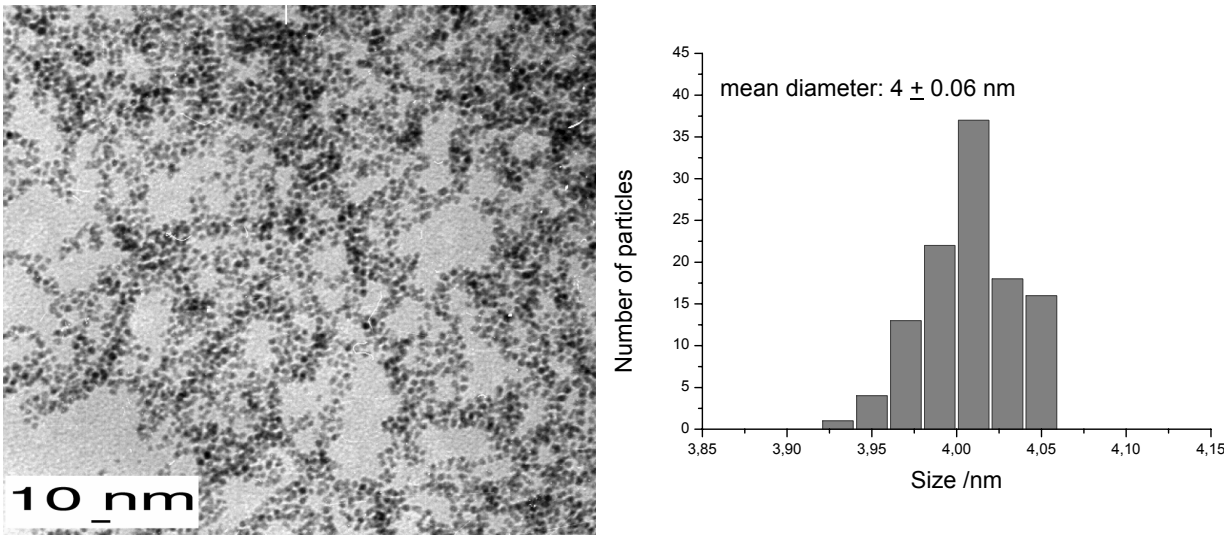

Figure 2-3: TEM micrograph and size histogram of Ru particles synthesised in pure n-propanol

2.3.2 Stabilisation of Ru nanoparticles in pure iso-propanol

The decomposition is faster when iso-propanol is used instead of n-propanol, which is indicated by a rapid colour change: after only two minutes of pressurisation it changes from yellow to brown. The results of synthesis in n-propanol and iso-propanol are similar, but the colloidal solution in iso-propanol is darker than the one obtained in n-propanol, and less stable

(1 month). Nevertheless, the solution obtained is homogeneous. TEM analyses indicate a slightly larger mean size of 5.2 nm and a slightly greater size distribution (Figure 2-4). The mean diameter is between 4.4 and 6 nm which means that the size control in pure iso-propanol is less efficient. By contrast, the particles seem to be organised in chain-like formations.

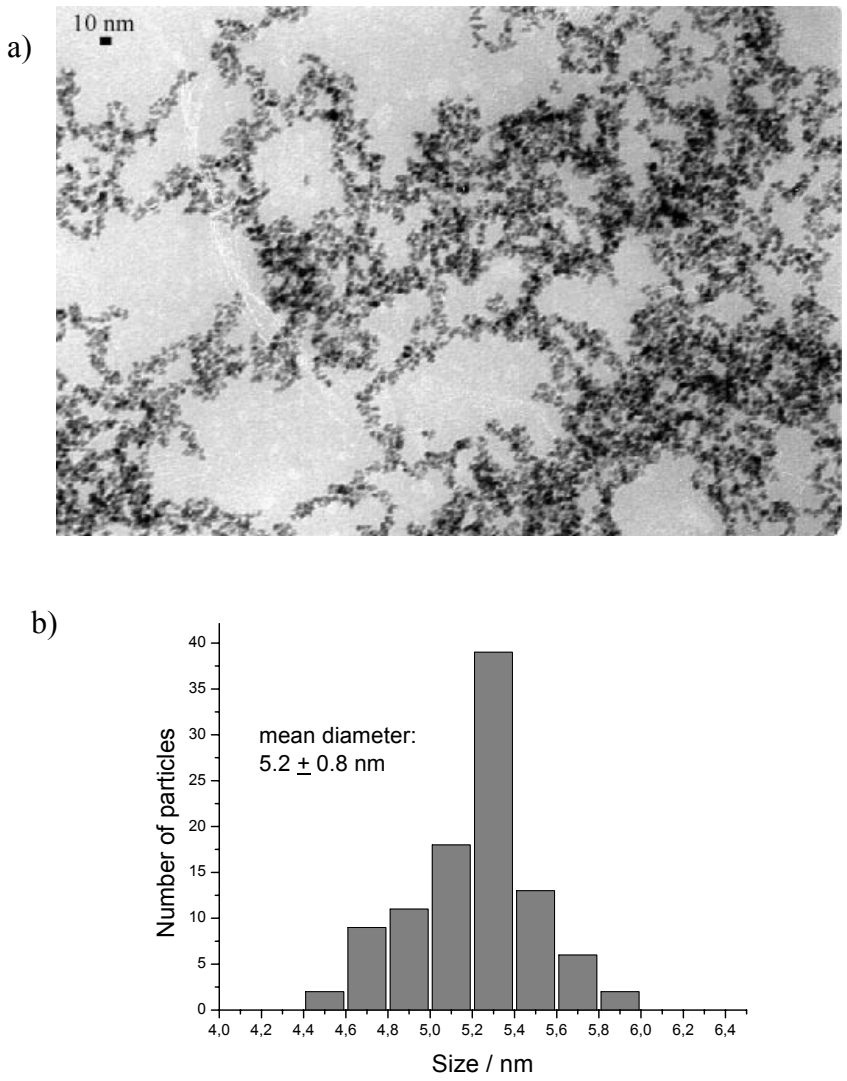

Figure 2-4: TEM micrograph (a) and size histogram (b) of Ru particles synthesised in iso-propanol

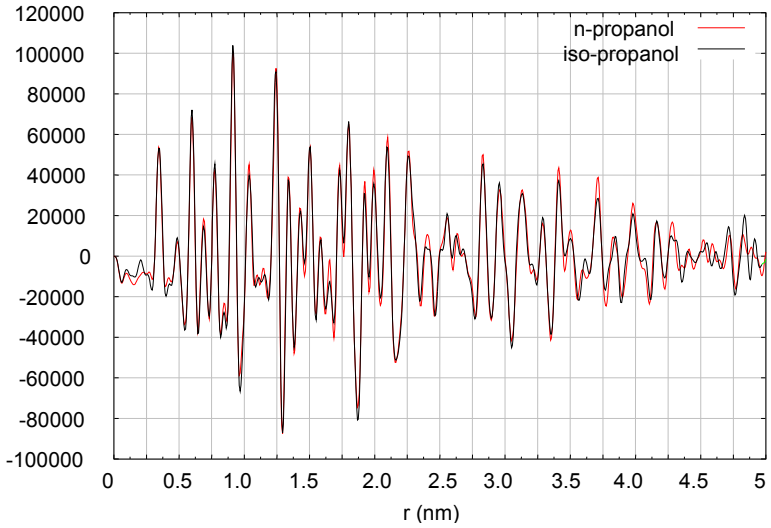

Figure 2-5: Comparison of WAXS measurements of Ru particles prepared in n- and iso- propanol

The comparison of the WAXS measurements of the ruthenium particles synthesised in n- and iso-propanol indicates that their structure is also the hcp structure of bulk ruthenium. A similar coherence length of approx. 5 nm for n-propanol and for iso-propanol synthesised particles is confirmed.

2.3.3 Stabilisation of Ru nanoparticles by pure pentanol

The decomposition of Ru(COD)(COT) in pentanol leads to the formation of very small Ru particles which are in close contact, as seen by TEM (Figure 2-6). The solution obtained is clear brown and stable for several weeks. Particle mean size is estimated to be around 2-3 nm since the corresponding size distribution is large. They appear to be well crystallised and homogeneous in size, but they tend to organise themselves into cloudy aggregates, inside which they remain separated.

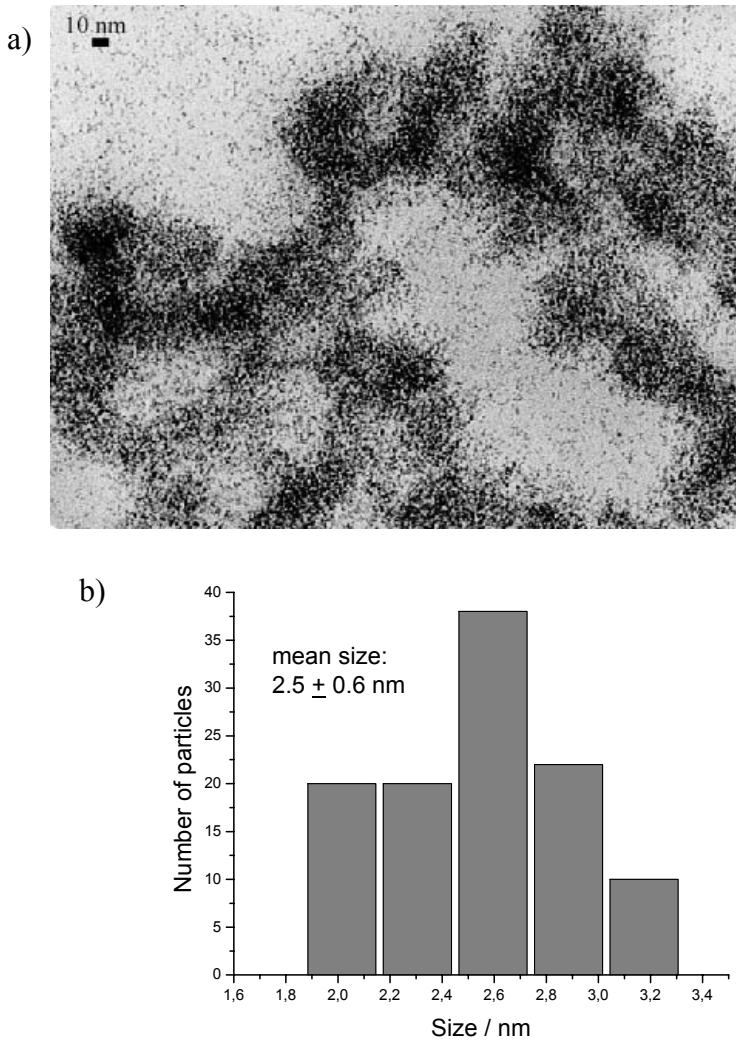

Figure 2-6: TEM micrograph (a) and size histogram (b) of Ru particles synthesised in pentanol

The determination of a precise size was difficult by TEM due to the strong agglomeration of the particles. WAXS measurements (Figure 2-7) validate the mean size of 2.5 nm estimated by TEM and verify crystallisation in the hcp structure.

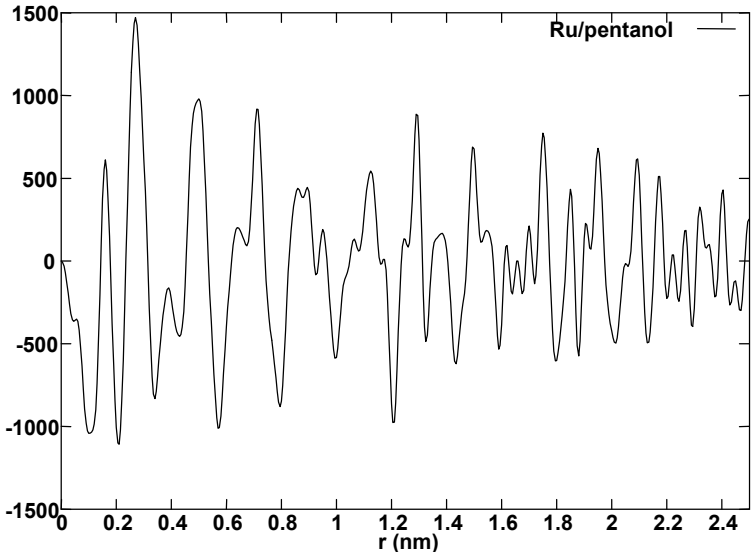

Figure 2-7: WAXS measurements of Ru particles prepared in pentanol

When the particles are visualised at higher magnification in HREM (Figure 2-8), the aspect of the particles seems to be crystalline: the presence of atomic planes can be observed. The particles are assembled into clouds inside of which they remain separated, in contrast to the "cauliflowers" observed earlier. In addition, the particle size is homogeneous.

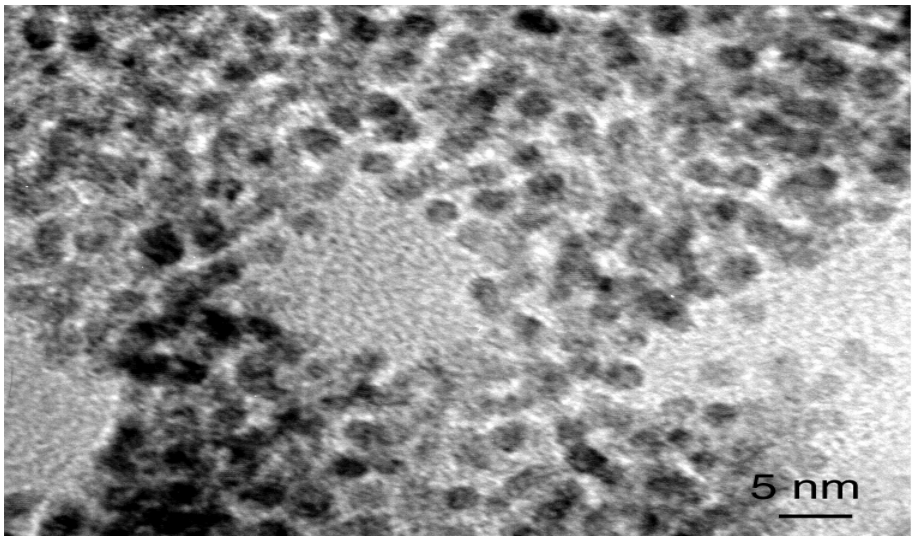

Figure 2-8: HREM micrograph of Ru particles synthesised in pentanol

2.3.4 Stabilisation of Ru nanoparticles by pure heptanol

When the decomposition is realised in pure heptanol the obtained colloidal solution is extremely stable and its colour is very clear brown. Figure 2-9 shows a TEM micrograph of these particles. In contrast to the particles gained in pentanol, these particles are well

dispersed and no agglomerates are observed. Although the size histogram shows a large base, the majority of the particles (69 %) possesses a mean size of 3 nm, showing that the size control of the particles is efficient. The alkyl chain of this alcohol, which contains seven carbon atoms appears to enable a better dispersion of the particles.

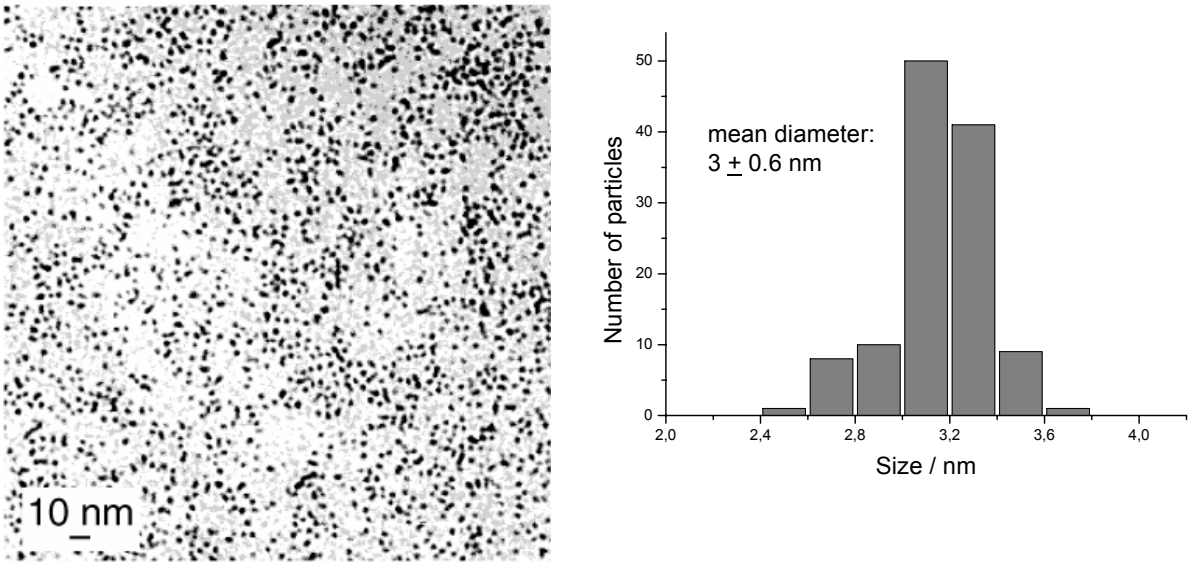

Figure 2-9: TEM micrograph and size histogram of Ru particles synthesised in heptanol

To try to obtain more information concerning the stabilising effect of this alcohol and the surface state of the particles, we considered the study of these particles through the use of solution NMR spectroscopy. A special part is dedicated to the characterisation of ruthenium particles synthesised in pure heptanol using solution NMR investigation which is presented later in chapter 4.

2.3.5 Stabilisation of Ru nanoparticles by pure dodecanol

When pure dodecanol was used as solvent for the decomposition of Ru(COD)(COT), the TEM image of the colloidal solution evidences the agglomeration of fairly small particles with a mean size of 2.5 nm (Figure 2-10). WAXS measurements (Figure 2-11) were performed which confirmed the mean diameter of the particles and the monocrystalline aspect of the particles. The hcp character of bulk ruthenium was confirmed. This brown colloidal solution is stable for over a year and the reception of a black powder was more difficult than for the other systems described before: the precipitation of the particles in cold pentane was very slow.

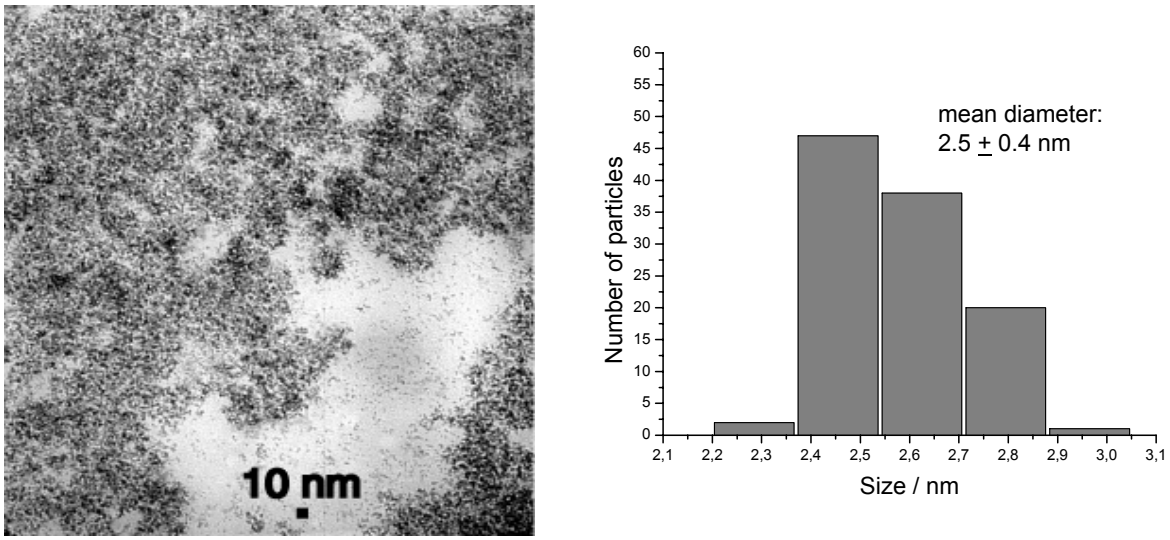

Figure 2-10: TEM micrograph and size histogram of Ru particles synthesised in dodecanol

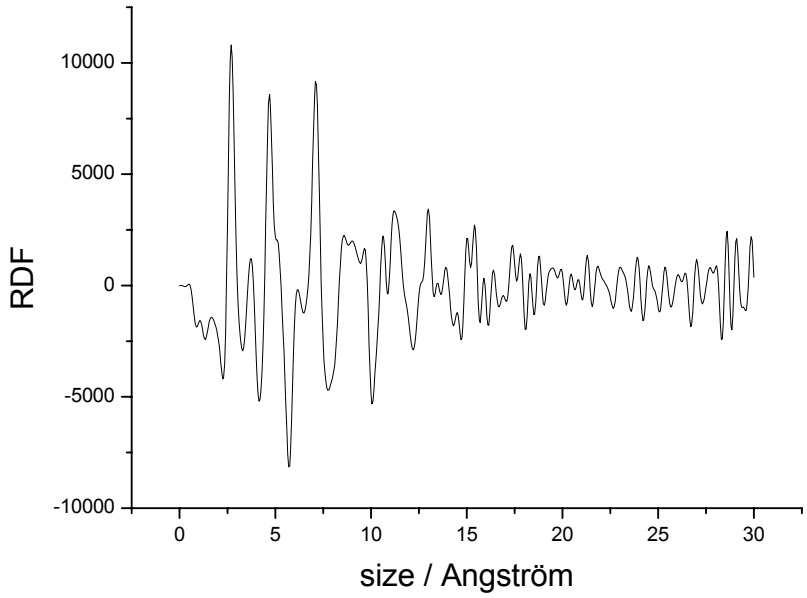

Figure 2-11: WAXS measurements of Ru particles synthesised in dodecanol

2.3.6 Stabilisation of Ru nanoparticles by pure oleylalcohol

In order to test a different alcohol, the decomposition of Ru(COD)(COT) was also realised in pure oleylalcohol. This alcohol possesses a C=C double bond in its alkyl chain containing 18 cabon atoms. In this case, we observed the formation of a light brown solution which was very stable even in the presence of oxygen. Nevertheless, a dispersion of the particles as the one observed for the particles prepared in pure heptanol could not be achieved.

Here, the small particles (~ 2-3 nm) seem assembled in larger agglomerates in the range of 20 nm (Figure 2-12). In addition, precipitation of the particles was not possible. Therefore, further investigation with this solvent was not considered.

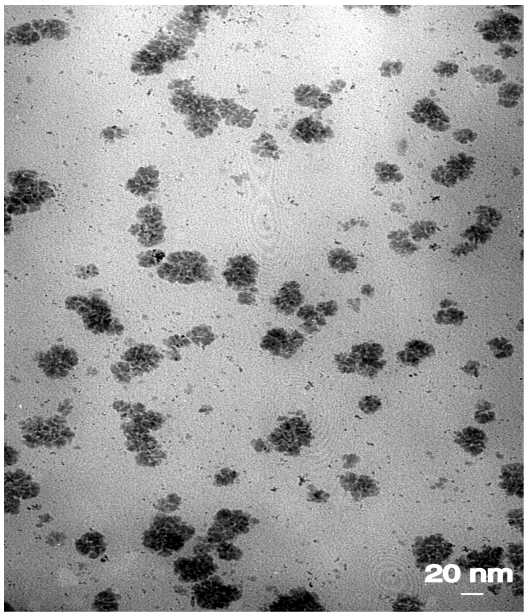

Figure 2-12: TEM micrograph of Ru particles synthesised in oleylalcohol

2.4 Conclusion

The easy and high yield hydrogenation of the organometallic precursor Ru(COD)(COT) in pure alcohols results in the formation of nanoparticles of various sizes. This synthesis of ruthenium particles is perfectly reproducible. Microscopy studies show that the particles display different morphologies according to the alcohol used. The decomposition was performed in solutions of methanol, n-propanol, isopropanol, pentanol, heptanol, dodecanol and oleylalcohol. The characteristics of the particles synthesised in pure alcohols are summarised in Table 2-1. After evaluation of these results, the capability of an alcohol for the stabilisation of ruthenium nanoparticles can be stated. All of the alcohols tested stabilise the particles. The highest stability of the colloidal solution is observed for the particles synthesised in oleylalcohol, which is stable even in air. The particle sizes are found to be similar for all the tested pure alcohols (2 to approx. 5 nm) except for methanol (76 nm) and oleylalcohol (~20 nm).

Table 2-1: Summary of the synthesis of Ru nanoparticles in various pure alcohols

Alcohol	Observations	Size / nm	Morphology	Ru/%	C/%	H/%
methanol CH_3-OH	very dark brown stable for 2 weeks	76	aggregates	68.4	7.7	1.4
n-propanol CH_3-CH_2-CH_2-OH	brown stable for 4 month	4	aggregates	67.0	4.6	1.2
isopropanol $(CH_3)_2$-CH-OH	brown stable for 4 weeks	5.2	aggregates	63.0	4.1	1.0
pentanol CH_3-$(CH_2)_4$-OH	very clear brown stable for several weeks	2-3	monocrystalline	69.4	5.1	2.0
heptanol CH_3-$(CH_2)_6$-OH	clear brown stable for a year	3.1	monocrystalline	70.0	5.2	1.8
dodecanol CH_3-$(CH_2)_{11}$-OH	light brown stable for over a year	2.5	monocrystalline	69.0	8.9	1.9
oleylalcohol $CH_3(CH_2)_7CH{=}CH(CH_2)_8OH$	dark brown stable in air	~2-3	agglomerates	not determined		

Various mean diameters and stability levels, depending on the nature of the alcohol, have been observed. Only two cases revealed disparate results. In the first case, when the decomposition of Ru(COD)(COT) was realised in pure methanol, large particles are formed which are perfectly crystalline and present a porous morphology with irregular contours. Under larger magnification they show a sponge-like aspect and the existence of channels. On account their porous surface, the particles are called “cauliflower”. This could result from the segregation in the solution between cyclooctane, resulting from COD and COT hydrogenation, and the rest of the solvent. In this way, the larger droplets would be formed in the most polar solvent systems and hence the most segregated medium. This fits well with the particle sizes obtained in pure alcohols. The mesoporous, polycrystalline nature of the large particles is surprising. It suggests that during the growth process nanocrystals synthesised at the early stage of the reaction may be linked together by ruthenium atoms or particles

resulting from the decomposition of the remaining starting material. The particles possess a homogeneous size distribution, which shows that the size control is efficient.

In the second case, concerning the synthesis in pure oleylalcohol, which is the most lipophilic alcohol employed in this study, agglomerates of around 20 nm are obtained. Inside these agglomerates small particles of 2.5 nm are observed. In this case, individual small particles are organised in larger structures but not chemically linked to each other.

In all cases, the stable colloidal solutions present a colour which seems related to the size of the particles: from clear brown (pentanol: 2-3 nm, dodecanol: 2.5 nm) to very dark brown (methanol: 76 nm). In addition, the alcohol employed allows a stabilisation of the nanoparticles in solution for several weeks. The stability of the solutions seems to depend on the nature of the stabilising alcohol since it increases with the length of the alkyl chain of the alcohol used for the synthesis, except in the case of n-propanol which gave a very stable colloidal solution. The particles could be isolated by pentane or cyclooctane addition and purified by solvent washing. A drawback of this synthesis method is that none of these colloids could be dissolved again in THF or pure alcohols after isolation as solids.

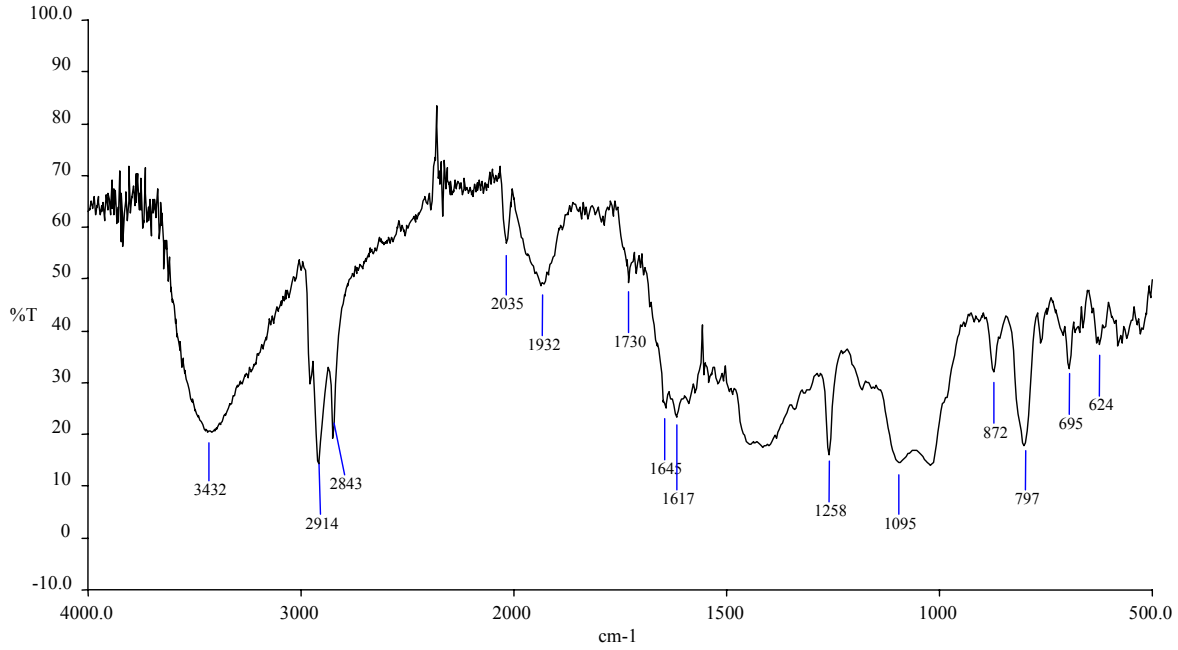

Figure 2-13: IR spectrum of Ru/pentanol particles as an example for Ru/alcohol particles

In each case, the particles are homogeneous in size suggesting that the alcoholic media are efficient in controlling the particles' growth. Since this efficient stabilising effect was unexpected, it seemed necessary to understand this behaviour and therefore to perform IR characterisation and microanalysis. High Ru contents between 63 and 70 % could be observed for all samples. Contents only up to 9 % of carbon and 2 % of hydrogen could be found on the particles. This suggests a relative clean surface of the particles. The presence of the alcohol molecules on the surface of the particles is confirmed by the microanalysis results (see Table 2-1), since carbon is detected. Thinking that the polar heads of the alcohols play an important role in the stabilisation, IR spectra have been registered and the presence of alcohol molecules could be verified by the observation of vibration bands which could be attributed to –OH (3432 cm^{-1}) and $-CH_2$ (2914-2843 cm^{-1}) groups. The band at 1932 cm^{-1}could indicate the presence of Ru-H species. The spectra are similar for all the tested alcohols. Figure 2-13 shows a typical infra red spectrum of ruthenium nanoparticles stabilised with pure alcohols. The comparion with the IR data for the free pentanol confirms the presence of the alcohol molecules at the metal surface (Table 2-2).

Table 2-2: IR data for Ru/pentanol particles

ν pentanol[101] / cm^{-1}	ν Ru/pentanol particles / cm^{-1}	assignment
3335	3432	-OH
2886	2914, 2843	$-CH_n$

Then, the stabilisation is probably achieved by the –OH groups which are attached to the surface. In addition, the length of the alkyl chain of the alcohol stabiliser seems to play an important role since in methanol the particles are large (76 nm), while in the other alcohols the size of the particles is in the range of 2-5 nm. This is probably related to the miscibility of the alcohol with cyclooctane, resulting from hydrogenation of Ru(COD)(COT). From pentanol upwards a good solubility leads to the formation of small monocrystalline particles. This contrasts with the results obtained in methanol, in which the large size of the particles could result from the formation of alkane droplets inside which ruthenium decomposition and particle growth would be achieved. Intermediate situations could then be observed for n- and iso-propanol. The particles prepared in pure alcohols are very air sensitive and burn in the open air. Only a small amount of oxygen leads to precipitation of the particles. The ruthenium zerovalent is sensitive to air and ruthenium oxide is formed quickly in contact with air. It is probably the passivation layer of ruthenium oxide that provokes the precipitation, which is characteristic of a very reactive surface state and most likely of a rather naked surface. This synthesis method therefore appears to be an excellent way for the preparation of reactive metal particles. These novel materials could be applied in catalysis.

Since pure alcohols could be used as stabilisers for the synthesis of ruthenium nanoparticles in contrast to the THF, which leads to the immediate precipitation of the particles, it seemed interesting to study the influence of methanol/THF mixtures on the particles synthesis.

3 Ruthenium particles stabilised by MeOH/THF mixtures

3.1 Introduction

Since the decomposition of Ru(COD)(COT) in pure THF leads to the formation of a precipitate of ruthenium metal, while stable ruthenium particles are obtained in different alcohols, a study of the stabilising effect of alcohols inside a non-stabilising solvent was performed considering the decomposition of this precursor in MeOH/THF mixtures of various compositions.

The reactions were carried out following the standard conditions previously described in chapter 2: room temperature, under pressure of 3 bar H_2 for at least 45 minutes and vigorous stirring. The only varied parameter is the ratio of methanol and THF in the reaction mixture. The volume quantity of methanol was 2.5 %, 5 %, 10 %, 15 %, 25 %, 50 % and 75 % in comparison to the THF.[102]

In all cases the decomposition is fast: the colour solution change from yellow to brown is observed a few minutes after pressurisation under dihydrogen. The solutions then remain unchanged and stable for at least several weeks.

The colloidal solutions have been characterised by transmission electron microscopy (TEM) and X-ray diffraction (XRD) measurements and some of them by wide angle X-ray scattering (WAXS).

3.2 Decomposition in a MeOH/THF 2.5/97.5 mixture (vol. %)

When the decomposition of Ru(COD)(COT) is performed in a MeOH/THF = 2.5/97.5 mixture (vol. %), a light brown and perfectly clear colloidal solution is obtained. TEM analyses indicate the formation of small monocrystalline particles which appear to be included in small agglomerates. The solution is stable for 3-4 months. The TEM micrograph (Figure 3-1) shows small agglomerated particles with a porous structure and an irregular outline.

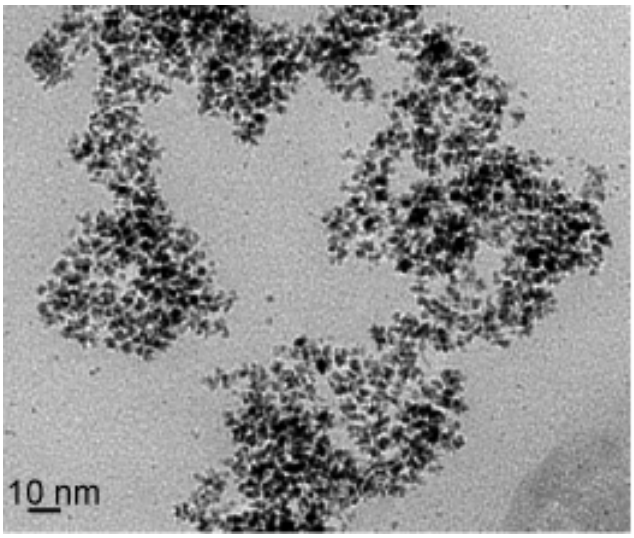

Figure 3-1: TEM micrograph of Ru nanoparticles synthesised in a mixture MeOH/THF 2.5/97.5

In this case a size histogram could not be gained, because the particles are too close inside the agglomerates to precisely distinguish their individual size. Nevertheless, their size can be estimated in the range of 3 to 6 nm. WAXS analysis (Figure 3-2) was performed and the diameter obtained for the particles is in the range of 4 nm. The structure of the ruthenium particles is found to adopt the hcp structure of the bulk metal.

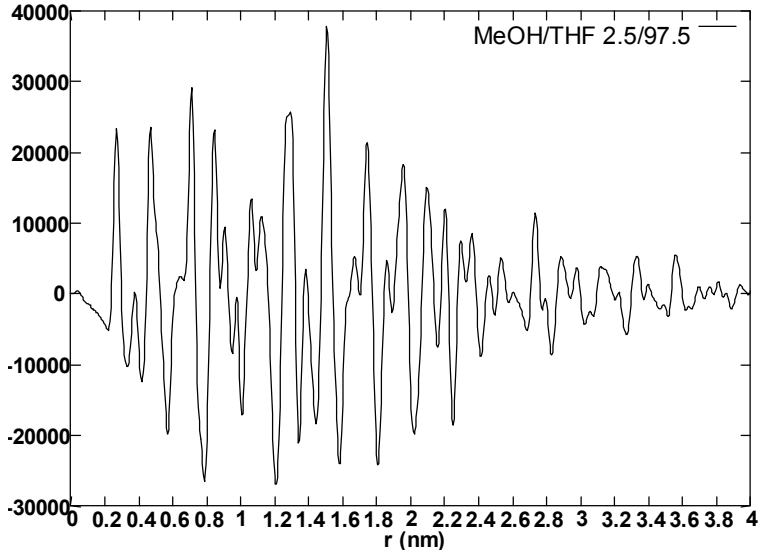

Figure 3-2: WAXS measurements on Ru nanoparticles synthesised in a mixture MeOH/THF 2.5/97.5

3.3 Decomposition in a MeOH/THF 5/95 mixture (vol. %)

When the methanol content of the MeOH/THF mixture is increased to 5 vol. %, a brown and clear colloidal solution is obtained which remains stable for at least 1 year. The particles formed in this case are distinctly larger than the previous ones. Nevertheless, these particles reveal a better separation from each other and the size distribution is symmetrical and narrow: no larger particles have been detected by TEM (Figure 3-3). This confirms an efficient size control of the particles by this method. The particles display a porous, polycrystalline aspect like ruthenium particles previously synthesised in pure methanol (see chapter 2)[67] and seem to also be constituted of aggregated small individual particles. The particles present a sponge-like morphology with a highly porous surface. The size is homogeneous and could be defined to be about 16.7 nm. The nanoparticles seem to have a regular outline and the size histogram presents a symmetric outward appearance, indicating an efficient size control.

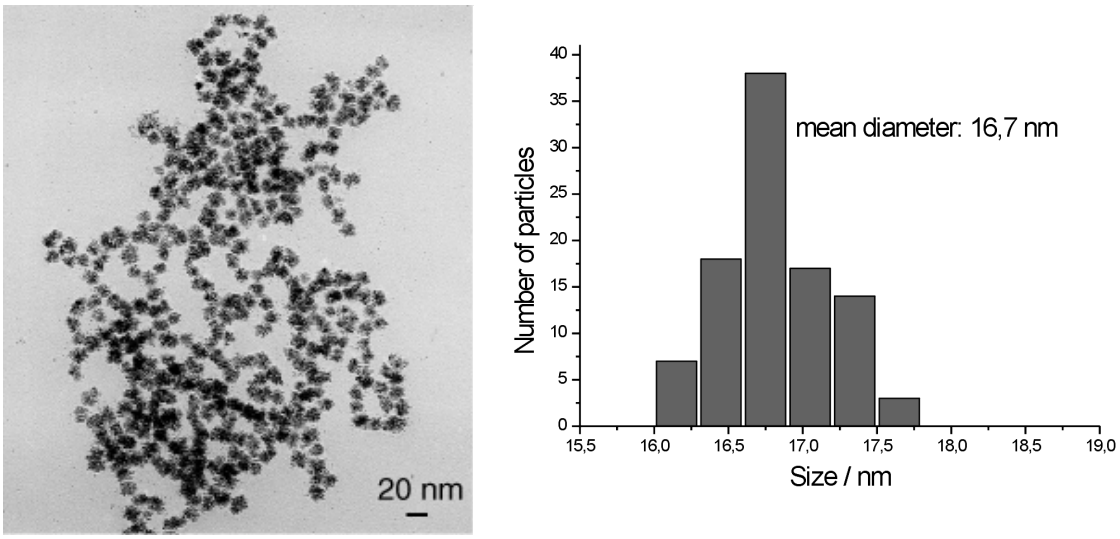

Figure 3-3: TEM micrograph and size histogram of Ru nanoparticles synthesised in a mixture MeOH/THF 5/95

3.4 Decomposition in a MeOH/THF 10/90 mixture (vol. %)

In the presence of 10 vol. % of MeOH, the colloidal solution is dark brown. The solution also remains stable for at least one year under argon. A microscopy grid was prepared immediately after depressurisation of the Fischer-Porter bottle. The mean size of the particles is around 20 nm as observed by TEM (Figure 3-4). The particles are homogeneous in

size, even if the base of the histogram appears broad: 68% of the particles adopt a mean diameter between 19.5 and 20.1 nm. They also display a polycrystalline morphology as can be seen in Figure 3-4. Their porous structure is remarkable and the "cauliflower" shape is very pronounced.

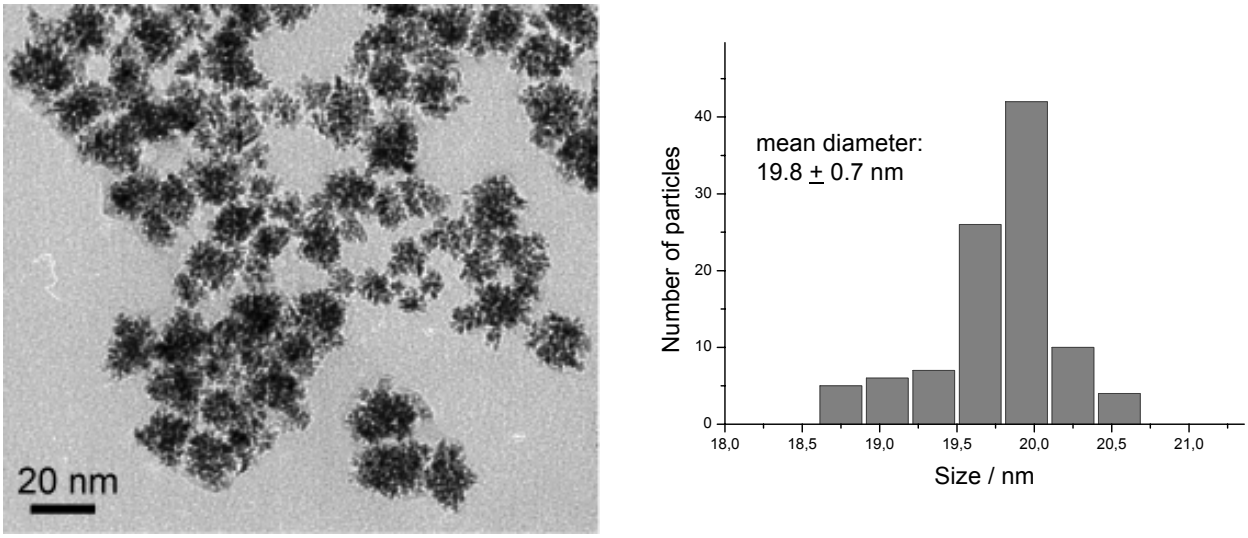

Figure 3-4: TEM micrograph and size histogram of Ru nanoparticles synthesised in a mixture MeOH/THF 10/90

3.5 Decomposition in a MeOH/THF 15/85 mixture (vol. %)

When the methanol content was further increased to 15%, a black–brown solution was obtained, which was perfectly homogenous and stable for at least four weeks under argon. Like the previous ones, they are homogeneous in size and well-dispersed on the TEM grid. Similar polycrystalline particles are formed, but with a slightly larger mean size (23.6 nm). They also display a very porous morphology, but the colloidal solution is less stable (one month). (Figure 3-5). Again, a "cauliflower" structure can be observed and the presence of channels can be stated. The histogram reveals a small size distribution which indicates a successful size control.

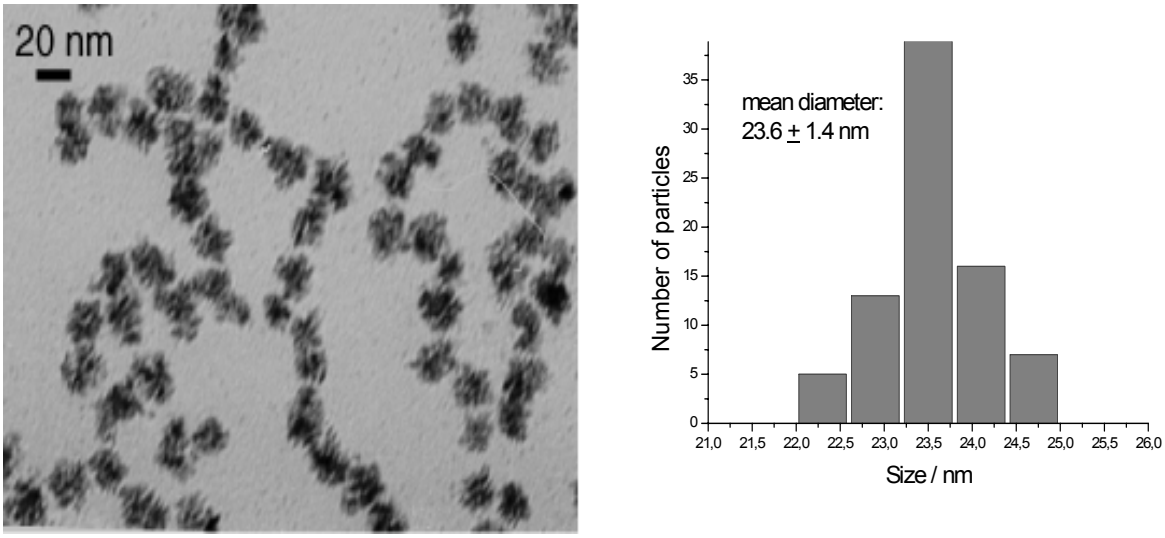

Figure 3-5: TEM micrograph and size histogram of Ru nanoparticles synthesised in a mixture MeOH/THF 15/95

3.6 Decomposition in a MeOH/THF 25/75 mixture (vol. %)

In a methanol/THF 25/75 mixture, the decomposition of the precursor leads to a brown and perfectly homogeneous colloidal solution. The TEM characterisation (Figure 3-6) shows the irregular contours of the particles whose mean diameter is of 33.8 nm. The increase of the methanol content in the reaction mixture drives to an augmentation of the particles size.

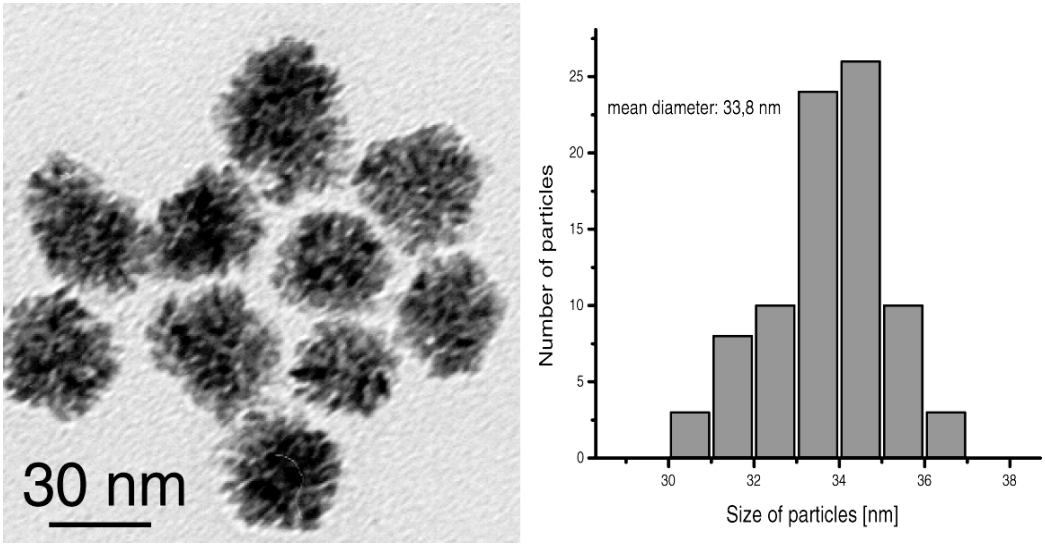

Figure 3-6: TEM micrograph and size histogram of Ru nanoparticles synthesised in a mixture MeOH/THF 25/75

3.7 Decomposition in a MeOH/THF 50/50 mixture (vol. %)

For the reaction mixture of methanol/THF 50/50, the aspect of the particles is again found to be porous. The particles formed in this mixture are stable for several months in the brown solution and their mean diameter is 47 nm (Figure 3-7). The particles are satisfactorily dispersed on the microscopy grid. The amplification in Figure 3-7 b) shows the sponge-like aspect of the particles morphology.

a)

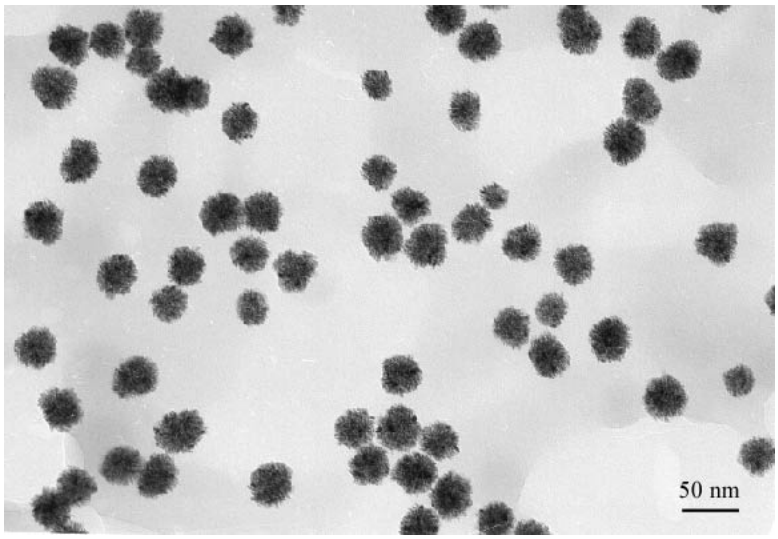

b)

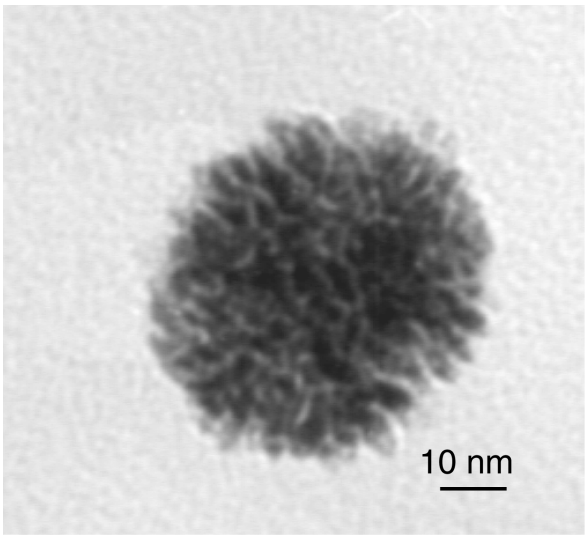

c)

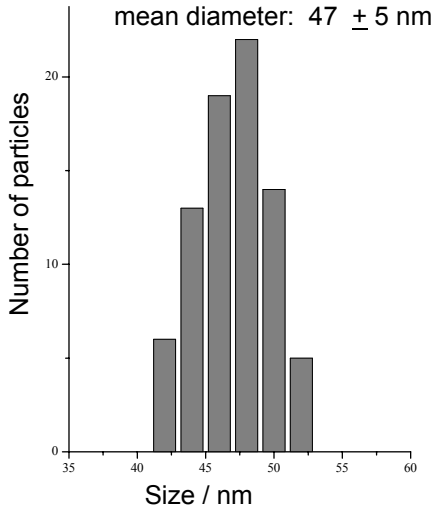

Figure 3-7: a) TEM micrograph, b) magnification of TEM micrograph and c) size histogram of Ru nanoparticles synthesised in a mixture MeOH/THF 50/50

The shape of the particles reveals the presence of small channels. Such nanoobjects could consist of an assembly of numerous small monocrystalline particles (~ 1-2 nm) which would have agglomerated to form bigger ones.[103] Therefore, the methanol content again seems to have an influence on the control of the size, since an increase to 47 nm in this mixture in contrast to 34 nm in the MeOH /THF 25/75 mixture can be observed.

3.8 Decomposition in a MeOH/THF 75/25 mixture (vol. %)

With a further increase of methanol in the reaction mixture to 75 %, a very dark brown colloidal solution was obtained, which was stable for one week. TEM analysis visualised larger particles of about 70 nm, displaying the sponge-like aspect seen before for the particles synthesised in mixtures containing a lower methanol content.

3.9 Decomposition in a MeOH/THF 90/10 mixture (vol. %)

When the content was raised to 90 %, the solution obtained is black, indicating the increased size of the particles. The mean diameter of the particles was about 86 nm (Figure 3-8). Nevertheless, the solution is stable for one week.

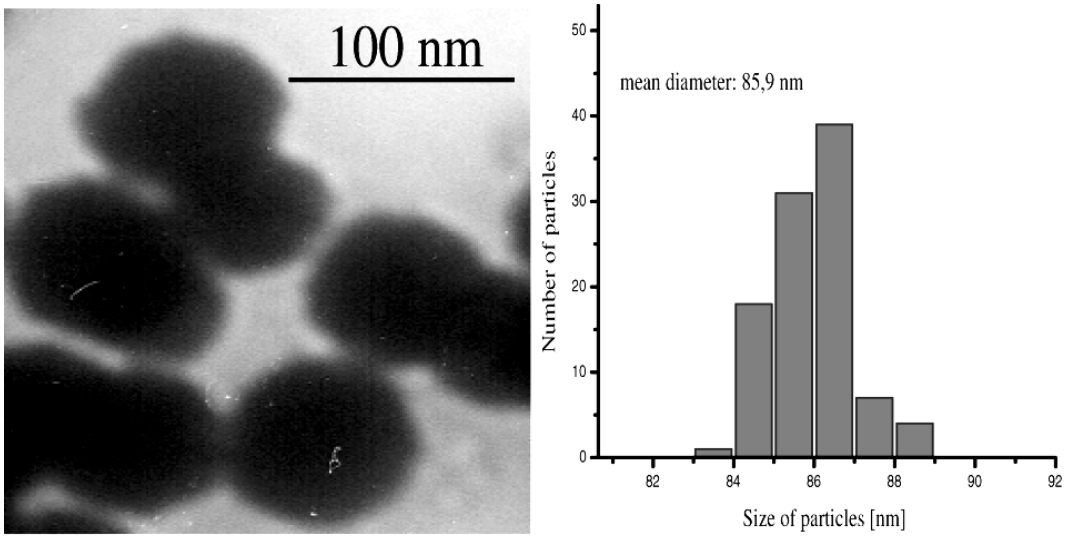

Figure 3-8: TEM micrograph and size histogram of Ru nanoparticles synthesised in a mixture MeOH/THF 90/10

3.10 Discussion and conclusion

Methanol/THF mixtures allow the preparation and stabilisation of well-dispersed ruthenium nanoparticles in the absence of any further stabiliser. The results obtained for the synthesis of ruthenium particles in the different methanol/THF mixtures are summarised in Table 3-1. Different particles sizes are obtained depending on the reaction medium composition.

Table 3-1: Characteristics of the particles as a function of the solvent composition

MeOH/THF volume rate /%	Observations	Ru/%	C/%	H/%	Particles mean size / nm
2.5/97.5	light brown stable for over a year	68.8	7.5	1.4	3-6
5/95	clear brown stable for 4 month	71.0	6.9	1.2	16.7
10/90	clear brown stable for 4 weeks	68.4	7.7	1.4	19.8
15/85	clear brown stable for several weeks	69.4	8.4	2.0	23.6
25/75	very clear brown stable for a year	69.9	7.9	1.6	33.8
50/50	brown stable for 2 weeks	70.3	7.8	1.7	47.0
75/25	very dark brown stable for one week	70.2	8.1	1.5	69.0
90/10	black stable for one week	69.2	8.3	1.3	85.9

From these results, it is clearly apparent that the size of the $[Ru]_0$ nanoparticles depends on the solvent mixture composition used for the precursor decomposition. One trend, the correlation between the methanol concentration and the size of the particles was confirmed by all results obtained for other MeOH/THF compositions from 5/95 to 90/10 volume ratio. The measured size of the particles increases regularly from 3-6 to 85.9 nm with rising methanol volume (Table 3-1). These results strongly suggest that the size of the "unprotected" Ru nanoparticles can be controlled to some extent by changing the preparation

conditions. The correlation between the MeOH/THF ratio and the particles size is linear, as can be seen from Figure 3-9.[102]

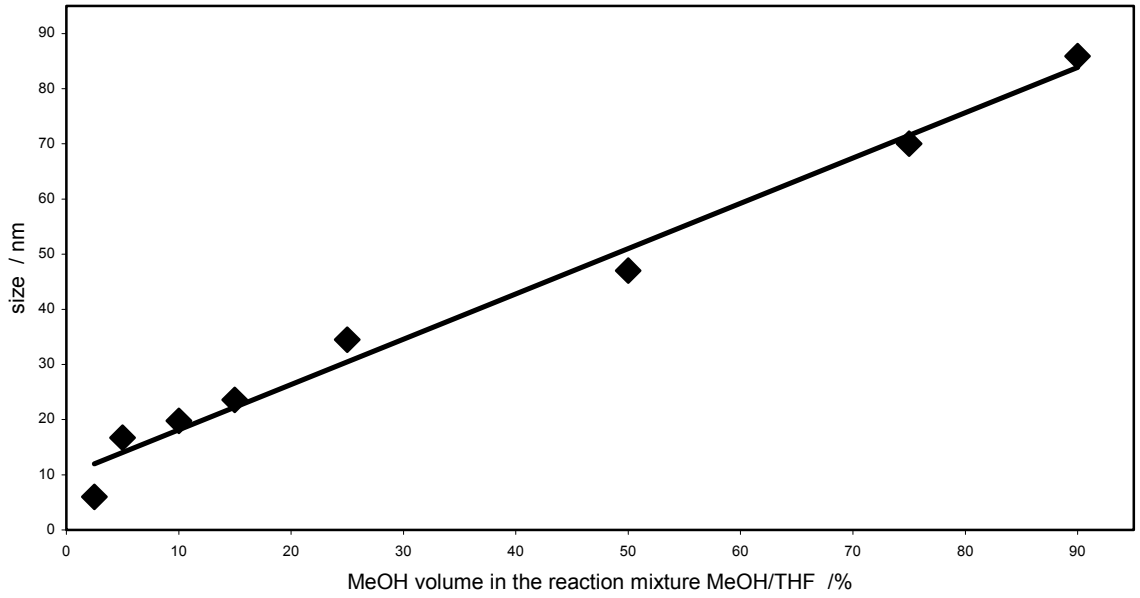

Figure 3-9: Relation between Ru particle size and MeOH/THF ratio in the reaction mixture

This linear correlation between the MeOH content and the size of the particles is surprising and reflects the increase in polarity of the solution upon adding MeOH in THF and perhaps the easier segregation of cyclooctane.

To explain the stabilisation of the ruthenium nanoparticles in the solvent mixtures, the following model (Figure 3-10) is suggested: a nano-emulsion could exist in the reaction medium, formed by nano-drops of cyclooctane which could be considered as "nano-reactors". Since the Ru(COD)(COT) is favourably soluble in cyclooctane, we can hypothesise that its decomposition would take place in these nano-reactors and that the size of the particles would depend on the dimensions of the "nano-reactors". The methyl groups of the methanol molecules would be orientated towards the apolar phase consisting of the cyclooctane while the polar –OH groups would be directed towards the THF.

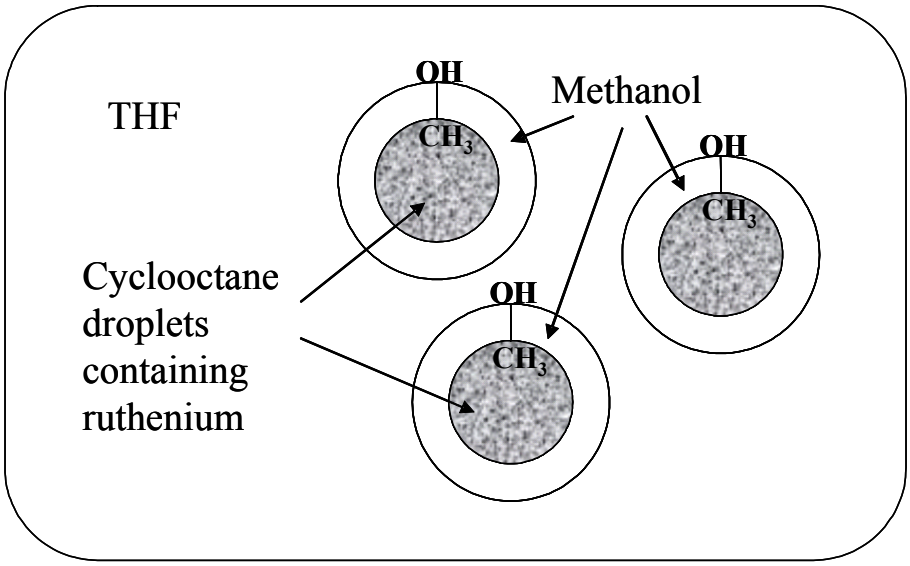

Figure 3-10: Hypothetical nano-reactors for the size control and stabilisation of Ru nanoparticles

Under these conditions, the stabilisation would be assured by an organisation of the solvents in the reaction mixture depending on the affinity between molecules. Several experiments were realised to confirm this hypothesis. When a cyclooctane excess was added to a MeOH/THF 10/90 solution the particle size increased by a factor 1.5 or 2. This is consistent with an increase in size of the droplets or nano-reactors inside which the ruthenium particles may form.[67] The size of the particles can therefore easily be controlled by a proper choice of the solvent mixture. In these MeOH/THF mixtures, the change in polarity of the medium resulting from the composition changes may account for the apparent correlation observed between the size of the particles and the MeOH content. In highly polar mixtures, the large size of particles may result from large droplets of cyclooctane. The linearity of the correlation is surprising but may be a good argument for the segregation hypothesis. This is also consistent with the observations carried out at various temperatures, solvent segregation increasing when the temperature decreases. The methanol is indispensable for the stabilisation since a stabilisation in pure THF is not possible, although the exact mechanism of the particles growth needs to be investigated further. Also, the size is directly dependent on the methanol content in the mixture. Only with a low volume ratio of methanol can very small particles can be obtained.

The colloidal solutions obtained in these reaction conditions are very stable and can be kept under argon from a few weeks to several months without precipitation (and even 1 year for some of them: 5/95 and 10/90 mixtures), the least stable solutions being those prepared in MeOH-rich solutions which also contain the largest particles. During the experiments, it was

noticed that the colour of the colloidal solutions becomes progressively darker with the increase of the methanol content in the reaction mixture and their stability decreases to a few weeks. The change of colour observed for this series of experiments at different temperatures appears to be a good indication of the size of the particles. When the colloidal solution is black or dark-grey, the particles are large while they are smaller when the colour is brown. In addition, the particles are better separated from each other when the methanol volume in the reaction mixture is increased. They are well-dispersed and homogeneous in size. Their high air sensitivity (they burn in the presence of oxygen) confirms their clean surface state since they are stabilised only by weakly coordinated alcohol and THF molecules.

As shown by TEM micrographs, the Ru particles display highly porous, sponge-like structures of regular spherical shape. In the MeOH rich mixtures, this sponge-like aspect is more pronounced than in the MeOH poor media. BET measurements have been performed on two samples resulting from the decomposition of Ru(COD)(COT) in 5/95 and 10/90 MeOH/THF mixtures. A 40 $m^2 \cdot g^{-1}$ specific area has been obtained for the two products but different pore sizes and shapes were determined. Cylindrical pores with a size in the range 60-180 Å have been found for the particles synthesised in the 5/95 MeOH/THF mixture while the 10/90 Ru particles display "ink bottle" shape pores with a mean size of 40Å. These results confirm the porous character of these materials.

In conclusion of this study, it can be said that methanol/THF mixtures allow for the preparation and stabilisation of well dispersed ruthenium nanoparticles in the absence of any further stabiliser giving then particles of adjustable size with a “clean” surface which is demonstrated by the reaction with air leading in some cases to a combustion of the particles. The main advantage of this method is that the size of the particles can be controlled by adjustment of the reaction mixture composition, since a linear correlation was observed. The results are surprising and rather difficult to explain in a non-ambiguous manner. What we do know is that the methanol is indispensable for the stabilisation since a stabilisation in pure THF was impossible, but the exact mechanism of the particles growth needs to be further investigated. The best hypothesis seems to be the segregation of the reaction medium. Another advantage of the synthesis mode is that the formed particles appear as porous and reactive materials. This high reactivity is probably due to the absence of strong stabilisers as the methanol in not usually referenced as a strong one.

These ruthenium nanoparticles can then be considered as quasi-naked particles and are expected to display high activity in catalytic application.

A special part hereafter describes the stabilisation of Ru nanoparticles by pure heptanol since a good dispersion of the crystalline particles was observed.

4 Stabilisation of ruthenium particles by pure heptanol

4.1 Introduction

There is a growing need for characterizing and understanding the surface state of the particles which may have a strong influence on their chemical and physical properties. It has been shown for example that surface ligands could strongly influence the magnetic properties of cobalt[68] and nickel[104] particles. Many studies are therefore devoted to the precise synthesis in solution of nanoparticles of defined size and shape using long chain ligands in organic solution, very few of them focus on the precise characterisation of the metal surface-ligand interactions. Infrared spectroscopy using CO as a probe molecule has been successfully used for surface characterisation: for palladium[105,106] and platinum[107] nanoparticles. In contrast, there are only a few reports available in the literature which concern the NMR characterisation of surface ligands.[43,108,109,110]

In the previous chapters, we have described the synthesis of ruthenium nanoparticles which are efficiently stabilised in the presence of an alcohol and without any further stabilising agent like organic molecules (amines, thiols,…)[102] Mono- or polycrystalline sponge-like particles are formed in these conditions, depending on the nature of the alcohol, in particular the length of its alkyl chain. In addition, these particles appear to be very reactive which indicates the probability of a quasi-naked surface. However, chemical and Infrared analysis attest to the presence of alcohol molecules on their surface. For this reason we considered to carry out NMR studies on one of these materials to try to obtain more information about the surface state of the ruthenium nanoparticles. For these studies, ruthenium particles, synthesised in pure heptanol, were chosen. Its alkyl chain is long enough to use it as a sort of probe, in particular the methyl group, which is probably far enough from the metal surface to be influenced by the metal core too extensively. A free tumbling of the methyl group in the solvent is possible.

The stabilisation of the colloids was achieved in pure heptanol and the characterisation of the surface of the particles was addressed by NMR spectroscopy in solution and infrared analysis. NMR spectroscopy could help in characterising the surface chemistry of ruthenium nanoparticles stabilised by pure heptanol and assist in understanding the crystalline morphology of these particles and IR confirms the presence of the ligand at the metal surface.

4.2 Synthesis of Ru / heptanol particles

Ruthenium nanoparticles were then prepared by decomposition of the organometallic precursor Ru(COD)(COT) (COD = 1,5-cyclooctadiene, COT = 1,3,5-cyclooctatriene) following the conditions previously described: under an H_2 atmosphere (3 bar), at room temperature and in pure heptanol as solvent for 45 minutes and in the absence of any additional stabilisers. This produces a brown colloidal solution which is stable for months when kept in the absence of air. The nanoparticles formed in the reaction may be isolated upon evaporation of the solution to dryness or concentration of the solution and precipitation from pentane yielding a black powder in both cases.

TEM analysis of the colloidal solution after deposition onto a carbon covered copper grid (Figure 4-1) shows the presence of well-dispersed particles of homogeneous size. The nanoparticles display a regular spherical shape and a monocrystalline composition with a plane surface. The histogram of Figure 4-1 evidences a mean size of 3 nm and a very narrow size distribution for the particles.

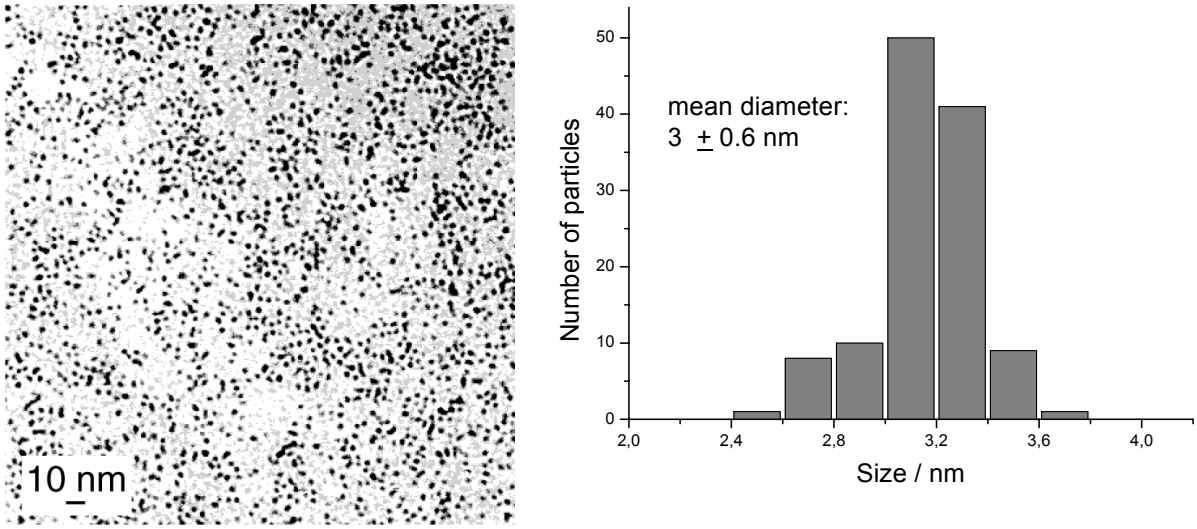

Figure 4-1: TEM micrograph and size histogram of Ru nanoparticles synthesised in pure heptanol

A HREM study demonstrates the crystalline character of the particles. This study was especially done by high resolution CRYO-transmission electron microscopy. The colloidal solution was deposited on a special copper grid with a carbon layer and plunged into liquid nitrogen. The sample was frozen at once and a thin frozen film was obtained for the CRYO-

TEM studies. By this means the original dispersion of the particles in solution is conserved and can be observed under the microscope. The high resolution TEM image (Figure 4-2) clearly shows well-separated mono crystalline particles. The atomic plans can be observed.

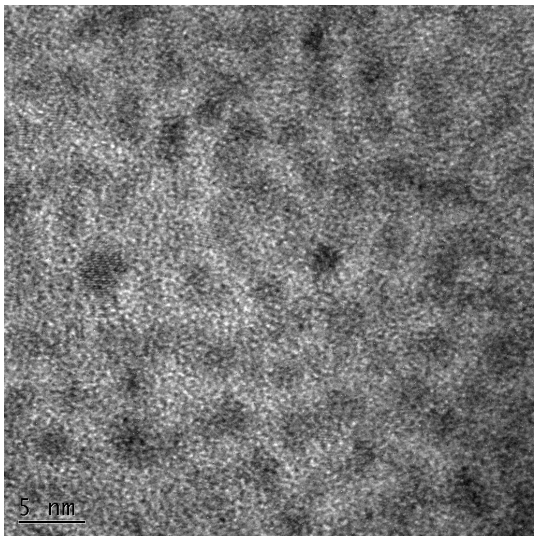

Figure 4-2: CRYO-HREM micrograph of Ru nanoparticles synthesised in pure heptanol

The estimated size and the crystalline character of the particles is confirmed by WAXS experiments (Figure 4-3). The particles display the hexagonal close packed structure of bulk ruthenium with a first metal-metal distance of approx. 0.270 nm, close to that of bulk ruthenium (Ru-Ru distance: 0.267 nm). In addition, the coherence length of the particles is found near 3 nm, in agreement with the size resulting from TEM images analysis. Overall, these data evidence the formation in the reaction conditions of crystalline nanoparticles of homogeneous size.

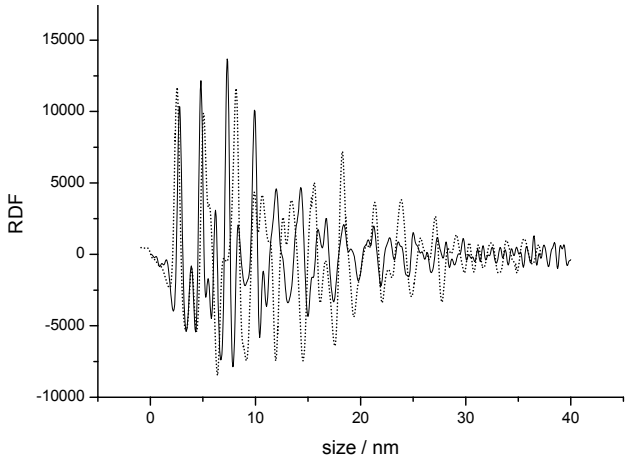

Figure 4-3: WAXS analysis of Ru nanoparticles synthesised in pure heptanol (plein line) and simulated RDF for bulk Ru in hcp structure (dotted line)

The data obtained from microanalysis realised on the black powder after purification indicate the presence of approx. 70 % Ru in the sample. Since the particles have a mean size of 3 nm as defined by TEM analysis and a compact structure confirmed by WAXS measurements, the associated "magic" number is 923 atoms, of which 362 atoms are located on the surface. The ratio is approx. 1 heptanol : 7.5 Ru. This means that approximately 123 heptanol molecules are associated to the ruthenium surface, which may not all be directly coordinated to the ruthenium surface. This approximate calculation only provides an estimation of the quantity of ligands present in the vicinity of the particles.

4.3 Solution NMR studies on Ru / heptanol particles

In order to obtain details on the stabilisation and the surface chemistry of the ruthenium particles stabilised by heptanol molecules on the surface, the use of NMR spectroscopy in d^8-THF solution was considered: both ^{1}H and ^{13}C NMR experiments on Ru / heptanol colloids were carried out.

4.3.1 Solution ^{13}C NMR studies on Ru / heptanol particles

For comparison with the experimental spectra, a ^{13}C NMR spectrum for pure heptanol was calculated (Figure 4-4).

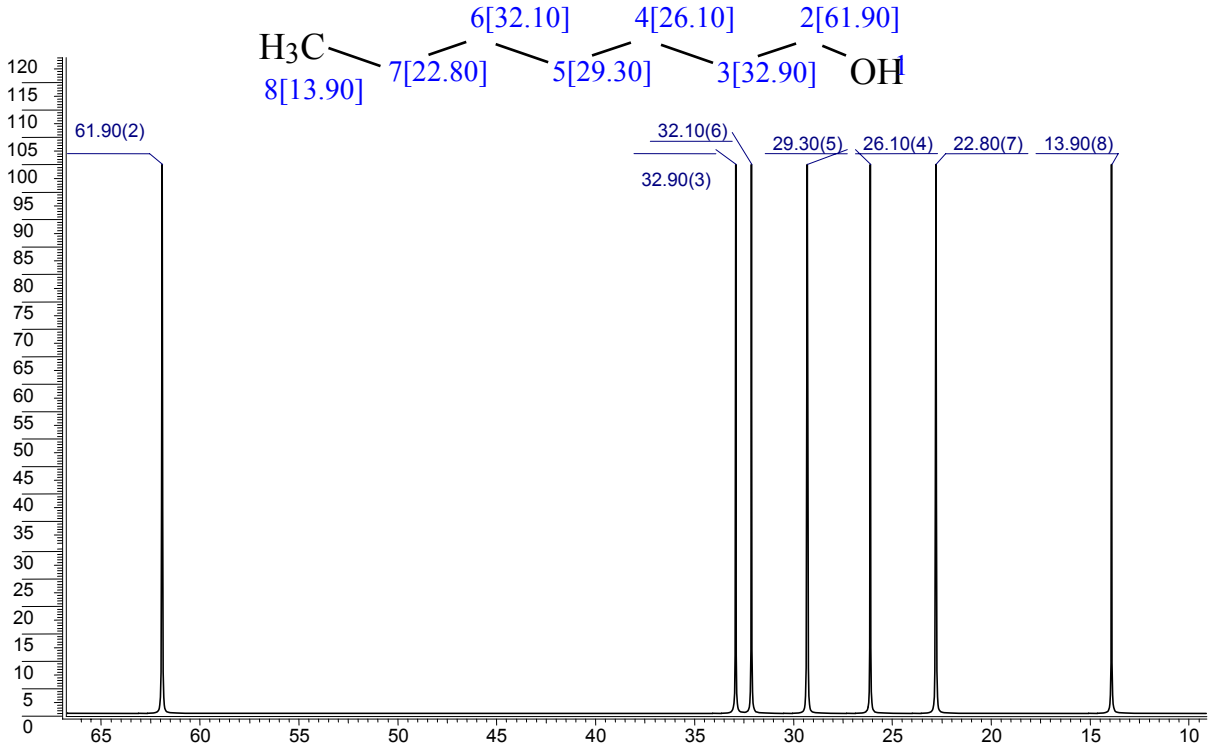

Figure 4-4: Simulated ^{13}C NMR spectrum for heptanol ($C_7H_{15}OH$)

The ^{13}C NMR spectrum (Figure 4-5) obtained for the purified colloid shows peaks which can be attributed to the different carbons of the heptanol. The spectrum obtained in the presence of a slight excess of heptanol due to purification difficulties shows the signals of the corresponding seven carbons of heptanol with a half-height width larger for the α and β carbons (respectively 7 and 5 Hz at 62.1 ppm (α-C) and 33.7 ppm (β-C)) than for the other signals (approx. 2.5-3 Hz). This result can be interpreted as resulting from a fast exchange between free and coordinated heptanol.

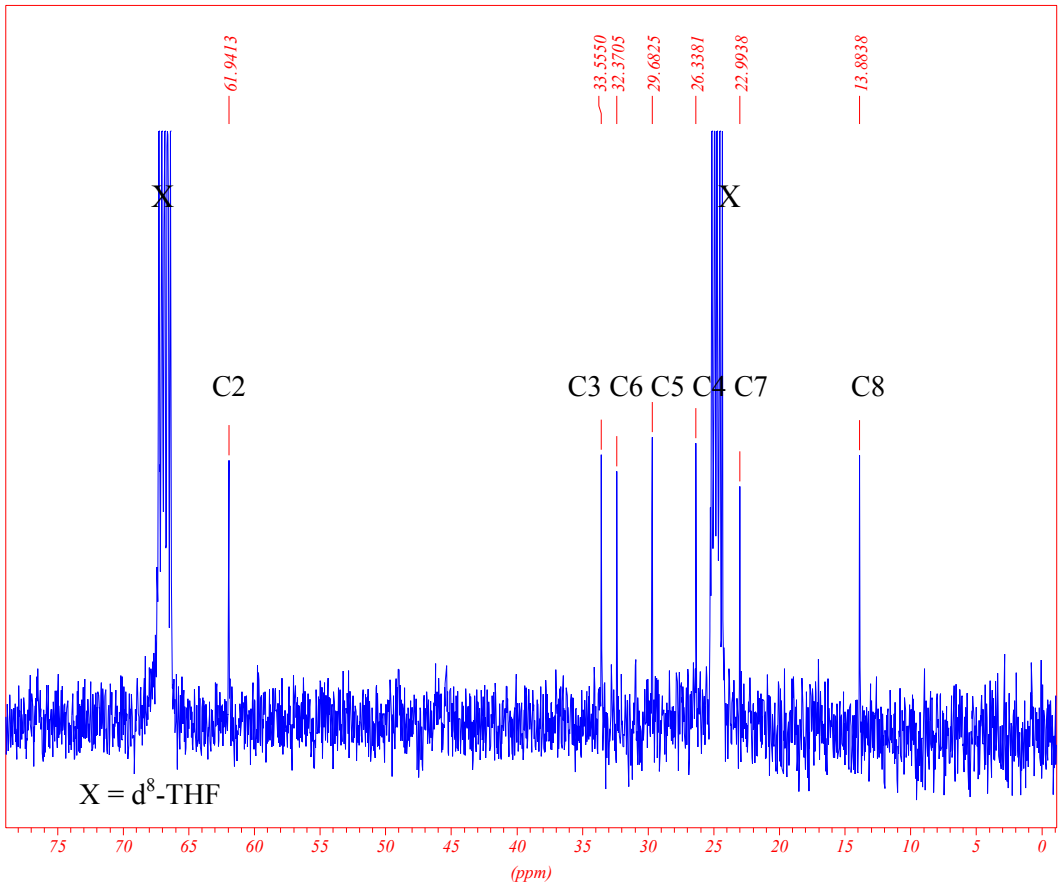

Figure 4-5: ^{13}C NMR spectrum (d^8-THF, 100.71 MHz) of purified Ru/heptanol particles with a small excess of free heptanol

When the particles are synthesised in pure heptanol, some free heptanol seem to stick in the sample due to purification problems since no precipitation was possible (see Table 4-1).

Table 4-1: Simulated and experimental ^{13}C NMR data for pure heptanol and Ru/heptanol colloids

Carbon	n C	Simulated shift heptanol / ppm	Experimental shift Ru / $C_7H_{15}OH$ / ppm
8	3	13.9	13.9
7	2	22.8	22.9
6	2	32.1	32.4
5	2	29.3	29.7
4 (γ)	2	26.1	26.3
3 (β)	2	32.9	33.6
2 (α)	2	61.9	61.9

4.3.2 Solution ^{1}H NMR studies on Ru / heptanol particles

A ^{1}H NMR spectrum of pure heptanol (Figure 4-6) was simulated for comparison with the experimental spectra. This allows the attribution of the peaks in the registered spectra. In the case of the simulated spectrum, no difference could be made between the OH-group and the α-carbon, while in the experimental spectrum these siganls are split up.

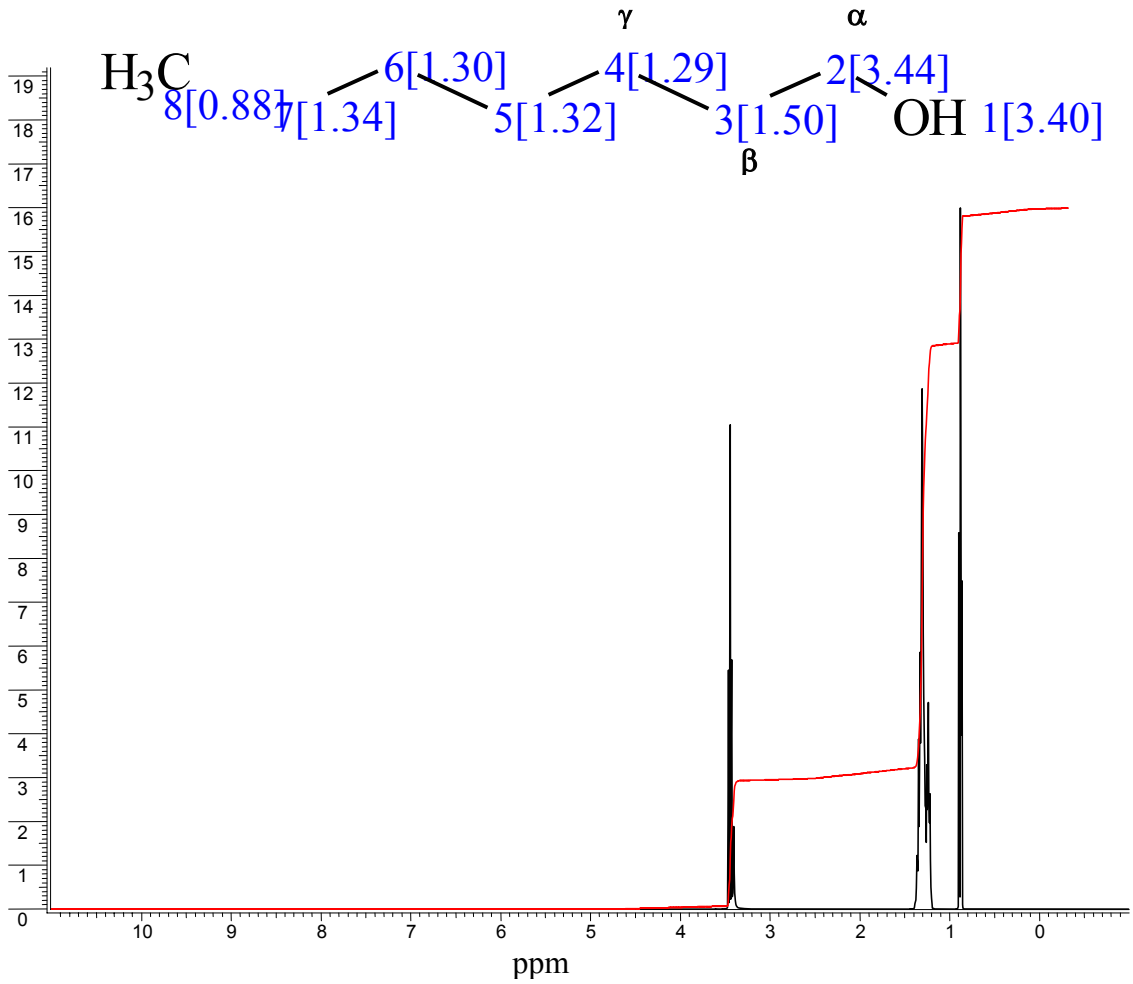

Figure 4-6: ^{1}H NMR spectrum simulated for pure heptanol ($C_7H_{15}OH$)

The ^{1}H NMR spectrum of a colloid purified by precipitation after pentane addition and drying in vacuum (Figure 4-7 c) was recorded in d^8-THF. It shows broad peaks at 0.93 and 1.34 ppm which can be attributed to coordinated heptanol after comparison with the spectrum of pure heptanol. The peak at 0.93 ppm is ascribed to the methyl group and the peak at 1.34 ppm to the methylene groups 7, 6 and 5 of the alkyl chain of the heptanol. This large signal at 1.34 ppm could cover the signal corresponding to the γ– protons normally expected near 1.29 ppm. No signal is visible for the β– protons located around 1.50 ppm. It should be noted that

the protons located on the carbon in α– position to oxygen and the proton of the OH-group are not visible (see Table 4-2). Only very small peaks can be seen whose intensity is not significant. In addition, another signal is observed at 2.5 ppm corresponding respectively to water. Of note is the presence of a sharp peak at 4.8 ppm attributed to the presence of dihydrogen in solution which will be discussed later. Some smaller peaks can be observed which are probably due to impurities present in the sample.

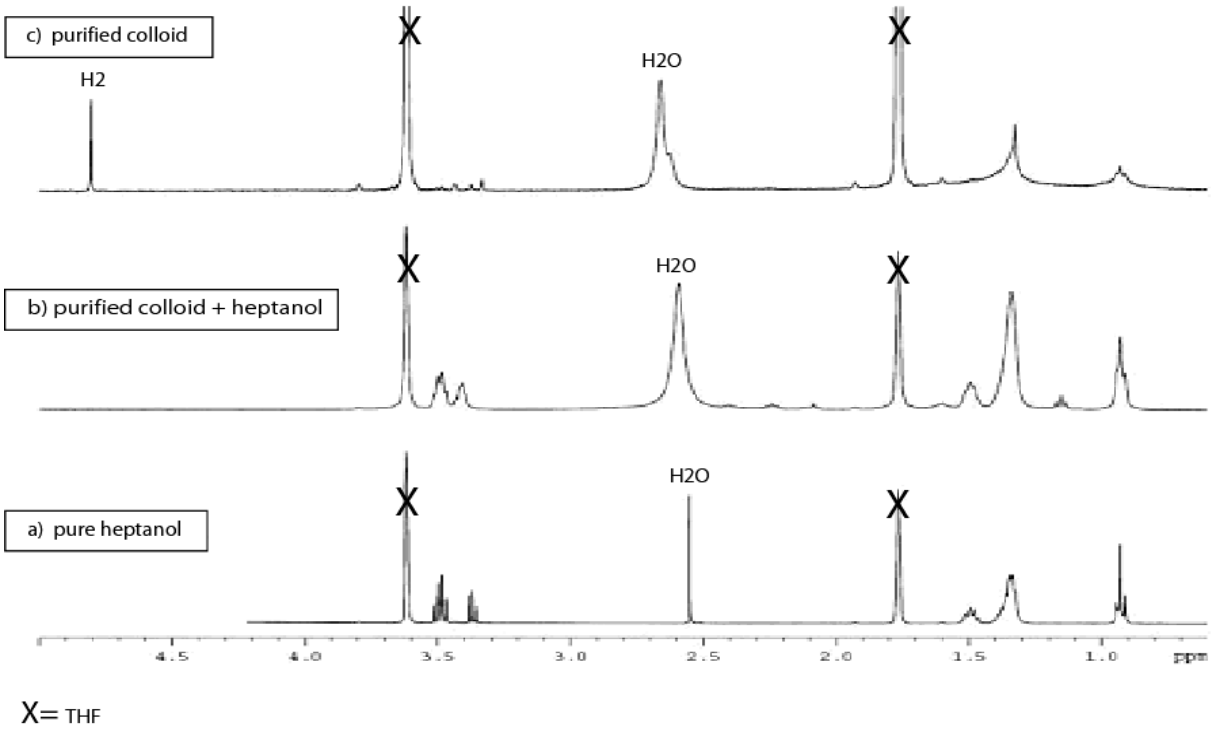

Figure 4-7: ^{1}H NMR spectrum (d^{8}-THF; 400MHz) a) heptanol as reference b) purified Ru/heptanol colloid with an additional amount of free heptanol and c) purified Ru/heptanol colloid

Table 4-2: Simulated and experimental ^{1}H NMR data for pure heptanol and purified Ru/heptanol colloid

Proton	n H	Simulated shift heptanol / ppm	Experimental shift Ru / $C_7H_{15}OH$ / ppm	After addtion of heptanol
8	3	0.88	0.93	0.93
7	2	1.34	1.49	1.49
6	2	1.30	1.34	1.34
5	2	1.32	1.34	1.34
4 (γ)	2	1.29	-	1.3
3 (β)	2	1.50	-	1.5
2 (α)	2	3.44	-	3.4
1	1	3.40	-	3.5

Since the protons in β position (1.5 ppm) could not be observed and those located on the γ carbon are very broad and not distinguishable from the other CH_2-groups of the alkyl chain a small amount (1 μL) of pure heptanol was added to the NMR tube. Upon that addition, the appearance of broad peaks previously not visible is observed: respectively signals at 1.5 ppm for the protons in β position, 3.5 ppm for the protons in α position and at 3.4 ppm for the proton located at the OH-group. A small shift can be noticed in comparison with the simulated spectrum which is probably due to the proximity to the metal particles.

When a ^{13}C NMR spectrum of this purified sample was registered, no peaks could be observed which is probably due to the lower sensivity.

A very interesting phenomenon became apparent when recording the ^{1}H NMR spectra of different Ru / heptanol colloids. Each time a peak at 4.8 ppm was observed shortly after dissolution of the sample in the NMR solvent which disappeared with time. After that, a series of experiments in a closed tube showed that this peak is not present immediately after dissolution, but that it grows rapidly within one hour and then remains constant, except when opening the NMR tube and while storing over night. In addition, it can be restored by bubbling dihydrogen in the NMR tube (Figure 4-8). This peak was attributed to dihydrogen desorbing from the particles. This observation suggests that surface hydrides are present on the surface of the colloid but disappear as a result of several factors, likely ones being

competition with THF for surface co-ordination and, possibly, the presence of water in the NMR solvent.

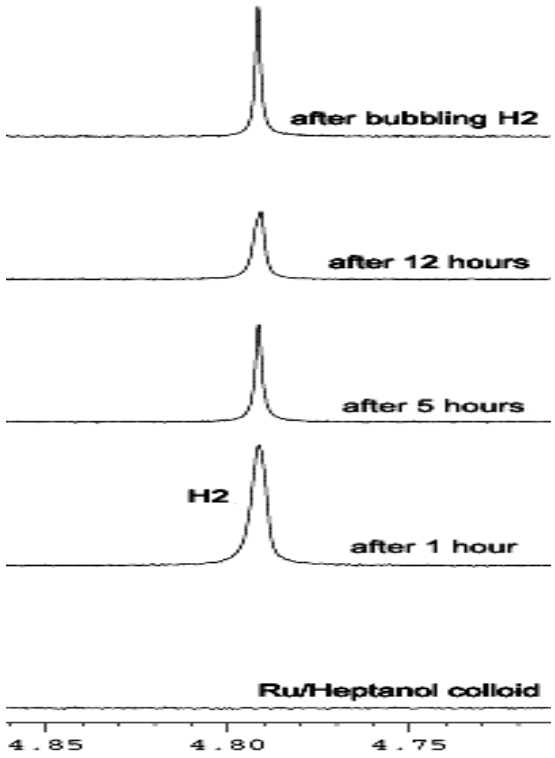

Figure 4-8: Comparsion of the ^{1}H NMR spectrum (d^{8}-THF; 400MHz) of Ru/heptanol colloid presented in Figure 4-7 showing the evolutiont of the dihydrogen peak at 4.8 ppm with the time

4.4 Infrared experiments

As another characterisation technique, we considered infrared spectroscopy and registered a spectrum of the Ru / heptanol colloid just after purification (Figure 4-9 a). In this spectrum, the presence of the ligand molecules on the colloid surface could be confirmed. Bands corresponding to the OH-group at 3408 cm^{-1} and to the CH_2-groups at 2917 cm^{-1} are seen. Additionally, a large band is observed at 1927 cm^{-1} which could be assigned to the presence of Ru-H species. This band is unsymmetrical and displays shoulders. The IR technique can be used to detect terminal hydrogen adsorbed on a transition metal surface. Adsorbed hydrogen atoms give peaks in the 1900-1960 cm^{-1} region.[111] The vibration bands observed in the spectrum can be assigned to twin or dihydrogen-like type which are terminally bonded on the metal crystal.[112,113]

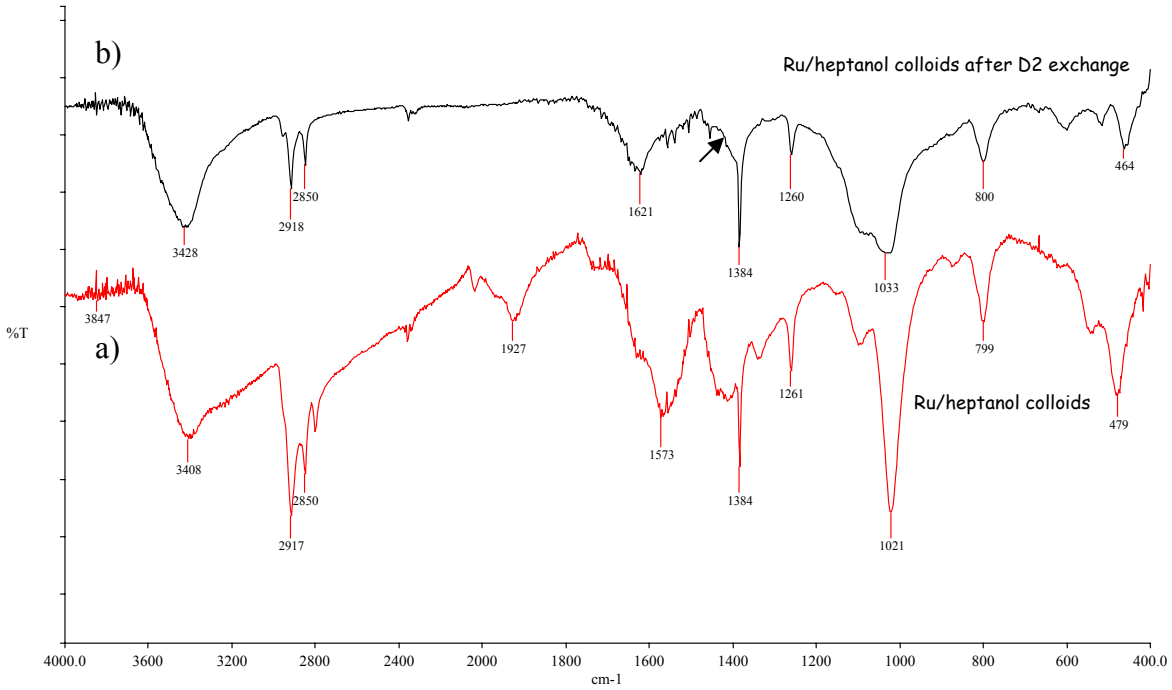

Figure 4-9: Infrared spectrum of Ru/heptanol particles

Table 4-3: IR data for Ru/heptanol particles in comparison with pure heptanol

ν heptanol[101] / cm^{-1}	ν Ru/heptanol particles / cm^{-1}	Assignment
3335	3408	-OH
2892	2917, 2850	$-CH_n$
-	1927	Ru-H

The band at 1927 cm^{-1} could correspond to a pure Ru-H mode since the possibility to find a Ru-H_2 mode is very low. When a deuterium exchange on the sample is accomplished, the band at 1927 cm^{-1} can not be observed any longer (Figure 4-9 b). For this the purified powder of the Ru / heptanol colloids is put under pressure of 3 bar of deuterium for 72 hours. If the deuteration was complete, the Ru-D modes should appear between 1380 and 1400 cm^{-1}.[114] A broad peak become visible around 1400 cm^{-1} but it may be hidden by other strong absorptions. This would underline the hypothesis of the presence of Ru-H species since a deuterium exchange would cause a shift of a Ru-D signal towards smaller wavelengths.

4.5 Conclusion

In conclusion, the decomposition of the Ru(COD)(COT) precursor in pure heptanol leads to the formation of nanocrystalline and well-dispersed nanometre-size ruthenium particles of 3 nm in a reproducible way. The heptyl chain allows the medium to be homogeneous and therefore the particles remain well separated. The different analysis are in agreement with the presence of heptanol molecules at the surface of the metal particles. In addition, the ^{13}C and ^{1}H NMR studies evidence the weak co-ordination of heptanol on the surface of the particles and the presence of a fast exchange between free and coordinated ligands. This strongly suggests the concomitant presence of both attached ligands at the surface of nanoparticles and free ligands in the reaction mixture. But the most interesting observation which has been obtained by both NMR and IR investigations is the existence of hydrides at the surface of the colloids. This does not come from a dehydrogenation of the heptanol since the reaction stops rapidly and that no heptaldehyde could be detected. It is hence probably due to dihydrogen desorption resulting from the formation of surface hydrides in the synthesis conditions.

This evidence is very interesting because of the relevance of Ru catalyst in the Fischer-Tropsch synthesis, ammonia synthesis[115] and hydrogenation of aromatics such as benzene.

5 Organic ligand-stabilised ruthenium nanoparticles

Nanoparticles can be coordinated by ligands to prevent reactions between each other and in order to stabilise them in solution. When the particles are protected by a ligand shell they can be handled as stable compounds. However, the utilisation of ligands coordinated at the surface of the particles has been considerably developed in the last years.[69,70,109,116] A new class of metal colloids has emerged resulting from their stabilisation by ligand molecules containing phosphorus, sulphur, nitrogen,… Organic ligands like pyridine,[37] triphenylphosphine (PPh_3),[36] trioctylphosphine oxide (TOPO),[117,118] long chain thiols[119,120] and amines[40,42,121] are already known to act as stabilisers for platinum,[36,90] indium[231] and nickel[104] nanoparticles. The most common tools used for stabilizing nanoparticles have so far been polymers.These ligands suggest strong interactions with the metal surface. This stabilisation mode presents several advantages such as the high solubility of the colloids, their behaviour as molecular systems, control of the size, size distribution and adjustment of the surface state. When self-assembly is achieved by ligand stabilisation, the particles can be used in selected chemical or physical applications. The chemical environment due to the presence of the ligands can influence the chemical and physical properties of the particles, since considerable consequences can arise from the interaction of the ligand shell with the metal surface, their electronic behaviour being then heavily influenced. It is well-known that the physical and the chemical properties of nanoparticles depend on the surface of the particles and the organisation of the particles into a nanomaterial and their dispensability. These factors will depend on the successful control, including reproducibility, of the synthetic process and the stability of the particles. The ligand shell favours the solubility of the particles in organic solutions. The interaction of the ligand shell with the metal surface can undergo several consequences due to: the particle size and their dispersion, the structure of the particles, the shape and the surface of the particles can all be affected by a ligand. A regular growth of the initial germs in the reaction mixture is essential to arrive at a regular consistency of the particles size in solution. The condition of the ligand on the surface of the particles has to be studied by different techniques to give an idea of the energetics and of the dynamics of the ligands co-ordination.

Gold is the most studied metal in this focus.[122,123,124,125,126,127] For example, G. Schmid[69] stabilised gold colloids with phosphines applying the reduction of $HAuCl_4$ with citrate. The synthesised colloids are well dispersed and show a regular size of 20 nm. HREM

studies proved the presence of the organic ligands forming a layer at the surface. The variation of the size of gold particles in the presence of a ligand was achieved by Klabunde et al.[128] who added dodecylamine at low temperature to a solution of gold colloids obtained by vaporisation of metallic gold. The size of the so-obtained particles depends on the quantity of the added amine, the colloids size decreases from the initial size of 7 nm to 2-5 nm and they become crystalline. M. Brust et al. obtained particles stabilised with dodecanethiol by using tetraoctylammoniumbromide as a phase transfer agent to facilitate the transfer of the precursor $AuCl_4^-$ from the water phase to the organic phase. The reduction agent (sodium borohydrate) and the dodecanethiol are added to this organic phase where the reduction takes place. The mean size of the particles is between 2 and 2.5 nm. The results of microanalysis show that 1/3 of the surface atoms are linked to the thiol. Recently G. Thomas[129] extended these observations by NMR studies and evidenced a strong interaction between the functional group of the ligand and the gold surface. Only a few studies have addressed the problem of the co-ordination mode of the ligand on the particles using techniques of molecular chemistry such as ^1H and ^{13}C NMR.[41,43,110] Nuclear magnetic resonance is a powerful method to investigate ligand behaviour on the particles surfaces in solution or in the solid state. It can provide information about the ligand-metal bond. Numerous ^{195}Pt experiments on small platinum particles have been carried out to date, as it is best suited for these experiments because it exhibits one of the largest Knight Shifts.[130] These analytical techniques are expected to demonstrate the presence of the ligand on the surface of the particles but could also give an idea of the energetics and of the dynamics of the ligands co-ordination.

In B. Chaudret's group the stabilisation of platinum with carbon monoxide, triphenylphosphine and octanethiol has been studied.[36,90] The particles have been prepared by the decomposition of the organometallic precursor $Pt_2(dba)_3$ dissolved in either toluene or THF under pressure of 1 bar CO at room temperature. The structure of the obtained particles is cfc and their size varies between 1 and 2 nm depending on the chosen solvent. When a ligand like PPh_3 or octanethiol is added a strong interaction with the particles surface can be detected although their size does not change as monitored by HREM and WAXS analysis.

In the previous chapters, the reproducible synthesis of stable ruthenium nanoparticles in pure alcohols or methanol/THF mixtures has been reported. More particularly in the case of heptanol, the co-ordination of the alcohol at the surface of the particles could be observed by

IR and solution NMR investigation. But, since alcohols are not refered as good organic stabilisers, the use of thiols and amine as ligands has been decided.

In this chapter the preparation of ligand protected ruthenium nanoparticles from organometallic derivatives will be described. The decomposition of Ru(COD)(COT) was accomplished in the presence of long chain alkyl thiols and amines as stabilisers to obtain ruthenium nanoparticles. These long alkylchain ligands offer the possibility to study the surface state of the particles when being considered as probe molecules. The study was extended to the use of chiral amino alcohols and oxazoline ligands as stabilisers for the ruthenium particles with the objective to test these new materials in asymmetric catalysis.

The study of the influence of the ligands on the size and the shape of the nanoparticles has been studied and their characterisation both by techniques of material characterisation methods like electron microscopy (TEM and HREM), wide-angle X-ray scattering (WAXS) and powder X-ray diffraction (XRD) and by techniques of the molecular chemistry methods as infra red measurements (IR) and solution nuclear magnetic resonance (NMR) studies will be described.

5.1 Thiols as a ligand for ruthenium nanoparticles

5.1.1 Synthesis of thiol stabilised ruthenium nanoparticles

To obtain thiol stabilised ruthenium particles, the organometallic precursor Ru(COD)(COT)[96] was decomposed in the presence of 0.2, 0.5 and 1 mole eq of an alkyl thiol. 1-octanethiol ($C_8H_{17}SH$), 1-dodecanethiol ($C_{12}H_{25}SH$) and 1-hexadecanethiol ($C_{16}H_{33}SH$). A solution of the complex was added to varying amounts of selected alkyl thiols in THF at 193 K. The resulting solution was then pressurized with 3 bar of dihydrogen at 193 K and allowed to react for 24 hours while the temperature was slowly raised up to room temperature (Scheme 5-1). The absence of residual amounts of Ru(COD)(COT) was confirmed by column chromatography. A brown solution formed, from which a black powder could be obtained following depressurization, concentration of the solution and addition of pentane. This brown material can be washed with pentane, dried in vacuum and dissolved soluble in THF. These reaction conditions were followed for all the thiols tested.

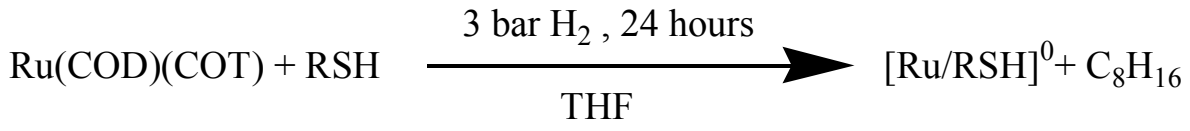

$R=C_8H_{17},C_{12}H_{25},C_{16}H_{33}$

Scheme 5-1: Decomposition of Ru(COD)(COT) in the presence of an alkyl thiol as stabilising agent

5.1.1.1 1-octanethiol as stabilizing agent for Ru particles

When a small amount of ligand (e.g. 0.1 eq) / 1 eq precursor was used, the particles could not be stabilised in solution: large agglomerates (100 nm) precipitated shortly after pressurisation with 3 bar of dihydrogen. Therefore the quantity of used ligand was enhanced to 0.2 eq.

In the case where 0.2 eq 1-octanethiol ($C_8H_{17}SH$) compared to the precursor were used, a fine powder of particles could be obtained. TEM analysis (Figure 5-1) of the colloidal solution evidenced the presence of small crystalline particles of spherical aspect which are found to be strongly agglomerated. The particles size is estimated to be of about 2.3 nm.

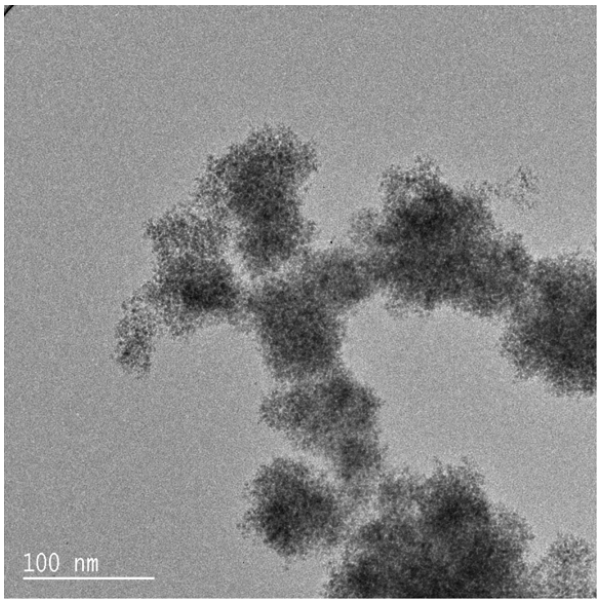

Figure 5-1: Transmission electron micrograph (TEM) of ruthenium nanoparticles synthesised in the presence of 0.2 eq 1-octanethiol ($C_8H_{17}SH$)

WAXS analysis performed on this colloid after isolation revealed that the particles are crystalline and adopt the hcp structure of bulk ruthenium with the same small deviation in the

cell dimensions of the hcp network was also observed as well for Ru particles stabilised with PVP as stabilising agent.[90] The WAXS experimental data were compared with simulated ones using a 100 atoms model adopting the hcp structure. This simulation suggests a relaxation of the lattice parameters of the hcp structure: a = 2.66 Å and b = 4.36 Å compared to a = 2.7058 Å and b = 4.2811 Å in bulk ruthenium. The metal-metal distance was found equal to that found in bulk ruthenium: 2.670 Å

The estimated size of the particles obtained by WAXS analysis is 2.3 nm which is in a very good accordance with the size calculated by TEM analysis.

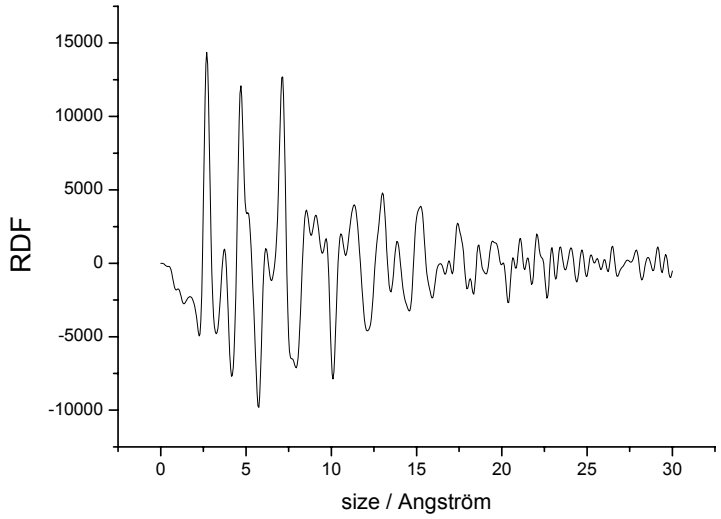

Figure 5-2: WAXS analysis of ruthenium nanoparticles synthesised in the presence of 0.2 eq of 1-octanethiol

In the presence of a higher amount of 1-octanethiol (0.5 eq) compared to Ru(COD)(COT) the precipitate obtained was very sticky and these colloids could not be isolated as powders. The TEM micrographs could not reveal exactly the structure of the particles, therefore HREM analysis have been performed. By HREM analysis (Figure 5-3) spherical agglomerates containing larger particles were witnessed for the particles stabilised with 0.5 eq of 1-octanethiol. The mean diameter of the small particles was estimated of about 2.5 nm although the agglomeration of the particles makes an approximation of their size difficult. WAXS analysis of a colloidal solution in THF performed on these colloids again evidences the hcp structure of the bulk ruthenium as was the case for the particles prepared in the presence of a smaller amount of 1-octanethiol (0.2 eq). The particles are agglomerated in spherical structures consisting of smaller particles.

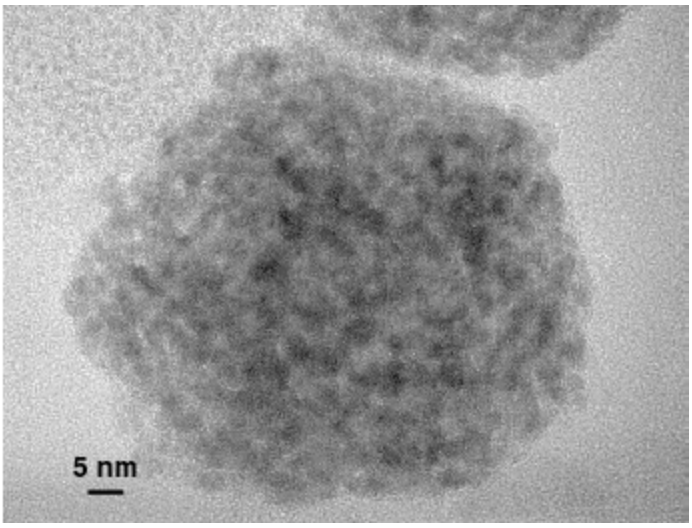

Figure 5-3: High resolution electron micrograph (HREM) of ruthenium particles stabilised in the presence of 0.5 eq of 1-octanethiol

When the quantity of added 1-octanethiol is increased to 1 eq, the size of the particles does not seem to increase significantly. The size of the particles remained near 2.5–3 nm.

Table 5-1: Summary of results obtained after colloid synthesis in presence of 1-octanethiol as stabilising agent

1-octanethiol / eq	mean size of Ru particles / nm
0.1	agglomerated
0.2	2.3
0.5	2.5
1	2.5-3

5.1.1.2 1-dodecanethiol as stabilizing agent for Ru particles

In order to study the influence of the length of the alkyl chain, the stabilisation of the particles has been carried out with different concentrations of 1-dodecanethiol ($C_{12}H_{25}SH$).

For the application of 1-dodecanethiol as a ligand on the particles the following 1-dodecanethiol ($C_{12}H_{25}SH$) / Ru(COD)(COT) ratios were used: 0.2 eq, 0.5 eq and 1 eq in comparison to the introduced ruthenium metal. A stabilisation of the particles in solution with lower amounts than 0.2 eq of this ligand could not be achieved. TEM analysis and WAXS measurements were carried out on all samples prepared in the presence of 1-dodecanethiol.

When 0.2 eq. of 1-dodecanethiol was used, spherical agglomerates containing 2.3 nm particles were observed (Figure 5-4). The observed agglomerates consist of smaller particles which seem to be crystalline since atomic plans can be noticed in the HREM micrograph.

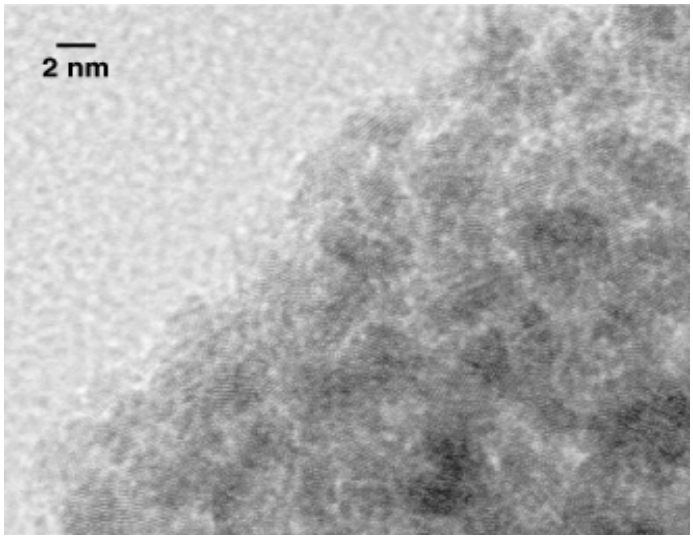

Figure 5-4: High resolution electron micrograph (HREM) of Ru particles stabilised with 0.2 eq 1-dodecanethiol

The decomposition in the presence of 0.5 and 1 eq of 1-dodecanethiol compared to the ruthenium also results in strongly agglomerated particles. The mean size for 0.5 eq added ligand is approx. 1.8 nm, while for 1 eq of 1-dodecanethiol the diameter is approx. 1 nm. The particles were found crystalline and to adopt the hcp structure of bulk ruthenium with small deviations in the cell dimensions of the hcp network.

Table 5-2: Summary of results obtained after colloid synthesis in the presence of 1-dodecanethiol as stabilising agent

1-dodecanethiol / eq	mean size of Ru particles / nm
0.1	agglomerated
0.2	2.3
0.5	1.8
1	1

All particles prepared in the presence of 1-dodecanethiol were found to be strongly coalesced and incorporated into spherical agglomerates as was the case for particles prepared in the presence of 1-octanethiol. In each case the hcp crystal structure was evidenced by WAXS experiments and when the colloids are stabilised using the highest quantity of 1-dodecanethiol (1 eq) a drop of the coherence length of the particles from 2.3 to 1 nm is observed. This observation is in contrast with the results obtained for the particles stabilised with 1-octanethiol which could be explained by the different length of the alkyl chain.

5.1.1.3 1-hexadecanethiol as stabilizing agent for Ru particles

In the presence of 0.2 eq of 1-hexadecanethiol ($C_{16}H_{33}SH$), in marked contrast to the shorter alkyl chain thiols, no agglomeration was observed, but individual particles of spherical aspect are formed as evidenced in the TEM image (Figure 5-5). This different result is probably caused by the influence of the stabilising agent's longer chain length. The particles mean size is approx. 2 nm. Nevertheless, the size distribution obtained form the TEM micrograph is large (between 1.6 and 2.4 nm) which is probably due to the difficulties while measuring the particles because of their irregular shape.

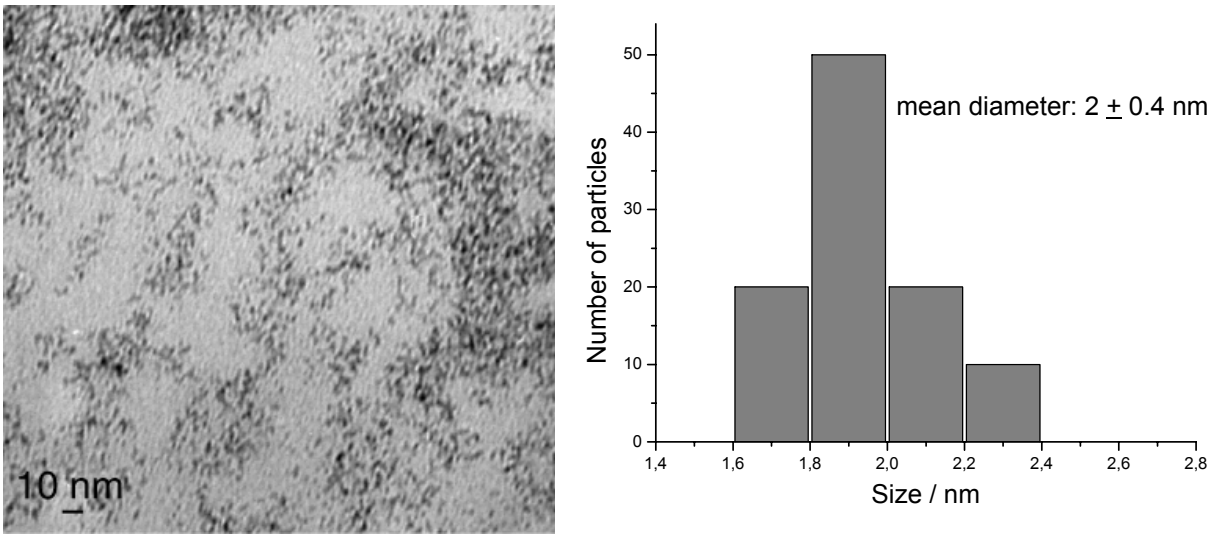

Figure 5-5: Transmission electron micrograph (TEM) and the corresponding size histogram of ruthenium nanoparticles synthesised in the presence of 0.2 eq of 1-hexadecanethiol

When the particles are stabilised with a higher amount of 1-hexadecanethiol (0.5 and 1 eq), their dispersion on the grid does not change considerably. For the addition of 0.5 eq, a mean diameter of 2 nm is observed. In contrast to the 1-octanethiol used before, but in agreement with the 1-dodecanethiol, a net decrease for the mean size is noticed for the use of 1 eq of 1-hexadecanethiol (Figure 5-6). Indeed, the particles prepared with 1 eq of ligand have a mean size of about 1 nm. But, they tend to be very sticky after evaporation of the solvent and are difficult to purify as the addition of pentane could not undergo the formation of a precipitate.

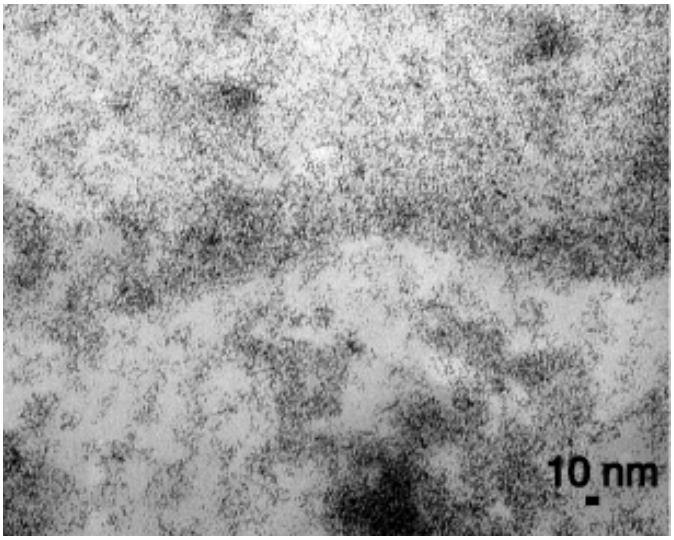

Figure 5-6: Transmission electron micrograph (TEM) of nanoparticles synthesised in the presence of 1 eq 1-hexadecanethiol ($C_{16}H_{33}SH$)

Table 5-3: Results obtained for the synthesis of ruthenium nanoparticles in the presence of 1-hexadecanethiol ($C_{16}H_{33}SH$) as stabilising agent

1-hexadecanethiol / eq	mean size of Ru particles / nm
< 0.2	not determined
0.2	2
0.5	2
1	1

The WAXS measurements performed on these three samples (Figure 5-7) evidence the crystalline character of the particles and underscore the relationship between the increase in particle size and the variation in ligand concentration. Their hcp structure was confirmed when the particles were compared with a simulation for a 100-atom model for the bulk ruthenium and the metal-metal distance was found to be equal to that in bulk ruthenium (2.670 Å). These data also confirm the effect of the ligand on the size of the particles depending on its concentration. The higher the thiol quantity in the reaction medium, the smaller are the particles.

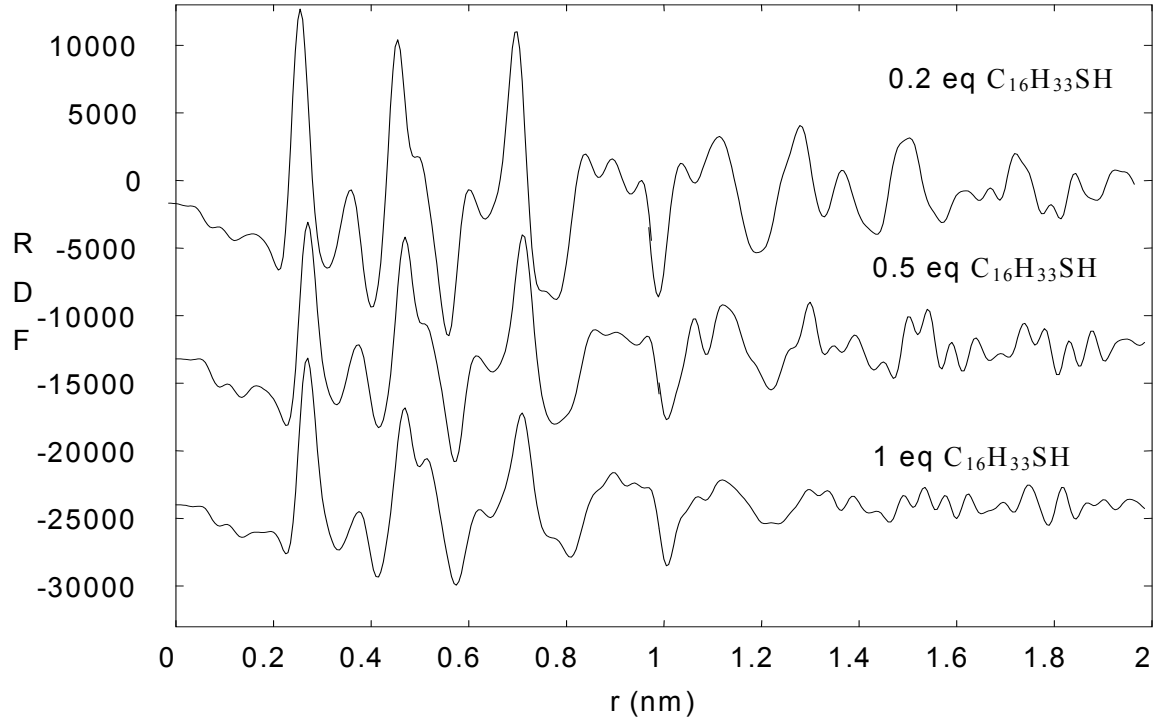

Figure 5-7: WAXS measurements on nanoparticles synthesised in the presence of 0.2, 0.5 and 1 eq 1-hexadecanethiol ($C_{16}H_{33}SH$)

From these results, it can be said that the ruthenium particles can be stabilised by a ligand shell consisting of thiol ligands with alkyl chains of varying lengths. A different effect has been observed depending on the quantity of added ligand and also on its alkyl chain length. The particles obtained in the presence of 1-octane- and 1-dodecanethiol have undergone the formation of agglomerates at a very low concentration of ligand (0.1eq). They have different mean diameters depending on the used quantity of the added ligand. Particles of a mean size around 2-2.5 nm were formed at higher concentrations (0.2, 0.5 and 1eq) of 1-octanethiol while the 1-dodecanethiol allowed the formation of smaller particles when its concentration is increased. This effect on the size of the particles that means the decrease of the size when the ligand concentration increases has also been observed with 1-hexadecanethiol. In all cases, the particles are crystalline and adopt the hcp structure of the bulk Ru.

In order to better understand the influence of the thiol ligands on the stabilisation of the particles, a solution NMR study has been undertaken with 1-octanethiol- and 1-hexanethiol-stabilised ruthenium particles.

5.1.2 Solution NMR studies on thiol-stabilised ruthenium particles

Previously, an approach of characterisation of ligand stabilised particles had been realised with Pt/1-octanethiol colloids.[90] In this case, the ^{13}C NMR spectrum of the colloid showed the peaks which could be attributed by comparison with the free octanethiol to the methylgroup (C 8) of the thiol chain, to the methylene (C 7), to two overlapping methylene groups, namely C 4 and C 5, and to the methylene group C 6. The α, β and γ carbons (C1, C2 and C 3) are not seen, probably as a result of shielding by the platinum particle. A similar effect has been observed by Reven et al. in alkanethiol-capped gold colloids.[108] In these cases, the resonances of the three α, β and γ carbons could not be located. It is possible to observe both a broad signal assigned to the coordinated 1-octanethiol and a minor sharp one attributed to the free ligand. These resonances do not exchange which suggests that there is not exchange between the free and the coordinated 1-octanethiol. It was not possible to determine whether the thiol molecules are coordinated.

For this work, NMR experiments were carried out concerning ruthenium nanoparticles stabilised by 1-octanethiol.

5.1.2.1 Ru/1-octanethiol particles: Solution NMR studies

To provide a better comparison and to verify the experimental data, the ^{1}H NMR data of 1-octanethiol ($C_8H_{17}SH$) were calculated for the free ligand as shown in Table 5-4 and in Figure 5-8.

Table 5-4: Calculated ^{1}H NMR data of 1-octanethiol

Number	9 (-CH_3)	8	7	6	5	4 (γ)	3 (β)	2 (α)	1
Number H	3	2	2	2	2	2	2	2	1
Chem. shift / ppm	0.88	1.34	1.29	1.25	1.25	1.33	1.52	2.44	1.28

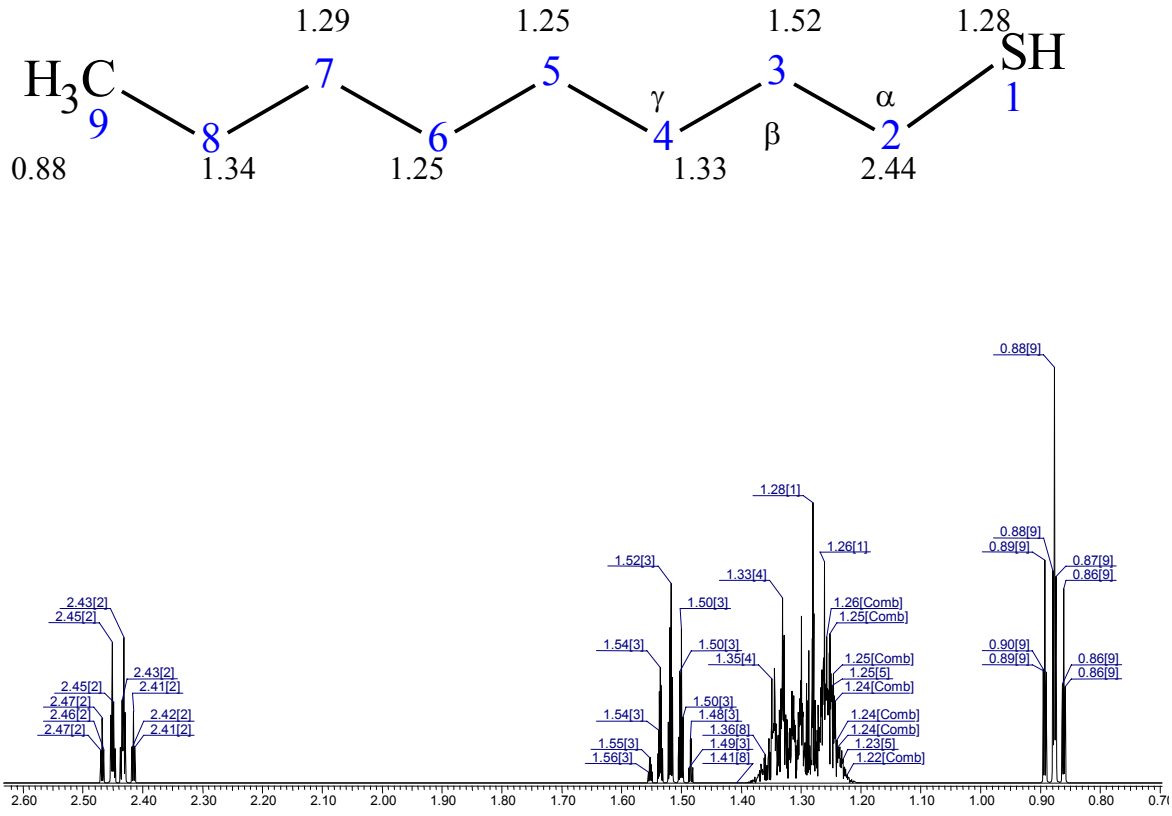

Figure 5-8: Simulated ^{1}H NMR spectrum of 1-octanethiol

The NMR study was carried out at room temperature in d^{8}-THF (400 MHz for ^{1}H NMR and 100 MHz for ^{13}C NMR) on a colloid stabilised with 0.2 eq of 1-octanethiol ($C_8H_{17}SH$). Tests at low temperature resulted in the precipitation of the particles. The following spectra (Figure 5-9) were obtained from the purified colloid spectrum and the colloid after progressive addition of free ligand:

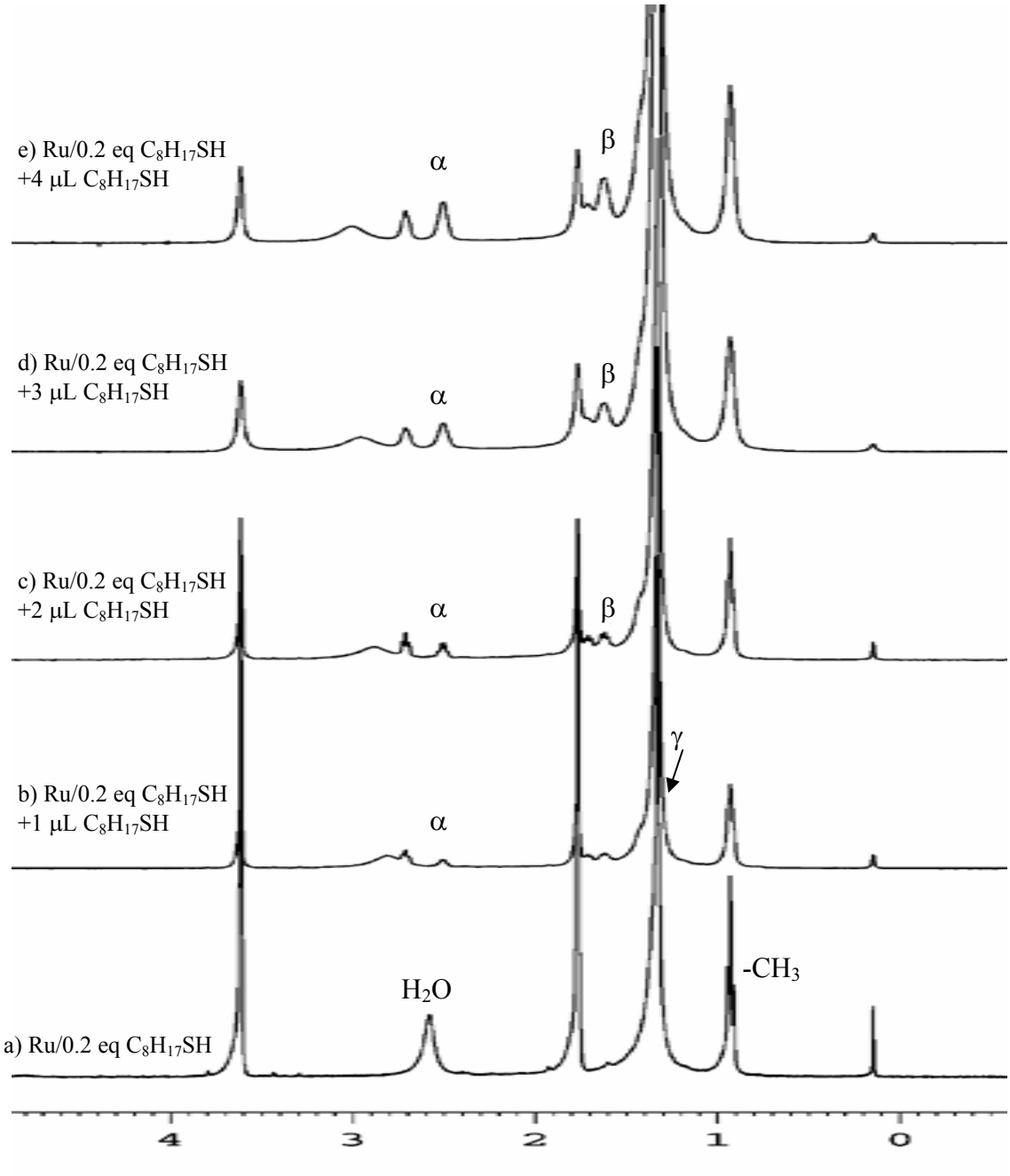

Figure 5-9: ^{1}H NMR spectra (d^8-THF, 400 MHz, 293 K) of colloids a) Ru / 0.2 eq $C_8H_{17}SH$, b) Ru / 0.2 eq $C_8H_{17}SH$ + 1 µL $C_8H_{17}SH$, c) Ru / 0.2 eq $C_8H_{17}SH$ + 2 µL $C_8H_{17}SH$, d) Ru / 0.2 eq $C_8H_{17}SH$ + 3 µL $C_8H_{17}SH$, e) Ru / 0.2 eq $C_8H_{17}SH$ + 4 µL $C_8H_{17}SH$

The initial ^{1}H NMR spectrum of the purified colloid (Figure 5-9 spectrum a) clearly shows the methyl groups of the ligand near 0.93 ppm and broad peaks for the methylene between 1.2 and 1.5 ppm but not the peaks attributed to the protons next to the sulphur atom which was expected at 2.44 ppm.

When additional amounts of 1-octanethiol was added (Figure 5-9 spectrum b), the peaks which can be attributed to the protons in α- and β- positions began to appear. The peaks

for the protons in α- and β- positions are already observable after addition of 1 µL of $C_8H_{17}SH$ to the purified colloid. The peak for the proton in α- position becomes visible at 2.5 ppm and the signal for the proton in β- position at 1.6 ppm. The peak corresponding to the protons in γ- position is difficult to detect because it is situated under the broad signal of the other methylene peaks around 1.3 ppm. The proton located on the sulphur atom at 1.28 ppm is also not observed. With progressive addition of $C_8H_{17}SH$ to the purified colloid the signals of the peaks became sharper (Figure 5-9 spectrum c, d, e).

Table 5-5 summarises the experimental ^1H NMR data collected for 1-octanethiol-stabilised colloids.

Table 5-5: ^1H NMR data of 0.2 eq 1-octanethiol stabilised Ru colloid and after adding free ligand

Colloid / added 1-octanethiol	Spectrum	Chemical shift / ppm				
		$(-CH_2)n$ (5-8)	$-CH_3$ (9)	α (2)	β (3)	γ (4)
Ru / 0.2 eq $C_8H_{17}SH$	a	1.2 - 1.5	0.93	-	-	-
Ru / 0.2 eq $C_8H_{17}SH$ + 1 µL $C_8H_{17}SH$	b	1.2 - 1.5	0.93	2.5	1.6	-
Ru / 0.2 eq $C_8H_{17}SH$ + 2 µL $C_8H_{17}SH$	c	1.2 - 1.5	0.93	2.5	1.6	~ 1.3

Finally, ^{13}C NMR spectra have been recorded for this colloid and the ^{13}C NMR spectrum for 1-octanetiol was simulated for the comparison with the experimental spectrum (see Figure 5-11 and Table 5-6).

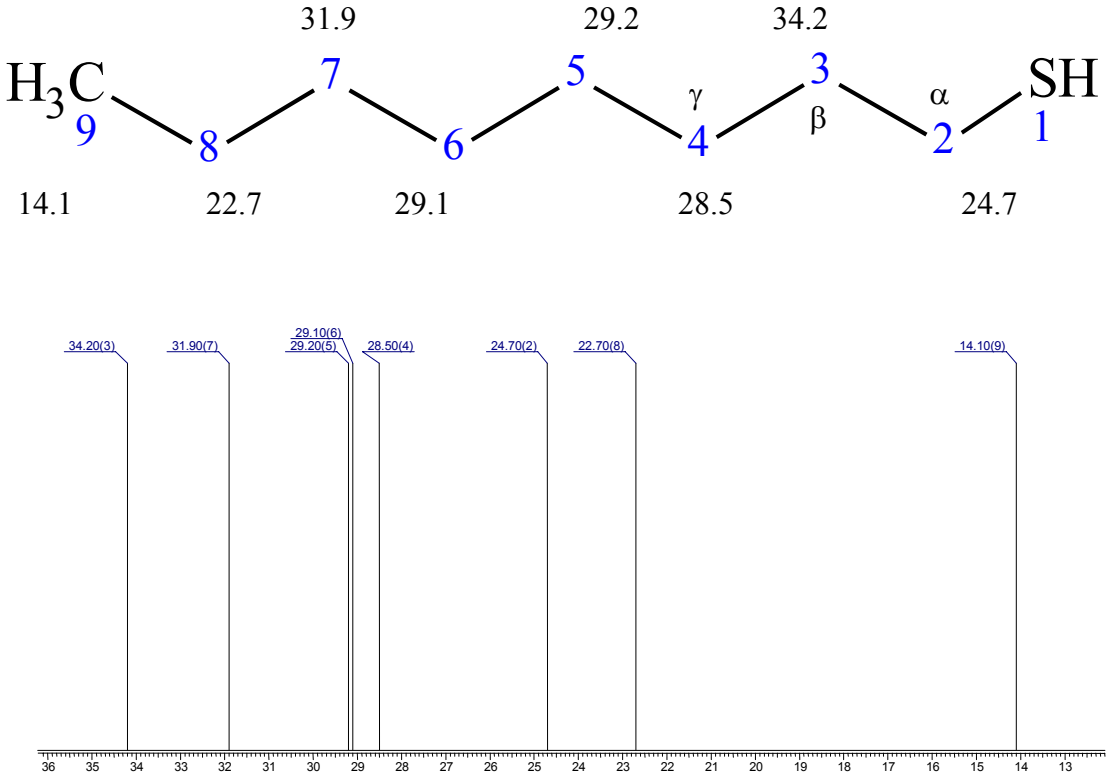

Figure 5-10: Simulated ^{13}C NMR spectrum of 1-octanethiol

Table 5-6: Calculated ^{13}C NMR data of 1-octanethiol

Group	9 (-CH_3)	8	7	6	5	4 (γ)	3 (β)	2 (α)
Carbon type	CH_3	CH_2	CH_2	CH_2	CH_2	CH_2	CH_2	CH_2
Chem. shift / ppm	14.1	22.7	31.9	29.1	29.2	28.5	34.2	24.7

The ^{13}C NMR spectrum of the purified colloid shows the peaks corresponding to the carbons of the ligands coordinated to the nanoparticles (Figure 5-11, spectrum b). They are broad and, as expected, at least two peaks corresponding to the α and β carbons are missing since the chemical surrounding of the colloid is shielding the protons of the attached ligand from detection by NMR. Only the peaks corresponding to the methylene groups can be recognized as large signals at 23.0 and near 30 ppm. A very diffuse peak is observed at 13.9 ppm for the CH_3-group. When an excess of free thiol (approx. 7 µL) was added to the solution (Figure 5-11, spectrum c), the appearance next to the colloid peaks, of sharp signals can be observed. Their chemical shifts are very close to those of the free ligand for all carbons. Just one is very different: a new peak is noticed at 39.0 ppm which could not correspond to the α

carbon of $C_8H_{17}SH$. This peak should be found at 24.7 ppm as in Figure 5-11, spectrum a for the free ligand. The observed information are summarised in Table 5-7.

Table 5-7: Experimental ^{13}C NMR data of Ru/0.2 eq 1-octanethiol and after adding free ligand

Colloid / added 1-octanethiol	Spectrum	Chemical shift / ppm			
		$-CH_3$ (9)	α (2)	β (3)	γ (4)
$C_8H_{17}SH$	a	13.8	24.7	34.2	28.8
Ru / 0.2 eq $C_8H_{17}SH$	b	13.9	-	-	-
Ru / 0.2 eq $C_8H_{17}SH$ + 7 µL $C_8H_{17}SH$	c	13.9	39.0	25.7	28.9
$C_8H_{17}S_2C_8H_{17}$	Figure 5-12	13.9	38.8	25.6	29.7

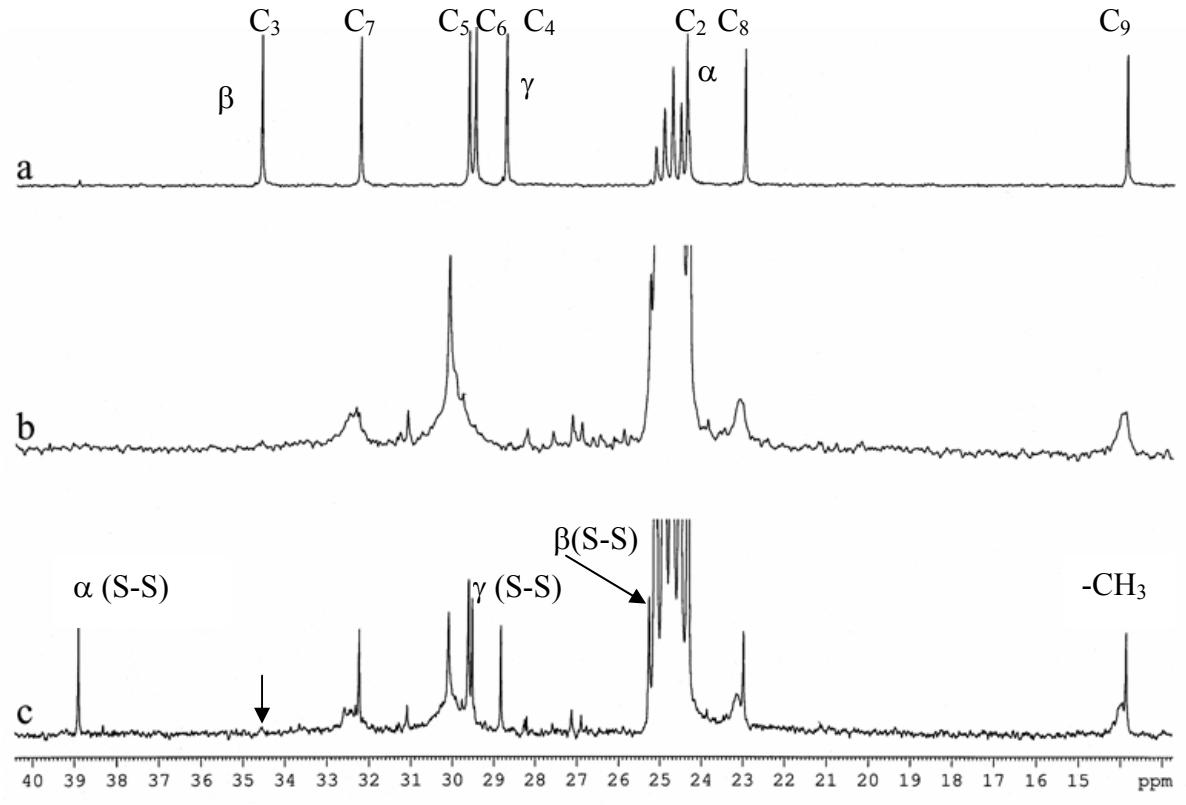

Figure 5-11: ^{13}C NMR spectra (101 MHz, d^8–THF, 293 K) of a) $C_8H_{17}SH$, b) Ru / 0.2 eq $C_8H_{17}SH$, c) Ru / 0.2 eq $C_8H_{17}SH$ + 7 µL $C_8H_{17}SH$,

This new peak observed at 39.0 ppm could not be attributed as belonging to the thiol ligand, but it could correspond to an α-carbon located on a disulfide. Then the formation of a disulfide has been suggested and the experimental spectra were compared with a calculated one for a octanedisulfide (Figure 5-12 and Table 5-8). The chemical shift for the α carbon was found at 39 ppm which corresponds to the α-carbon of the octanedisulfide. As this value

corresponds to the new peak detected at 39 ppm in spectrum c, the conversion of 1-octanethiol into the corresponding disulfide $C_8H_{17}S_2C_8H_{17}$ has been proposed.

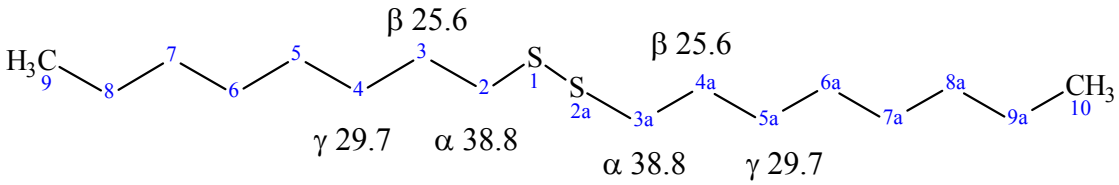

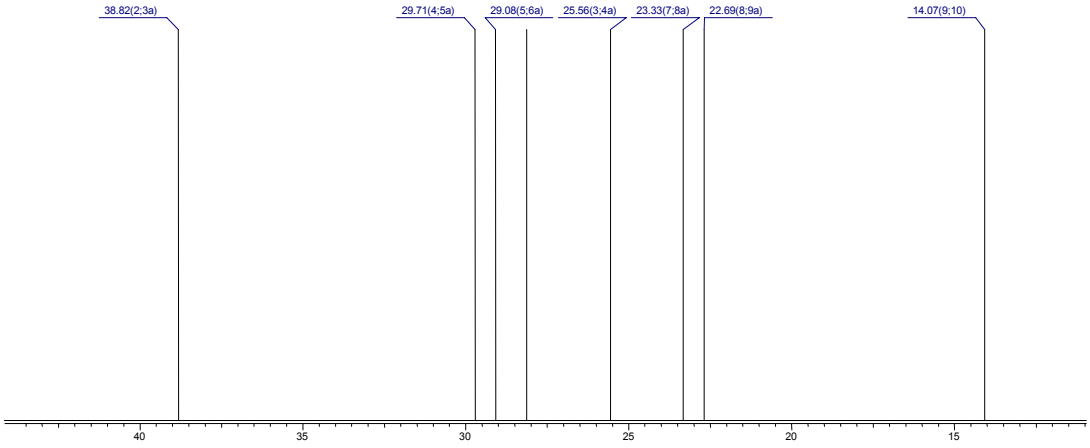

Figure 5-12: Simulated ^{13}C NMR spectrum of 1-octanedisulfide ($C_{16}H_{34}S_2$)

Table 5-8: Calculated ^{13}C NMR data of 1-octanedisulfide ($C_{16}H_{34}S_2$)

Number	2, 3a (α)	3, 4a (β)	4, 5a (γ)	5, 6a	6, 7a	7, 8a	8, 9a	9, 10
Carbon type	CH_2	CH_2	CH_2	CH_2	CH_2	CH_2	CH_2	CH_3
Chem. shift / ppm	38.8	25.6	29.7	29.1	28.1	23.3	22.7	14.1

A similar observation of new peaks which could not be attributed to the 1-octanethiol was also made by ^1H NMR (Figure 5-14). The transformation of the quartet at 2.50 ppm corresponding to the protons located on the α–carbon in $C_8H_{17}SH$ into a triplet at 2.70 ppm for the corresponding protons in $C_8H_{17}S_2C_8H_{17}$ could be observed (Figure 5-15). This reaction was monitored during several days by ^1H NMR. The ^1H NMR spectrum for 1-octanedisulfide was simulated for 1-octanedisulfide for comparison to the experimental results (Figure 5-13 and Table 5-9). It is possible to establish a correspondence with the attributed signal.

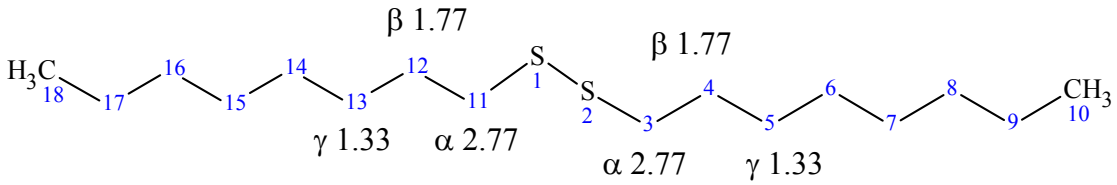

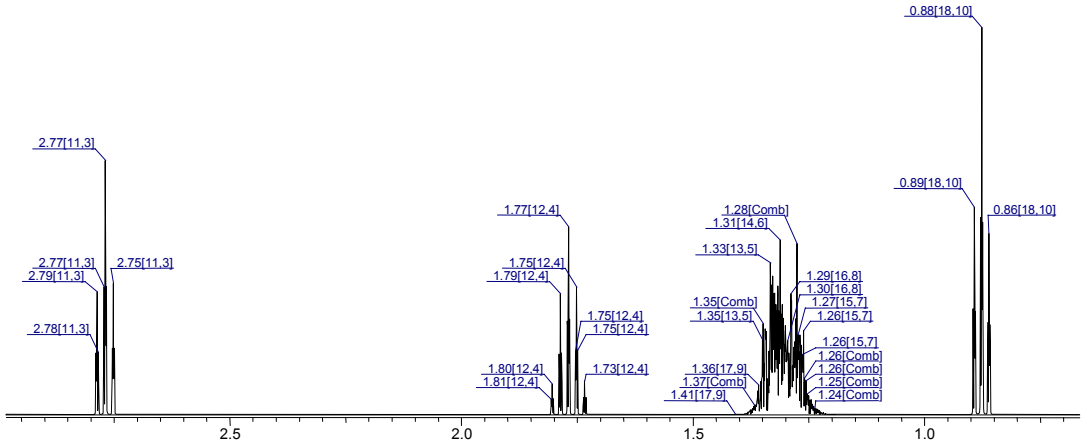

Figure 5-13: Simulated ^{1}H NMR spectrum of 1-octanedisulfide ($C_{16}H_{34}S_2$)

Table 5-9: Calculated ^{1}H NMR data of 1-octanedisulfide ($C_{16}H_{34}S_2$)

Number	3, 11 (α)	4, 12 (β)	5, 13 (γ)	6, 14	7, 15	8, 16	9, 17	10, 18 (-CH_3)
Number H	2	2	2	2	2	2	2	3
Chem. shift / ppm	2.77	1.77	1.33	1.31	1.26	1.29	1.34	0.88

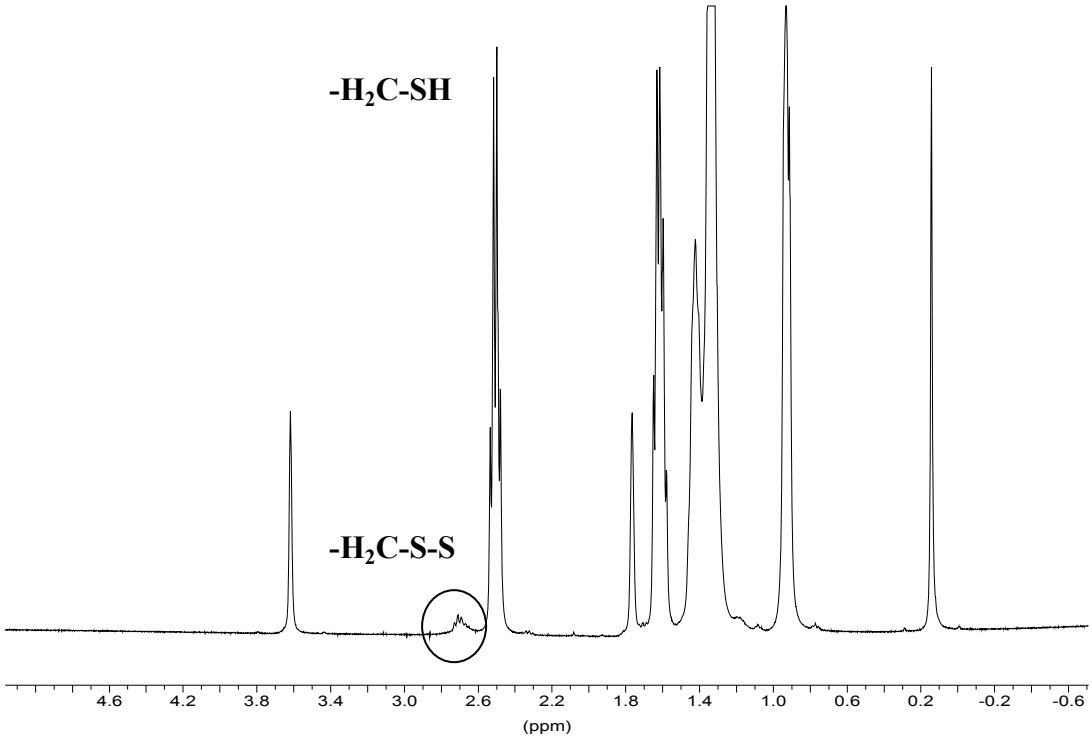

Figure 5-14: ^{1}H NMR spectrum (200 MHz): Ru / 0.2 eq $C_8H_{17}SH$ in d^8-THF at 293 K after 1 day

It seems clear that the 1-octanethiol is consumed continiously while the quantity of disulfide increases (Figure 5-14 and Figure 5-15). These experiments therefore demonstrate the catalytic oxidation of a thiol into a disulfide at the surface of the ruthenium nanoparticles. The information obtained from the NMR experiments is that if the colloids are stable and if the ligands which are present at the surface of the colloids are disulfides, they do not rapidly exchange with the free ligands on the NMR time scale.No precipitation of the particles was observed during this time. A microscopy grid prepared at the end of this NMR study revealed the presence of ruthenium nanoparticles similar to those resulting from the synthesis of ruthenium particles stabilised with 0.2 eq of 1-octanethiol. Probably the formed disulfide can assist the stabilisation of the particles. We know that stabilisation of particles is possible by disulfides, since disulfide protected gold clusters have already been reported.[131]

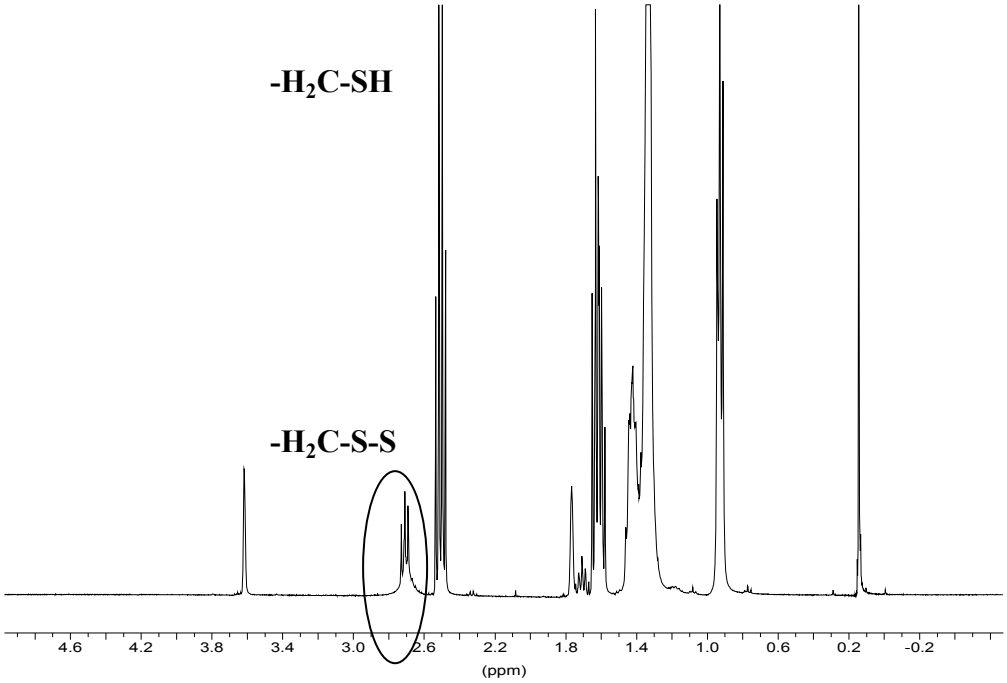

Figure 5-15: ^1H NMR spectrum (200 MHz): Ru / 0.2 eq $C_8H_{17}SH$ in d^8-THF at 293 K after 2 days

A catalytic coupling of thiolate ligands leading to the production of dihydrogen can account for this transformation (Figure 5-16).

Another important observation is the detection of free dihydrogen by ^1H NMR at an early stage of the reaction. Dissolved H_2 was identified by its chemical shift (4.8 ppm in d^8-THF) and its long relaxation time (T_1 = 2.1 s). This signal is broad but sharpens when the temperature of the sample is cooled to 193 K. This line width results from an equilibrium, detectable at the NMR time scale, between dissolved and attached H_2 present in the solution (d^8-THF) which demonstrates the ability of the particles to split H-H bonds. This process could not be studied thoroughly because of the elimination of H_2 from the reaction solution: as H_2 concentration decreases, the shape of the spectrum changes and the H_2 peak vanishes. It has therefore not been possible to observe the formation of H_2 during the catalytic coupling of thiols, probably because the reaction is very slow and the concentration of H_2 in solution remains very low. In order to test an alternative oxidation mechanism, two parallel reactions between the ruthenium colloid and excess 1-octanethiol were carried out, one in a rigorously controlled atmosphere whereas the other was in the presence of air (approx. 500 µl) which has been injected into the solution just before running the first NMR spectrum. In the first case, we observed the formation of disulfide while, in the second one, the presence of air stopped

the reaction. This demonstrates that the coupling needs a controlled atmosphere and involves oxidative addition of thiol followed by reductive elimination of dihydrogen. In this respect, the initial observation of dissolved H_2 is most probably the result of oxidative addition of thiols on ruthenium particles producing surface hydrides and from the recombination of these hydrides. The elimination of H_2 from the reaction solution may be a driving force for the coupling.

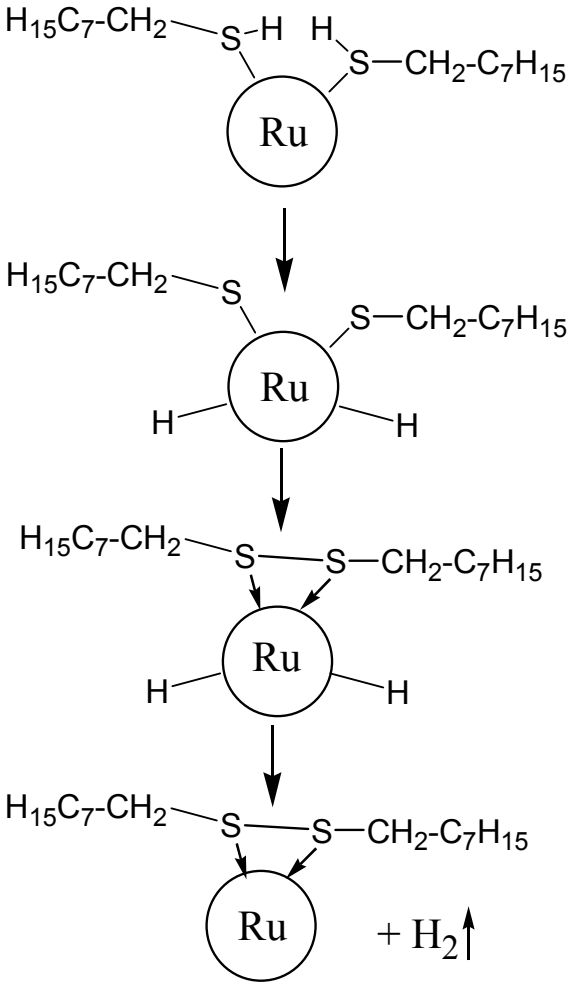

Figure 5-16: Possible mechanism for the formation of disulfide catalysed at the particles surface

This NMR study demonstrates the coupling of thiols into disulfides at the ruthenium particles surface and the presence of dihydrogen in the solution. When excess thiol is present, a catalytic coupling of thiol into disulfide, slow on the NMR time scale, is observed. This indicates that the ruthenium particles are active materials for catalytic applications even in the presence of sulphur which is commonly considered to be a poison for catalytic materials.

In order to study the influence of the length of the alkyl chain of the ligand, solution NMR studies with Ru/0.2 eq 1-hexadecanethiol particles have been undertaken.

5.1.2.2 Ru/1-hexadecanethiol particles: Solution NMR studies

NMR studies have been carried out on ruthenium particles synthesised with 0.2 eq of 1-hexadecanehiol ($C_{16}H_{33}SH$).

A ^{1}H NMR spectrum was simulated for comparison (Figure 5-17 and Table 5-10) and an analogy for the peaks could be stated.

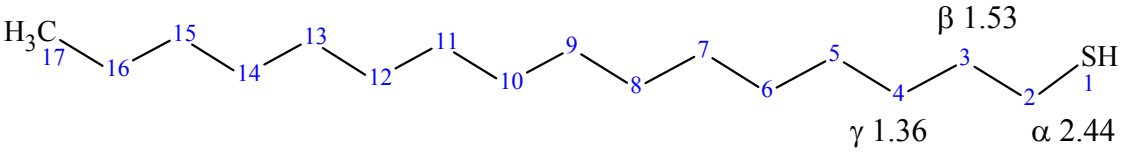

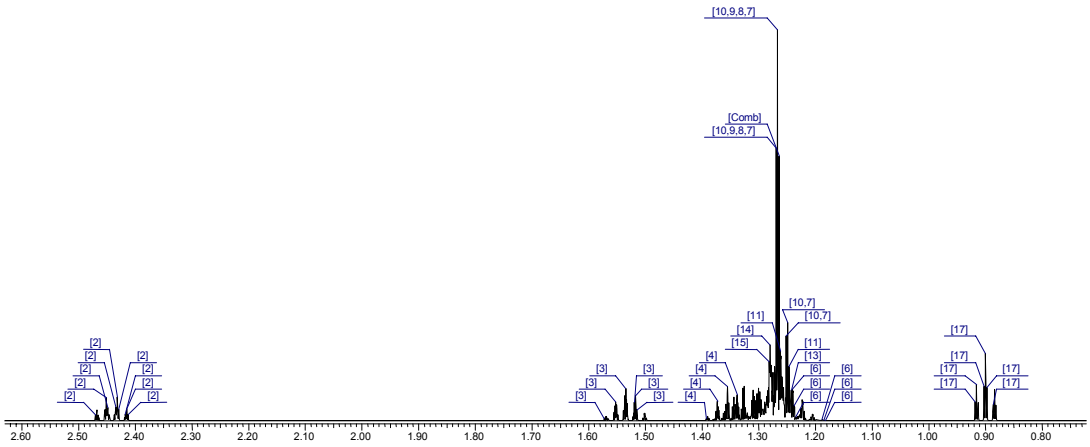

Figure 5-17: Simulated ^{1}H NMR spectrum of eq 1-hexadecanethiol ($C_{16}H_{33}SH$)

Table 5-10: Calculated ^{1}H NMR data of eq 1-hexadecanethiol ($C_{16}H_{33}SH$)

Number	2 (α)	3 (β)	4 (γ)	5	6	7,8,9,10	11	12	13	14	15	16	17
Number H	2	2	2	2	2	2	2	2	2	2	2	2	32
Chem. shift / ppm	2.44	1.53	1.36	1.28	1.22	1.27	1.25	1.24	1.27	1.28	1.29	1.34	0.90

A ^{13}C NMR spectrum (100.71 MHz) in d^8-THF of the colloid has been recorded at room temperature to avoid the precipitation of the particles. The spectrum of the colloid after purification does not show any excess of free ligand (Figure 5-18 spectrum a). No peaks neither for the α, β and γ carbons nor for the CH_3-group are observed. Nevertheless, the presence of the ligand can be confirmed by the peaks for methylene groups of the alkyl chain of the thiol. After addition of free ligand in the NMR tube the appearance of the corresponding peaks for the α, β and γ carbons can be observed. With the emergence of the peak associated to the α carbon another signal can be observed. The chemical shift of this peak is 39 ppm. (Figure 5-18 spectrum e). This new peak can be attributed to the α carbon next to a newly formed disulfide as previously observed for the 1-octanethiol. The peak for the α carbon is still visible which indicates the presence of both species in the medium. These results are summarised in Table 5-11.

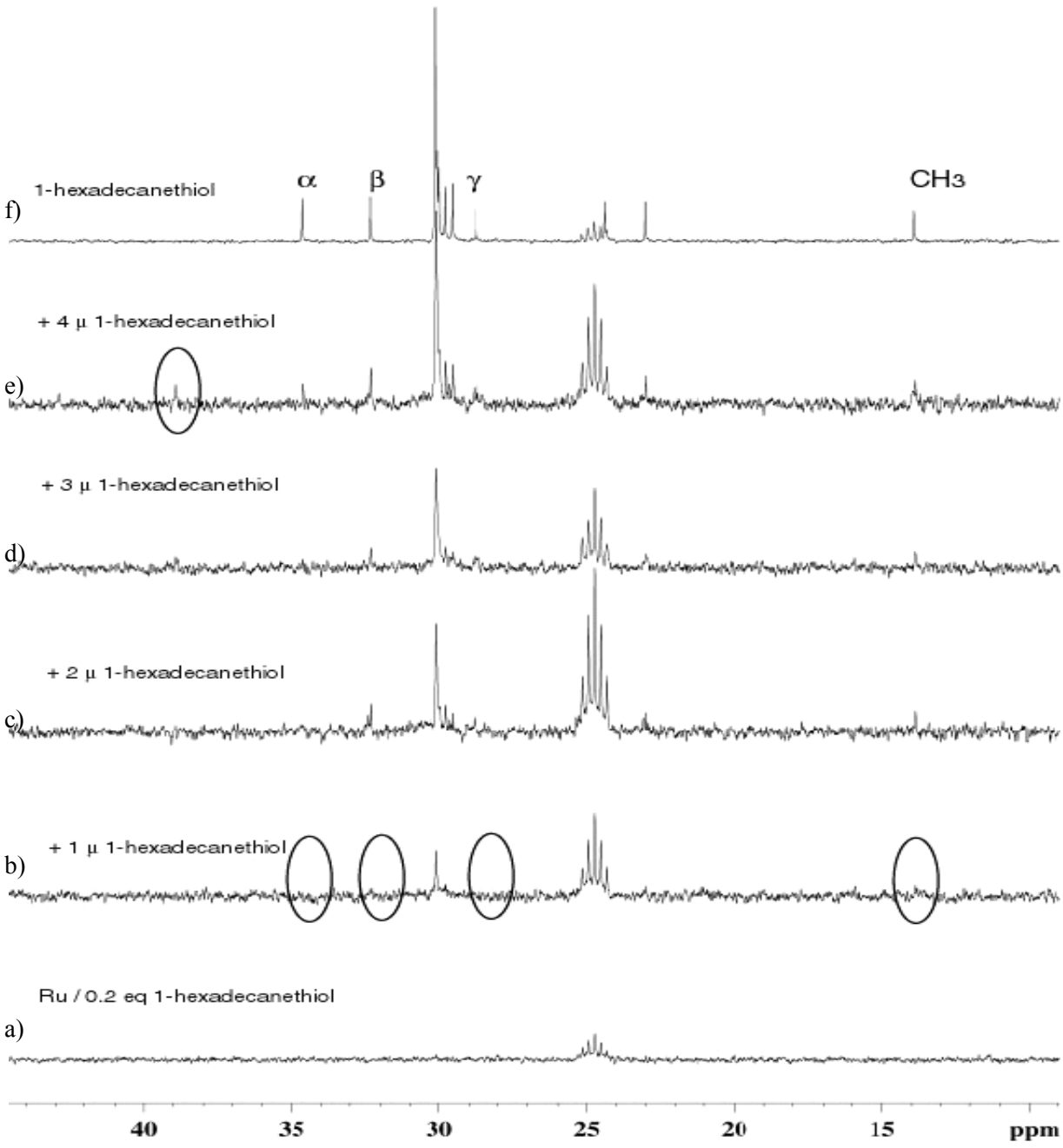

Figure 5-18: ^{13}C NMR spectra (101 MHz, d^8-THF, 293 K) of ruthenium particles synthesised with 0.2 eq 1-hexadecanethiol and addition of free ligand

Table 5-11: Experimental ^{13}C NMR data of eq 1-hexadecanethiol after adding free ligand

Colloid / added 1-octanethiol	Spectrum	Chemical shift / ppm			
		$-CH_3$ (17)	α (2)	β (3)	γ (3)
$C_{16}H_{33}SH$	f	13.9			28.7
Ru / 0.2 eq $C_{16}H_{33}SH$	a	-	-	-	-
Ru / 0.2 eq $C_{16}H_{33}SH$ + 1 µL $C_{16}H_{33}SH$	b	13.9	-	-	-
Ru / 0.2 eq $C_{16}H_{33}SH$ + 3 µL $C_{16}H_{33}SH$	d	13.9	-	32.3	28.7
Ru / 0.2 eq $C_{16}H_{33}SH$ + 4 µL $C_{16}H_{33}SH$	e	13.9	34.7	32.3	28.7
$C_{16}H_{33}S_2C_{16}H_{33}$	e	13.9	39.0	32.2	28.7

The formation of a disulfide could be confirmed by ^1H NMR. The signal at 2.4 ppm (note that 0 ppm here is calibrated at 0.4 ppm) is assigned to the protons in α-position and an additional peak at 2.6 ppm for the disulfide is clearly visible after 3 days as can be seen in Figure 5-19.

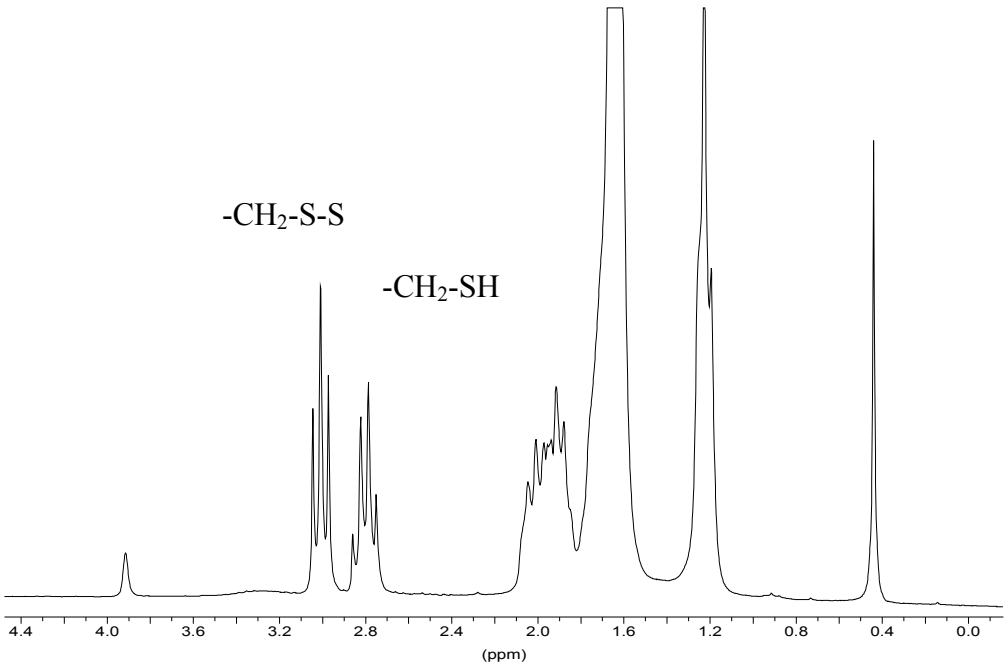

Figure 5-19: ^1H NMR spectrum (200 MHz, d^8-THF, 293 K) of ruthenium particles synthesised with 0.2 eq 1-hexadecanethiol after 3 days

The increase in intensity of the peak attributed to the disulfide was observed over time which indicates that the 1-hexadecanethiol is being continuously transformed into the corresponding disulfide.

These NMR investigations monitored the presence of this ligand at the surface of the particles and the formation of disulfide could be stated.

5.1.3 Conclusion

Ruthenium particles can be stabilised by long chain alkyl thiols to give colloids some of which can be obtained in powder form. In the cases where thiol / Ru(COD)(COT) ratios of 0.5 eq / 1 eq and 1 eq / 1 eq were used, the precipitates obtained were so sticky after complete evaporation of the solvent that the corresponding colloids could not be purified. When less than 0.2 eq of ligand were used, the colloids were not stable in solution. For an added quantity other than 0.2 eq, the particles were found to be stable in solution for several weeks and a fine powder could be obtained after purification.

WAXS analysis were performed on the colloids and in each case the particles were found to be crystalline and to adopt the hcp structure of bulk ruthenium with the same small deviation in the cell dimensions of the hcp network. The RDF of the colloids evidence a tendency for a decrease in the coherence length when colloids are stabilised with relatively long alkyl chains like 1-dodecanethiol and 1-hexadecanethiol ($C_{12}H_{25}SH$ and $C_{16}H_{33}SH$) as the concentration of the thiol is increased. But, in contrast to that, the colloids stabilised with 1-octanethiol show a growth in size as the concentration of ligand is increased. A reduction in particle size depending on the added ligand concentration as indicated by WAXS experiments was also observed by Klabunde et al.[132] and Yasui et al.[133]

TEM and HREM analysis confirm the presence of crystalline particles of spherical aspect. The particles prepared in the presence of 1-octane- and 1-dodecanethiol were found to be strongly agglomerated and incorporated into large superstructures. In the presence of 1-hexadecanethiol, probably because of the chain length, no agglomeration was observed but individual particles are of spherical aspect. However, the size of the particles remains around 1-3 nm.

The observation of agglomerated particles in the case of thiol stabilised particles is in marked contrast with the observation that nanoparticles of comparable size of gold or of platinum are perfectly stabilised by the same ligands (1-octanethiol, 1-dodecanethiol), do not agglomerate and can be deposited as monolayers on various substrates.[37,40,41,69,70]

NMR studies were undertaken to shed some light on the behaviour of the ligands on the particle surface. It is shown that the thiols are oxidatively attached to ruthenium and when an excess of free thiol is added to the NMR tube a reductive elimination of disulfides released into the solution is observed. Apparently, they do not exchange with the ligands present at the surface of the particles. This may be the reason why the ruthenium colloids adopt such different structures from those known for gold and platinum colloids, even though the alkyl chains are the same and the functional groups similar. Platinum particles of similar sizes do not aggregate when 0.2 eq of 1-octanethiol are employed but display a regularly space between each other.[90] The alkyl chains of the sulphur ligands most likely encircles the particles and interpenetrate with the alkyl chains of other ligands either free or located at the surface of other particles, thereby leading to the formation of superstructures and agglomeration of the particles. The observation of a slow catalytic coupling of thiols into disulfides which may be removed from the colloid surface is in agreement with Schmid et al. who demonstrated recently that the removal of ligands from the surface of gold particles force the particles to organise into superstructures.[134]

Only a very few NMR studies evidenced this process of catalytic coupling of molecules at the surface of metal nanoparticles. This study demonstrates a relation between the behaviour of co-ordinated ligands on the surface with the shape of the particles. The combination of methods of characterisation of nanomaterials such as TEM and WAXS with simple techniques of organometallic chemistry such as NMR provides useful information on the chemical reactivity of the surface of the nanoparticles. Elementary surface reaction steps such as oxidative addition and reductive elimination of thiols can be pictured. Such a study may also help to understand the shape and structure of nanoparticles. These results are encouraging for the use of ligand stabilised metal particles as catalysts.

5.2 Amines as a ligand for ruthenium nanoparticles

The previous chapter described the stabilisation of ruthenium nanoparticles by thiols. The use of this type of ligands allowed the stabilisation of the particles, but their dispersion was not sufficient. The gained particles could not be well-separated. It is known that the nature and the applied quantity of the stabilising agent can have an influence on the shape of the particles. Therefore another type of organic ligand has been used in different quantities for the stabilisation of ruthenium nanoparticles.

In this chapter the preparation of amine protected ruthenium nanoparticles, the study of the influence of the ligands on the size and shape of the nanoparticles and their characterisation by both material characterisation methods (electron microscopy, X-ray scattering) and molecular chemistry methods such as solution NMR studies will be described.

In order to compare the interaction of thiol and amine molecules with the surface, the stabilisation of Ru particles by similar ligands as those prepared in the previous chapter, but bearing a $–NH_2$ function instead a –SH one, was studied. Alkylamines with various chain lengths have then been selected to stabilise Ru nanoparticles. These amines are not often mentioned in the literature although the use of alkylamines has been applied in a few cases in the past.[14,15,16] The amines are known as a good ligand capable of interacting with the surface of the metal, the functional $–NH_2$ group being attached to the reactive sites at the metal surface.

It will be shown that the size and organisation of the particles fluctuate with the nature and quantity of the ligand used and that in some cases superstructures are obtained.

5.2.1 Study of different alkyl chain length amines

The preparation of the amine-stabilised nanoparticles has been carried out in a similar way to that described in the presence of a thiol (chapter 5.1). A solution of Ru(COD)(COT) is added to a solution of a selected alkyl amine in THF at 193 K. The resulting solution is then pressurised with 3 bar of dihydrogen at 193 K and allowed to react for 24 hours while the temperature is slowly raised up to room temperature (Scheme 5-2). A brown solution is formed. The absence of residual amounts of Ru(COD)(COT) can be monitored by column chromatography. To obtain a black powder from the solution the particles are precipitated

after depressurisation, the crude solution is concentrated and dripped into a big volume of cold pentane. The fine particles are washed several times with pentane to remove the excess of ligand. The powder that is obtained can be dissolved in THF. For the characterisation of their size, morphology and dispersion, the particles were visualised by transmission electron microscopy (TEM) as well as high resolution electron microscopy (HREM). The measurement of the nanoparticles diameters were made using these images (approximately 200 or 300 particles are considered), from which size distribution histograms can be created and the average diameter obtained. The particles crystal structure is determined by WAXS experiments and their coherence length could be compared to the particles sizes obtained from the TEM micrographs. In the case of the amine ligands that were used a very good accordance between the two characterisation modes was found.

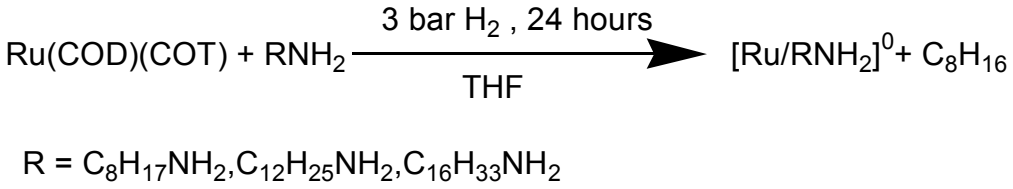

Scheme 5-2: Decomposition of Ru(COD)(COT) in the presence of an amine as stabilising agent

This procedure was applied for reactions of Ru(COD)(COT) with various mole equivalents of alkyl amines compared to the ruthenium introduced. 1-aminooctane ($C_8H_{17}NH_2$), 1-aminododecane ($C_{12}H_{25}NH_2$) and 1-aminohexadecane ($C_{16}H_{33}NH_2$) were tested to investigate the influence of the alkyl chain length of these ligands on the size, the shape and the dispersion of the particles.

5.2.1.1 1-aminooctane as stabilising agent for Ru particles

When the stabilisation of ruthenium nanoparticles was attempted with amounts lower than 0.2 eq 1-aminooctane ($C_8H_{17}NH_2$) compared to ruthenium, a precipitate formed shortly after pressurisation and a clear solution was obtained. As a result, the amount of the stabilising ligand was increased.

With 0.2 eq 1-aminooctane ($C_8H_{17}NH_2$) compared to ruthenium, individual spherical particles of mean diameter 2.5 nm are observed which are well separated on the microscopy grid as seen from the TEM micrograph in Figure 5-20. WAXS measurements (Figure 5-21) have been performed and the crystalline character of the particles was established. The particles adopt the hcp structure of bulk ruthenium and only a small deviation in the cell

dimensions of the hcp network was observed. The size of the particles obtained from the TEM micrograph was in agreement with the coherence length resulting from the WAXS analysis (2.4 nm). Nevertheless, the size distribution of the particles is large from 2.2 to 3.0 nm which can be due to the irregular shape of the particles.

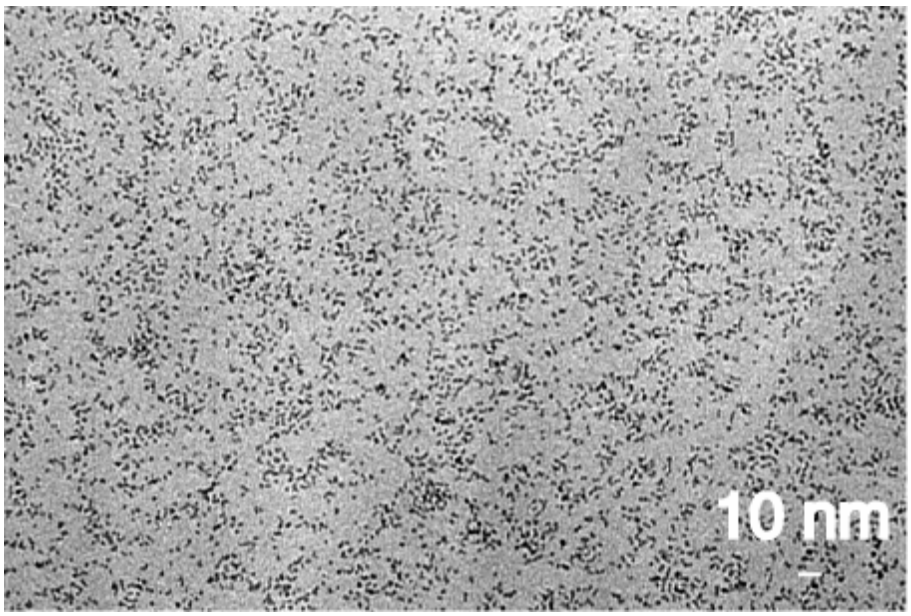

Figure 5-20: TEM micrograph of Ru nanoparticles stabilised with 0.2 eq. 1-aminooctane

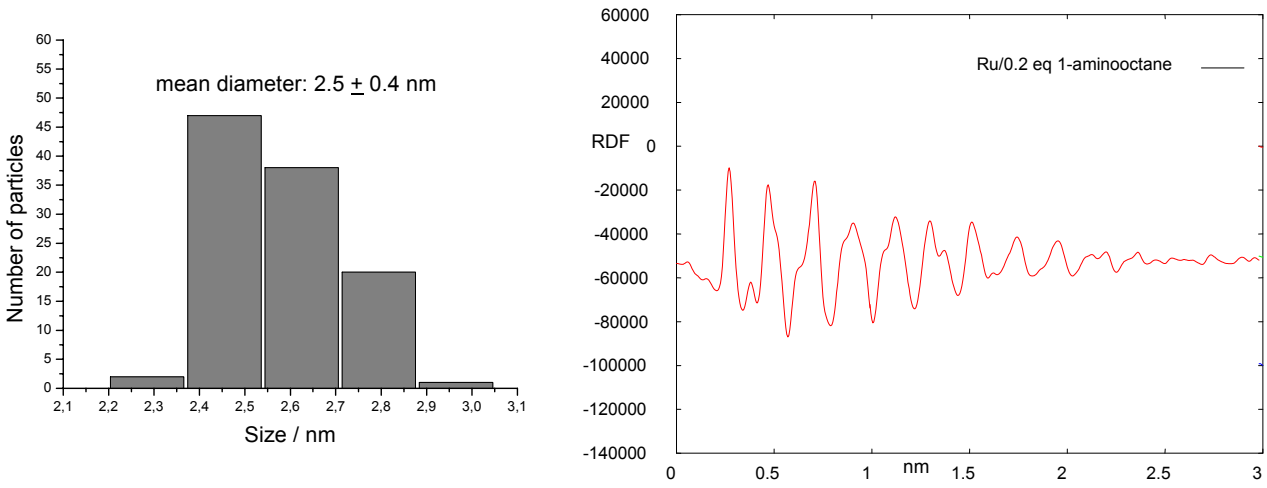

Figure 5-21: Size diagram built from the TEM micrograph and WAXS measurements of Ru nanoparticles stabilised with 0.2 eq. 1-aminooctane

In the presence of 0.5 eq 1-aminooctane, the size of individual particles does not seem to change much but the particles are agglomerated into more diffuse structures which renders their observation difficult (Figure 5-22). Nevertheless, their mean diameter can be estimated at 2.5 nm.

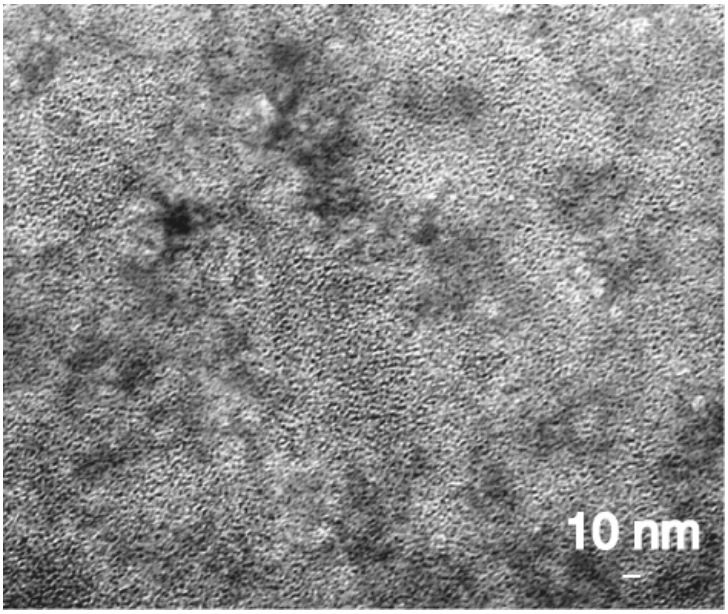

Figure 5-22: TEM micrograph of Ru nanoparticles stabilised with 0.5 eq. 1-aminooctane

It was not possible to observe individual particles when colloids were prepared in the presence of larger amounts of 1-aminooctane since the excess of ligand renders the TEM micrographs blurred and only cloudy species can be observed.

Table 5-12 summarises the results obtained for the stabilisation of ruthenium nanoparticles with 1-aminooctane.

Table 5-12: Obtained mean diameters for Ru particles stabilised with 1-aminooctane

eq / 1-aminooctane	Size / nm (TEM)	Coherence length / nm (WAXS)	Shape	Ru / %	N /%
0.1	-	-	not stable	-	-
0.2	2.3	2.4	spherical	62.24	1.07
0.5	2.5	2.5	clouds	83.03	1.85

Amounts lower than 0.2 eq of 1-aminooctane do not allow stabilisation of the particles in solution and for amounts higher than 0.2 eq of 1-aminooctane no good dispersion of the particles could be observed. In the presence of 0.2 eq of 1-aminooctane spherical particles which are homogeneous in size and well dispersed are observed. In order to achieve a better or a different stabilisation of the particles, longer alkyl chain amines have been employed.

5.2.1.2 1-aminododecane as stabilising agent for Ru particles

In the case of 1-aminododecane, with amine / ruthenium ratio equal to 0.2, 0.5 or 1, the particles display an unusual aspect: The particles are well dispersed and show an elongated form. When the amount of ligand is 0.2 eq, the particles are well separated as shown in Figure 5-23. Their mean size is about 1.9 nm. WAXS analysis evidenced the hcp structure of the particles and confirmed a coherence length of 1.9 nm.

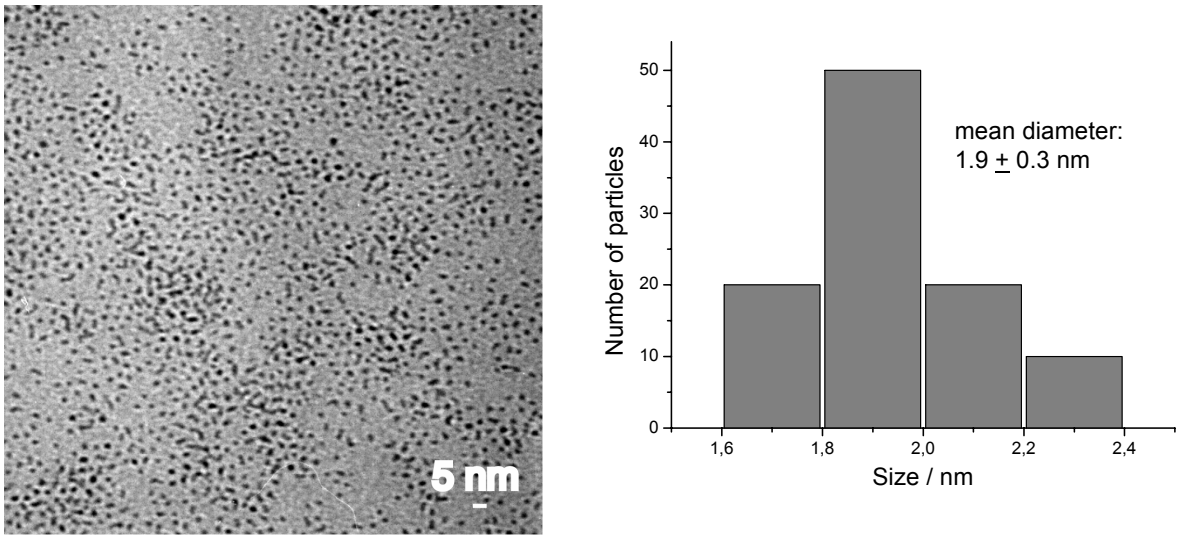

Figure 5-23: TEM micrograph and size histogram of Ru nanoparticles stabilised with 0.2 eq. 1-aminododecane

Upon increasing the relative concentration of the ligand compared to ruthenium to 0.5 eq, the aspect ratio of the particles decreased and the particles are more agglomerated and evidenced a tendency to form elongated particles. It is difficult to measure the size of such particles, but the shortest mean diameter can be estimated at 2.3 nm. In this work, the shortest mean diameter have always been measured. The particles are monocrystalline as established by HREM analysis and a careful observation of some electron micrographs reveals the presence of spherical particles (Figure 5-24) near the elongated ones.

a) b)

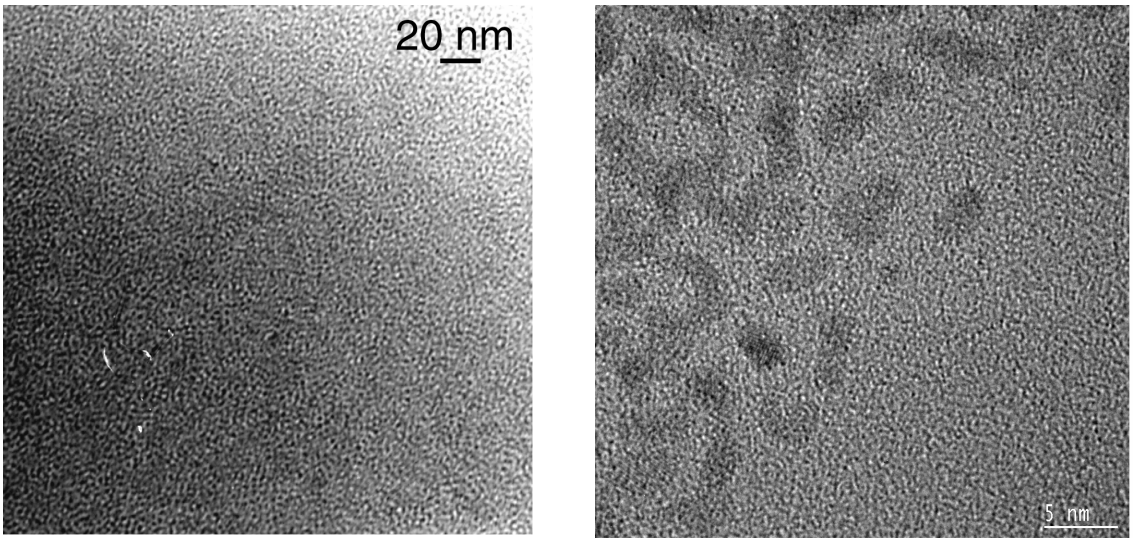

Figure 5-24: TEM (a) and HREM (b) micrographs of Ru nanoparticles stabilised with 0.5 eq. 1-aminododecane

Observation by TEM was difficult for the stabilisation of the particles with 1 eq 1-aminododecane, because of the agglomeration of the particles into large clouds. The particles size is estimated from 2.3 to 2.6 nm for 1 eq ligand.

The size of the particle is found to be regular for the 1-aminododecane ligand (near 1.9 nm for 0.2 eq ligand, 2.3 for 0.5 eq ligand and 2.3 to 2.6 nm for 1 eq ligand). WAXS analysis (Figure 5-25) evidenced the hcp structure of the particles and the similarity of the coherence lengths for particles prepared using different quantities of 1-aminododecane.

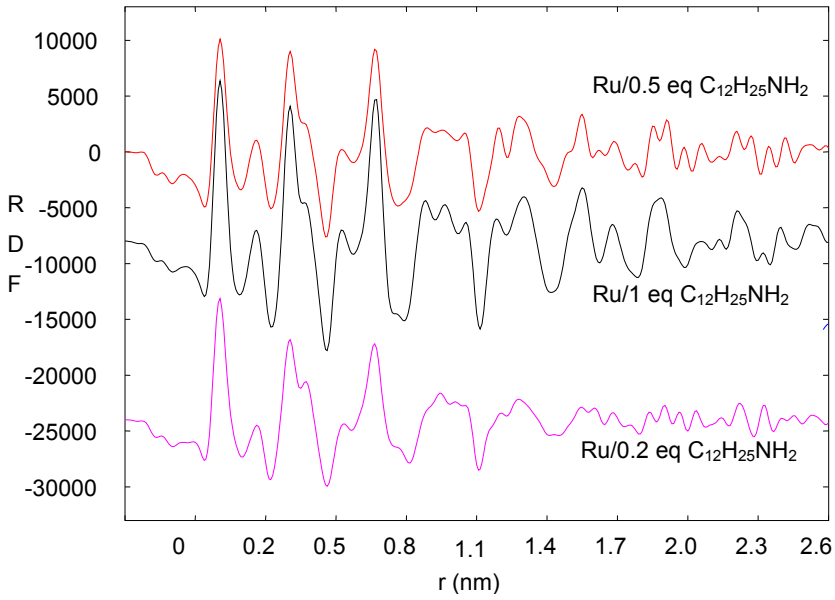

Figure 5-25: WAXS measurements for Ru particles synthesised with 0.2, 0.5 and 1 eq of 1-aminododecane

Table 5-13 summarises the results collected for Ru particles stabilised with 1-aminododecane.

Table 5-13: Obtained mean diameters for Ru particles stabilised with 1-aminododecane

eq / 1-aminododecane	Size / nm (TEM)	Coherence length / nm (WAXS)	Shape	Ru / %	N /%
0.1	-	-	not stable	-	-
0.2	1.9	1.9	elongated	69.2	1.64
0.5	2.3	2.3	elongated	79.8	1.58
1	2.3-2.6	2.6	agglomerates	80.2	1.57

An influence on the size of the particles of the quantity of used ligand and a tendency to form elongated particles in the presence of 1-aminododecane is noticed. As this was not the case with the 1-octylamine, is it possible that the longer alkyl chain could influence the shape of the particles. Therefore, the study was pursued employing 1-aminohexadecane ($C_{16}H_{33}NH_2$).

5.2.1.3 1-aminohexadecane as stabilising agent for Ru particles

A test series of various concentrations of the HDA (Table 5-14) was undertaken to determine the influence of the ligand concentration on the particles and their behaviour in the reaction medium (THF) at room temperature. For each synthesis 50 mg of Ru(COD)(COT) was used to assure a sufficient quantity of colloidal powder for the characterisation. The series was done using tetrahydrofurane as the solvent and always under 3 bar of dihydrogen. In the case of 1-aminohexadecane, with amine / ruthenium ratio equal to 0.1, 0.2, 0.5 or 1, the particles display a new aspect.

Table 5-14: Series of test for different amounts of HDA for the precursor

HDA /eq.	Stability
0.04	not stable
0.06	not stable
0.1	little stable
0.2	stable
0.5	stable
1	stable
5	stable
10	stable

In the presence of very small quantities (< 0.1 eq) of HDA, the yellow solution turned very dark brown but changed quickly into a clear liquid and the particles precipitated at the bottom shortly after pressurisation. Very small quantities of HDA are then not able to stabilise the particles in solution.

For example, In the presence of a very small amount of 1-aminohexadecane (0.04 eq) a powder was obtained which presented agglomerated, ill-defined nanoparticles of small size in TEM micrograph (Figure 5-26). The particles size is approx. 1 nm and the building of a size histogram was impossible because of the clogging of the particles. These nanoparticles do not remain stable in solution.

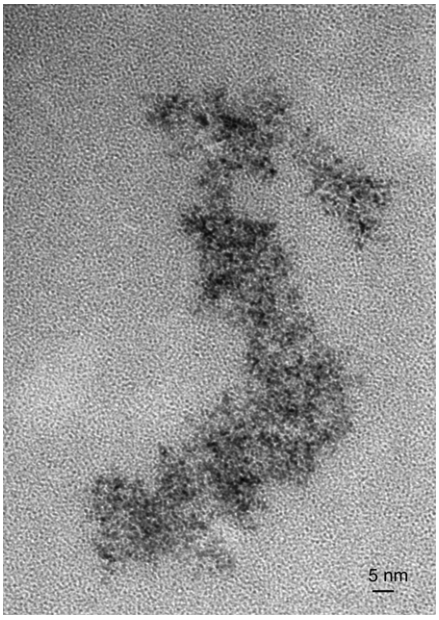

Figure 5-26: TEM micrograph of Ru nanoparticles stabilised with 0.04 eq. HDA

The same behaviour was observed when 0.06 eq of HDA were added to the precursor. The particles did not remain stable in the solution and rapidly formed a precipitate following pressurisation. Agglomerates of small particles in the range of 1 nm were also observed by TEM analysis.

It can be concluded that the particles stabilised with a low amount of ligand (0.04 and 0.06 eq.) are very small but show a tendency to agglomerate into bigger superstructures in the range of more than 100 nm and they do not remain stable in solution as a precipitate is observed. The quantity of ligand added was possibly not enough to avoid the interaction between the particles and achieve their stabilisation. In order to attain a better separation of the particles, the quantity of ligand was then increased to prevent agglomeration.

In the case of 0.1 eq of HDA / Ru, the colloids were still found to be not very stable in solution and they precipitated after one day. Nevertheless, a better separation of the particles could be noticed by TEM (Figure 5-27). The visualised particles do not form agglomerates, but are more regularly dispersed on the TEM grid than the particles stabilised by a lower amount of hexadecylamine. In addition, they show a lengthened shape.

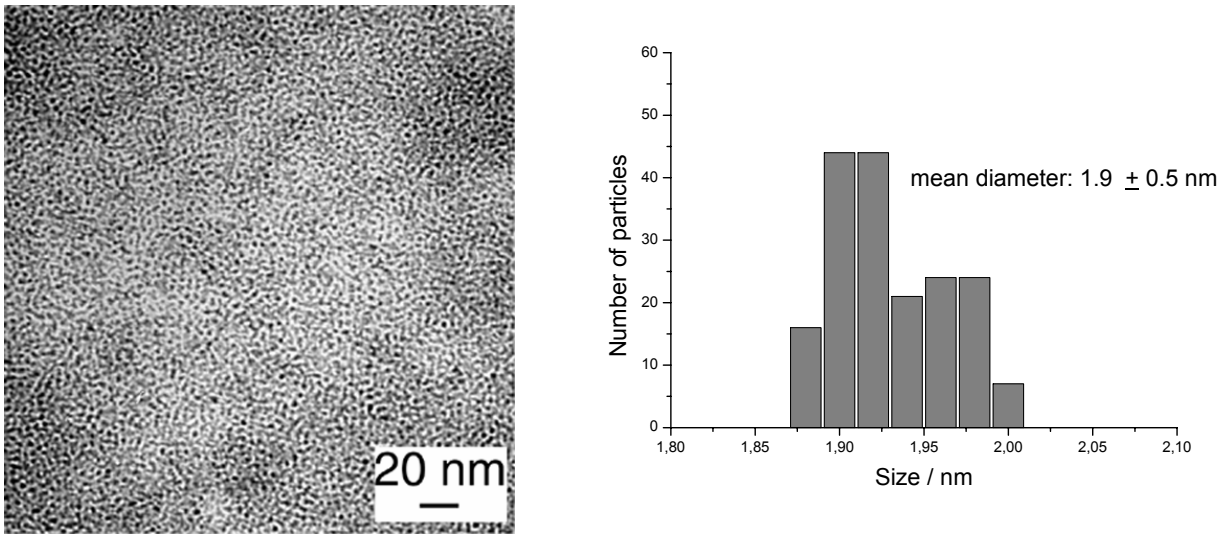

Figure 5-27: TEM micrograph of Ru nanoparticles stabilised with 0.1 eq. HDA and size histogram built from the TEM micrograph

In this case the particles form a homogenous colloidal solution from which they precipitate after 24 hours. The aspect of the particles is very regular and seem to be somehow arranged on the microscopy grid. They show an elongated shape, which can be obtained in a reproducible way.

The size distribution elaborated from the TEM micrographs is wide and found between 1.87 and 2 nm and the mean diameter for these particles is about 1.9 nm as shown in Figure 5-27.

WAXS analysis was performed in the solid state on all the colloids prepared in the presence of 0.1 eq HDA, except for the colloids which were found to be too sticky. In each case, the particles are crystalline and adopt the hcp structure of bulk ruthenium. The coherence length is found to be larger than those found in polymers[34] but similar to the coherence length for particles prepared using different quantities of amine. The size suggested by WAXS measurements (Figure 5-28) is about 19 Å (1 nm = 10 Å) which is in agreement with the size determined by TEM.

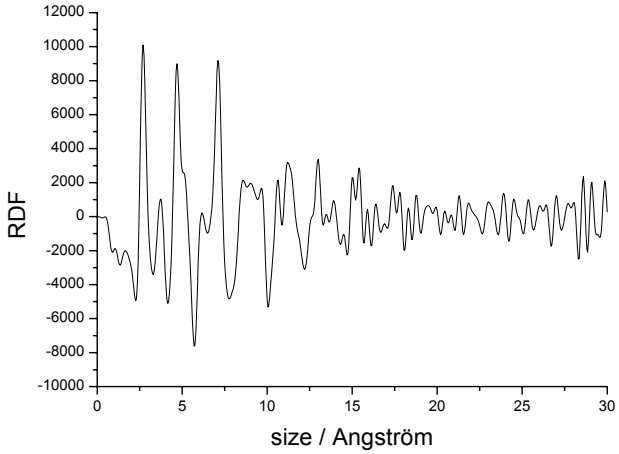

Figure 5-28: WAXS measurements of Ru nanoparticles stabilised with 0.1 eq. HDA

From 0.1 equivalents upwards the particles remained stable in solution for at least several weeks. As revealed by TEM analysis, the particle size increases with the increase of ligand quantity in the reaction medium.

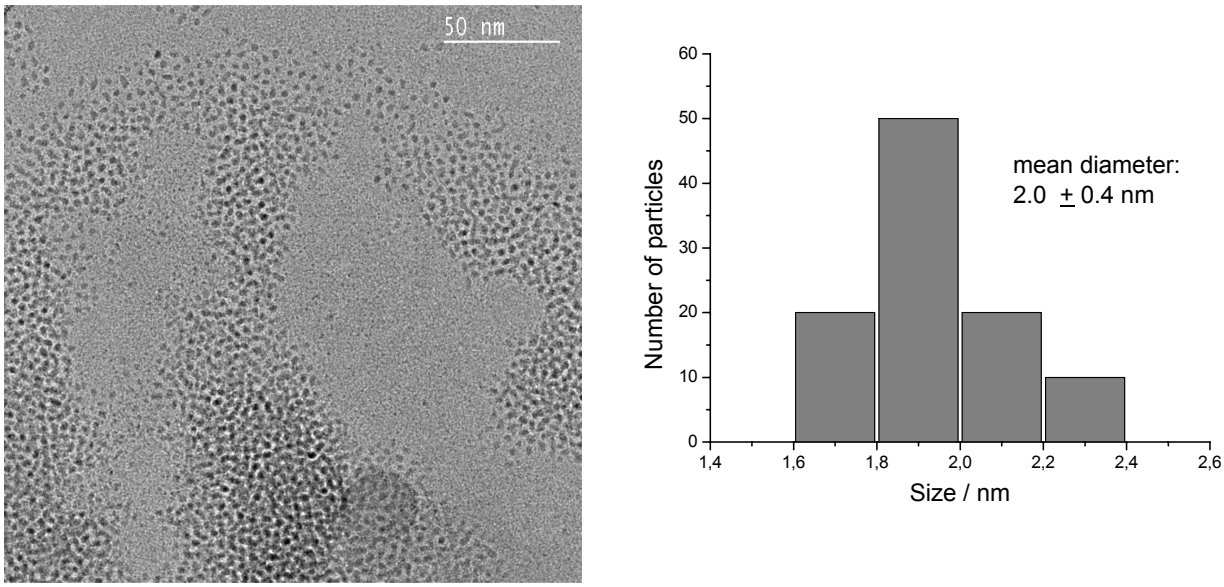

Figure 5-29: TEM micrograph of Ru nanoparticles stabilised with 0.2 eq. HDA and size histogram built from the TEM micrograph

In the presence of 0.2 eq of HDA, a homogenous solution was obtained which was stable for at least several weeks. A fine powder could be isolated by precipitation in cold pentane. The aspect of the particles does not seem to vary much from the previous case. The TEM micrograph (Figure 5-29) shows the tendency of the particles to be lengthened: they

appear like “worms”. This tendency to present an elongated shape was previously observed in the presence of 0.1 eq of this ligand and is here confirmed. The mean diameter obtained from the TEM micrograph is 2.0 nm (Figure 5-29). This means that the size of the particles stabilised with 0.2 eq HDA remains nearly unchanged in comparison with the particles stabilised with only 0.1 eq HDA: 2.0 nm against 1.9 nm.

The particles are well separated from each other. Nevertheless, they present a tendency to be organised into superstructures since in some areas of the grid the particles are absent (Figure 5-29). The particles are well-crystallised as evidenced by HREM analysis. The HREM micrograph (Figure 5-30) clearly shows the atom layers of the particles. Some elongated particles present long atom layers which can be interpreted as a coalescence of two particles in the same crystalline direction.

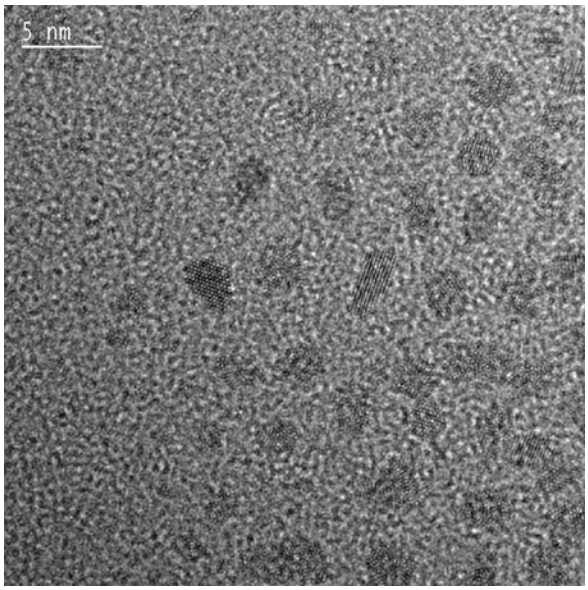

Figure 5-30: HREM micrograph of Ru nanoparticles stabilised with 0.2 eq. HDA

A careful observation of some electron micrographs reveals the presence of spherical particles which are in the process of coalescing. After some time in solution (48 hours), the particles display an elongated or “vermicular” aspect (Figure 5-31).

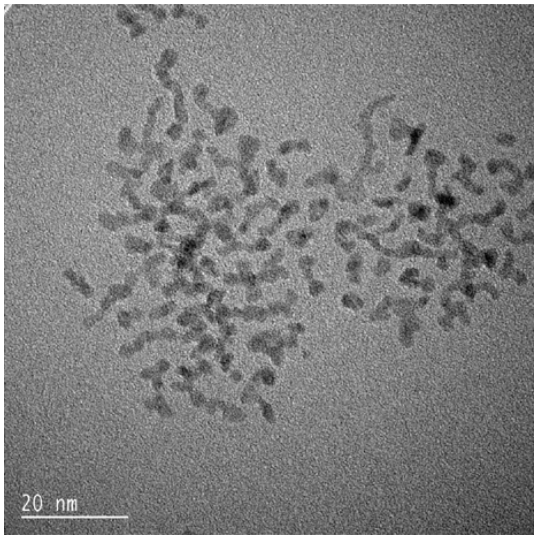

Figure 5-31: Transmission electron micrograph of Ru particles stabilised with 0.2 eq HDA showing the elongated aspect of the particles after 48 hours

It is difficult to measure a size for such particles, but taking into account the shortest diameter, the mean diameter of the "worms" can be estimated at 2 nm. The particles also adopt the hcp structure of ruthenium, and a coherence length of 20 Å was found by WAXS which is in agreement with the size of the particles determined by TEM (Figure 5-32) The particles are crystalline.

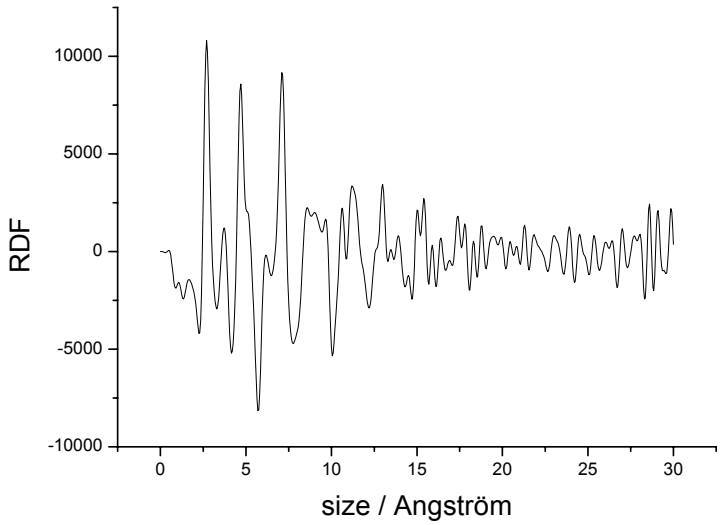

Figure 5-32: WAXS measurements of Ru nanoparticles stabilised with 0.2 eq. HDA

Upon increasing the relative concentration of the ligand 0.5 eq compared to ruthenium, the particles obtained seem to diverge quite obviously from the particles stabilised with only

0.2 equivalents HDA. Indeed, TEM micrographs (Figure 5-33) reveal that the particles are not agglomerated but seem to organise themselves into nanorods, which remain separated from each other. The formation of Ru nanorods could be favoured by a better organisation of the HDA when present in higher quantities in the reaction mixture. Some areas of the grid display parallel rods. The nanorods are regularly dispersed on the grid.

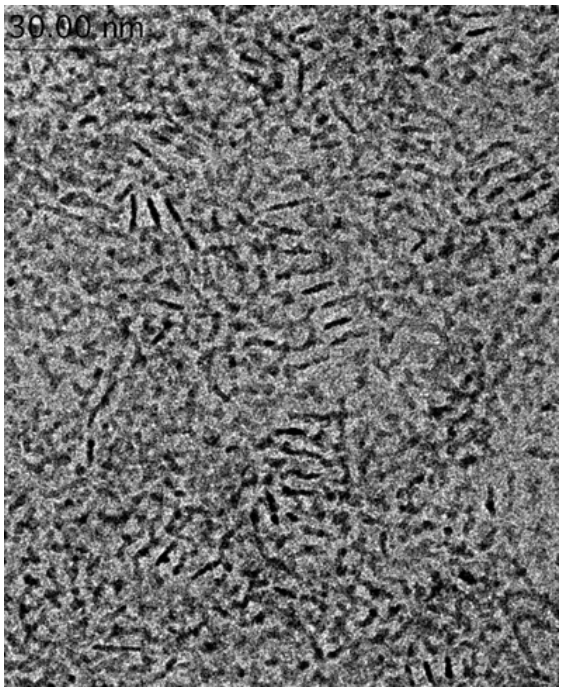

Figure 5-33: TEM micrograph of Ru nanoparticles stabilised with 0.5 eq. HDA

It is difficult to measure a size for such particles but still the diameter of these "worms" can be estimated to 2.4 nm. WAXS analysis (Figure 5-34) performed on these colloids confirmed the crystalline character and the hcp structure of the particles. After evaporation of the solvent, they do not form a fine precipitate, probably because of the excess of ligand which makes the material sticky.

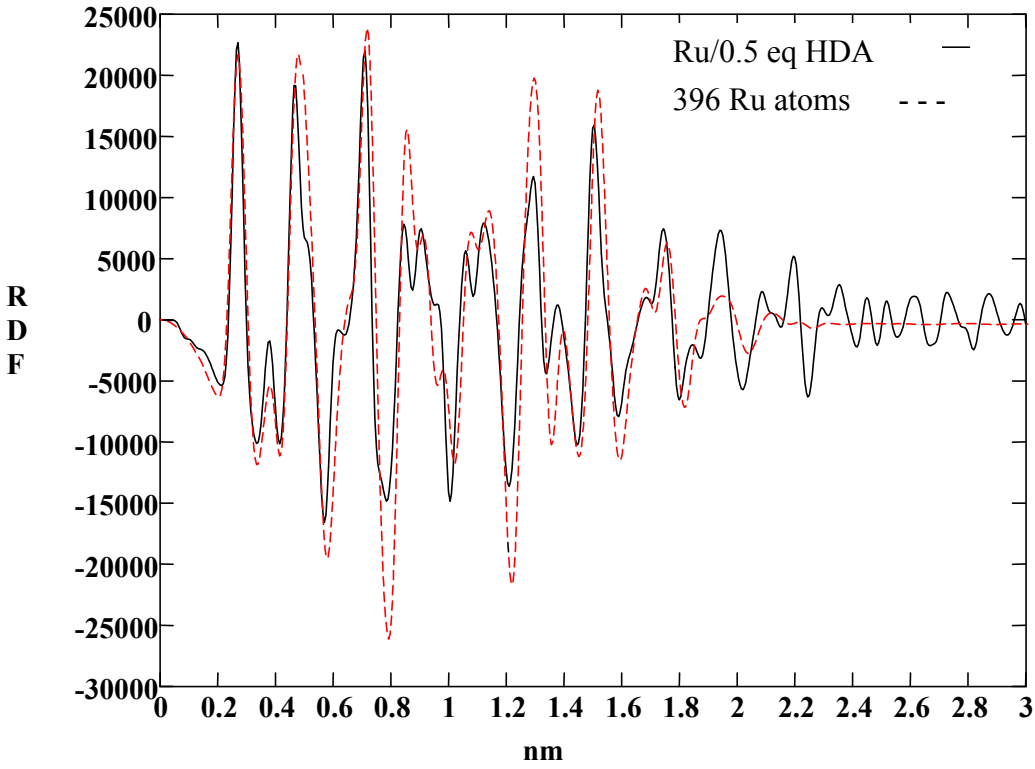

Figure 5-34: Comparison between a model of 396 Ru atoms adopting the hcp crystal structure (----) and Ru particles stabilised by 0.5 eq of HDA (—)

When the amount of the stabilising agent was later increased up to 1 eq a development in the shape of the particles took place. All the solutions were stable and homogenous, but for the purification of the particles some difficulties were experienced. The particles do not precipitate easily in cold pentane and it was not possible to separate them from the excess of ligand. The TEM micrograph (Figure 5-35) reveals spherical particles with a mean diameter of 2.6 nm. WAXS experiments confirmed the presence of metal ruthenium particles with hcp structure and a coherence length of 2.6 nm was determined. The increasing concentration of stabilising HDA does not seem to favour the formation of nanorods.

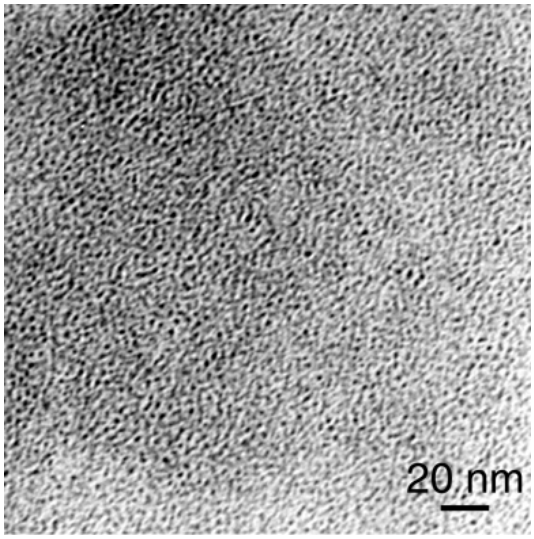

Figure 5-35: TEM micrograph of Ru nanoparticles stabilised with 1 eq. HDA

In the presence of larger amounts of 1-aminohexadecane (5 and 10 eq), TEM micrographs revealed the presence of cloudy agglomerates in which isolated nanoparticles could not be seen. The particles seem to be embedded in a large ligand matrix which makes their observation impossible. The influence of the quantity of ligand become more evident in this case.

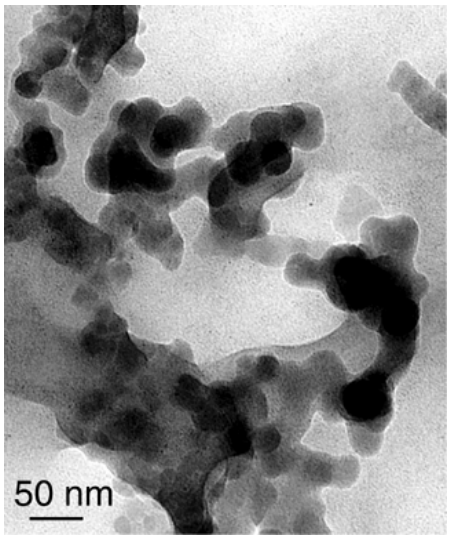

Figure 5-36: TEM micrograph of Ru nanoparticles stabilised with 5 eq. HDA

The different results obtained in the presence of various quantities of HDA are summarised in Table 5-15. The mean diameters of the particles increase with the added ligand quantity from ~ 1 nm for 0.04 and 0.06 eq HDA to 2.6 nm for 1 eq HDA. Upon increasing the relative concentration of the ligand compared to ruthenium, the aspect of the particles

evidenced a tendency to form "worms". It is difficult to determine a size for such materials, but a mean diameter of the "worms" could be measured.

Table 5-15: Summary of results obtained after colloid synthesis through hydrogenation of Ru(COD)(COT) by 3 bar H_2 in the presence of HDA as stabilising agent

HDA / eq.	Size / nm (TEM)	Coherence length / nm (WAXS)	Ru / %	N / %	Shape	Superstructure
0.04	approx. 1	-	-	-	spherical agglomerates	not stable
0.06	approx. 1	-	-	-	spherical agglomerates	not stable
0.1	1.9	1.9	50.4	1.37	spherical	little stable
0.2	2.0	2.2	53.2	1.45	elongated	-
0.5	2.4	2.5	52.5	2.65	nanorods	organisation of rods
1	2.6	2.6	53.1	2.33	elongated	-
5	-	-	-	-	not detectable	cloudy
10	-	-	-	-	not detectable	cloudy

WAXS analyses could be performed in the solid state on almost all the colloids prepared in the presence of HDA, except for colloids with a high excess of amine (> 0.5 eq), which were found to be too sticky. Therefore, WAXS analyses were performed in these cases on the colloidal solutions. In each case, the particles are crystalline and adopt the hcp structure of bulk ruthenium. The coherence length is found to be above 2 nm revealing a size larger than those found in polymers.[34] Examples of RDF of colloids stabilised by 0.1 eq (Figure 5-28), 0.2 eq (Figure 5-32) and 0.5 eq (Figure 5-34) of 1-aminohexadecane have been separately shown. They confirm the hcp structure of the particles and the similarity of the RDF obtained for the particles prepared using various quantities of this amine. Figure 5-37 evaluates the results for the particles obtained with 0.2, 0.5 and 1.0 eq. of 1-aminohexadecane.

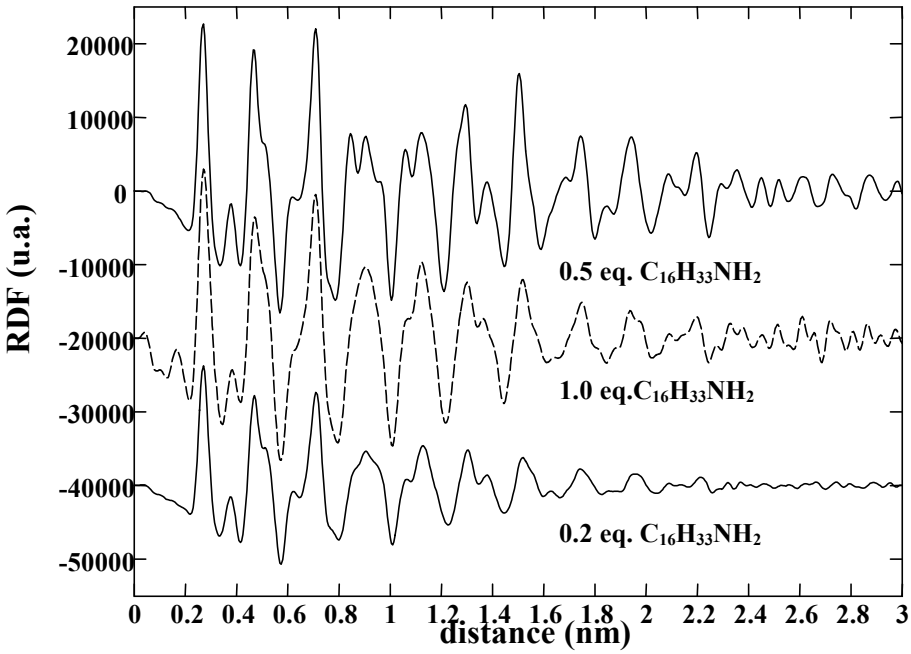

Figure 5-37: Experimental RDF of Ru particles stabilised by 0.2, 0.5 and 1.0 eq HDA

The coherence length of the particles increases with the increase in the concentration of added ligand from 2.2 to 2.6 nm. The "vermicular" aspect of the particles as shown by TEM is surprising, as is their tendency to grow in diameter with increasing ligand concentration.

5.2.1.4 Conclusion

In summary, amine ruthenium nanoparticles are easily prepared at room temperature by hydrogenation of the organometallic precursor Ru(COD)(COT). The particles can be stabilised by long chain amines to give, after appropriate work-up, colloids which can be obtained as powders and handled like molecular compounds. The colloids adopt different dispersions on the microscopy grid, although the alkyl chains are similar and the functional group is the same.

The possible organisation of the amines in THF could influence the growth of the ruthenium particles in the solution and their tendency to present different aspects such as spherical particles and nanorods. In the case of 0.1 eq HDA/Ru the aspect of the particles is spherical, while in the case of 0.2 eq HDA/Ru a beginning formation of elongated particles can be observed which continued with the time. For the use of 0.5 eq HDA/Ru, the presence of nanorods could be stated.

This study demonstrates application of traditional techniques of characterisation of nanomaterials (TEM, HREM, WAXS). They provide useful information on the structure, the morphology and the dispersion of the nanoparticles. Such a study may help in designing nanoparticles of defined shape and organisation.

The previous studies showed that the quantity of the stabilising agent clearly has an influence on the growth of the metal particles, but the manner of its attachment on the metal atoms as well as its behaviour is not yet understood. This led us to attempt to characterise precisely the mode of co-ordination of these ligands by methods commonly used in molecular chemistry, namely IR and NMR spectroscopy, as they could shed some light on the co-ordination of the ligand at the surface of the particles since this could be a factor related to the shape of the particles. By contrast, there are only a few reports available in the literature which concern the NMR characterisation of surface ligands. In an initial attempt, we have demonstrated that thiolate ligands are firmly fixed to the surface of ruthenium particles (see chapter 5.1).

5.2.2 Infrared studies

Via infrared analysis the presence of amine ligands at the particles surface and an influence of the metal surface on the vibration bands can be observed. This study has been performed on ruthenium particles stabilised with 0.2 eq HDA. The spectra of the colloidal powder have been registered in KBr. The comparison of the infra red spectra (Figure 5-38) of the free 1-aminohexadecane and the one of the stabilised colloid with 0.2 eq of that ligand after the usual pentane washing, attests to the presence of the ligand around the colloid. For the free ligand, a sharp signal at 3326 cm^{-1} for the $–NH_2$ group is detected while for the colloid a shoulder around 3300 cm^{-1} located under a broad water signal can be attributed to this group. The stretching bands for the $–CH_2$ groups of the alkyl chain around 2914 and 2843 cm^{-1} do not change. By contrast, the signals for the colloid are less sharp than for the free ligand. Two signals are observed for the colloid at 2035 and 1932 cm^{-1} which are not visible in the spectrum of the free ligand. These bands could possibly result from hydrogen species that could be present at the surface of the metal particles due to the precursor decomposition which was carried out under 3 bar H_2. However, this needs to be demonstrated.

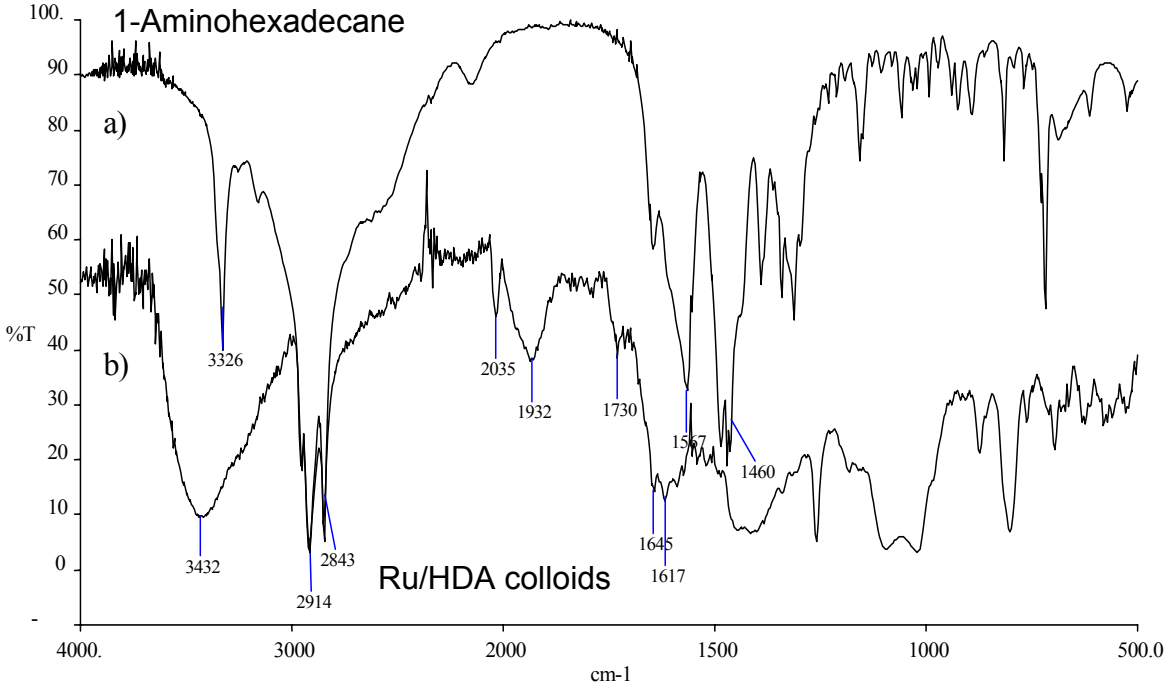

Figure 5-38: Comparison of the infra red spectra of a) 1-aminohexadecane and b) ruthenium nanoparticles stabilised with 0.2 eq 1-aminohexadecane

This observation made for these colloids is representative for all other amines used for the stabilisation of rutheium nanoparticles.

In conclusion of this point, infrared studies monitored the existence of the ligand at the surface of the particles: the corresponding bands are present in the experimental spectrum of the stabilised colloid. NMR studies were then begun in order to obtain more information about the co-ordination and the dynamic of the ligand at the surface of the particles since the behaviour of the ligands at the particles surface could not be explained yet.

5.2.3 NMR Studies of Ru / HDA colloids

Solution NMR studies were considered to help in understanding the mode of co-ordination and to study the arrangement of amine ligands on the particles surface. Previous studies had been carried out with gold particles.[43] The ^{1}H and ^{13}C NMR spectra of 1-octanethiol protected platinum[90] and ruthenium (chapter 5.1) nanoparticles demonstrated the absence of dynamics between free and coordinated ligands.

The NMR studies were carried out on a representative purified sample: the colloid stabilised with 0.2 eq $C_{16}H_{33}NH_2$ (HDA). The Ru/HDA particles were previously precipitated in cold pentane and finally washed several times to remove all unattached ligand. d^8-THF was chosen as the solvent because of the better solubility of the particles. ^{1}H NMR (400 MHz) and ^{13}C NMR (100.71 MHz) spectra could not be measured at lower temperature than room temperature, since the ruthenium particles have the tendency to precipitate in the NMR tube.

5.2.3.1 Solution ^{1}H NMR studies on Ru / HDA colloids

In Figure 5-39, a simulated ^{1}H NMR spectra of 1-aminohexadecane ($C_{16}H_{33}NH_2$) is shown which was calculated for a frequency of 400 MHz (Table 5-16).

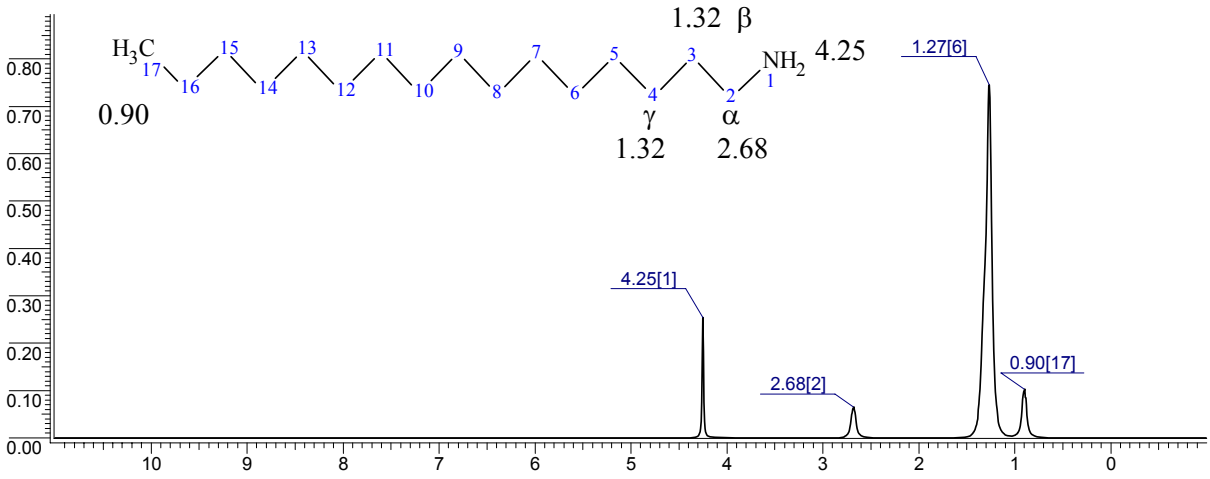

Figure 5-39: Simulated ^{1}H NMR spectrum (400 MHz) of 1-aminohexadecane($C_{16}H_{33}NH_2$)

Table 5-16: Calculated ^{1}H NMR data of 1-aminohexadecane ($C_{16}H_{33}NH_2$)

Group	17 (CH_3)	5 - 16	4(γ)	3(β)	2(α)	1
Number H	3	24	2	2	2	2
Chem. shift / ppm	0.90	1.26-1.29	1.32	1.32	2.68	4.25

The ^{1}H NMR spectrum (Figure 5-40) obtained for Ru colloid stabilised with 0.2 eq HDA, only shows the methyl groups of the ligands near 0.92 ppm and broad peaks for the methylene groups of the alkyl chain between 1.25 and 1.4 ppm but not the peaks attributed to the protons next to nitrogen that means the α-position which are expected at 4.25 ppm. The peaks at 1.75 and 3.6 ppm result from the natural abundance of the solvent protons (THF). At 2.5 ppm a peak is specified as water protons which can be present in the solvent. In this spectrum a peak near 4.8 ppm is observed which can be attributed to H_2 gas dissolved in the solvent. The formation of dihydrogen is probably due to the presence of hydrides at the metal surface, as already observed in the IR spectrum of the colloid. This will be discussed further in this work.

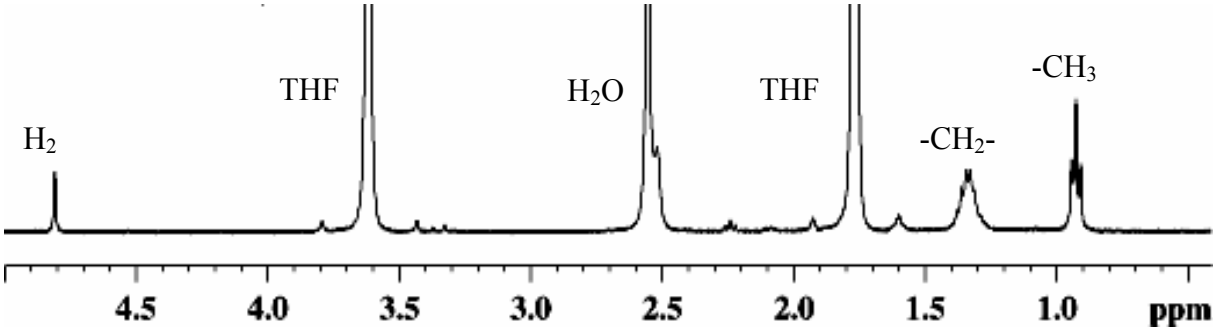

Figure 5-40: ^{1}H NMR spectrum (400 MHz, d^{8} THF, 293 K) of Ru colloid stabilised with 0.2 eq HDA

When small quantities of free ligand are added to the sample, variations can be detected on the spectra (Figure 5-41), depending on the ligand concentration. The peak near 0.92 ppm for the methyl group increases and the one corresponding to the methylene groups between 1.2 and 1.5 ppm begins to sharpen giving a more well-defined peak.

A signal near 2.6 ppm can be attributed to the α-CH_2 group. It sharpens with the addition of free ligand in the NMR tube. The protons in β- and γ- positions are not easy to detect, because of their location under the signals of the alkyl chain protons between 1.3 and 1.6 ppm.

The sample was then heated up to 333 K. In that case, we could observe a displacement of the water signal at 2.5 ppm undergoing then a better observation of the expected peak for the α- protons near 2.7 ppm. Even with a large excess of free ligand the peak corresponding to the $–NH_2$ group is not visible. Table 5-17 summarises the obtained results.

Table 5-17: ^{1}H NMR data of 1-aminohexadecane after adding free ligand HDA

	Spectrum	Chemical shift / ppm				
Carbon		$(-CH_2)_n$	$-CH_3$	α	β	γ
Ru / 0.2 eq HDA	a	1.2 - 1.5	0.92	-	-	-
Ru / 0.2 eq HDA + 1 µL HDA	b	1.2 - 1.5	0.92	-	1.4	1.4
Ru / 0.2 eq HDA + 2 µL HDA	c	1.2 - 1.5	0.92	2.55	1.4	1.4

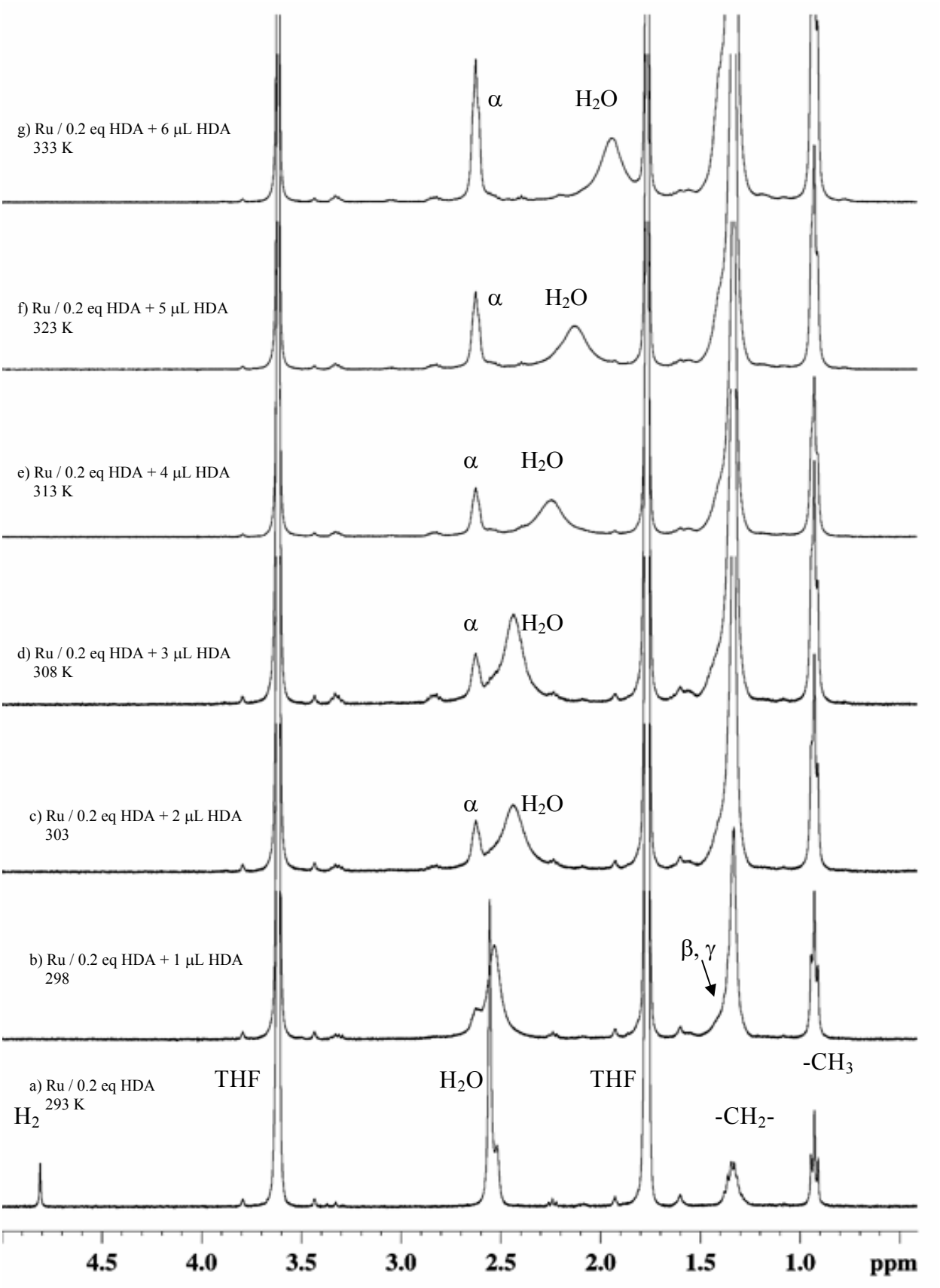

Figure 5-41: ^{1}H NMR (400 MHz, d8 THF, a)293 K, b)298 K, c)303 K, d) 308 K, e) 313 K, f) 323 K, g) 333K) of Ru / 0.2 eq HDA colloid and additional amounts of free ligand at various temperatures

In conclusion of this study, one can say that the ligand is present at the surface of the particles, and that it is attached by the amine group to the metal surface since on the spectrum of the purified colloid, the protons in α-, β- and γ- position can not be detected by NMR due to chemical shift anisotropy resulting from the slow tumbling of the particles in solution.[43] These peaks only become visible in the presence of added ligand in the NMR tube. In addition, the methyl signal increases when the ligand concentration is higher. It can be suggested that this phenomenon is due to an exchange of ligands between ligands attached at the surface and free ligands in solution. Only the free ligand tumbling in the solution can be observed, as well as the end of the long alkyl chain when a tumbling of the chain is possible.

At this level of the study, the peak corresponding to the dihydrogen seen in the first spectrum was no longer observed since the NMR tube was not sealed and the gas could escape from the sample. This point will be discussed further.

5.2.3.2 Solution ^{13}C NMR studies on Ru / HDA colloids

The ^{13}C NMR spectra are much more informative. The ^{13}C NMR spectrum (Figure 5-42) of 1-aminohexadecane has been calculated to compare the chemical shifts with the experimental spectrum (Table 5-18).

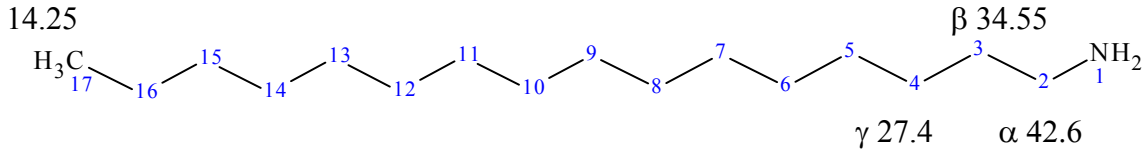

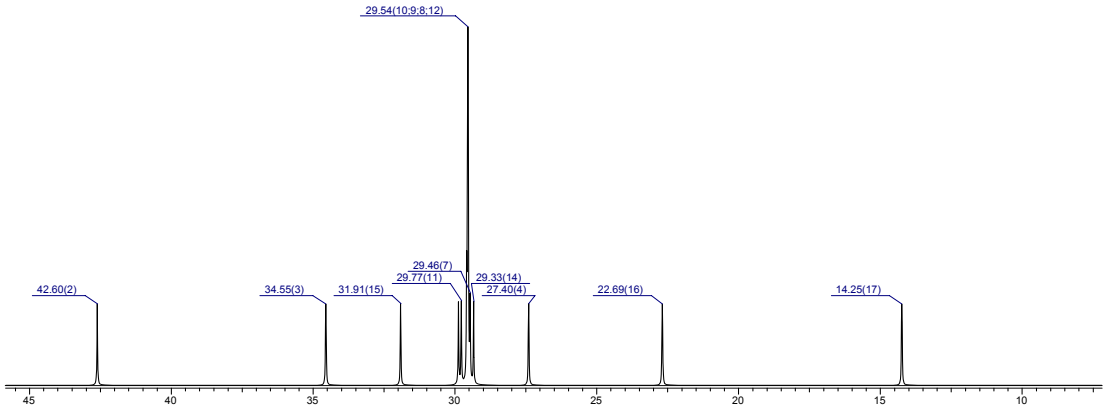

Figure 5-42: Calculated ^{13}C NMR spectrum of 1-aminohexadecane

Table 5-18: Calculated ^{13}C NMR data of 1-aminohexadecane($C_{16}H_{33}NH_2$)

Number	17 (CH_3)	16	15	5-14	4(γ)	3(β)	2(α)
CH_n	CH_3	CH_2	CH_2	CH_2	CH_2	CH_2	CH_2
Chem. shift / ppm	14.25	22.69	31.91	29.33-29.87	27.4	34.55	42.6

Figure 5-43 shows the room temperature spectrum of an isolated sample of the colloid Ru / 0.2 eq HDA, purified by precipitation and washing with pentane, as well as the effect of the addition of known amounts of excess HDA and finally the spectrum of pure HDA, all recorded in d^8-THF at 100.71 MHz and at the same temperature (303 K).

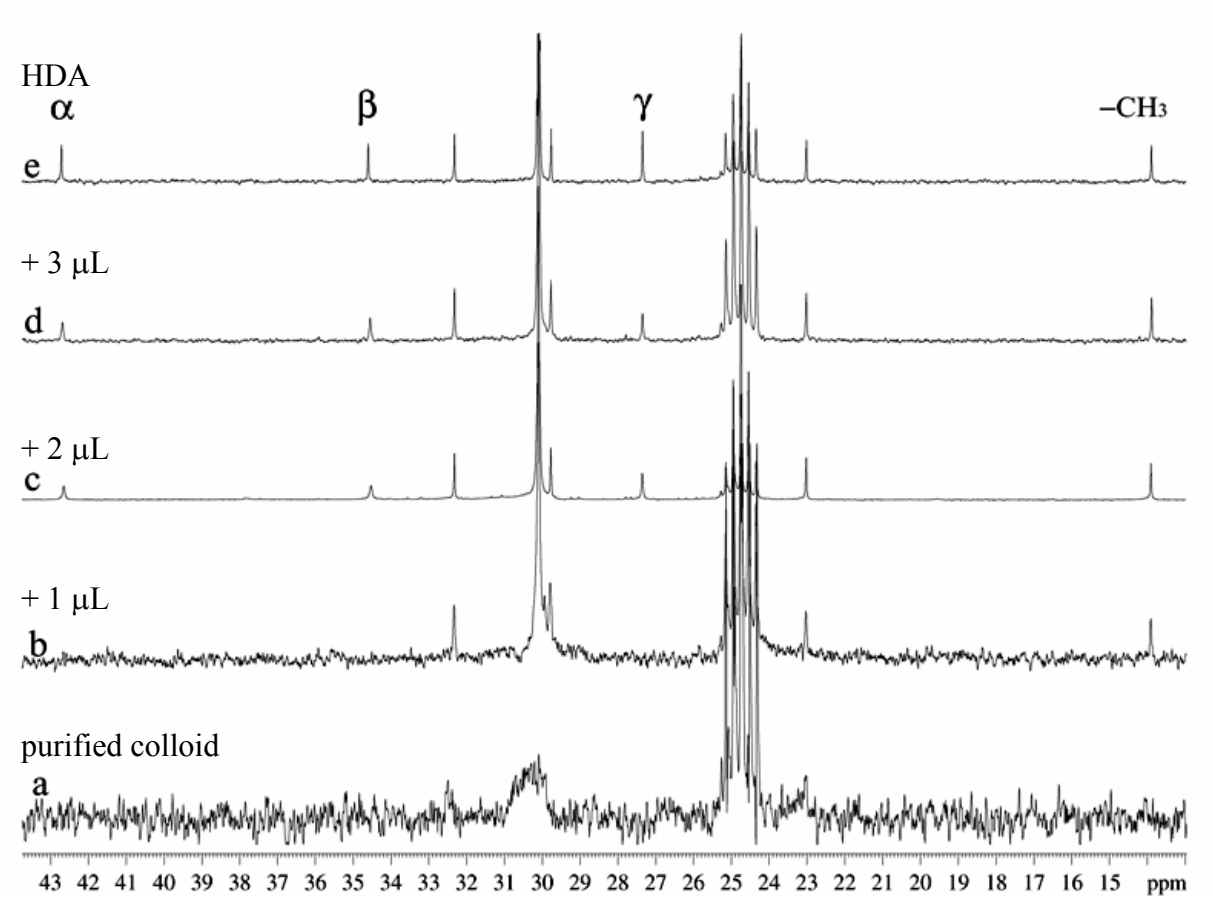

Figure 5-43: ^{13}C NMR spectra (100.71 MHz, d^8 – THF, 303 K) of a) Ru / 0.2 eq HDA, b) Ru / 0.2 eq HDA + 1 μL HDA, c) Ru / 0.2 eq HDA + 2 μL HDA, d) Ru / 0.2 eq HDA + 3 μL HDA, e) $C_{16}H_{33}NH_2$

The first spectrum (Figure 5-43 a) corresponding to the initial isolated colloid only shows three broad signals centred near 32.5, 30.5 and 23 ppm. These signals correspond to the methylene groups of the alkyl chain of the amine. Both the carbons located in α–, β– and γ– positions relative to the amino group and, more surprisingly, the carbon of the methyl group are not observed. In contrast, the ^1H NMR spectrum showed the peak for the -CH_3 group. Upon progressive addition of excess amine from 1 to 3 μL, one can observe first the sharpening of the methylene peaks at 32.3, 29.8, 23.0 ppm previously noticed on spectrum a) (Figure 5-43 b) and secondly the presence of a peak attributed to the methyl group at 13.9 ppm, but still no resonance for the α–, β– and γ– carbons. All the peaks observed are relatively sharp, but significantly broader than those of the free ligand (Figure 5-43 e), and resonate at the same place as those of the free ligand. Table 5-19 reviews the ^{13}C NMR chemical shifts for the studies realised with the Ru/0.2 eq HDA colloid and in the presence of added ligand and summarises the values obtained for the half-height width. The influence of the metal on the characteristics and the behaviour of the ligand at the surface is shown.

Table 5-19: Summary of the ^{13}C NMR data: chemical shifts for the colloid Ru / 0.2 eq HDA and the free ligand and the comparison of the variation of half height width between free and metal surface coordinated ligand for the Ru / 0.2 eq HDA colloid

		Chemical shift / ppm				Half height width / Hz			
Spectrum	Colloid/addition of HDA	α	β	γ	$-CH_3$	α	β	γ	$-CH_3$
a	Ru / 0.2 eq HDA	-	-	-	4.2	-	-	-	-
b	Ru / 0.2 eq HDA + 0.1 eq HDA	4.8	6.4	2.5	0.9	-	-	-	13.9
c	Ru / 0.2 eq HDA + 0.3 eq HDA	3.5	3.15	2.2	0.8	42.7	34.5	27.3	13.8
d	Ru / 0.2 eq HDA + 0.7 eq HDA	0.9	0.92	0.69	0.65	42.6	34.4	27.2	13.7
e	free HDA					42.5	34.3	27.1	13.6

When additional amounts of 1-hexadecylamine (2 et 3 µL) were added to the colloid, the peaks corresponding to the α–, β– and γ– carbons became visible at 42.7, 34.5 and 27.3 ppm but they present a half-height width broader than that of the other peaks and that found for the peaks of the free ligand (Figure 5-44).

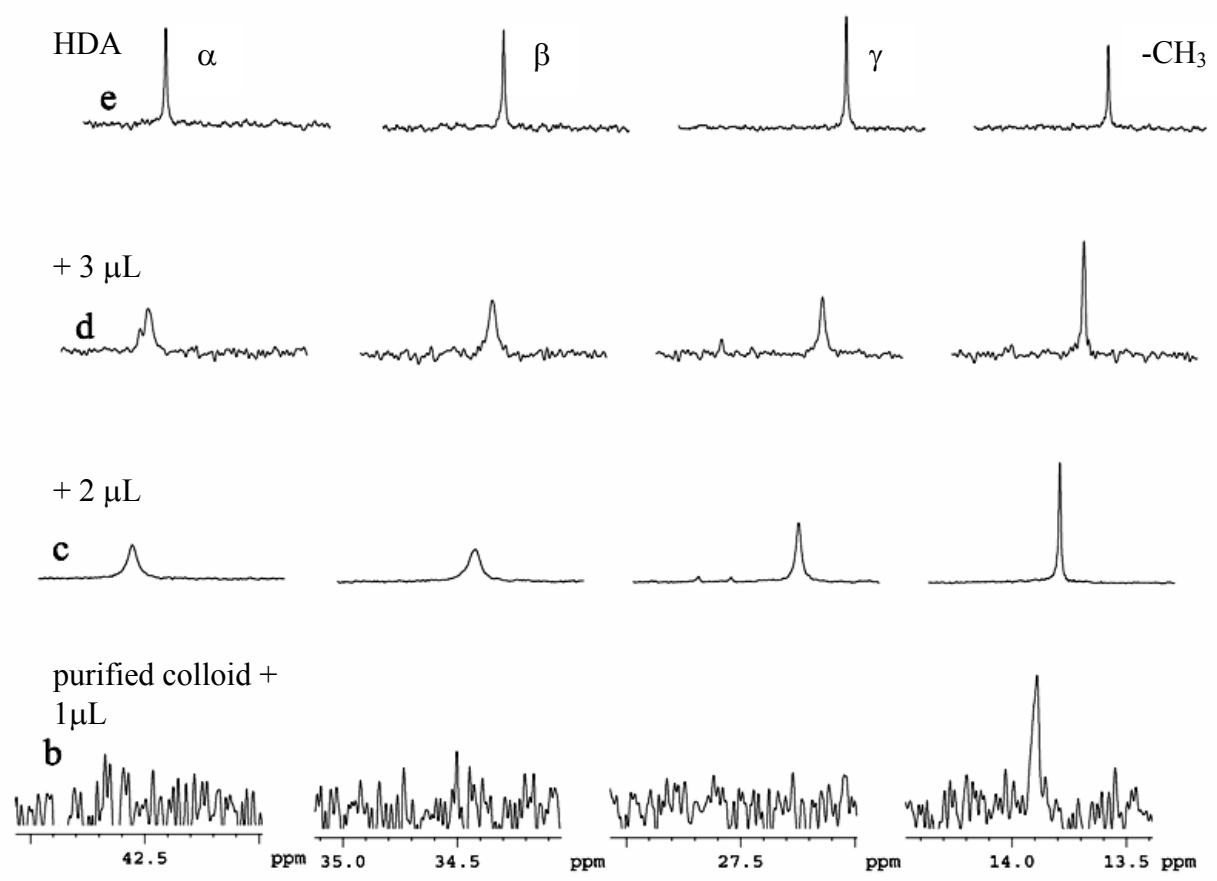

Figure 5-44: Enlargement of Figure 5-43 for comparison of the half-height width of the ^{13}C NMR spectra (100.71 MHz, d^8 – THF, 303 K) of b) Ru / 0.2 eq HDA + 1 μL HDA, c) Ru / 0.2 eq HDA + 2 μL HDA, d) Ru / 0.2 eq HDA + 3 μL HDA, e) $C_{16}H_{33}NH_2$

The half-height width of the signals of the free ligand is smaller than that observed for the ligand peaks surrounding the colloid. In addition, a displacement of the chemical shift for the groups of the ligand attached to the particle surface to the high field is noticeable because of the influence of the metal.

The interpretation of these results is the following : when only a small amount of HDA is present in solution, the α–, β– and γ– carbon resonances are missing because of the proximity of the metal core. This phenomenon has been observed previously for gold and platinum colloids and is attributed to chemical shift anisotropy resulting from the slow tumbling of the particles in solution.[43,90,110,110] The α–, β– and γ– carbons are in proximity to the metal surface due to the NH_2 group which is attached to it. Addition of excess ligand leads to the appearance of the resonances of the α–, β– and γ– carbons but they present a half-height width broader than that of the other peaks. Further addition of amine leads to the sharpening of these resonances. This observation is characteristic of a fast equilibrium at the

NMR time scale between two species; in the present case, free and coordinated amines. Attempts to observe a decoalescence of the exchange process at low temperature have failed because of precipitation of the colloids and of the HDA in the NMR tube. Only by using a larger amount of ligand is it possible to achieve a good solubility of the particles. Therefore the accumulation time for the NMR often varied by several hours to one night at room temperature.

There is one more interesting observation: when a very small amount of ligand is present (Figure 5-43 a) neither the α–, β– and γ– carbons nor the methyl group are detected for the purified colloid but some methylene carbons of the chain are observable. Only in the first spectrum can the $–CH_3$ group not be seen. The $–CH_3$ group becomes visible upon addition of free ligand to the NMR tube. An hypothesis could be that the end of the long alkyl chain is not yet attached to the metal surface, therefore the signal for the $–CH_3$ group would become visible in the spectrum due to its fast tumbling. This might be due to a bending of the group towards the surface of the metal where an interaction could take place and make the detection of the protons impossible by NMR. This suggests that for a very low HDA content, there may be a coverage of the ruthenium surface by the ligand and an interaction of the methyl groups with free Ru atoms, perhaps through an agostic interaction, well-known in molecular chemistry. That would explain why the carbon of the methyl group is not observed on the NMR spectrum at this low quantity of HDA. Addition of a small amount of HDA then results in the displacement of this weak interaction by an amino group (Figure 5-45) and consequently the observation of the HDA methyl group as a sharp singlet thanks to its fast tumbling at the end of the alkyl chain. This scheme (Figure 5-45) illustrates the dynamics of the ligand at the surface as a function of the amine concentration.

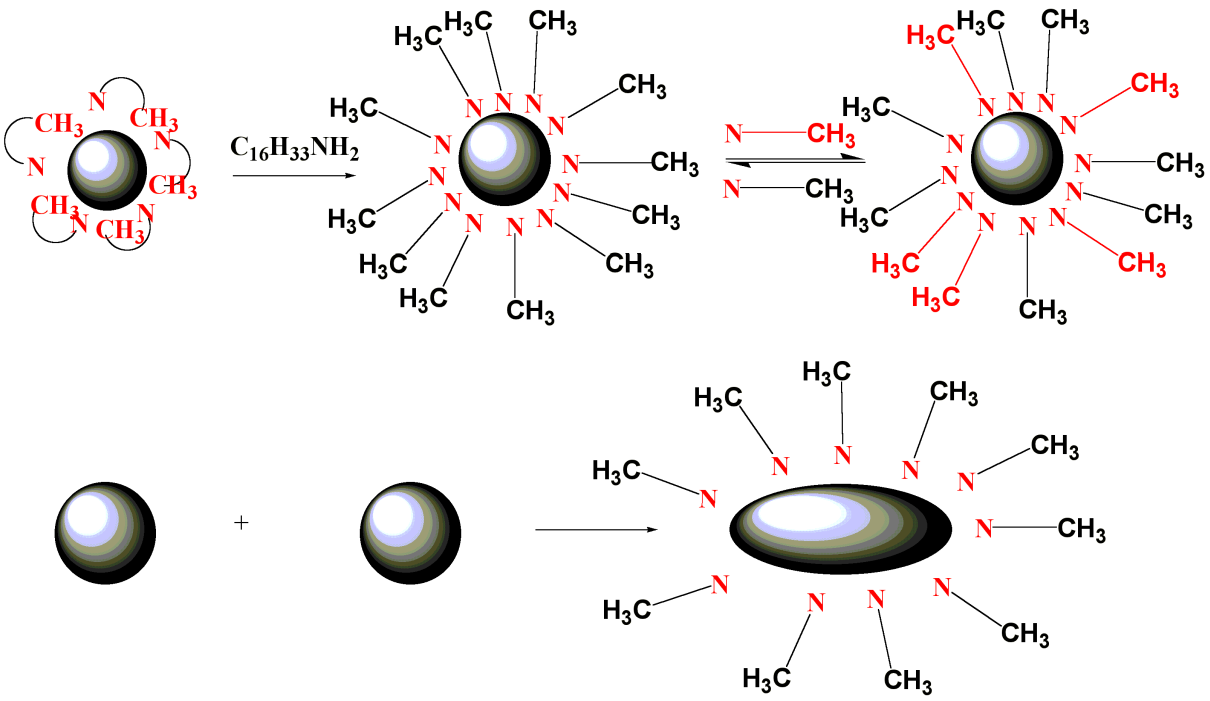

Figure 5-45: Hypothetical co-ordination of 1-aminohexadecane on ruthenium particles conducted by the amine concentration

In conclusion of this part, it can be stated that solution NMR experiments evidence a dynamic process at the surface of ruthenium nanoparticles between amine molecules which present a fast exchange at the NMR time-scale between free and coordinated ligand molecules. Bradley et al. have previously reported the dynamic exchange of ^{13}CO at the surface of palladium particles[135] and Schmid et al. the phosphine exchange at the surface of gold and rhodium particles.[136,137] The originality of the present system lies in the observation of both the signals for coordinated ligands and those of free ligands and for their rapid exchange. This result explains the different behaviours observed for nanoparticles accommodating these ligands, for example towards the coalescence in solution into "worm-like" structures as observed by TEM studies. The formation of "worms" could result from the co-ordination mode of the amine at the surface depending of its concentration in the reaction mixture and the possible coalescence between close particles as shown in Figure 5-45. One point stays to be discussed: the detection of hydrogen in the NMR tubes.

5.2.3.3 Discussion of the presence of dihydrogen by NMR studies on Ru/HDA

The formation of dihydrogen in the NMR tube could be stated for all the samples of amine-stabilised ruthenium nanoparticles that were studied: dissolved H_2 was identified by its chemical shift (4.8 ppm in d^8-THF) and its long relaxation time (T_1 = 2.1 s). This peak is not present immediately after dissolution of the particles, but it grows rapidly within one hour and then remains constant when the NMR tube was sealed. The presence of dihydrogen in the reaction medium was followed by ^{1}H NMR (Figure 5-46). The peak for H_2 at 4.8 ppm was observed from the beginning of the preparation of the NMR sample.

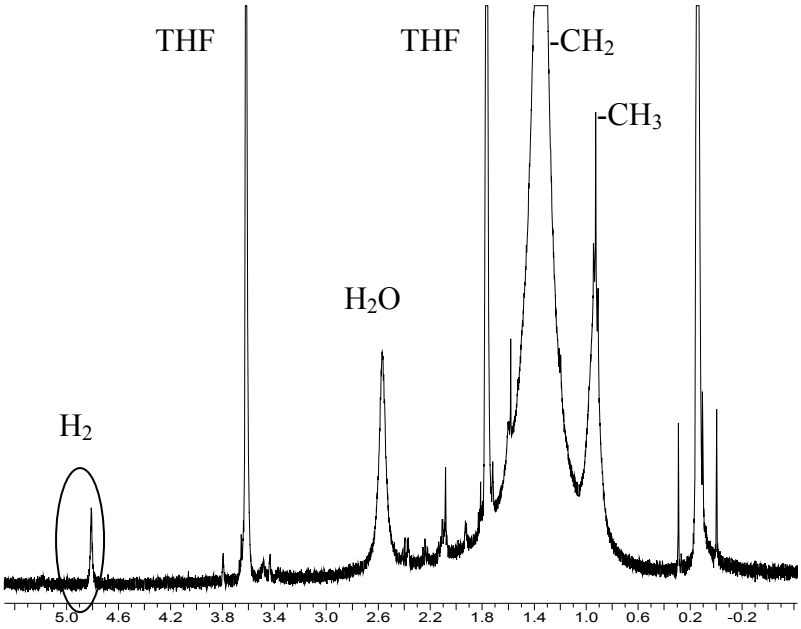

Figure 5-46: ^{1}H NMR (200 MHz, d^8-THF, 293 K) of Ru colloid stabilised with 0.2 eq HDA

In order to characterise this peak, some complementary experiments have been done (Figure 5-47). After two hours in the NMR rotor a reduction of the intensity of the peak attributed to dihydrogen could be detected (Figure 5-47 b). The addition of an excess of free H_2 by bubbling leads to an increase of the same signal as seen in Figure 5-47 c). It reappears at the same chemical shift and with the same shape / line width. If the NMR tube is opened under argon, the peak vanishes from the spectrum, probably because of a degassing of the dihydrogen from the solution (Figure 5-47 d).

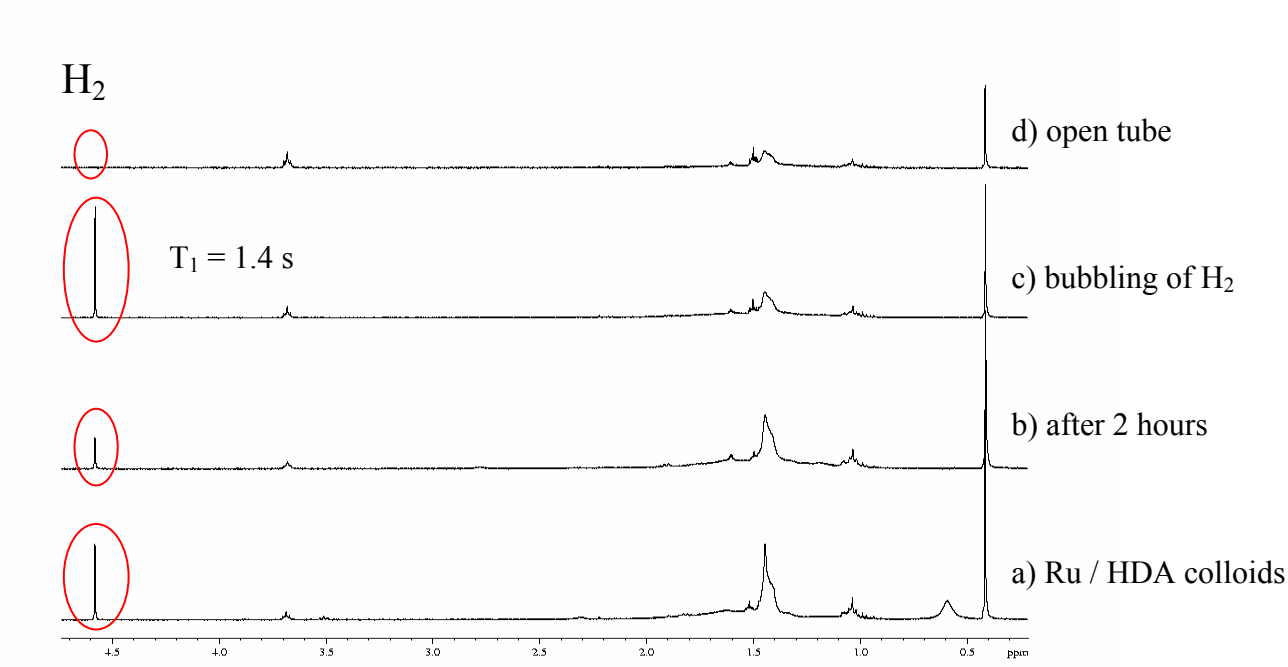

Figure 5-47: ^{1}H NMR (400 MHz, C_6D_6, 293 K): Pursuing of the H_2 peak at 4.6 ppm in presence of Ru / HDA particles

This phenomenon can therefore be attributed to dihydrogen desorbing from the particles. This suggests that surface hydrides are present on the initial colloid but disappear as a result of several factors, likely ones being competition with HDA and solvent for surface co-ordination and, possibly, the presence of water in the NMR solvent. By taking into account the IR results described in part 5.2.2, we can consider that hydrides might be attached to the active surface sites ensuing from the decomposition of the precursor. Hydrogen is released into the solution, resulting from the liberation of surface hydrides formed under this synthesis conditions. Figure 5-48 shows a hypothetical interaction of the amino ligand with the metal surface and the resulting liberation of dihydrogen in the solution.

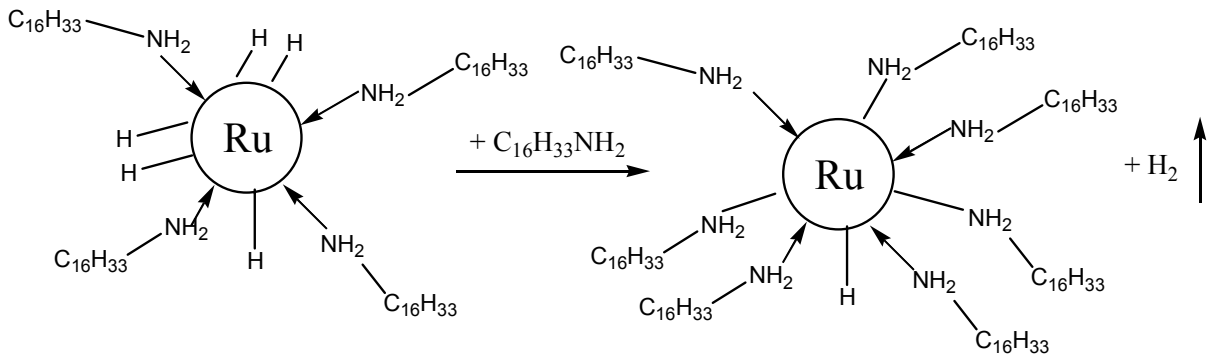

Figure 5-48: Hypothetical interaction of the stabilising amine on the metal surface: Formation of H_2

An interaction between these surface hydrides and the ligands and/or water in the reaction medium could also take place on the surface of the colloids undergoing the release of hydrogen.

In conclusion, ^{13}C NMR studies in d^8-THF led to the observation of a fast exchange between free and coordinated amine ligands. When a sample of Ru / HDA is dissolved in d^8-THF in a NMR tube and analysed after a standard degassing procedure, the ^1H NMR spectrum consists of broad peaks attributed to the alkyl chain of the amine with the notable exception of the methylene group adjacent to nitrogen. Upon leaving the tube in the NMR apparatus for a few minutes, a new peak becomes visible at 4.6 ppm which is attributed to free H_2. This peak rapidly reaches a maximum value and then remains constant. If the NMR tube is opened under argon, this peak disappears and if H_2 is bubbled into the NMR tube, it reappears at the same chemical shift and with the same shape/line width. The experiment is reproducible and suggests the desorption of H_2 from the ruthenium surface. Although the mechanism of this reaction is not known, it probably involves either thermally induced reductive elimination from the ruthenium surface or a reaction of the colloid surface with d^8-THF or traces of water present in it.

Solid state NMR spectroscopy was considered to obtain more information about the binding of the ligands and their mobility at the ruthenium surface.

5.2.4 Solid NMR spectroscopy: mobility of ligands on the surface

Metal nanoparticles are of great interest for current research because of their novel properties and their potential application in catalysis.[138,139] Most of these physical properties concern the core of nanoparticles. However, there is a growing need for characterising and understanding the surface chemistry which is known to have a strong influence on the physical properties of the particles.[68] Studies are progressively devoted to the controlled synthesis in solution of nanoparticles of defined size and shape, using for example long chain ligands in organic solution. But, there are only few reports available in the literature which concern the NMR characterisation of surface ligands.[43,108,110,108] In the previous section, it was demonstrated that solution NMR studies could help for characterising the surface of ruthenium nanoparticles stabilised by 1-aminohexadecane (HDA) and for understanding the shape evolution of these particles.[34] The following section is devoted to solid state NMR investigations.

Indeed, solid state NMR is a tool widely applied for the characterisation of compounds in the area of surface chemistry as organometallic compounds grafted on metal surfaces. Therefore, it could be assumed that this technique might be a good method to characterise the surface of ruthenium particles. Quantitative investigations of catalytic reactivity can also be investigated by gas phase NMR spectroscopy. As the catalysis takes place at the surface of the particles, a complete characterisation of the active surface sites is required. The nanoparticles investigated are Ru colloids which are stabilised by 0.2 eq 1-aminohexdecane for which the presence of the ligand and dihydrogen at their surface was observed by solution NMR. By solid NMR studies we expect more information concerning the structure of the particles' surface, the mobility of different surface species and the reactivity of surface hydrogen species.

This work was performed in collaboration with the group of Professor H.-H. Limbach at the Institut of Chemistry of the Freie University of Berlin in Germany.

5.2.4.1 Solid State ^{1}H and ^{13}C MAS NMR spectroscopy on Ru/HDA colloid

A definitive characterisation of the surface hydride would of course result from a direct observation. This is in principle possible given that ruthenium displays little or no Knight shift and the studied ruthenium particles are in the 2 nm range.

Solid state MAS NMR experiments were performed on Ru / 0.2 eq HDA particles after purification, in order to investigate the co-ordination of the protecting ligand HDA at the surface of the particles. Magic angle spinning was employed for these experiments to obtain a good signal resolution. The anisotropy of the chemical shift and dipolar coupling can be averaged by this method and a good resolution can be achieved. ^{1}H and ^{13}C NMR spectra were recorded and compared with the corresponding simulated spectra of the free ligand.

The ^{1}H MAS NMR spectrum of the nanoparticles and the simulated ^{1}H spectrum of the free ligand are shown in Figure 5-49.

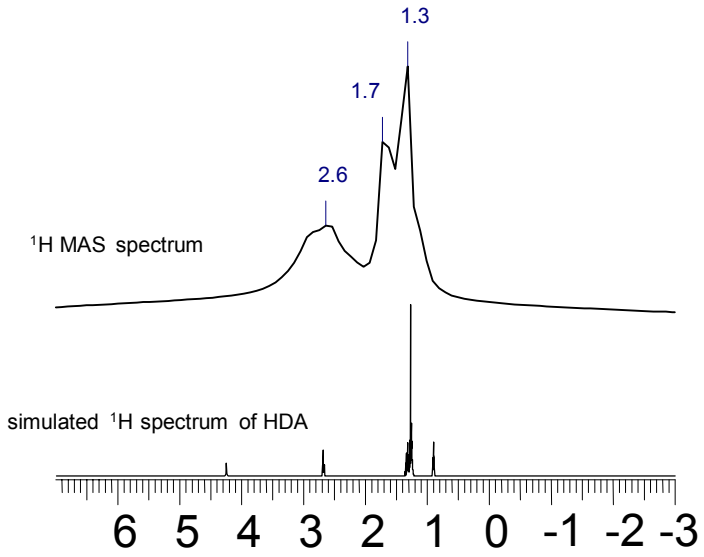

Figure 5-49: ^{1}H MAS NMR spectrum of Ru / 0.2 eq HDA and the simulated ^{1}H spectrum of HDA

The peaks of the recorded spectrum match well with the peaks of the simulated one. The peaks observed at 1.3 ppm and 1.7 ppm correspond to the $–CH_2$ groups of the alkyl chain of the amine. In contrast to the solution NMR spectrum of the Ru/HDA colloid, it is possible to observe the proton in α-position at 2.6 ppm. The small deviations of the chemical shifts can be explained by the interaction of the protecting ligand with the metal atoms at the surface of the particles. The signal attributed to the protons of the NH_2-group at 4.25 ppm is not visible. The absence of the peak corresponding to the NH_2-group has also been noticed by liquid NMR studies.[34] For solution NMR, this fact is related to the slow tumbling of the ligand at the surface of the metal particles.

The ^{13}C MAS spectrum with the corresponding simulated spectrum of the free ligand is represented in Figure 5-50. It presents a better match with the simulated spectrum than the ^{1}H spectrum.

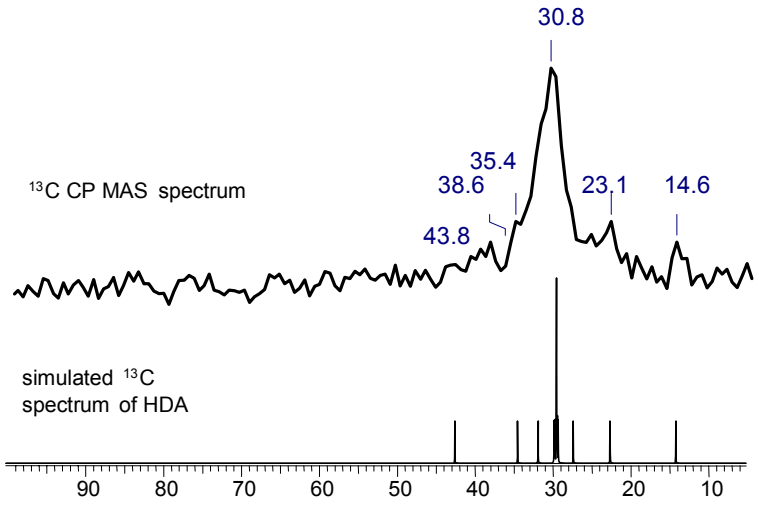

Figure 5-50: ^{13}C MAS NMR spectrum of Ru / 0.2 eq HDA and the simulated ^{13}C spectrum of HDA

The peak at 14.6 ppm can be attributed to the $-CH_3$ group at the end of the alkyl chain. The signal corresponding to the $-CH_2$ group is visible at 23.1 ppm for the carbon next to the methyl group. A large signal corresponding to the carbons of the alkyl chain can be observed at 30.8 ppm. The γ-carbon is probably hidden below this large signal. The signal at 35.4 ppm can be attributed to the β-group of the ligand. At 38.6 ppm another peak can be seen which is corresponding to the α-carbon. The signal is very broad and can not be clearly separated from the signal at 43.8 ppm. Nevertheless, a shift of this peak has to be noticed which is probably due to the influence of the metal surface on the ligand.

In ^{1}H NMR the relation between the signals and the background noise is much better because of the natural abundance of hydrogen which is 100 %. The nucleus is more sensible to the magnetic field.

The ^{1}H and ^{13}C MAS spectra of the nanoparticles are in agreement with the simulated spectra of the free ligand and show the co-ordination of the protecting ligand at the surface of the particles. The ^{13}C MAS spectrum of the colloid shows the expected signals for the carbons of the ligand shift where they appear in the free ligand, which fully validates the previous solution experiments and the presence of the ligand at the metal surface. The peaks are

between 38.6 and 43.8 ppm are very broad. This cannot be a result of its reduced mobility and so indicates the presence of magnetic interaction. The ^{1}H MAS spectrum only shows broad peaks corresponding to the hydrocarbon chain of the amine but no peak resulting from the NH_2 group and no signal which could be attributed to surface hydrides which could be hidden in the background noise or behind the signals of the protecting ligand. No direct evidence of a hydrogen surface species could be supplied by ^{1}H MAS NMR.

5.2.4.2 Deuterium exchange experiments

The previous IR and NMR studies on ruthenium nanoparticles using IR, solution and solid state NMR spectroscopy suggested the presence of hydrogen species. We attempted to characterise the surface hydrides by using different NMR techniques.

The question that had to be answered was whether H_2 was present on the surface of the colloids due to the synthesis conditions. Solid state MAS NMR studies after H/D exchange on the particles were applied to characterise the presence and the binding of hydrogen and deuterium species on the surface of the particles. Since H_2 was used as the decomposition agent in excess during the synthesis of the particles we attempted to determine how the hydrogen species are bound to the particles' surface. The mode of co-ordination and the question of H_2 or/and H adsorption at the surface have been investigated. The detection of a protonated surface species was not directly possible, therefore an H / D exchange was performed and a ^{2}H NMR spectrum was recorded. Since this signal could be hidden by the hydrocarbon ligands as well, the experiment was carried out again in ^{2}H NMR using a sample prepared as described above but treated with D_2 in solution immediately after the synthesis.

An exchange of H_2 with D_2 was then achieved by bubbling deuterium gas through the solution for 30 minutes in order to substitute possible hydrogen surface species by deuterium surface species. A ^{2}H MAS NMR spectrum of the nanoparticles was recorded after the H/D exchange , which is shown in Figure 5-51.

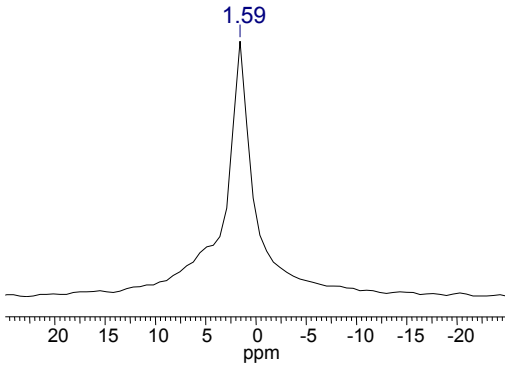

Figure 5-51: ^{2}H MAS solid state NMR Spectrum of Ru /0.2 eq HDA after H/D exchange by bubbling at 4 kHz rotating frequency

In this spectrum, a peak at 1.59 ppm with a full width at half maximum of 120 Hz (at a spinning frequency of 4 kHz) could be detected (Figure 5-51). Comparison of the chemical shift and the full width at half maximum with values of free D_2 (δ=4.46 ppm and $w_{1/2}$=126 Hz @ 4kHz sample spinning) (Figure 5-52) with the experimental spectrum confirm the presence of D_2. It shows that the signal of the deuterium species diverges from the D_2-gas signal by almost 3 ppm. This could be a consequence of the interaction of D_2 with the surface metal atoms. The observation of a D_2 signal different from the free D_2 gas is a consequence of the synthesis conditions (excess H_2).

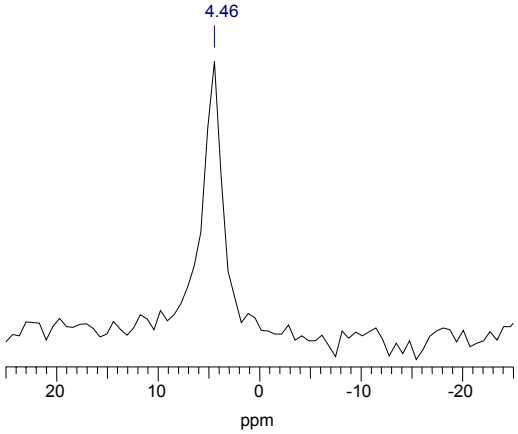

Figure 5-52: ^{2}H MAS solid state NMR spectrum of D_2 at 4 kHz rotating frequency

For colloid Ru / 0.2 eq HDA, D_2 on the surface could clearly be verified by solid state ^{2}H MAS NMR spectroscopic investigation and therefore supports the hypothesis of the presence of free adsorption sites on the surface of the nanoparticles. In addition, it demonstrates the accessibility of small molecules to these free sites.

5.2.4.3 Study of the mobility of surface species by solid state MAS NMR

Studies of the mobility of surface species are a very important part of catalysis research, because for catalysis the reactants have to coordinate to the catalyst's active sites before interacting together. If the bond is too strong, the adsorbed reactants cannot interact strongly enough with other reactants to form new molecules which desorb.

In order to gain information about the mobility of the deuterated surface species described in the previous section, spectra were recorded with different rotation frequencies. By stopping the rotation of the sample, the "simulated" motion of the molecules is switched off and only "real" motion affects the averaging of interactions. This means that the width of the NMR signals of rigid molecules becomes very broad when rotation is stopped, while the signals of mobile molecules remain relatively narrow.

^{2}H MAS NMR spectra of the 0.2 eq HDA ruthenium nanoparticles after the hydrogen / deuterium exchange were recorded at 4 kHz, 2 kHz rotating frequency of the sample and without rotation in order to gain some information on the mobility of the deuterated surface species which were detected previously. These spectra are shown in Figure 5-53.

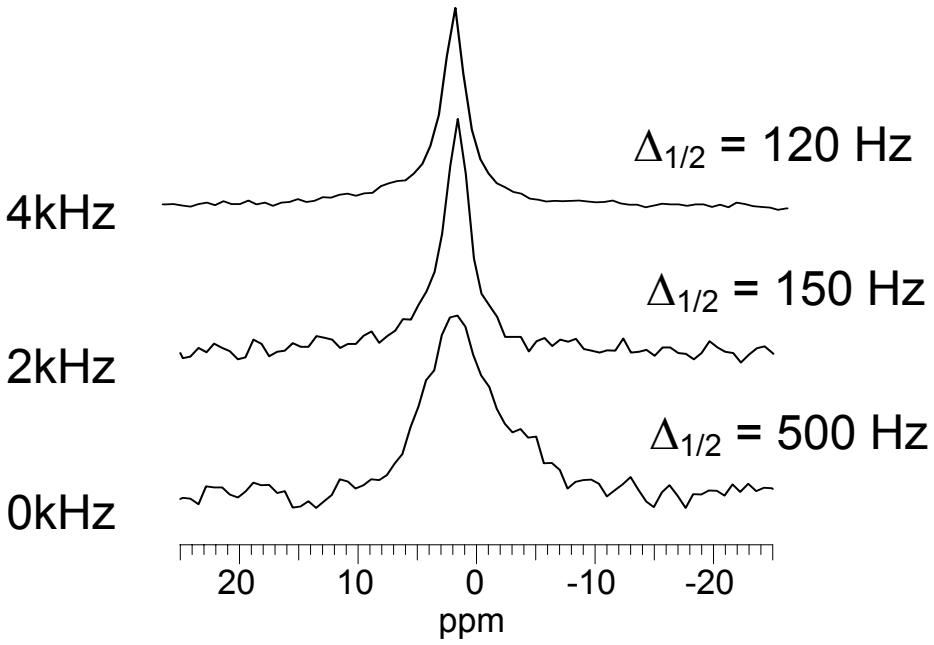

Figure 5-53: ^{2}H MAS solid state NMR spectra at various rotating frequencies of deuterated species at the surface of Ru / 0.2 eq HDA after H/D exchange by bubbling

The half intensity width (Δ1/2) of the signal of the deuterated species at 1.59 ppm increases from 120 Hz at 4 kHz rotating frequency to 150 Hz at 2 kHz rotating frequency and

reaches 500 Hz when the rotation is stopped. These values were compared on the one hand with half intensity widths of the signal of D_2 gas, as an example of a totally mobile system. On the other hand the values were compared with half intensity widths of a signal of the protecting ligand, as an example of a rigid system. The half intensity widths were obtained by analysis of ^2H (D_2 gas) and ^1H (protecting ligand) MAS NMR spectra of the nanoparticles. All half intensity widths are summarized in Table 5-20. The half-intensity width of the observed peak of the rigid protecting ligand increases greatly from 60 Hz at 4 kHz rotation frequency to 7800 Hz without rotation while the half-intensity width of D_2 gas hardly increases from 120 Hz at 4 kHz rotation frequency to 145 Hz without rotation. The growth rate of the half-intensity width of the deuterated species lies between those two "model systems".This result suggests that this species is well adsorbed to the surface of the nanoparticles, but seems to be very mobile on the surface. By contrast, the HDA at the surface of the particles is strongly fixed since the half-intensity width of the ligand without rotation is much higher than for the D_2 species (7800 kHz).

Table 5-20: Comparison of half intensity widths of surface species on Ru particles

MAS rotating frequency /kHz	$\Delta_{1/2}$ HDA	$\Delta_{1/2}$ D_2 at the surface (1.59 ppm)	$\Delta_{1/2}$ free D_2
4	60	120	120
2	65	150	130
without rotation	7800	500	145

From these results we can say, that information on the mobility of the ligand can be gained by recording solid state NMR spectra at different rotation frequencies and without rotation. By rotation of the sample along the magic angle, many interactions are averaged by a "simulated" motion of the molecules and signals narrow. By stopping the rotation of the sample, NMR signals of rigid species get very broad while those of mobile species stay relatively narrow. The line width of the deuterated surface species at different rotating frequencies and that comparison with the values of mobile and rigid model systems show that these surface species are well attached to the surface. However, they are very mobile on the particles' surface. Since the signal for hydrides could be hidden by the hydrocarbon ligands, the experiment was carried out in ^2H NMR using a sample prepared as described above but treated with D_2 in solution immediately after synthesis. In this case, a peak is clearly visible at 1.59 ppm ($w_{1/2}$=120 Hz). It differs from the peak of free D_2 recorded in a blank experiment

and which appears at 4.6 ppm ($w_{1/2}$=126 Hz) under similar conditions. In order to be able to attribute the peak at 1.59 ppm, we compared this signal to those corresponding on one side to the free ligand and, on the other, to that of D_2 in the gas phase at 3 different rotation rates, namely 4, 2 and 0 kHz. The results are shown in Table 5-20. It is clear that the signal at 1.59 ppm is not due to free D_2 but instead to a species displaying a large mobility on the ruthenium surface. We propose that this results from surface deuteride groups. Alternatively, it could result from a fast exchange between these groups and free D_2.

5.2.5 Study of Ru /HDA nanoparticles by ^{1}H gas phase NMR

Since it was not possible to detect the surface hydrogen on the nanoparticles directly with solid state MAS NMR spectroscopy, an indirect method was chosen to prove its presence on the surface. The Ru(COD)(COT) has been dedecomposed in the presence of 02. eq HDA in pure THF under 3 bar dihydrogen for 24 hours. The particles have been purified by precipitation in cold pentane and have been dried under vacuum for 24 hours before preparing the NMR sample.

The catalytic activity of colloids for the reaction H_2+$D_2 \rightarrow$ 2 HD was investigated both qualitatively and quantitatively by gas phase NMR spectroscopy. If a hydrogen species is adsorbed on the surface and if the ruthenium nanoparticles catalyses the reaction $H_2 + D_2 \rightarrow$ 2 HD, it should be possible to detect HD in the gas phase of an NMR tube which is filled with D_2 and the nanoparticles.

When the tube was sealed in vacuum, no H_2 signal was observed, even after heating at 360 K. However, when the tube was filled with D_2 at room temperature and the gas phase analysed by ^{1}H NMR, a peak rapidly grew at 4.5 ppm, reaching a maximum value after about 2 hours and then remaining constant (Figure 5-54). In Figure 5-54, ^{1}H gas phase NMR spectra before and during the reaction are shown. A peak at 4.5 ppm can be observed after 10 minutes of contact time between the reactive particles and D_2. This chemical shift could correspond to H_2 or HD. Measurement of the line-width of this peak gives a value of 230 Hz, and comparing with pure samples of H_2 (1200 Hz) and HD (200 Hz) strongly suggests that the gas observed is indeed HD, resulting from an easy H/D exchange reaction with surface hydrides. Furthermore, the amount of surface hydrides could in principle be quantified since the signal reaches a maximum value.

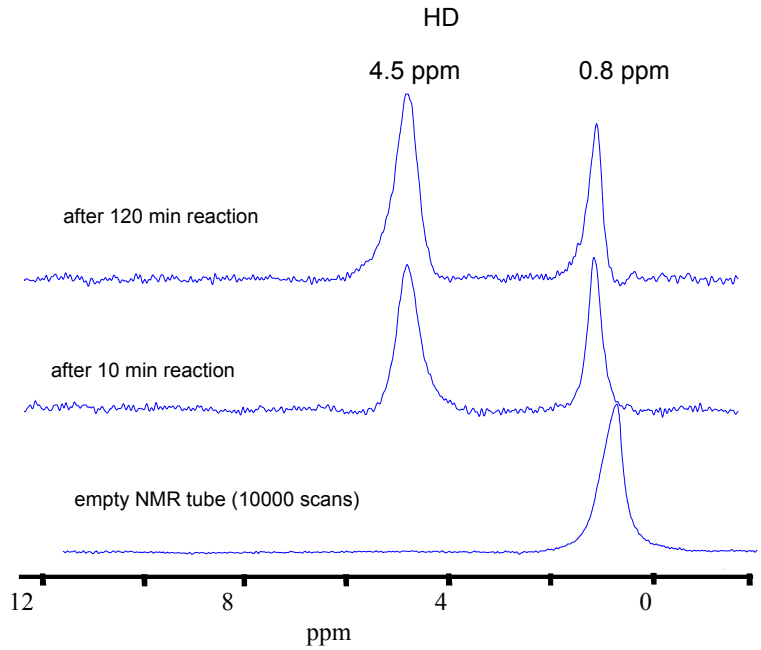

Figure 5-54: ^{1}H gas phase NMR spectrum before and during the reaction of Ru particles with D_2

The reaction $H_2 + D_2 \rightarrow 2$ HD could be quantitatively followed by ^{1}H gas phase NMR. The hydrogen was supplied by adsorbed hydrogen species on the surface of the nanoparticles. The evolution of the catalytic reaction in a glass sealed NMR tube (filled with Ru / 0.2 eq HDA and H adsorbed on the surface of the particles as shown above) and 600 mbar of D_2 gas was followed by ^{1}H gas phase NMR as shown in Figure 5-55.

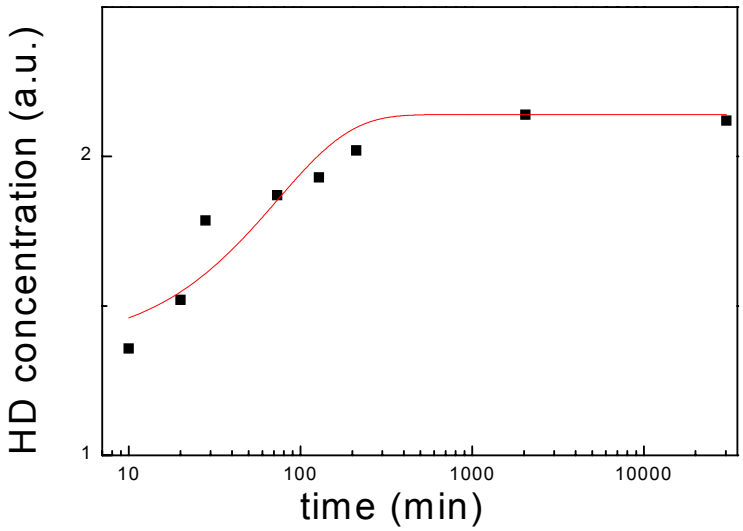

Figure 5-55: Evolution of the catalytic reaction $H_2 + D_2 \rightarrow 2$ HD on Ru/HDA colloids in a glass sealed NMR tube

In addition, a gas phase NMR spectrum of another NMR tube which was evacuated reveals no signal of H_2. Even after heating the sample up to 360 K no H_2 signal was detected. This excludes the possibility that the detected signal in the NMR tube with D_2 and the Ru nanoparticles results from desorbed H_2. This experiment proves the presence of H_2 on the surface of the particles.

5.2.6 Discussion

These studies demonstrate that the synthesis method commonly used, the hydrogenation of an organometallic precursor in the presence of an amine ligand, produces particles which accommodate both a coordinated ligand and surface hydrides. The presence of amine molecules and hydride species was observed by IR and NMR analysis.

By solution ^{1}H NMR studies the presence of the ligand at the surface of the particles could be confirmed. It could be stated that the ligand is attached by the amine group to the metal surface since on the spectrum of the purified colloid, neither the protons in α-, β- and γ-position nor the –NH_2-group protons can be detected by NMR. The observation of a peak at 4.8 ppm suggests the adsorption of H_2 onto the ruthenium surface.

Solution ^{13}C NMR showed that long chain amines are present at the ruthenium surface and that they are involved in a fluxional process that means a fast exchange at the NMR time-scale between free and coordinated ligand molecules. The solution NMR experiments evidence a dynamic process at the surface of ruthenium nanoparticles.

The ^{1}H and ^{13}C MAS spectra of the nanoparticles are in agreement with the simulated spectra of the free ligand and show the co-ordination of the protecting ligand at the surface of the particles.

H/D exchange experiments attest of the adsorption of hydrogen at the surface of the ruthenium particles stabilised with 0.2 eq 1-aminohexadecane. The *in situ* detection of the reaction was possible by gas phase ^{1}H NMR spectroscopy. The reaction could be followed quantitatively and furthermore, the presence of an adsorbed H-species was proven indirectly. In fact, the signal of HD at 4.5 ppm could be detected. The half intensity width of the detected species (about 230 Hz) was compared with those of H_2 (about 1200 Hz) and HD (about 200

Hz) to confirm the attribution of HD to this signal. It furthermore evidences the reactivity of the surface hydrides/deuterides for H/D exchange, which is present at room temperature, and the mobility of these hydrides/deuterides on the ruthenium surface.

In conclusion, after observation of the behaviour of amine ligands at the surface of ruthenium nanoparticles by infrared measurement, solution and solid state NMR studies, the indirect observation of hydrides at the surface was made by gas phase NMR. The catalytic reaction of $H_2 + D_2 \rightarrow 2$ HD could be quantitatively followed by ^1H gas phase NMR.

It is interesting to note that K. Honkala and J. Nørskov have recently calculated hydrogen adsorption energy on ruthenium surfaces.[140] The adsorption energy of a hydride on a flat Ru (0001)-surface is 0.38 eV on a fcc hollow and 0.25 eV on a bridge site whereas it is 0.49 eV on a step. The diffusion barrier on a flat surface is 0.126 eV. This data agrees with both the possibility of thermally induced dihydrogen desorption or substitution and with the observation of mobile hydrides on the ruthenium surface.

5.2.7 Conclusion for Ru particles stabilised with long chain amines

In summary, ruthenium nanoparticles are easily prepared at room temperature by hydrogenation of the organometallic precursor Ru(COD)(COT) in the presence of long chain amines as stabilisers.

Whereas the thiols are oxidatively added to ruthenium and excess thiol leads to the reductive elimination of disulphides which are released into the solution and do not exchange with the ligands present at the surface of the particles, the amine ligands exchange rapidly at the surface of the particles with free amines. This may be the reason why the colloids adopt such different structures and superstructures, even though the alkyl chains are the same and the functional groups similar. The alkyl chains of the sulphur ligands will encircle the particle and interpenetrate with the alkyl chains of other ligands, either free or located at the surface of other particles, leading to the formation of superstructures. The observation of a slow catalytic coupling of thiols into disulphides was described previously in chapter 5.1. They may be removed from the colloid surface. This is in agreement with recent observations demonstrating that the removal of ligands from the surface of gold particles force the particles to organise into superstructures.[141]

By contrast, the dynamics of the amine at the surface of the particle may allow the self-organisation of these amines, which are known to produce in water micellar arrangements and even hexagonal phases which are used for templating the synthesis of mesoporous materials.[142,143] The presence of some organisation of the amines in THF could allow the growth of ruthenium particles in the channels created and then explain the "vermicular" aspects of the particles stabilised with 1-amonihexadecane . Alternatively, the dynamics of the amines could also provoke changes in the co-ordination sites at the surface of the particles, and therefore the preferred co-ordination of the amine along the growth axis of the hcp structure, perpendicular to the basal plane. In any case, the dynamics of the amine will favour the coalescence of particles that were initially spherical shaped and consequently the formation of worm-like particles.

This study demonstrates that the coupling of traditional methods for the characterisation of nanomaterials (TEM and WAXS) with simple methods of organometallic chemistry (NMR) may provide useful information on the chemical reactivity of the surface of the nanoparticles and shed light on elementary surface reaction steps such as substitution, oxidative addition and reductive elimination.

Very few NMR studies have focused on such processes as dynamic ligand exchange at the surface of metal nanoparticles, and this is probably the first one relating the dynamics of coordinated ligands with the shape of the particles.

5.3 Stabilisation of Ru nanoparticles by chiral aminoalcohol and oxazoline ligands

When considering the field of asymmetric catalysis, the only systems that so far have displayed a selectivity comparable to that of molecular complexes associate cinchonidine to platinum particles, both in heterogeneous and colloidal catalysis.[144] The use of new systems associating metal nanoparticles and organic ligands for selective catalytic transformations is very attractive but not well studied yet. In order to adjust the properties of such materials in catalysis and to obtain reproducible catalytic activities, the particles must have a controlled size and surface composition. They should also be stable under the reaction conditions.

Stabilisers with nitrogen donor atoms such as chiral oxazolines, easily prepared from β-aminoalcohols were used for the stabilisation of ruthenium nanoparticles.[145] The application of these new colloids in different enantioselective catalytic processes, such as Ru-catalysed reduction of aryl/alkyl ketones have been studied.[146,147,148] Asymmetric hydrogen transfer from isopropanol to acetophenone is catalysed by Ru nanoparticles. β-aminoalcohols, shown to be excellent chiral auxiliaries in Ru-catalysed asymmetric hydrogen transfer processes, were also studied. This part describes the synthesis of new Ru nanoparticles stabilised by β-aminoalcohols and oxazolines. Preliminary results concerning their application in asymmetric hydrogen transfer and hydrogenation reactions will be given and compared to more conventional molecular systems in chapter 7.

Ruthenium nanoparticles can be stabilised by organic thiol and amine ligands as discussed previously (see for example parts 5.1 and 5.2).[34,149] Our capability to make reproducible small nanoparticles (between 1 and 10 nm) with a large surface area and a controlled surface composition, which are mono dispersed and stable in solution, suggests their preparation for catalytic applications. The catalytic properties of ruthenium nanoparticles in solution have been relatively little studied.[150] In order to test their potential in asymmetric catalytic reactions, chiral aminoalcohols and oxazoline ligands were considered for the stabilisation of Ruthenium nanoparticles. These types of ligands have been used in homogeneous catalysis for the last ten years.[151,152]

Although ruthenium molecular systems are extensively used in homogenous catalysis, ruthenium colloids as catalysts remain little investigated.[94,153,154] These systems could be used

with stabilisers containing nitrogen or oxygen donor atoms such as chiral amino and hydroxy oxazolines, easily prepared from β-aminoalcohols and carboxylicacid or nitrile derivates.[155,156,157] Their co-ordination chemistry to metal centres has been studied[158] for applications to different enantioselective catalytic processes,[151] such as Ruthenium-catalysed reduction of aryl/alkyl ketones.[159,160,161,162] β-aminoalcohols, previously shown to be excellent chiral auxiliaries in ruthenium-catalysed asymmetric hydrogen transfer processes were also studied.[163,164,165,166] This chapter describes the synthesis of new ruthenium nanoparticles stabilised by β-aminoalcohols and amino and hydroxy oxazolines.

Chiral ligands stabilised ruthenium colloids were prepared following the procedure previously described for ruthenium particles stabilised with more simple ligands like alcohols, thiols or amines but using asymmetric ligands as stabilisers. In a typical experiment Ru(COD)(COT) is dissolved in a Fischer-Porter bottle at 193 K in a THF solution containing 0.2 eq of the appropriate ligand L* (Scheme 5-4).[167,168] The resulting yellow solution is then exposed to a dihydrogen atmosphere (3 bar), allowed to warm to room temperature and left to react for 24 hours under vigorous stirring (Scheme 5-3). The stability of the ligands has previously been tested in these conditions and no C=N bond hydrogenation was undergone under H_2 pressure. The so-obtained brown colloidal solutions are stable for several weeks. The colloids can be purified by precipitation upon addition of pentane, filtration and drying in vacuum giving then dark brown powders which can be dissolved in THF or isopropanol. In all cases, the particles did not show any sign of decomposition and were then considered to be stable over time.

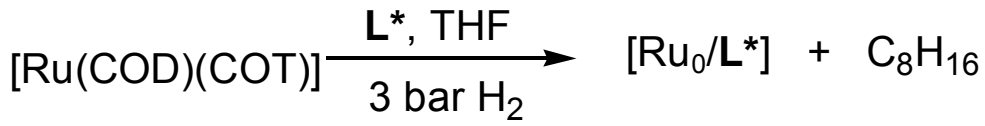

*Scheme 5-3: Decomposition of the organometallic precursor Ru(COD)(COT) in the presence of a chiral stabilising ligand L**

This work has been performed in collaboration with the Department of Inorganic Chemistry of the University of Barcelona, which provided the chiral ligands for the stabilisation of the Ru particles.

Three different types of chiral ligands have been used (Scheme 5-4):

I. β-aminoalcohols

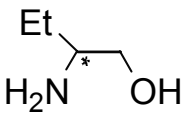

(R)-**1**

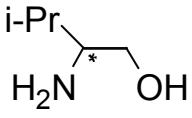

(S)-**2**

II. Mono-oxazolines:

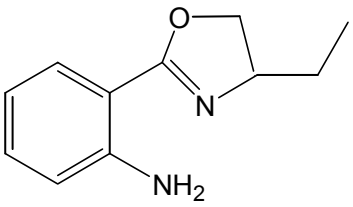

(R)-**3**

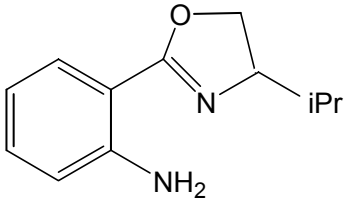

(S)-**4**

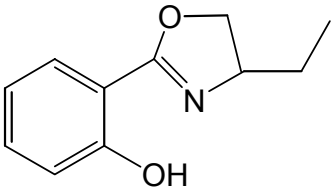

(R)-**5**

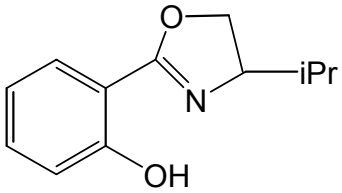

(S)-**6**

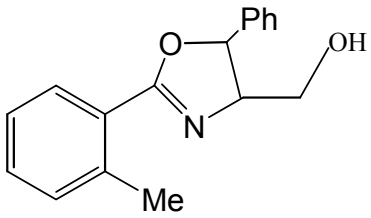

(S,S)-**7**

III. Bis-oxazolines:

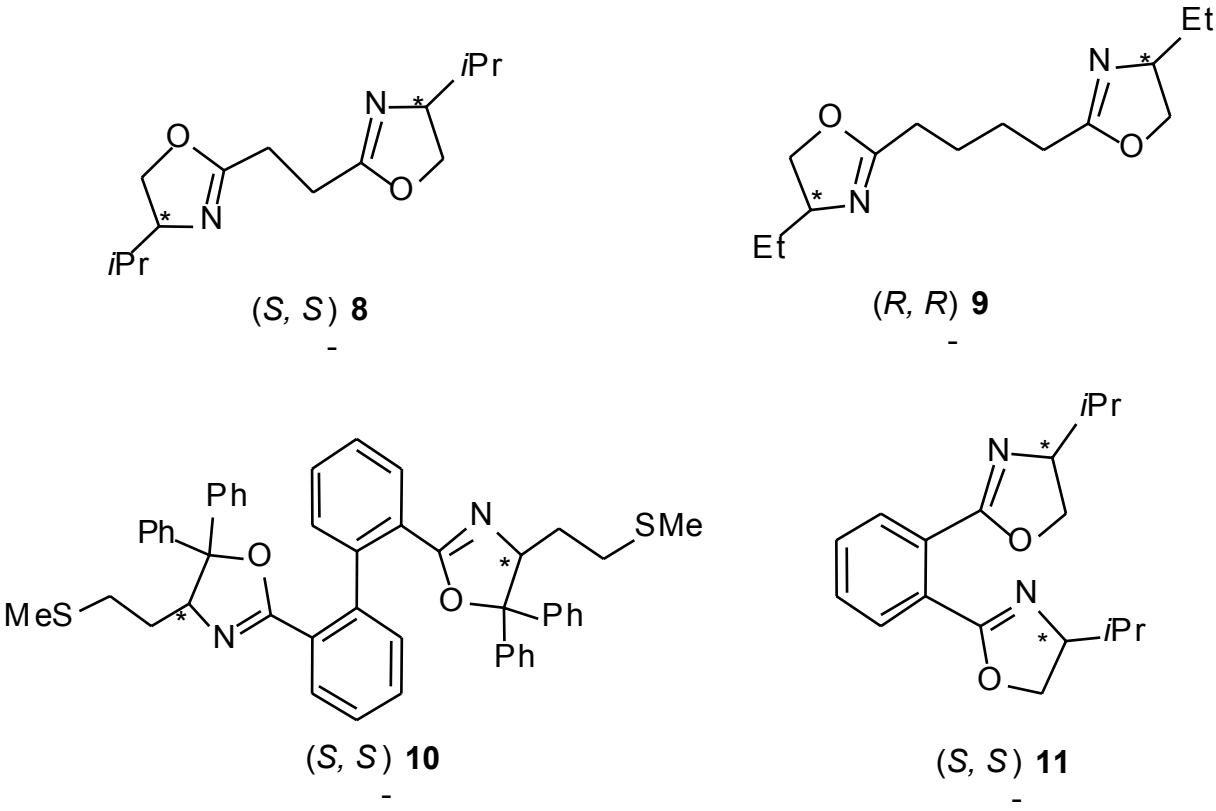

Scheme 5-4: Chiral ligands L employed for the stabilisation of ruthenium nanoparticles*

The following abbreviations will be used in the description of the Ru particles synthesis with these ligands as stabilising agents (Table 5-21):

Table 5-21: Employed aminoalcohols, mono- and bis-oxazolines for the stabilisation of ruthenium nanoparticles

I. β-aminoalcohols		
1	NH_2OH	(R)-(+)-2-aminobutanol
2	NH_2OHiPr	(S)-2-amino-3-methyl-1-butanol (L-Valinol)

II. Mono-oxazolines		
3	$MoxNH_2Et$	2-(4'R)-(4'-ethyl-3',4'-dihydrooxazol-2'-yl)-aniline
4	$MoxNH_2iPr$	2-(4'S)-(4'-isopropyl-3',4'-dihydrooxazol-2'-yl)-aniline
5	MoxOHEt	2-(4'R)-(4'-ethyl-3',4'-dihydrooxazol-2'-yl)-phenol
6	MoxOHiPr	2-(4'S)-(4'-isopropyl-3',4'-dihydrooxazol-2'-yl)-phenol
7	MoxOH-Me	2-(3'S, 4'S)-(3'-phenyl-4'-hydroxymethyl-3',4'-dihydrooxazol-2'-yl)-toluene

	III. Bis-oxazolines	
8	S,S-B	1,2-bis[(4'S)-(4'-isopropyl-3',4'-dihydrooxazol-2'-yl)]ethane
9	Bisox(CH_2)$_4$Et	1,4-bis[(4'R)-(4'-ethyl-3,4-dihydrooxazol-2'-yl)]butane
10	Bisox-SMe	2,2'-bis[(4'S)-[4'-(2-methylthio)propyl-3',3'-diphenyl-3',4'-dihydrooxazol-2'-yl]]
11	S,S-G	1,2-bis[(4'S)-(4'isopropyl-3',4'-dihydrooxazoly-2'-yl)]benzene

The several chiral ligands L*[169] bearing various functional groups like alcohols or amines (Scheme 5-4) have been used in the usually concentration ratio of 0.2 eq compared to the ruthenium and their influence on the size and shape of the nanoparticles was studied. The use of 0.2 eq ligand compared to the ruthenium was optimised beforehand as described in chapter 5.1 and 5.2. Lower quantities of ligand did not stabilise the particles in solution, while for higher amounts of ligand the particles were found to be sticky due to the ligand excess and could not be purified further. For the characterisation of these new colloids, both material characterisation methods (transmission electron microscopy, X-ray scattering, IR spectroscopy, microanalysis) and solution NMR studies have been applied.

5.3.1 Ruthenium particles stabilised by aminoalcohol ligands

(R)-(+)-2-aminobutanol (1) is a commercial chiral ligand and (S)-2-amino-3-methyl-1-butanol (L-Valinol) (2) is easily obtained from the first one.[170] They contain both an amino and an alcohol group. Since these functional groups have previously been employed for the stabilisation of Ru particles, we believed that a combination of these two groups could favourably stabilise the particles. In addition, we thought about possible applications in catalysis with this chiral ligands. Therefore, the stabilisation of ruthenium nanoparticles has then been performed with these two aminoalcohols respectively named L* = NH_2OH (1) and NH_2OHiPr (2) (Scheme 5-4).

The TEM micrograph (Figure 5-56) obtained from the colloidal solution prepared in the presence of 0.2 eq of (R)-(+)-2-aminobutanol (NH_2OH) shows the presence of small particles of a regular round shape of approx. 2.5 nm mean size: some particles are isolated but most of them are integrated into large superstructures, which in some cases show signs of self-organisation suggesting the formation of hydrogen bonds. The decomposition of the

precursor was fast indicated by the colour change of the solution from yellow to brown. The particles can be purified by precipitation in cold pentane and a black powder could be obtained.

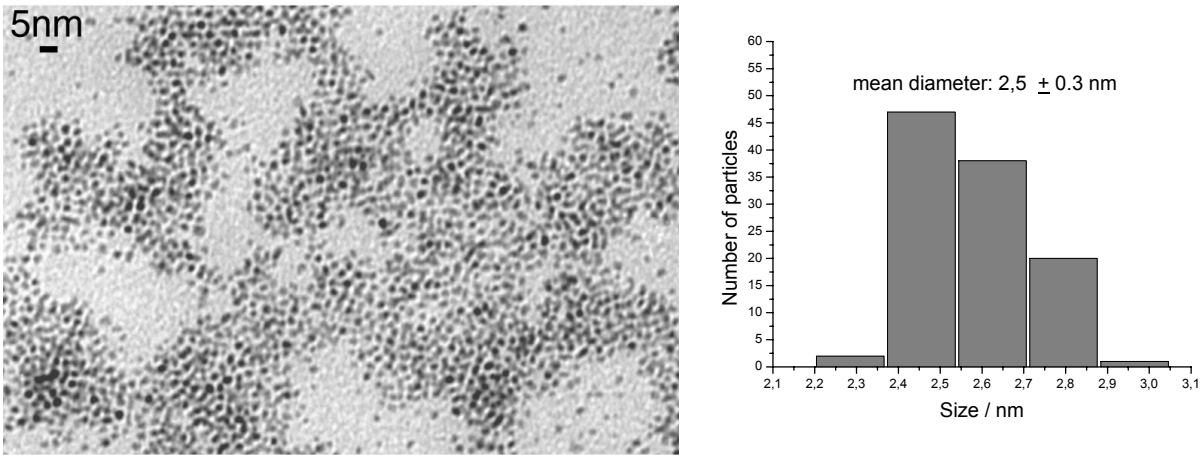

Figure 5-56: TEM micrograph and size histogram of Ru / 0.2 eq NH_2OH particles in pure THF

The infrared spectrum (Figure 5-57) of the purified colloid shows a similarity with the spectrum of the free ligand NH_2OH. The bands match up, which indicates the presence of the ligand at the colloids surface. Nevertheless, a variation of the bands can be noticed. This is a sign of the influence of the metal surface on the ligand.

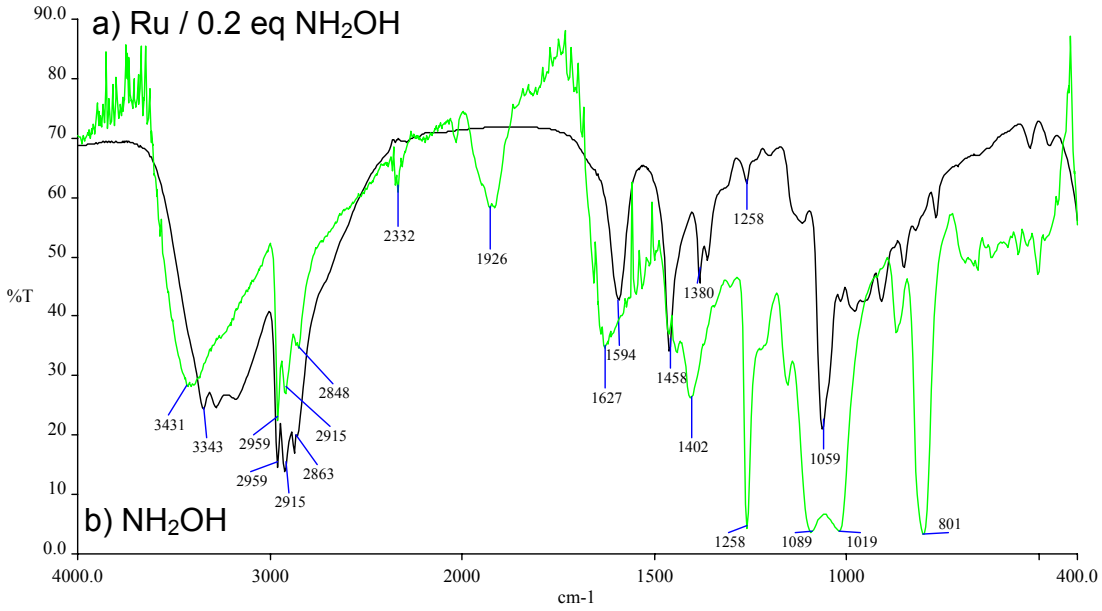

Figure 5-57: IR spectra of a) Ru / 0.2 eq NH_2OH colloids (KBr pellet) and b) free NH_2OH (NaCl cells)

Table 5-22: IR data for free NH_2OH and Ru / 0.2 eq NH_2OH colloids

ν NH_2OH / cm^{-1}	ν Ru / NH_2OH / cm^{-1}	Assignment
3343	3431	$-NH_2$, -OH
2959, 2915, 2868	2959, 2915, 2846	$-CH_2$
1594	1627	-C=N

Both spectra show in agreement the bands for the $-NH_2$ and the -OH group at 3343 cm^{-1} for the free ligand and at 3431 cm^{-1} for the stabilised colloid. The bands corresponding to the $-CH_2$ groups around 2900 cm^{-1} are also in conformity. The spectrum of the purified colloid shows a strong and large band at 1627 cm^{-1} which could correspond to the C=N stretching of the coordinated oxazoline. The sharp band for the free ligand is at 1594 cm^{-1}.The band at 1926 cm^{-1} is remarkable and could be attributed to Ru-H stretching. This suggests the presence of hydrogen at the particles surface as described in the previous section (see chapter 5.2).[171]

The presence of the ligand at the particles surface could be shown by elemental analysis (C = 7.6 %, H = 4.1 %, O = 1.2 %, N = 1.3 %).

The particles synthesised in the presence of 0.2 eq of (S)-2-amino-3-methyl-1-butanol (L-Valinol) (NH_2OHiPr) in 100 % THF present a regular aspect and a round shape as observed by the TEM microscopy (Figure 5-58). The size is estimated around 2.2 nm. In some areas the particles are agglomerated in packets, but well isolated particles can also be observed. The agglomerates give the impression of being linked in chain-like structures. WAXS measurements (Figure 5-58) revealed a coherence length of 2.3 nm for this sample whose crystal structure is hcp.

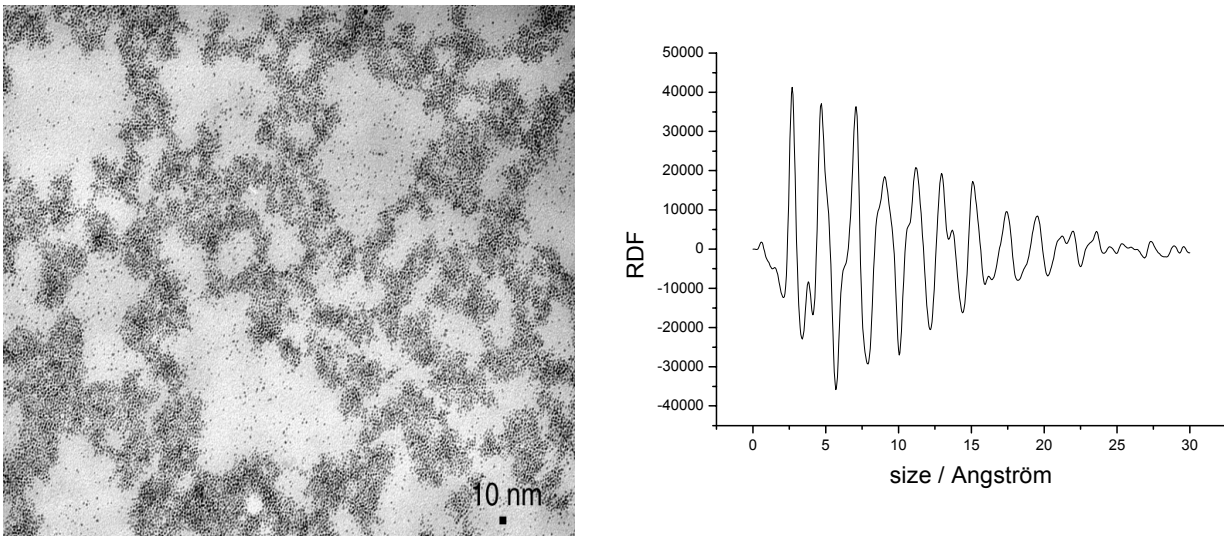

Figure 5-58: TEM micrograph and WAXS measurements of Ru / 0.2 eq NH_2OHiPr particles in pure THF

The experiments performed with the ligands NH_2OH and NH_2OHiPr allowed the stabilisation of ruthenium nanoparticles. Their characteristics are recapitulated in Table 5-23.

Table 5-23: Aminoalcohols as ligands for ruthenium nanoparticles

Ligand		Solvent	Particles	Size / nm	Ru %	C %	H %	N %	O %
1	NH_2OH	THF	self-organisation	2.5	48.9	7.6	4.1	1.3	1.2
2	NH_2OHiPr	THF	self-organisation	2.3	49.8	9.2	4.3	1.2	1.4

The ruthenium particles which have been stabilised with aminoalcohols remain stable in solution for several weeks. The content of Ru in all samples is about 50 %. An emerging self-organisation of the particles in THF has been observed. The particles are individual and present a mean diameter between 2.3 and 2.5 nm. Infrared measurements for NH_2OH confirm the presence of the ligand and hydrogen at the surface.

After these results, the particles have been stabilised with chiral oxazoline ligands bearing amine or alcohol groups but also different carbon skeletons susceptible to cause different dispersion and/or size for the particles.

5.3.2 Ruthenium particles stabilised by amino-oxazolines

At first, two oxazoline amines were used to stabilise the ruthenium particles: L^* = $MoxNH_2Et$ (3) and $MoxNH_2iPr$ (4) (Scheme 5-4).

The ligand was added to a solution of the precursor in 100 % THF and an *in situ* decomposition was carried out. For the use of 0.2 eq of 2-(4'R)-(4'-ethyl-3',4'-dihydrooxazol-2'-yl)-aniline ($MoxNH_2Et$) in THF the individual particles obtained are very regular in shape and well dispersed, and their colloidal solution is stable for several weeks. The TEM micrograph (Figure 5-59) shows the presence of small particles: some particles are isolated but most of them are included into large superstructures showing in some cases signs of self-organisation. The particles display a spherical shape. The corresponding mean diameter is 2.5 nm.

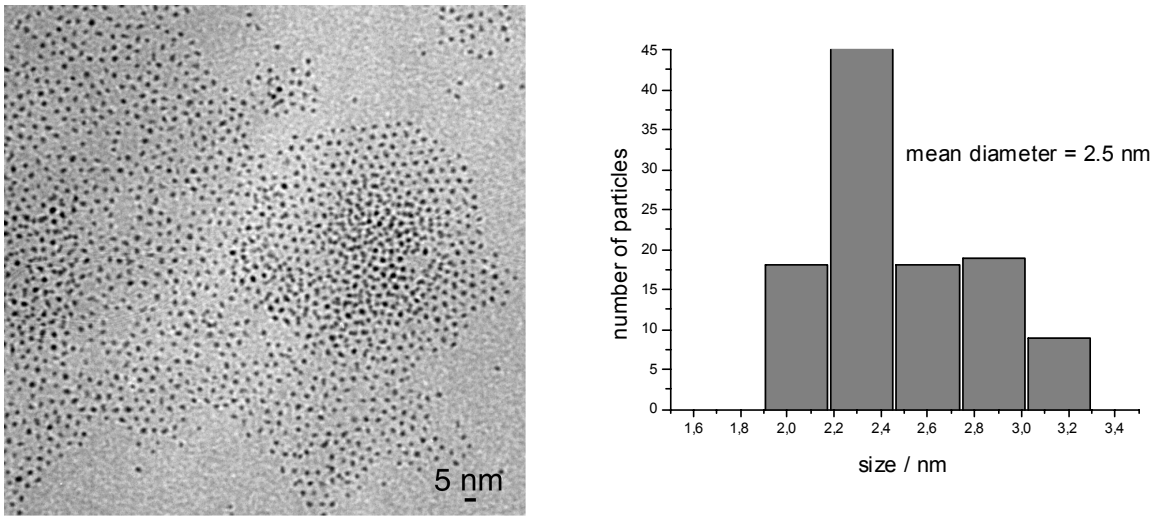

Figure 5-59: TEM micrograph and size histogram of Ru / 0.2 eq $MoxNH_2Et$ particles synthesised in THF

WAXS analyses on these colloids evidence the hcp structure of bulk ruthenium as previously observed for other ruthenium nanoparticles. The measurements show a coherence length of about 2.4 nm (Figure 5-60). The particles are monocrystalline and no coalescence of larger agglomerates is observed.

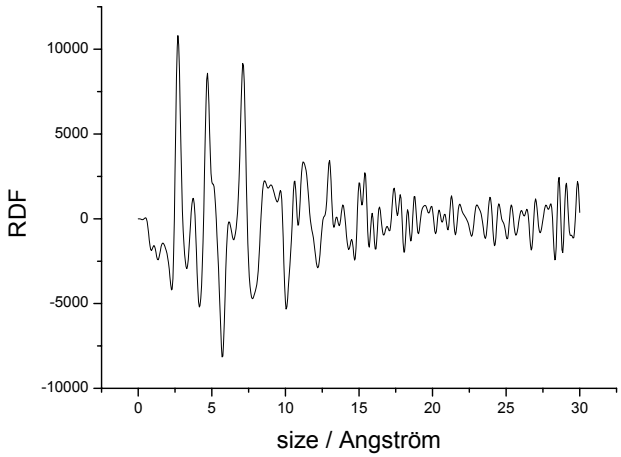

Figure 5-60: WAXS measurements on Ru / 0.2 eq $MoxNH_2Et$ colloids synthesised in THF

IR spectroscopy performed on these colloids shows a large band at 1610 cm^{-1} corresponding to the C=N stretch of the coordinated oxazoline. The corresponding band for the free ligand is at 1636 cm^{-1}. The characteristic stretching bands corresponding to the $–NH_2$ and $–CH_n$ groups of the ligand are also present in the IR spectrum of the stabilised colloid.

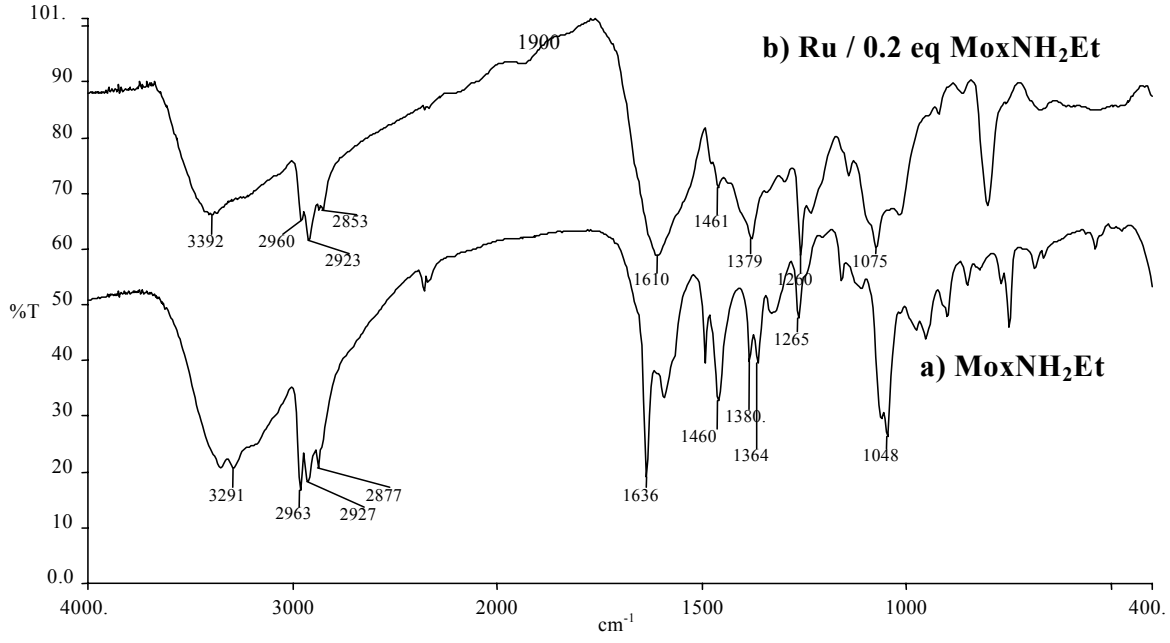

Figure 5-61:IR spectra of a) free $MoxNH_2Et$ (NaCl cells) and b) Ru / 0.2 eq $MoxNH_2Et$ colloids (KBr pellets)

Table 5-24: IR data for $MoxNH_2Et$ and Ru / $MoxNH_2Et$ colloids

ν $MoxNH_2Et$ / cm^{-1}	ν Ru / $MoxNH_2Et$ / cm^{-1}	Assignment
3291	3392	$-NH_2$
2963, 2927, 2877	2960, 2923, 2853	$-CH_n$
1636	1610	-C=N
1265	1260	-C-O

The wavenumbers corresponding to the bonds in the ligand can be found in the colloid spectrum, but a slight shift and an enlargement of the major bands can be observed probably due to the influence of the metal environment. A very weak signal at about 1900 cm^{-1} can be an indication of the presence of hydrogen at the surface of the particles. The infrared spectrum clearly shows the presence of the ligand from the similarity of the two spectra.

These colloids were examined by solution ^1H NMR spectroscopy and was compared with the spectrum of the free ligand $MoxNH_2Et$. The ^1H NMR spectrum of the stabilised colloid (Figure 5-62) does not show all the peaks corresponding to the attached ligand (Figure 5-63) as previously observed for the other ligands like 1-aminohexadecane, 1-octanethiol,… This phenomenon probably results from the greater proximity of the ligand to the metal particles. A tumbling in the magnetic field of the ligand is not possible when it is fixed to the metal surface. The corresponding peaks for the $–NH_2$ group (6-6.5 ppm) and the protons of the oxazoline ring (3-4 ppm) are not visible probably because of the proximity to the metal. The peaks observed near 6.7 ppm can be attributed to the aryl group. Concerning the ethyl group several peaks are observed between 0.6 and 1.1 ppm. The signal at 1.0 ppm probably corresponds to the $–CH_3$ group of the ethyl group (4'b).

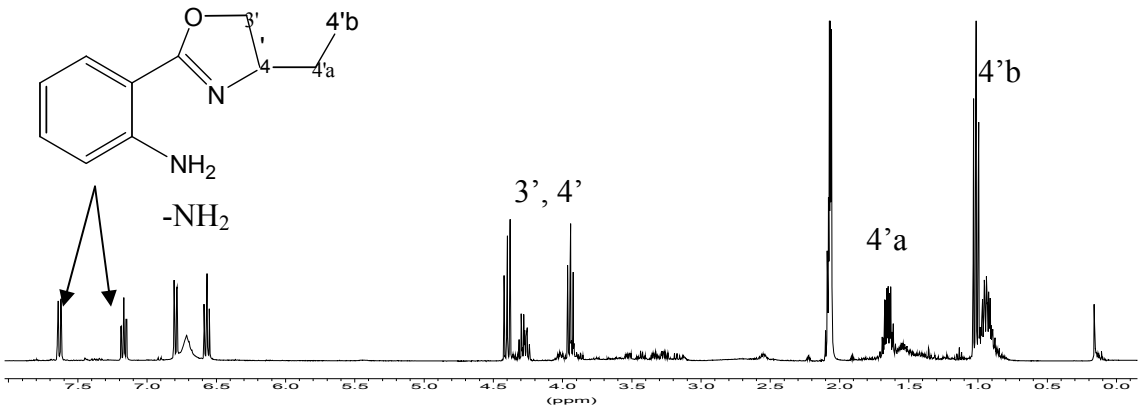

Figure 5-62: ^{1}H NMR spectrum (200 MHz, $CDCl_3$, 293 K) of free $MoxNH_2Et$

^{1}H NMR (250 MHz, $CDCl_3$, 298 K) δ: 1.02 (pt, *J* = 7.2 Hz, 3H, **4'b**), 1.65 (m, 2H, **4'a**), 4.32 (m, 1H, **4'**), 3.93 (pt, *J* = 8.5 Hz, 1H, **3'**), 4.38 (pt, *J* = 9.4 Hz, 1H, **3'**), 6.12 (bs, 2H), 6.68 (ptd, *J* = 9.4 Hz, *J* = 1.2 Hz, 1H, CH), 6.69 (pdd, *J* = 9.8 Hz, *J* =1.0 Hz, 1H, CH), 7.21 (ptd, *J* = 9.8 Hz, *J* = 2.2 Hz, 1H, CH), 7.69 (pdd, *J* =9.7 Hz, *J* =2.0 Hz, 1H, CH) ppm.

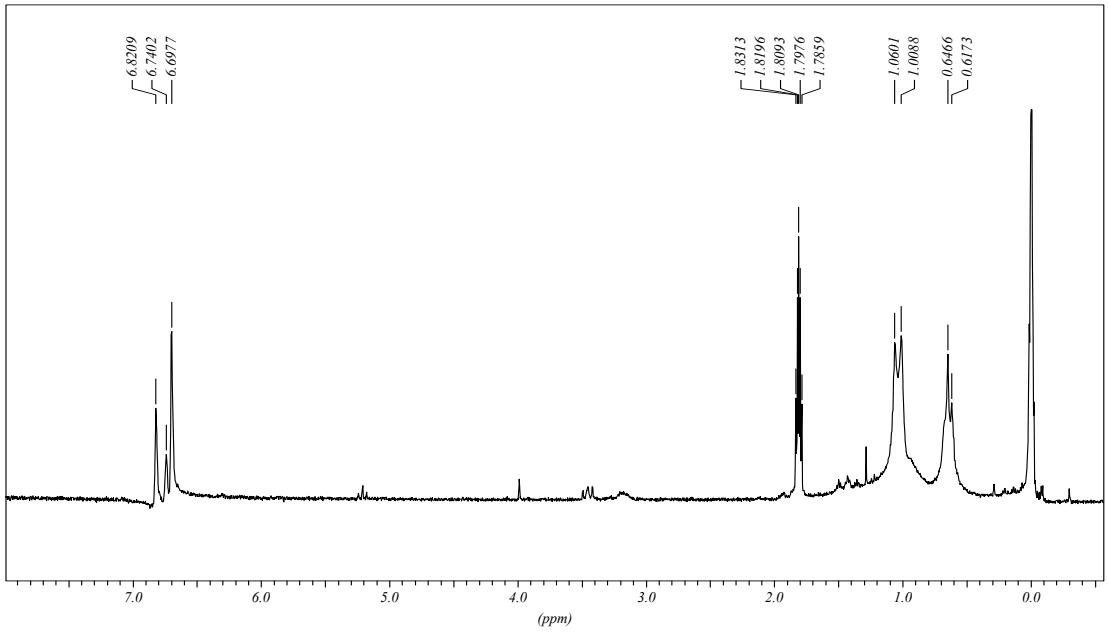

Figure 5-63: ^{1}H–NMR spectrum (200 MHz, d^6-acetone, 293K): Ru / 0.2 eq. $MoxNH_2$ colloid in toluene at 293 K

A similar oxazoline ligand has been employed in order to test the influence of a steric effect: the ethyl group was replaced by an isopropyl one. For this synthesis, 0.2 eq of 2-(4'S)-(4'-isopropyl-3',4'-dihydrooxazol-2'-yl)-aniline ($MoxNH_2iPr$) were added to the precursor for an *in situ* decomposition in pure THF. The particles obtained are nicely dispersed on the microscopy grid and have a spherical aspect (Figure 5-64).

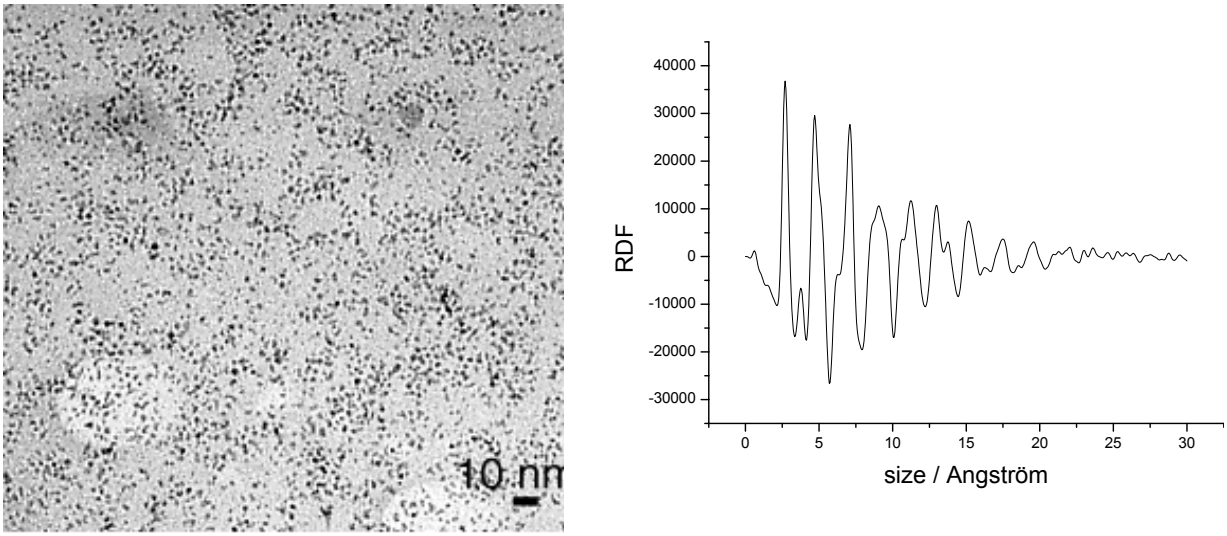

Figure 5-64: TEM micrograph and WAXS measurements of Ru / 0.2 eq $MoxNH_2iPr$ particles synthesised in 100 % THF

The coherence length of the particles was determined by WAXS measurements and estimated to be 2.1 nm.

Likewise for the samples prepared with $MoxNH_2iPr$, the presence of the ligand could be verified by IR spectroscopy. The bands for the characteristic groups of the ligand can be found on the colloid spectrum which was investigated after purification by precipitation and washing in pentane.

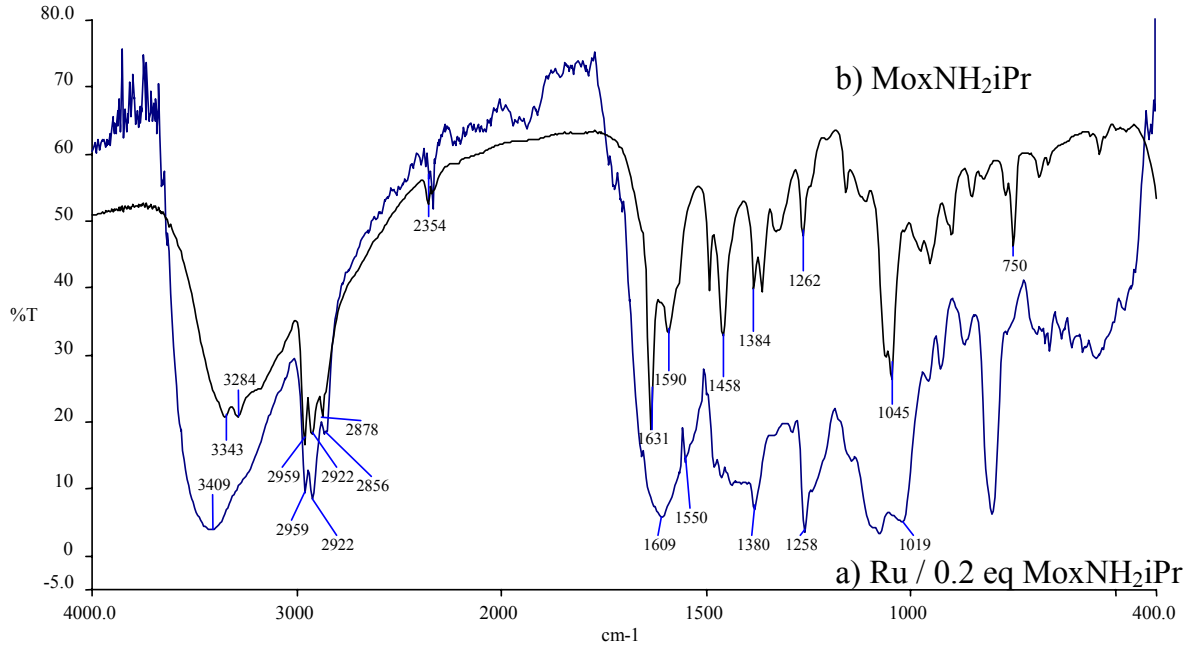

Figure 5-65: IR spectra of a) Ru / 0.2 eq MoxNH$_2$iPr colloids (KBr pellet) and b) free MoxNH$_2$iPr (NaCl cells)

As previously observed, the IR spectrum (Figure 5-65) shows different stretching bands which seem to correspond to the -C=N stretch of the coordinated oxazoline at 1609 cm^{-1}. The corresponding band for the free ligand is at 1631 cm^{-1}. The agreement of the bands for the free ligand and the stabilised colloid are shown in Table 5-25. As previously observed, a large and weak band at 1900 cm^{-1} attests of the presence of hydrogen on the metal surface. The metal has an influence on the ligand: the bands for the colloid are slightly broader than for the free ligand.

Table 5-25: IR data for free MoxNH$_2$iPr and Ru / 0.2 eq MoxNH$_2$iPr colloids

ν MoxNH$_2$iPr / cm^{-1}	ν Ru / MoxNH$_2$iPr / cm^{-1}	Assignment
3343	3409	-NH$_2$
2959, 2922, 2878	2959, 2922, 2856	-CH$_n$
1631	1609	-C=N
1262	1258	-C-O

The ^{1}H NMR spectrum (Figure 5-66) of this colloid shows the presence of peaks around 7 ppm corresponding to the aromatic protons of the MoxNH$_2$iPr (see Figure 5-62 for comparison) and the peaks corresponding the isopropyl group at 0.93 (-CH$_3$), 1.1 ppm (-CH$_3$)

and 1.8 ppm (-CH), but no peaks attributed to the heterocycle are visible. The peak at 4.8 ppm can be attributed to H_2.

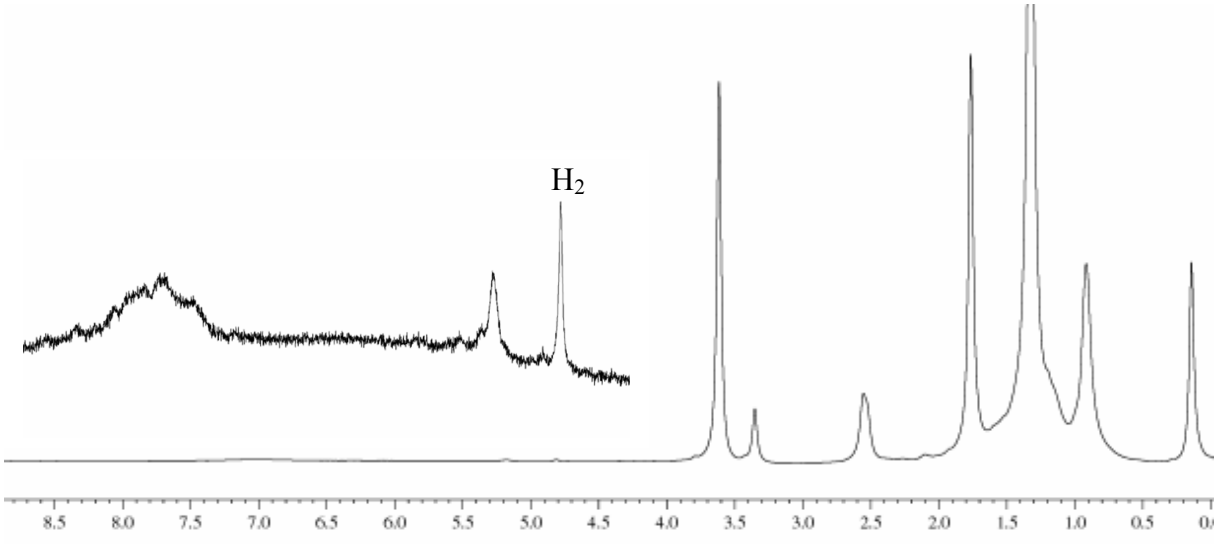

Figure 5-66: ^{1}H–NMR spectrum (200 MHz, d^{8}- THF, 293K): Ru / 0.2 eq. MoxNH$_2$iPr colloid with enlargment

The ^{13}C NMR spectrum of the free MoxNH$_2$iPr ligand is shown in Figure 5-67. In the ^{13}C NMR spectrum of the Ru / 0.2 eq MoxNH$_2$iPr colloids (Figure 5-68) the carbon corresponding to the C=N group (164 ppm) cannot be observed. Aromatic (129 and 127 ppm) and alkyl chain carbons (8 ppm) are seen. No signals at 66 ppm attributed to the five-ring are visible. This in in agreement with the presence of the ligand close to the surface of the particles.

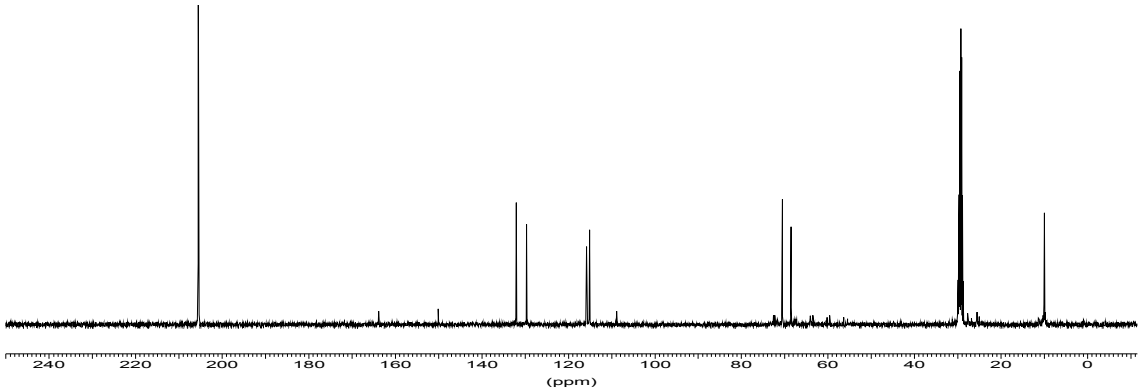

Figure 5-67: ^{13}C NMR spectrum (50 MHz, $CDCl_3$, 293 K) of free MoxNH$_2$Et

^{13}C NMR (50 MHz, $CDCl_3$, 293 K) δ: 8.2 (**4'b**), 26.9 (**4'a**), 66.1 (**4'**), 69.4 (**3'**), 129.5 (C, Ph), 127.5 (C, Ph), 113.5 (C, Ph), 113.8 (C, Ph), 129.8 (C, Ph), 127,5 (C, Ph), 164.5 (**C**=N) ppm.

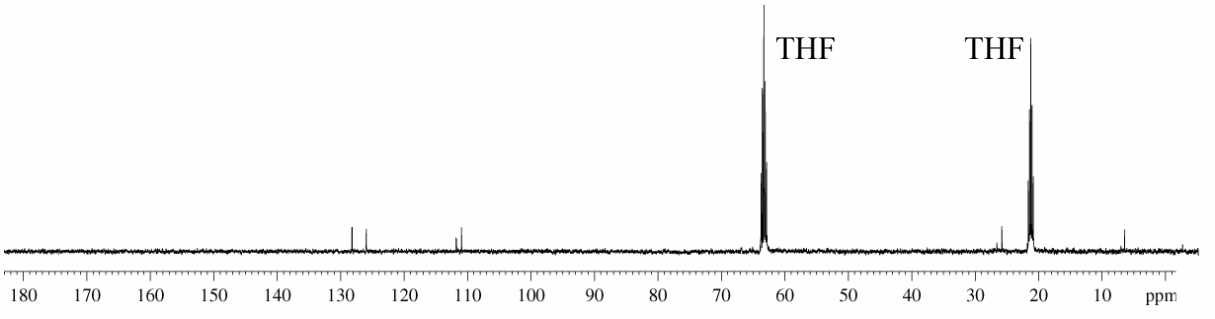

Figure 5-68: ^{13}C NMR spectrum (50 MHz, d^8- THF, 293K)of Ru / 0.2 eq MoxNH$_2$iPr colloid

Ruthenium particles could be stabilised by these two chiral amino-oxazoline ligands. The particles prepared in the presence of an oxazoline bearing an amine function showed a different organisation from the particles stabilised with oxazoline alcohols. For the use of MoxNH$_2$, the size of the particles is 2.5 nm while for the use of MoxNH$_2$iPr a lower size of about 2 nm is observed. This difference of size is probably due to the influence of the ligand on the particles size was observed. The presence of the chiral oxazoline ligands could be stated by NMR and IR spectroscopy. The ruthenium content determined for each sample by microanalysis is in all cases around 50 %. The characteristics of these two samples are summarised in Table 5-26.

Table 5-26: Ruthenium particles stabilised by amine-oxazoline ligands MoxNH$_2$Et and MoxNH$_2$iPr

	Ligand	Solvent	Size / nm	Structure	Ru / %	C %	H %	N %	O %
3	MoxNH$_2$Et	THF	2.5	individual	49.3	12.7	6.1	1.1	0.9
4	MoxNH$_2$iPr	THF	2	individual	49.6	12.1	5.3	1.2	1.3

5.3.3 Ruthenium particles stabilised by hydroxy-oxazolines

Several different oxazolines bearing alcohol substituents have been tested. The decomposition of the organometallic precursor has been accomplished in the presence of 0.2 eq of the chosen hydroxy-oxazoline ligand: L^* = MoxOH (5), MoxOH-2 (6) and MoxOHiPr (7) (Scheme 5-4)

The gathered mean diameter obtained in the case of addition of 0.2 eq 2-(4'R)-(4'-ethyl-3',4'-dihydrooxazol-2'-yl)-phenol (MoxOH) is about 2.7 nm, as can be seen in Figure 5-69. The particles appear well dispersed on the microscopy grid.

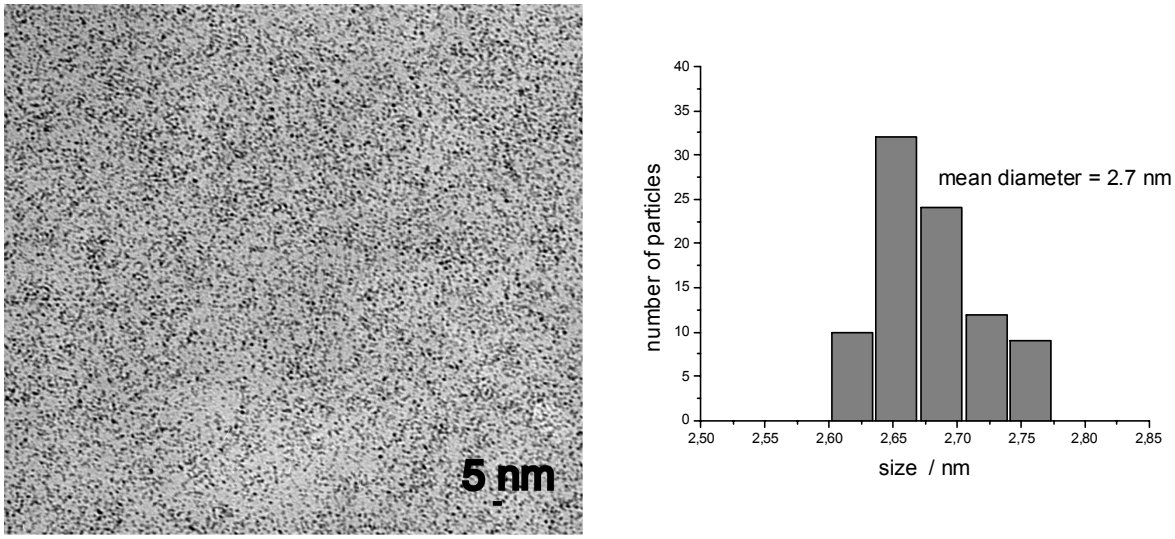

Figure 5-69: TEM micrograph and size histogram of Ru / 0.2 eq MoxOH particles in 100 % THF

An agreement between the IR spectra of the free ligand and the colloid can be stated (Figure 5-70). The bands of the characteristic groups of the ligand are visible in the presence of the metal. Nevertheless, the observed bands are larger for the colloid than for the free ligand which demonstrates the influence of the attachment to the metal surface. This attachment is also responsible for the shifting of the bands.

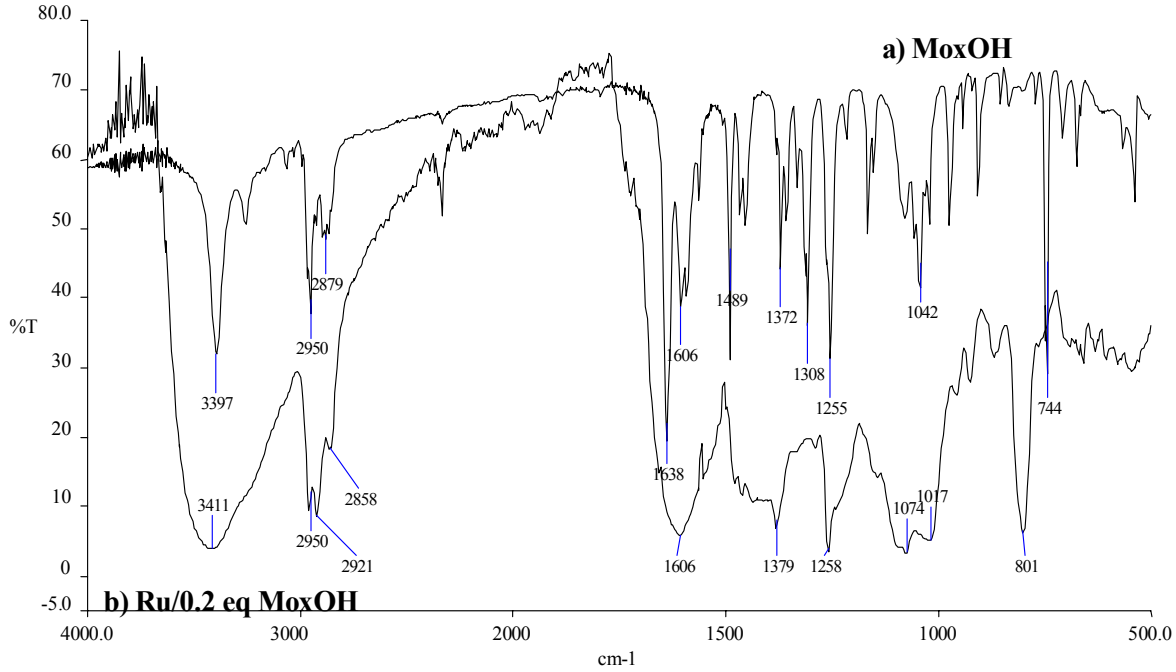

Figure 5-70: IR spectra of a) free MoxOH (NaCl cells) and b) Ru / 0.2 eq MoxOH colloids (KBr pellets)

Table 5-27: IR data for free MoxOH and Ru / 0.2 eq MoxOH colloids

ν MoxOH / cm^{-1}	ν Ru / MoxOH / cm^{-1}	Assignment
3397	3411	-OH
2950, 2879	2950, 2921, 2858	$-CH_n$
1638	1606	-C=N
1255	1258	R_3C-OR

Consequently, an alcohol–oxazoline with an isopropyl group was tested. 0.2 eq of 2-(4'S)-(4'-isopropyl-3',4'-dihydrooxazol-2'-yl)-phenol (MoxOHiPr) were used for the decomposition of the precursor. The small particles are found to be strongly coagulated and to form large round shaped structures which are connected to each other (Figure 5-71).

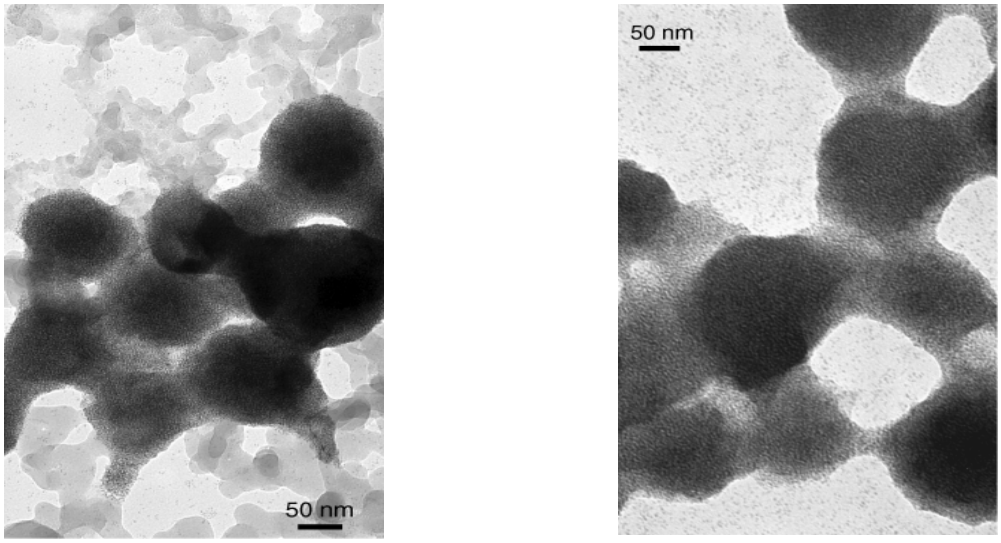

Figure 5-71: TEM micrographs of ruthenium particles synthesised with 0.2 eq MoxOHiPr in THF

An estimation of the size of the particles in the agglomerates was not possible, but individual particles outside these formations seem to be in the order of magnitude of 1-3 nm.

In the case of the use of 2-(3'S, 4'S)-(3'-phenyl-4'-hydroxymethyl-3',4'-dihydrooxazol-2'-yl)-toluene (MoxOH-2) in pure THF, we obtain particles in solution with a mean diameter of 2.5 nm (Figure 5-71). The particles appear slightly elongated and they are very clearly separated from each other.

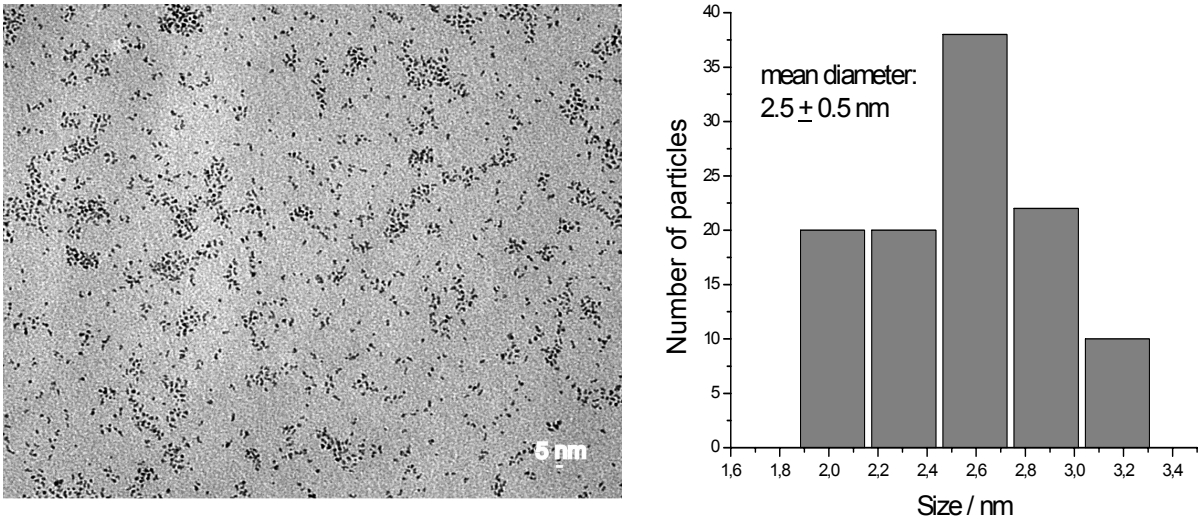

Figure 5-72: TEM micrograph and size histogram of Ru / 0.2 eq MoxOH-2 particles in THF

The following Table 5-28 collects the characteristics of hydroxy-oxazoline stabilised ruthenium particles.

Table 5-28: Ruthenium particles synthesised with alcohol-oxazoline ligands

Ligand		Solvent	Structure	Size / nm	Ru %	C %	H %	N %	O %
5	MoxOH	THF	individual	2.7	46.1	13.2	6.1	0.3	2.3
6	MoxOHiPr	THF	strongly agglomerated	1-3	44.7	13.1	6.3	0.3	2.5
7	MoxOH-2	THF	individual	2.5	45.8	12.9	5.8	0.4	2.4

The use of 0.2 eq of the appropriate ligand results in ruthenium particles with a ruthenium content of about 45 %. The Ru content observed for the amino oxazoline-stabilised particles was a little higher, at about 50 %. The particles could be stabilised with all alcohol oxazolines, but in contrast to the amino oxazoline-stabilised particles, their diameter varies from approximately 2 to 3.5 nm. In the case of MoxOHiPr agglomerates of particles have been observed, but in contrast to that, the particles stabilised with MoxOH and MoxOH-2 are well-dispersed on the microscopy grid. The presence of ligand at the surface was confirmed by IR spectroscopy.

5.3.4 Ruthenium particles stabilised bis-oxazolines ligands

For the stabilisation of ruthenium nanoparticles various bis-oxazolines have been considered which are displayed in Scheme 5-4.

For the decomposition of Ru(COD)(COT) with 0.2 eq 1,2-bis[(4'S)-(4'isopropyl-3',4'-dihydrooxazol-2'-yl)]ethane (S,S-B), the particles were found to be very small. The particles are not very well separated on the microscopy grid which makes the building of a size histogram difficult. The coherence length obtained by WAXS measurements is about 1.6 nm (Figure 5-73).

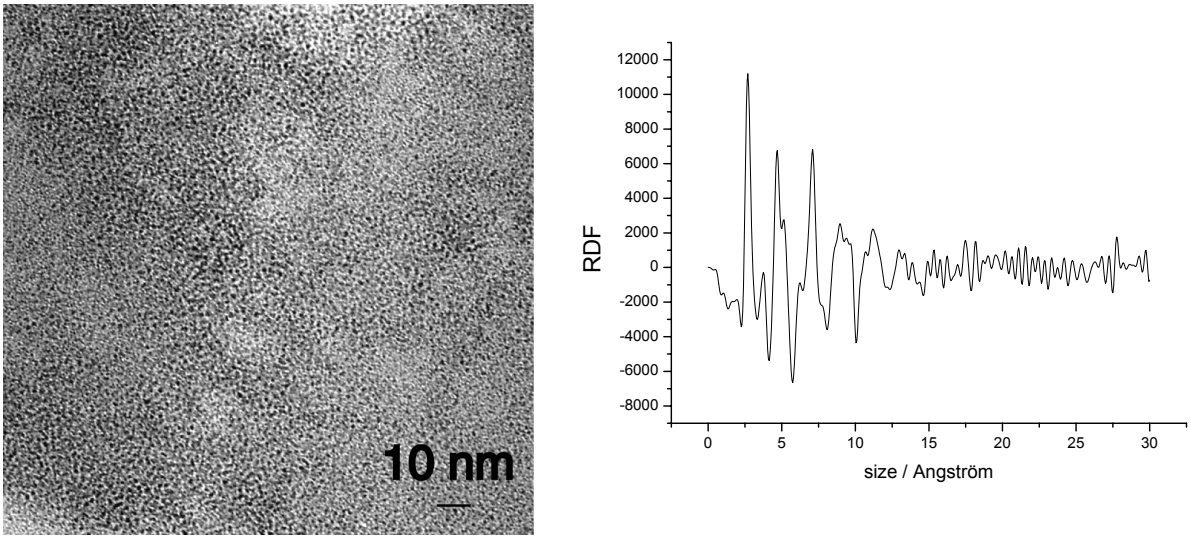

Figure 5-73: TEM micrograph and WAXS analysis of Ru / 0.2 eq S,S-B particles synthesised in THF

For the application of 0.2 eq 1,4-bis[(4'R)-(4'-ethyl-3,4-dihydrooxazol-2'-yl)]butane (Bisox$(CH_2)_4$Et) large and composite species could be detected: these agglomerates of more than 100 nm consist of smaller particles as revealed by the TEM micrograph in Figure 5-74. The particles display a regular sphere-shaped aspect. The coalescence only permits an estimation of a mean diameter of 1.5 nm.

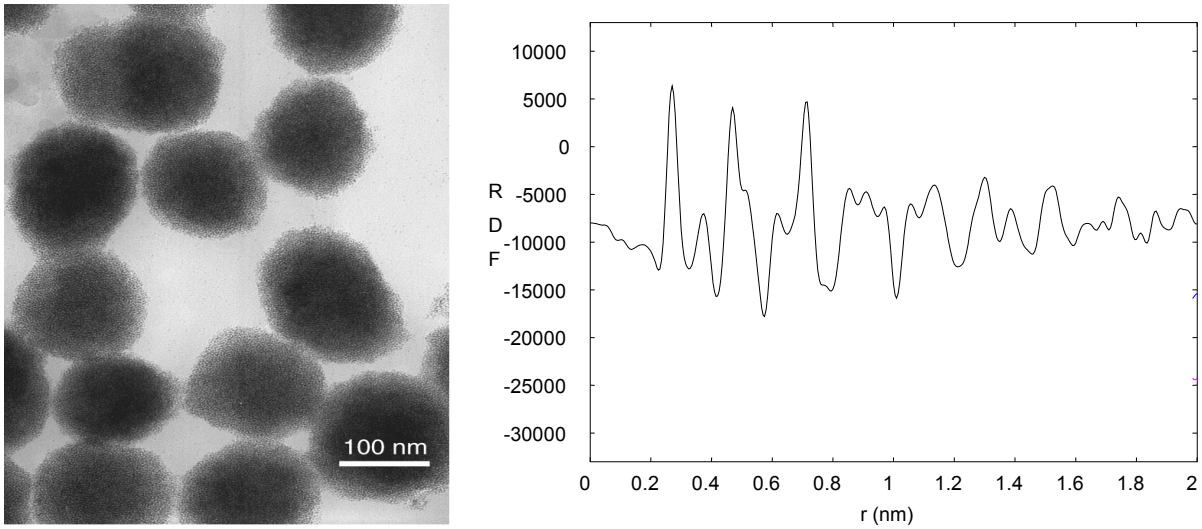

Figure 5-74: TEM micrograph and WAXS measurements of Ruthenium particles synthesised with 0.2 eq Bisox(CH_2)$_4$Et in THF

For the decomposition in the presence of 0.2 eq 2,2'-bis[(4,S')-[4'-(2-methylthio)propyl-3',3'-diphenyl-3',4'-dihydrooxazol-2'-yl]] (Bisox-SMe) in the reaction setting (100 % THF), small and very dense particles could be observed (Figure 5-75). The particles are strongly agglomerated and small: mean size about 1.6 nm. The particles viewed are crystalline, verified by WAXS measurements and they adopt the hcp structure of bulk ruthenium, as previously seen with other Ru nanoparticles.

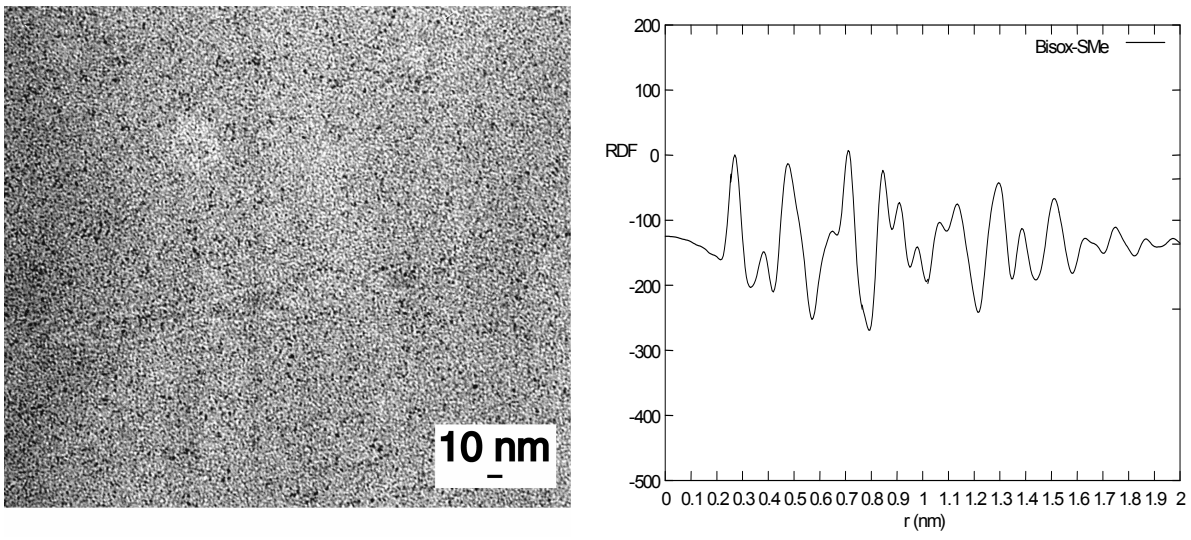

Figure 5-75: TEM micrograph and WAXS measurements of R u/ 0.2 eq Bisox-SMe particles in THF

1.6 nm particles are produced when the decomposition is performed in the presence of 0.2 eq 1,2-bis[(4'S)-(4'isopropyl-3',4'-dihydrooxazoly-2'-yl)]benzene (S,S-G) in THF (Figure 5-76). They display a spherical shape and most of them are separated. Nevertheless, some particles are very close to each other as seen in the TEM micrograph (Figure 5-77).

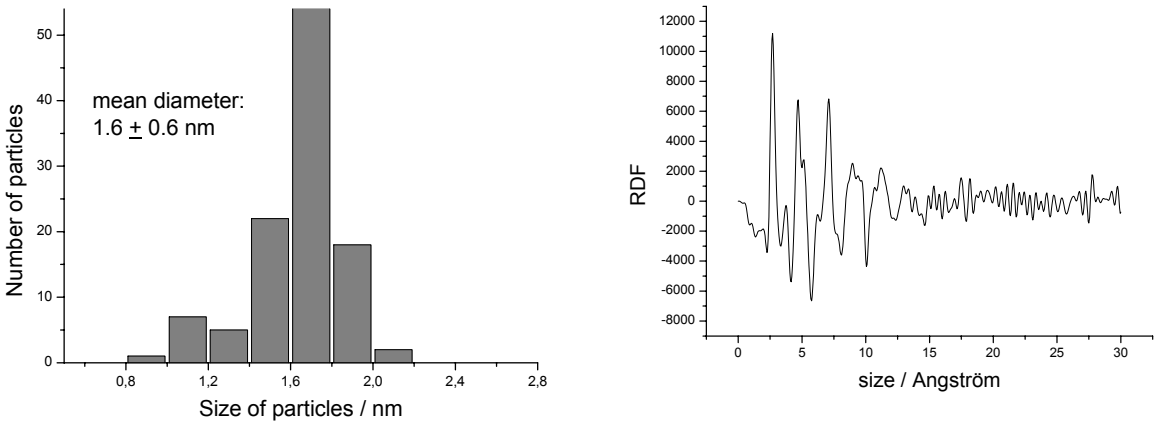

Figure 5-76: Size histogram and WAXS analysis of ruthenium particles synthesised with 0.2 eq S,S-B in THF

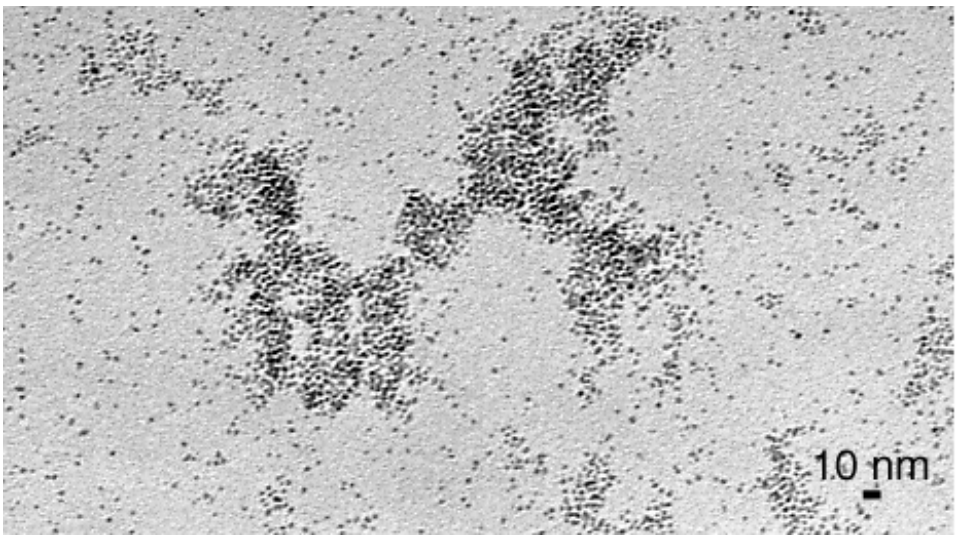

Figure 5-77: TEM micrograph of Ru / 0.2 eq S,S-G particles in THF

The particles stabilised with bis-oxazolines are found to be smaller than all other samples described in this work, with a mean diameter of 1.6 nm as seen in Table 5-29. The Ru content of the samples is likewise smaller (44 %).

Table 5-29: Bis-oxazolines as ligands for ruthenium nanoparticles

Ligand		Solvent	Particles	Size / nm	Ru %	C %	H %	N %	O %	S %
8	S,S-B	THF	dense particles	1.6	44.2	12.7	5.3	0.9	1.8	-
9	Bisox$(CH_2)_4$Et	THF	globes of agglomerates	1.5	44.3	16.4	9.3	0.9	0.7	0.9
10	Bisox-SMe	THF	dense particles	1.6	47.1	16.1	9.2	0.8	0.8	0.9
11	S,S-G	THF	separated	1.6	42.3/45.0	14.2	7.1	0.8	1.7	-

The coherence length of the Ru particles stabilised by chiral bis-oxazoline ligands are compared in Figure 5-78.

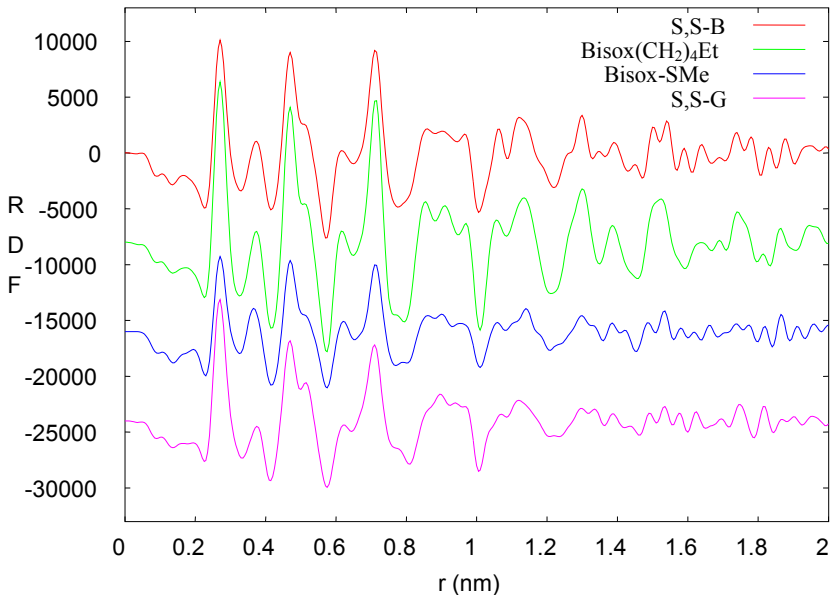

Figure 5-78: Comparison of WAXS analysis for Ru particles stabilised with bis-oxazolines

Infrared experiments for ruthenium nanoparticles stabilised with bis-oxazolines confirm the presence of the ligand. Nevertheless, the vibration bands are less pronounced in these cases than for the mono-oxazolines. Figure 5-79 shows a representative IR spectrum for Ru / bis-oxazoline colloids.

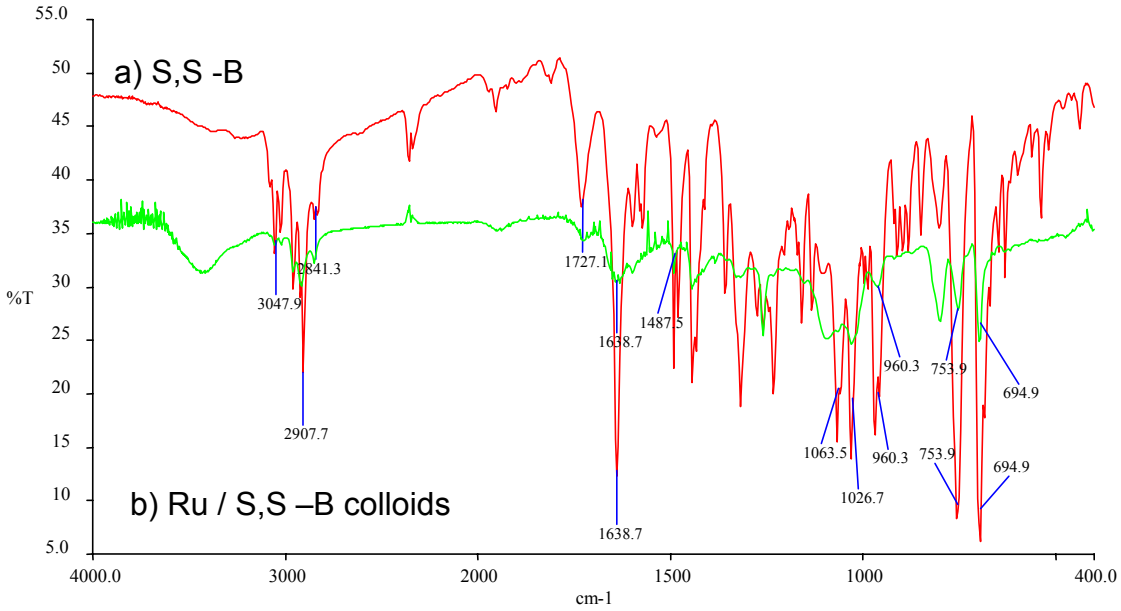

Figure 5-79: IR spectra of a) free S,S-B (NaCl cells) and b) Ru / 0.2 eq S,S-B colloids (KBr pellet)

Table 5-30: IR data for free S,S-B and Ru / 0.2 eq S,S-B H colloids

ν S,S-B / cm^{-1}	ν Ru / S,S-B / cm^{-1}	Assignment
3047	2907	$-CH_{ar}$
2841	2841	$-CH_{al}$
1638	1638	C=N

5.4 Conclusion for Ru nanoparticles by chiral aminoalcohol and oxazoline ligands

This is the first report on the synthesis of ruthenium nanoparticles stabilised by chiral ligands. This chapter describes the synthesis of ruthenium nanoparticles stabilised by aminoalcohols, hydroxy-, amino- and bis-oxazolines. The surface co-ordination of the ligands leads to an excellent stabilisation of the metal particles in solution. Different values of mean diameter and dispersion are obtained depending on the nature of the ligand. Around 1.6 nm for bis-oxazolines, 1.7 – 2.5 nm for aminoalcohols, a range from 1 to 3 nm for hydroxy-oxazolines and from 2 – 2.5 nm for amino-oxazolines. The dispersion and the structure of the particles is influenced by the stabilising ligand.

These particles have been tested in various catalytic systems, as will be described later in this work.

6 Inclusion of ruthenium nanoparticles in mesoporous materials

6.1 Organisation of ruthenium nanoparticles

There are not many efficient methods which allow control of the size and surface state of the particles. Therefore, the organisation of nanoparticles has been attempted. The advantages of organising particles in mesoporous systems is the constrained environment which limits of the amount of metal precursor and restricts its motion, and control of the size and size distribution.

Recent literature reports have highlighted the advantages of using nanostructured materials in many areas, especially in material science.[172,173] The motivation for this stems particularly from the unique electronic, optical, electro-optical, electrochemical and catalytic properties associated with colloidal metal particles of controlled size and composition. Mesoporous materials with variable composition have been receiving much attention because of their uses in organisation and separation.[174,175] The organisation of nanoparticles have attracted great attention because of their quantum size effects which are not only of a great theoretical interest, but also have potential for future application in catalysis as well as nanoreactors, sensors, electronic and optic devices.[70,176] Nanoparticles are usually synthesised by electrochemical or chemical deposition followed by decomposition or reduction in the confined channels of host materials such as carbon nanotubes[177], anodic alumina membranes[178] or microporous or mesoporous sieves.

6.1.1 Porous alumina membranes as templates for ruthenium particles

Nanoporous alumina membranes have turned out as ideal materials to generate and to organise nanosized materials.[176] This is due to their unique properties and easy synthesis.[179,180] This template material has been extensively examined for several years.[181,182] Anodization of flat aluminium surfaces in polyprotic acids gives transparent membranes with pores running throughout the material. The pores of these mesoporous materials can be generously varied between 5 and 250 nm. The pores are organised vertically to the metal surface. The most important advantage of these membranes is the variability of the pore widths which simply depends on the voltage applied for anodization. Other usable properties

are the temperature stability up to more than 1000 °C and the chemical activity of the pore walls which can easily be modified by various compounds for further use.[183] Therefore mesoporous aluminium oxide membranes are attractive for their application as templates to systematize nanoparticles.

Nanomaterials can be synthesised in these pores, and already prepared nanomaterials can be organised. The surface and pore structure can be elaborated by transmission electron microscopy as well as by high resolution transmission electron microscopy and atomic force microscopy.

Given the free choice of the pore diameter, these mesoporous materials are excellent templates for the organisation of small clusters. Therefore, Ruthenium nanoparticles have been included in the pores of nanoporous alumina membranes by filtration or vacuum introduction of pre-prepared colloidal solutions, or by *in situ* decomposition of the complex Ru(COD)(COT).

6.2 Nanoporous Alumina Membranes

The quantum size effect is not the only factor responsible for the characteristics of small particles. Beside this effect the one dimensional organisation leads to an anisotropy concerning their properties. Therefore, mesoporous alumina membranes are attractive for their application as templates to systematize nanoparticles[184,185] and have turned out as ideal materials to generate and to organise nanosized materials.[186,187,188] These materials are easy to synthesise and own unique properties.[189,190,191,192,193] The pores of those mesoporous materials are laid on in parallel and their diameter can be generously varied from 5 nm to 250 nm depending upon the anodizing voltage applied.[194] The channel length varies from the nanometer dimension to the micrometer dimension and depends on the anodizing time. Thin layers of the membranes are optically transparent and can withstand temperatures of up to 1000 °C.[195] Nanoporous alumina can be used as templates for organising nanosized materials that can be inserted or fabricated inside their pores. [196,197] The properties of materials change with the miniaturization when nanoparticles are formed.[2,198,199]

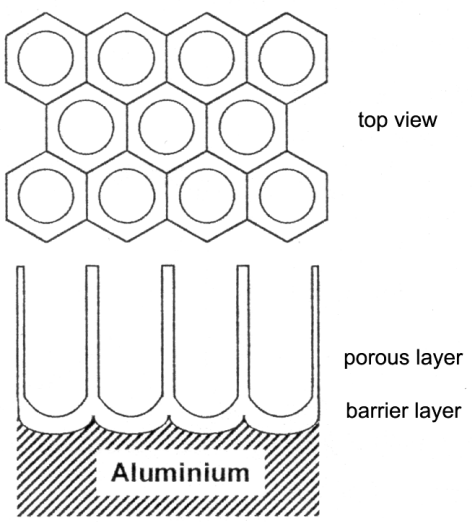

Figure 6-1: Scheme of a porous alumina membrane[183]

Porous alumina membranes can be obtained by anodic oxidation of very pure aluminium. Their constitution is shown in Figure 6-1. This template material has been extensively examined for years.[200,201] The surface and pore structure can be studied by transmission electron microscopy (TEM) as well as by atomic force microscopy (AFM).

When the aluminium metal is in contact with atmospheric oxygen, a thin passivation layer is formed which protects the metal from further oxidation. The so-called "Eloxal" process (**el**ectrolytic **ox**idation of **al**uminium) can extend this passivation layer and leads to a formation of a highly porous oxide layer on the metal surface by anodic oxidation in polyprotic acids like sulphuric acid. This layer of α-Al_2O_3 protects materials from corrosion and can be coloured by filling the surface pores with organic colours and colloidal metal compositions in the porous surface.[202] This material is very stable, and it is simple to both manufacture and to control in its properties.

Due to the freedom of choice of the pore diameter these mesoporous materials are excellent templates for the organisation of small clusters.

6.2.1 Formation of barrier oxide layers

Because of its electrochemical properties aluminium belongs to the group of the so called “valve metals” like titanium and hafnium.[192] The characteristics of those metals is the formation of a passivation layer on their surface. Aluminium carries the cathode current flow under formation of hydrogen. This isolating oxide layer is formed when the metal is used as the anode within an electrochemical redox reaction and the anodic power flow is blocked after a certain time in neutral electrolyte. The ion transport introduces a power flow which is inhibited by the formation of the passivation layer on the metal. The electrical field is reduced by the increasing thickness of the α-Al_2O_3 layer formed at the metal surface. The consequence is areduction of the electrical field by the barrier layer which behaves like a obstruction for the current. Aluminium oxide is a typical isolator with a energy gab of 7 to 8 eV.[203] This is the main difference between metals and valve metals.

If a very pure aluminium metal is anodized in neutral or slightly acidic solutions, e. g. in phosphate- or ammoniumborate solutions, the formation of a non-porous barrier layer can be observed.[204] When a constant electrical current between an aluminium plate as the anode and a cathode is applied, the electrical power decreases with time as an exponential function as shown in Figure 6-2.[192]

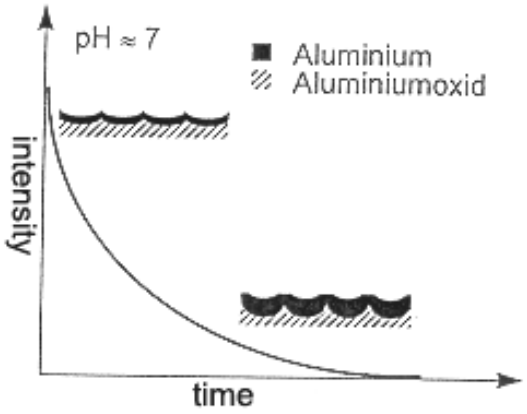

Figure 6-2 : Current-time deportment of anodic oxidation in neutral electrolyte[205]

The behaviour follows the equation :

$$I = I_0 \cdot e^{\beta E}$$

β and I_0 are temperature dependent material constants and E represents the electrical field power for the oxide. The anodic oxidation takes place in the presence of an applied electrical field which can be described as the quotient current reduction ΔU and the thickness of the oxide layer h. The electrical field power decreases with the increasing thickness of the barrier layer.

$$E = \frac{\Delta U}{h}$$

The barrier layer is situated on the aluminium surface and its thickness is directly proportional to the applied anodic current. The corresponding relation for the current and the thickness determined for the barrier layer is between 0.8 and 1.2 nm V^{-1}.[191,206] The resulting thickness of the compact layer is smaller because of the dissolution of the metal oxide by the electrolyte.

The thickness of the porous layer on top of the barrier layer depends on the time of the anodic oxidation. Depending on the transported current the thickness of the synthesised membranes has a wide range, from a few hundred nanometers up to several hundred micrometers.[207,208,209] The pores are organised vertically to the metal surface and their diameter have a well-defined proportionality to the applied anodic current (Figure 6-3). Pore diameters between 5 and 250 nanometers can be achieved.[20]

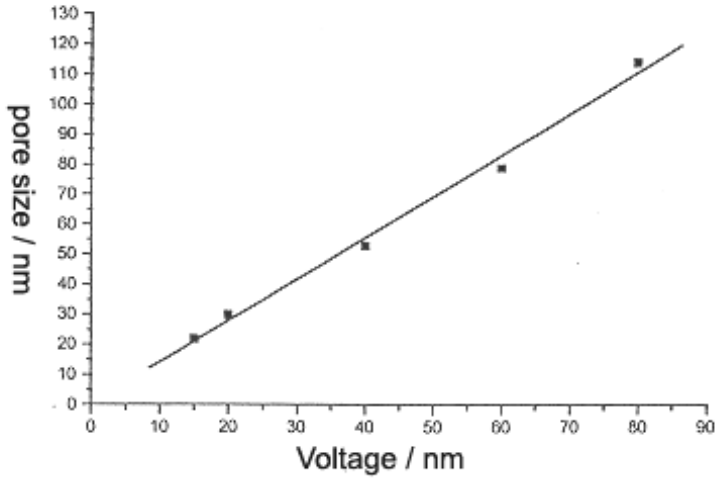

Figure 6-3: Dependency of the pore diameter from the applied voltage[205]

6.2.2 Formation of a porous structure

In a non-neutral electrolyte the barrier layer is dissolved by the action of the applied electric field. The formation of the pores begins at the defect sites of the barrier layer and is supported by the acidic electrolyte such as diluted oxalic acid, sulphuric acid or phosphoric acid. Figure 6-4 illustrates the formation of the pores.

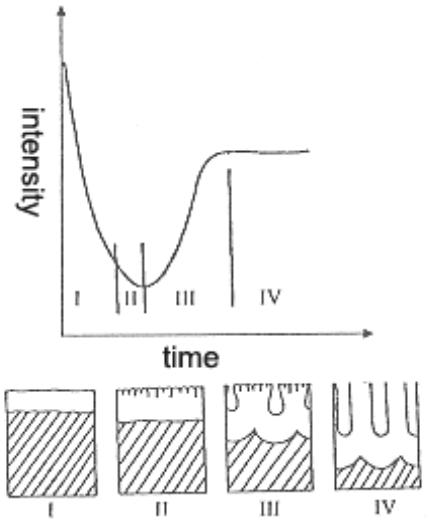

Figure 6-4: Oxidation of aluminium in a non neutral electrolyte[205]

The metal surface is at first covered with a thin oxide layer (barrier layer) (I). In part II starts to dissolve and it is possible to observe pores beginning to form in the oxide layer (III). The pores become wider and a regular pore structure is formed until an equilibrium is achieved (IV).[210] In a model for the dissolution of the barrier layer is the deformation of the oxide lattice by the applied electrical field[193] and can than be more easily attacked by the electrolyte. According to O´Sullivan et al.[193] the weakening of the Al-O bonding in the lattice by the applied electric field, responsible for the dissolution of the oxide (Figure 6-5). The lattice will be deformed and the Al cations will be displaced towards the electrolyte while the oxygen anions are pushed towards the barrier layer. The deformed lattice can now be more easily attacked by the electrolyte under formation of water and dissolved Al cations in the solution. Figure 6-5 illustrates the mechanism.

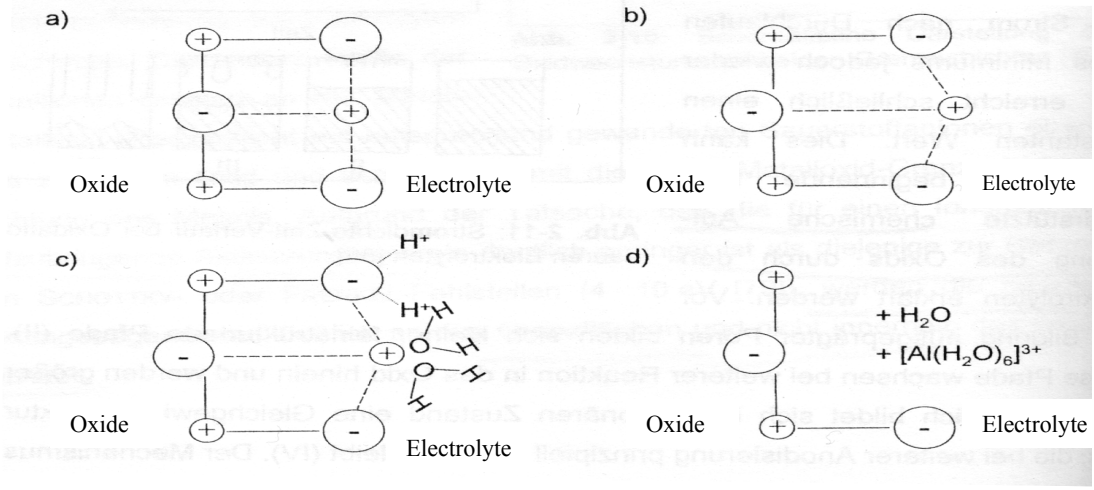

Figure 6-5: Field supported dissolution of the barrier layer[21]

The formation of regular pores is due to the applied electrical field. An equilibrium of the electric field on the bottom of the pores is responsible for their constant diameters as shown in Figure 6-6. For a bigger pore the electric field decreases at the pore base and the dissolution of the oxide is slower while in the case of a smaller pore, because the electric field increases and the dissolution of the oxide is quicker.[193]

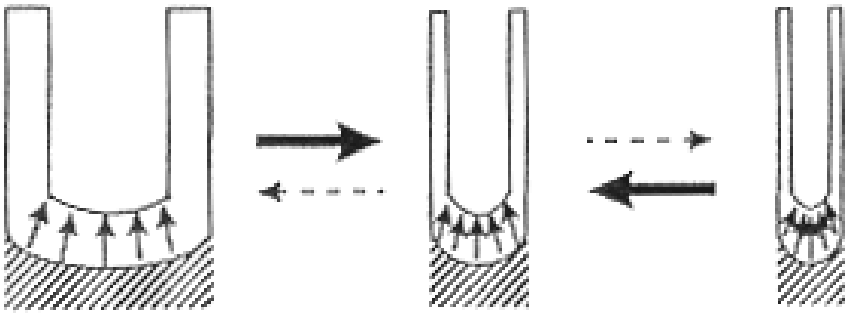

Figure 6-6: Control of a regular pore diameter by the electric field[205]

In conclusion the formation of pores can be described as competitive formation and dissolution of the oxide layer depending on the electric field. The formation of controlled porosity membranes from anodically oxidized aluminium can be obtained with a range of pore diameters regulated by the applied anodizing voltage.[211]

The alumina membranes are characterised by TEM and AFM. Figure 6-7 shows a TEM micrograph of the top view of a typical membrane with 24 nm pores prepared at 15 V. The pores size distribution was obtained from this micrograph.

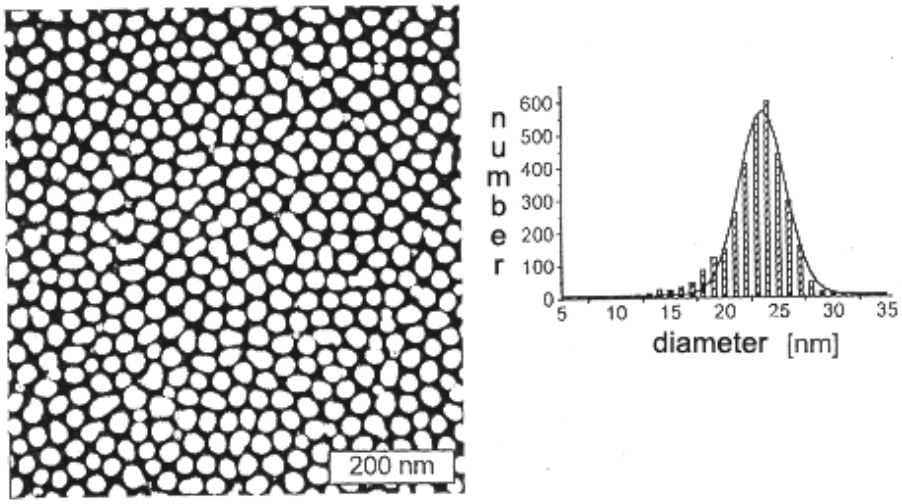

Figure 6-7: HRTEM micrograph of a 15 V Al_2O_3 membrane

The surface of the membranes can also be prospected by atomic force microscopy (AFM) as a means of obtaining more information about the pore diameters, the structure of the cells and the coarseness of the surface. Figure 6-8 shows a typical porous surface of a 50 V membrane. All samples show a regular porosity and the roughness of the surface is between 10 and 70 nm.

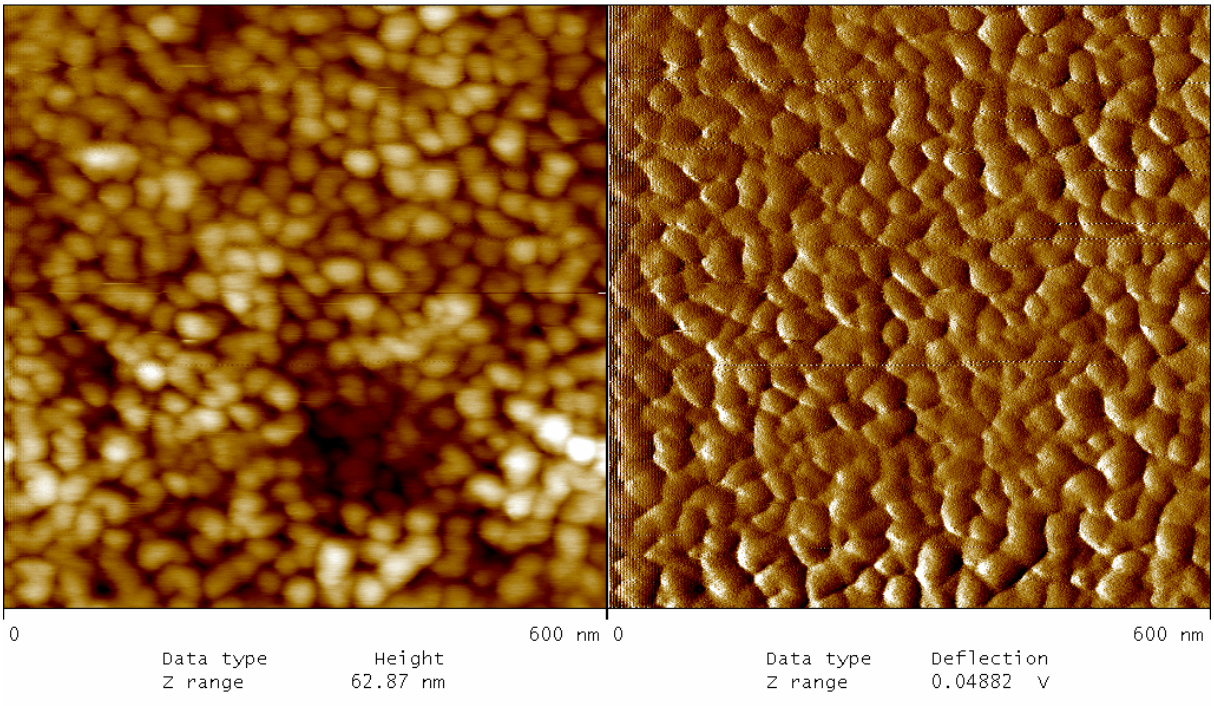

Figure 6-8: AFM image of a 50 V Al_2O_3 membrane

AFM[212,213] can claimed on these samples since it can be applied on non conducting surfaces in contrast to scanning tunnelling microscopy (STM). AFM can provide vertical resolutions up to atomic scale and can provide three-dimensional images of the surface.[214] Studies were performed using contact mode (V-shaped Si3N4 tip with radius of curvature R around 50nm) recording height (Figure 6-8 left) and deflection (Figure 6-8 right) images. The coarseness of the investigated membrane is about 60 nm.

6.2.3 Alumina membranes as templates for Ru nanoparticles

On account of their mesoporous structure, free standing membranes are used as templates to restrict the reaction area of chemical processes or as templates to organise the structure of various matertials.[196,215] Inside their pores nanomaterials can be synthesised as well as previously prepared nanomaterials can be structured.

Nanoparticles inside the porous alumina can be obtained by chemical[216] or electrochemical[217] deposition and by thermal decomposition.[218] In this chapter the filling of nanoporous alumina membranes of various pore widths with ruthenium nanoparticles. These catalytic materials were obtained employing three different methods. Ruthenium nanoparticles included in alumina membranes have been prepared either by dihydrogen decomposition of the organometallic complex Ru(COD)(COT)[96] to give pre-prepared colloidal solutions which were further used to fill the pores of nanoporous alumina membranes by filtration, vacuum induction or by in situ decomposition.

6.2.3.1 Preparation of pre-prepared colloidal solutions in MeOH/THF mixtures

Colloidal solutions of size controlled ruthenium nanoparticles can be prepared by decomposition of the organometallic precursor Ru(COD)(COT) under an H_2 atmosphere using a methanol/THF mixture as solvent and in the absence of any further stabiliser (Scheme 6-1).[219] The reactions were carried out following the standard conditions previously described in chapter 2: room temperature, under pressure of 3 bar H_2 for at least 45 minutes and vigorous stirring.

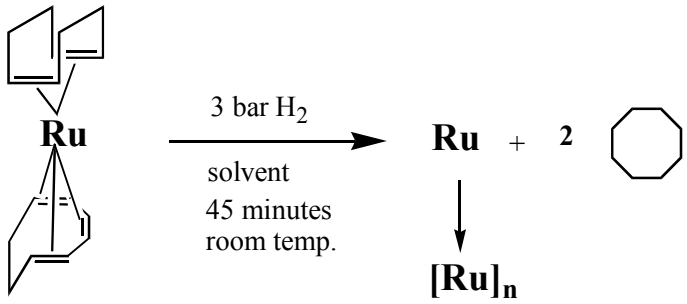

Scheme 6-1: Preparation of the colloidal solutions of Ru particles for membrane filling

In all cases the decomposition is fast: the colour of the solution changes from yellow to brown a few minutes after pressurization under dihydrogen. The so-obtained colloidal solutions then remained unchanged and stable for at least several weeks. Control of the particle size is possible through a proper choice of the solvent mixture. The particles display a more or less sponge-like aspect depending upon the medium composition. In the MeOH rich mixtures, this sponge-like aspect is more pronounced than in the MeOH poor media.[102]

As shown in chapter 2, the colloidal solutions have been characterised by transmission electron microscopy (TEM) and X-ray diffraction (XRD) measurements and some of them by wide angle X-ray scattering (WAXS). The Ru particles display highly porous, sponge-like structures of regular spherical shape. They are well-dispersed and homogeneous in size. Their high air sensitivity (they burn in the presence of oxygen) confirms their clean surface state since they are stabilised only by weakly coordinated alcohol and THF molecules. These quasi naked particles are then expected to display high activity in catalysis. An organisation in mesoporous Al_2O_3 membranes promises a increase of the reactivity of the particles since the organisation makes the active surface sites more accessible and augments the contact between the reactive gas and the surface atoms.

Such Ru colloidal solutions were further used to fill Al_2O_3 membranes of various pore diameters which were selected depending on the particles size (Table 6-1).

Table 6-1: Mean size of the particles as a function of the solvent composition and selected membranes sizes for the incorporation of the Ru particles

MeOH/THF volume rate / %	Particles mean size / nm	Pores diameter / nm	Anodising voltage / V
2.5/97.5	5	~ 21	15
5/95	16.7	~ 28	20
10/90	19.8	~ 42	30
15/85	23.6	~ 42	30
25/75	33.8	~ 56	40
50/50	47.0	~ 70	50
75/25	69.0	~ 84	60
90/10	85.9	~ 112	80

Concentrated pre-prepared nanoparticles solutions were transferred into membranes of adequate pore sizes via two different methods which are described below: filtration and vacuum incorporation.

6.2.3.2 Filling by filtration

The first approach to fill the pores of the membranes involved the use of pre-formed colloidal solutions which were put in contact with the membrane and then filtered through the membrane in order to fill the pores.

This method of filtration was applied to several nanoparticles sizes. For example, the results obtained in the case of 20 nm particles introduced inside a 20 V membrane (pore diameter: 28 nm) are shown in Figure 6-9. The TEM micrograph reveals that no particles are located inside the channels of the membrane but remain at the surface of the membranes suggesting a mismatch between the particle size and the pore widths. This observation is valid for all systems tested.

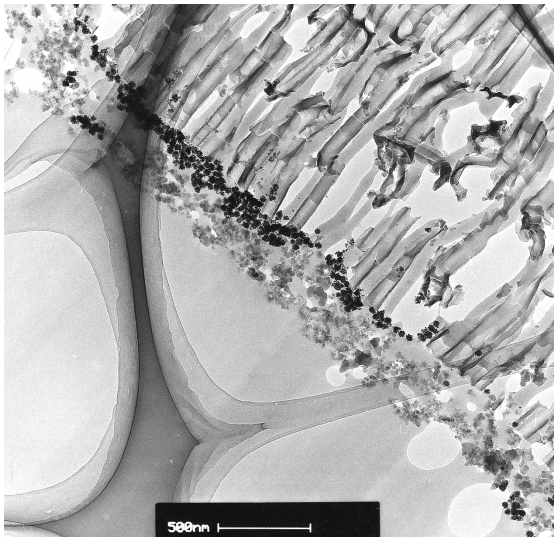

Figure 6-9: Filtration of a 20 V membrane (pores diameter: 28 nm) with Ru nanoparticles pre-synthesised in a MeOH/THF mixture of 10/90 ratio (particles size: 20 nm)

When the same solution was used with a 40 V membrane containing bigger pores (56 nm instead of 28 nm) the presence of particles inside the channels of the membrane could also not be observed.

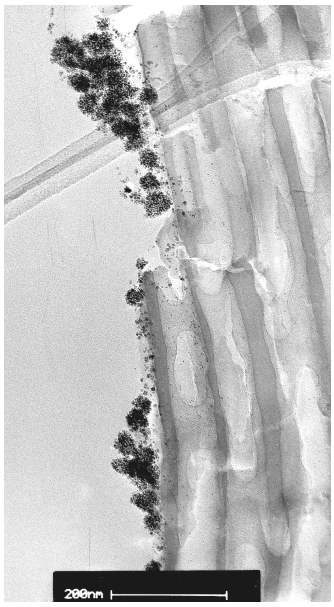

Figure 6-10: Filtration of a 40 V membrane (pores diameter: 56 nm) with Ru nanoparticles pre-synthesised in a MeOH/THF mixture of 10/90 ratio (particles size: 20 nm)

The TEM micrograph in Figure 6-10 shows a membrane after completion of the filling process. Agglomerations of particles are only found on the surface of the membrane. They do

not seem to enter the pores even when their size is distinctly inferior to that of the pore opening.[220]

6.2.3.3 Vacuum filling

The second method of filling consists of vacuum induction of pre-prepared solutions into the pores of the membranes. The combination of solutions and membranes are those listed in in Table 6-1. The TEM micrograph in Figure 6-11 shows a membrane after completion of the filling process. Only very few agglomerates are seen outside of the pores. In contrast to the filtration method, the diffusion of particles through the pores was possible in this case. It therefore seems that the difference between the diameter of the pores and the size of the particles has to reach a certain value for the particles to enter the pores, although this value can not be determined precisely.

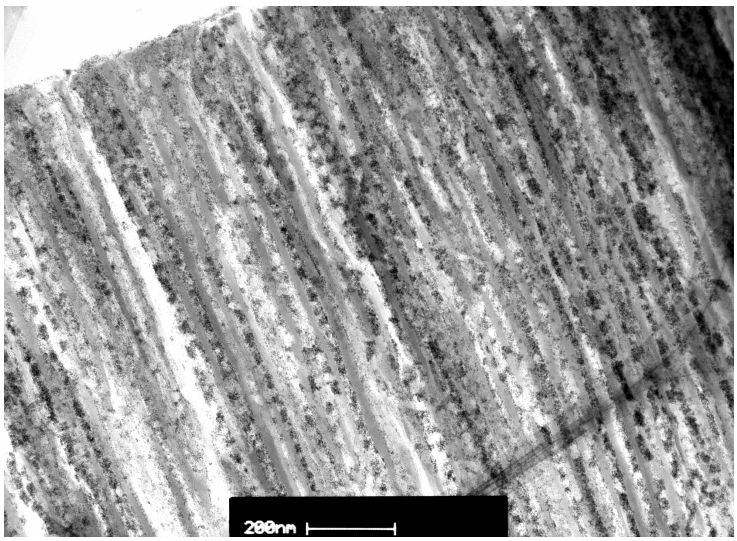

Figure 6-11: Regularly filled pores of a 20 V membrane (pores diameter: 28 nm) with nanoparticles synthesised from a mixture MeOH/THF 5/95 (particles size: 16 nm)

For all the combinations of colloidal solutions and membranes the membranes obtained showed pores with a regular fill of particles. Figure 6-12 shows an overview of a membrane which is regularly filled with particles. This confirms that a homogeneous and reproducible filling is possible using this method.

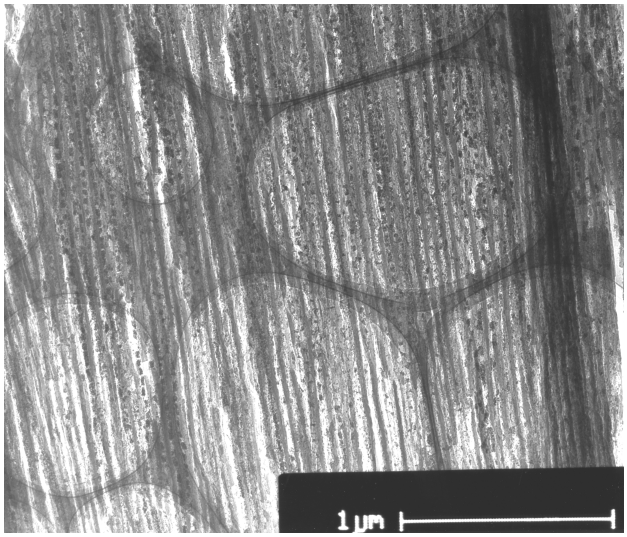

Figure 6-12: Regularly filled pores of a 30 V membrane (pores diameter: 42 nm) with nanoparticles synthesised from a mixture MeOH/THF 10/90 (particles size: 20 nm)

To use these materials in heterogeneous catalytic applications, a regular dispersion of the particles inside the pores is needed but not a complete clogging which would hinder the gas diffusion through the membrane. Therefore, given these encouraging but still not optimal results, we decided to improve the filling of the pores, *i.e.* to get a more regular particles dispersion and to avoid the formation of dense areas inside the pores, by using another route.

6.2.3.4 Decomposition in situ

This route consists of the decomposition of Ru(COD)(COT) under the usual conditions (3 bar H_2, 45 minutes, room temperature), but followed by deposition of the complex inside the pores using a concentrated solution and vacuum drying. The same membranes as with the pre-prepared colloidal solutions were used. In order to assist the diffusion of the molecular complex into the pores, the membrane remained in contact with a concentrated solution of Ru(COD)(COT) for 24h before (incomplete) solvent evaporation and decomposition of the precursor *in situ*. This procedure was repeated until the reception of a black coating on the membrane which indicates an organisation of the particles inside. TEM micrographs revealed that the formation of the ruthenium nanoparticles effectively takes place inside the pores .

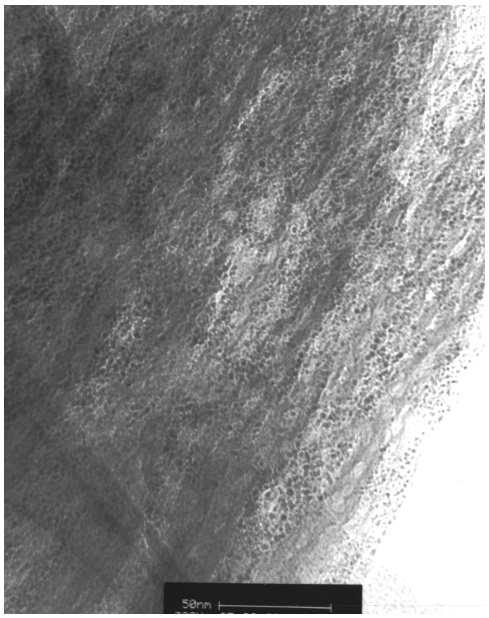

Figure 6-13: TEM micrograph of Ru particles obtained from in situ *decomposition of Ru(COD)(COT) in MeOH/THF 5/95 (particles size: 17 nm) inside a channel of 28 nm pores (20 V membrane)*

As an example, Figure 6-13 presents a typical TEM micrograph showing the one-dimensional arrangement of the Ru particles obtained in these conditions inside a membrane of 28 nm pores. The mean size of the particles determined by TEM analysis is around 17 nm, and this value was confirmed by XRD analysis. This size is similar to that obtained in the same solvent mixture but in the absence of alumina membrane. This result strongly suggests that the control of the particle size is also effective inside the membrane. Nevertheless, the morphology of the particles does not look as porous as previously found in solution. The particles appear denser, possibly because of the walls of the membrane which can have an influence on their growth or of the pressure inside the channels.

An example can be seen in Figure 6-14, where Ru particles are imaged inside a pore of approx. 42 nm. A regular dispersion of accessible nanoparticles is observed. The formation of aligned particles can be observed.

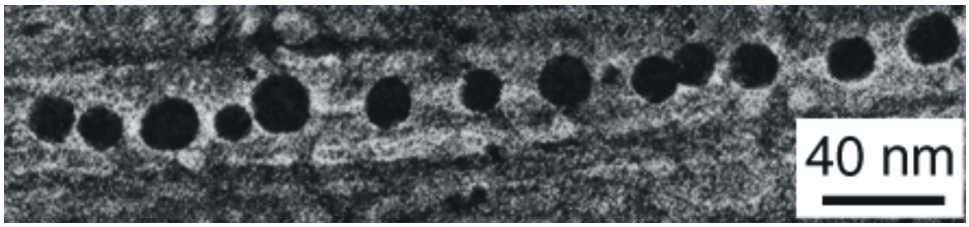

Figure 6-14: HRTEM micrograph of Ru particles obtained from in situ *decomposition of Ru(COD)(COT) in MeOH/THF 10/90 inside a channel of a 42 nm pore (30 V membrane)*

By this method, the dispersion of the particles inside the pores is more regular. In addition no particles are observed outside the pores and no dense areas are registered within the membrane channels.

This successful induction and regular organisation of the particles inside the alumina membrane pores, prompted us to use this method for different particle sizes. The selected pore widths are shown on Table 6-1.

6.2.4 Conclusion

Ruthenium nanoparticles of different sizes have been included in mesoporous alumina membranes of varying pore sizes. These new materials seem to correspond to the requirements for catalytic applications, since a homogeneous filling of the pores is expected to allow a perfect diffusion of the gas through the material and an optimized contact between the reactants and the particles active sites.

This method appears efficient for preparing homogenous materials for catalysis. Therefore, eight materials consisting of nanoparticles included into membranes of appropriate pore size (see Table 6-1) were prepared and tested in the catalytic hydrogenation reaction of 1,3-butadiene (see chapter 7).

6.3 Mesoporous silica materials as templates for ruthenium nanoparticles

6.3.1 Mesoporous silica as templates for ruthenium particles

Nanometer-sized metal particles with a narrow particle size distribution homogeneously dispersed in a SiO_2 matrix have been reported based on the incorporation of pre-formed nanoparticles within silica[221] or by sol-gel processing of metal complex.[222] In this last case, a transition metal complex-containing gel is oxidized in air leading to nano-sized metal oxide particles within the matrix which are then reduced under hydrogen to give metal particles. The metal dispersion and size distribution obtained by this approach depends on the kind of metal, the reaction conditions and the metal loading. Another approach consists of making use of the pore channels of hexagonal mesoporous silica[223] as matrices for controlling the nanoparticles size. Thus, the ordered mesoporous silica MCM-41,[224] MCM-48,[225] and FSM-16[226] materials have been used as templates for the growth of mono-[227] or bimetallic[228] transition metal nanoparticles. The general procedure used was based on impregnating the metallic precursor or grafting silaferrocenophanes[229] onto the support followed by calcination to generate the nanoparticles. The final nanoparticles size is dependent on both the pore size and the calcination temperature. Furthermore, the main problem of all these impregnation/calcination methods is the growth of nanoparticles outside the pores of silica. A new methodology consisting in co-ordination of an organo-gold precursor within the pore channels of functionalised mesoporous silica followed by metal nanoparticles growth under mild chemical reduction was optimised in our group.[230] The preparation of gold (0) nanoparticles within channels of mesoporous materials functionalised with mercaptopropyl groups was realised.

Additionally, the formation of indium nanoparticles within the pores of phosphonate-functionalised SBA-15 and MCM-41 type materials and their coalescence to indium nanorods was achieved. Oxidation of the as-obtained indium (0) nanometer scale objects leads to indium-oxide without modification of the initial size and shape was studied in our group. The incorporation of indium within organised mesoporous hybrid materials allowing a good control of the size of the obtained nanoparticles is described.[231]

Mesoporous silica materials with uniform pore diameters are a promising new kind of host for the preparation of ultra fine metal nanostructures. Their pore surface can be functionalised with many functional groups and their inner and outer surface can be selectively modified. For example, the surface of silica can contain organic functionality such as polar head groups like –SH or $–NH_2$.[232] They are excellent materials for studying host-guest interactions.[233] The host is usually passive and does not actively participate in the reduction of precursors to form nanoparticles followed by their entrapment in the host matrix. The organic functional groups act as anchors for the nanoparticles by binding them through covalent interactions, thereby avoiding the requirement of external capping agents like alkylamines or alkylthiols for the stabilisation of the particles. The porous host used in the present application is an SBA-15 type, which was originally developed by Stucky and co-workers.[234,235] Such ordered mesoporous materials with uniform morphology and large porosity have been used as the host materials for the organisation of nanoclusters. Generally, the sizes of particles prepared by this method span a broad range of sizes (3-30 nm)[236], which depends on metal support interactions, the solvent used and the drying and the reduction conditions. There are considerably practical advantages to synthesise more uniformly sized metal nanoparticles which are better dispersed in the solid support template.

The ruthenium nanoparticles have been introduced in the channels to form organised nano-objects inside. This new material is finally calcinated to obtain more information about the composites inside the pores. Another method is the stabilisation of ruthenium nanoparticles by ligands, which can be polymerised afterwards to synthesise mesoporous materials.

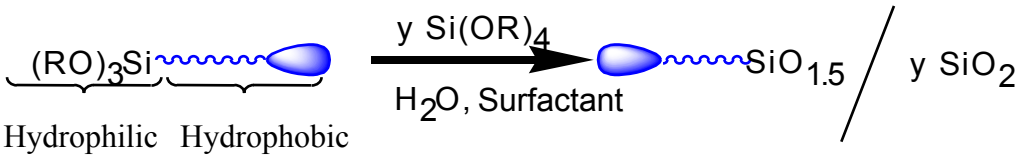

Figure 6-15: Synthesis of functionalised silica material

Figure 6-15 illustrates the synthesis of functionalised silica which were used for this work. These materials have been prepared in the University of Montpellier in the group of R.

Corriu. The porous structure of silica are used as templates for ruthenium particles as shown in Figure 6-16.

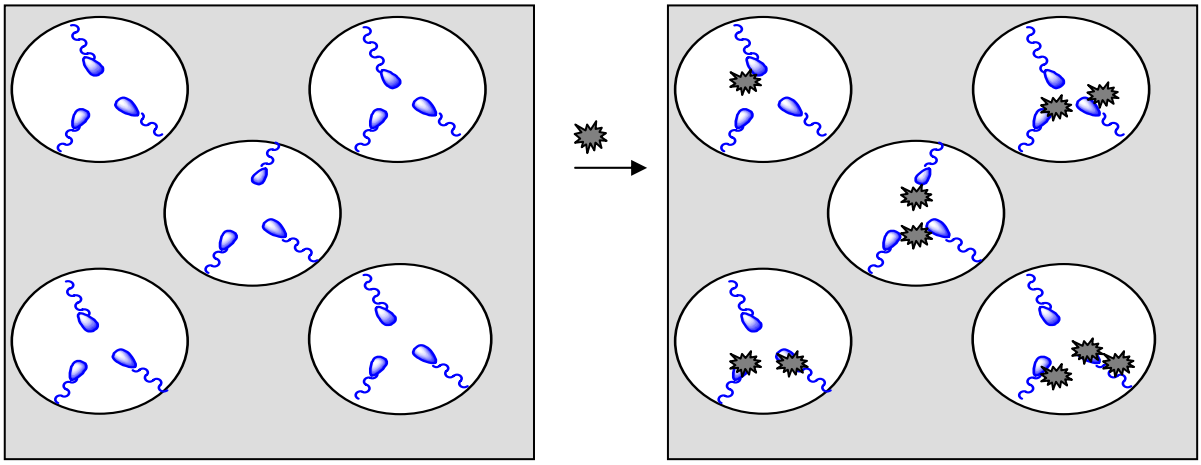

Figure 6-16 : Incorporation of metal nanoparticles inside mesoporous functionalised silica

In the work reported here, ruthenium nanoparticles have been successfully synthesised in the pore channels of selectively functionalised silica by a "in situ" reduction route (Scheme 6-2).

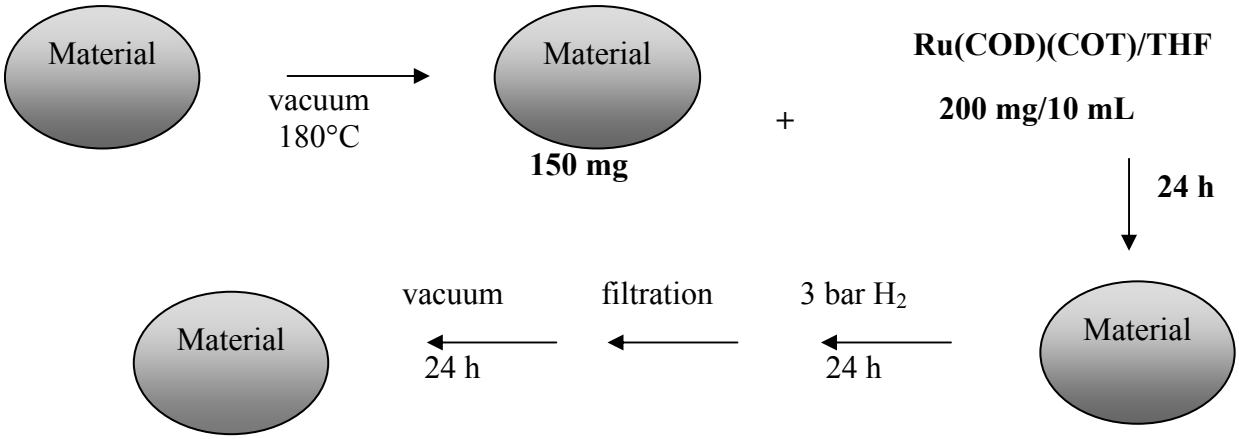

Scheme 6-2: Procedure for incorporation of Ru nanoparticles inside the mesoporous materials

The host materials used for the organisation of ruthenium nanoparticles inside their pores are new types of functionalised mesoporous silica which have been synthesised at the University of Montpellier. Such ordered mesoporous materials with uniform morphology and large porosity have a use in the organisation of Ru nanoclusters. The highly ordered mesoporous SBA-15 materials with high-yield rod-like morphology have been synthesised for

this purpose. Different functionalised materials as shown in Table 6-2 have been prepared to incorporate Ruthenium nanoparticles inside their pores.

Table 6-2: Functionalised mesoporous materials and their pore sizes

Mesoporous material	Pore size / Å
SBA-15	70
$HS(CH_2)_3SiO_{1.5}/9SiO_2$	45
$HO_2C(CH_2)_3SiO_{1.5}/9SiO_2$	72
$H_2N(CH_2)_3SiO_{1.5}/9SiO_2$	60
$(CH_3CH_2O)_2P(=O)(CH_2)_3SiO_{1.5}/9SiO_2$	52

The solid-supported metal particles were conventionally prepared by wet impregnation of a high surface area porous solid with the solution containing the organometallic precursor, followed by drying and decomposition of the precursor inside the pores under H_2 (Scheme 6-2). The colour of the porous material changes after incorporation of the metal particles from white to black. The incorporated ruthenium nanoparticles is uniform and comprised between 2,5 and 3 nm. In general, both a decrease of the specific surface of the material can be stated and a diminution of the observed peak in XRD studies can be asserted in agreement with pore filling of the host material.

6.3.2 SBA-15 as template for ruthenium nanoparticles

The incorporation of particles in the mesoporous silica SBA-15 material was achieved using a simple impregnation method. The pores of this material are organised parallel and their size is about 70 Å (Figure 6-17).

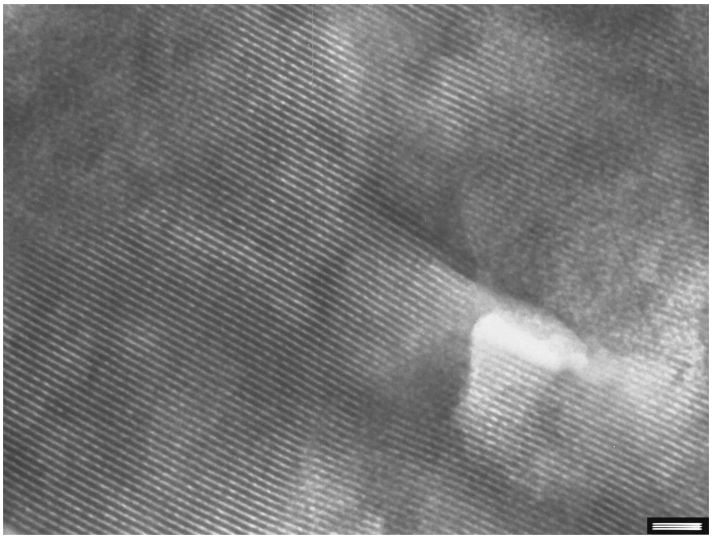

Figure 6-17: TEM micrograph of SBA-15

The support was brought in contact with the solution of THF containing Ru(COD)(COT) for 24 hours, then dried and pressurised under 3 bar dihydrogen for another 24 hours. The formation of nanoparticles inside the pores was observed. The ruthenium content demonstrated its dependency on the impregnation/reduction cycles. After two impregnation/reduction cycles the percentage of the metal inside the material amounts to 21 % ruthenium and with an additional impregnation/reduction cycle this goes up to 28 % ruthenium. In this case, utilising SBA-15, particles were formed both inside and outside the pores. Figure 6-18, showing a TEM micrograph of the SBA-15 with incorporated ruthenium, proves the presence of small particles inside the pores but also the presence of several small aggregates of particles at the surface of the material. Nevertheless, the ruthenium particles are confined in the pores and small Ruthenium particles are dispersed throughout the mesoporous silica. The size of the metal clusters is smaller than the pore diameter of the host (7 nm). The particles display a spherical aspect with an average size of 2.3 nm and are dispersed over all the areas that were investigated as shown in Figure 6-18.

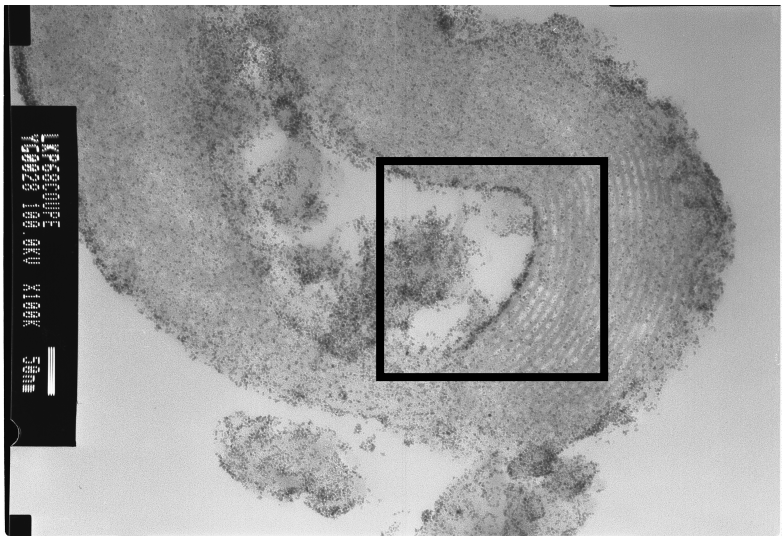

Figure 6-18: TEM micrograph of Ruthenium particles incorporated in SBA-15

In an enlargement of the TEM micrograph (Figure 6-19), it is possible to observe the presence of particles inside and outside of the mesopores. The particles display a spherical aspect with an average size of 2-2.5 nm.

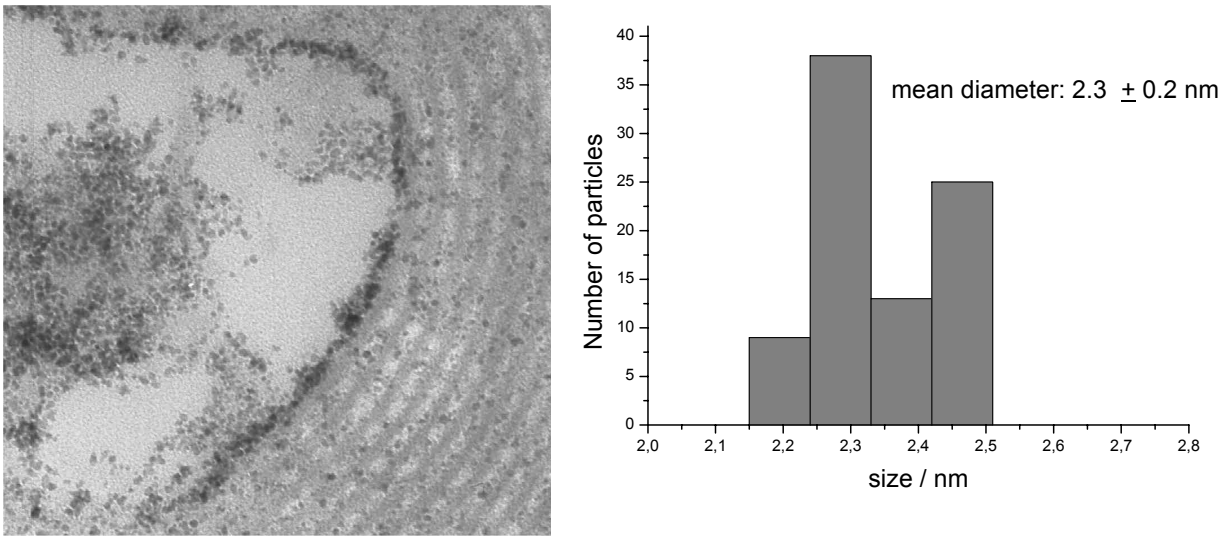

Figure 6-19: Enlargement of TEM micrograph and size histogram built form the TEM micrograph of ruthenium particles incorporated in SBA-15

The influence of the SBA-15 surface and the generation of the ruthenium nanoparticles inside its mesoporous structure was also investigated by X-ray diffraction (XRD). The detection of the main diffraction peaks indicates that the hexagonal framework of

the material has been retained very well after the incorporation of the ruthenium nanoparticles. The wide-angle X-ray diffractogram (Figure 6-20) displays that the size of the ruthenium particles inside the pores of the mesoporous silica is 2.3 nm.

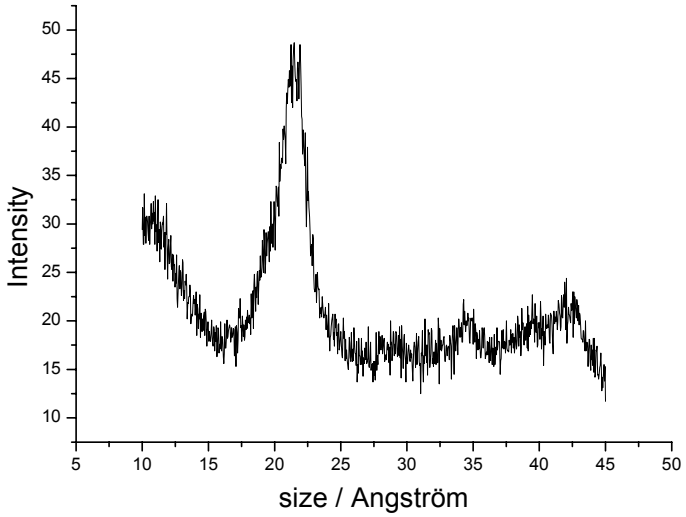

Figure 6-20: XRD measurements of ruthenium particles incorporated in SBA-15

In order to favour the incorporation of the ruthenium particles inside the mesoporous materials, we decided to synthesise functionalised silica as described below.

6.3.3 $HS(CH_2)_3SiO_{1.5}/9SiO_2$ as template for ruthenium nanoparticles

The first approach was the use of silica functionalised with –SH groups. In this case the pore diameter of the material is 45 Å. The formation of the particles took only place at the outer surface of the mesoporous silica. The reason is probably an immediate reaction of the metallic precursor with the thiol groups at the surface of the silica. After an additional impregnation/reduction cycle the amount of the ruthenium only increased from 10.62 % after two impregnation/reduction cycles to 11.30 % after three impregnation/reduction cycles: no further increase of the ruthenium content could be obtained after more impregnation/reduction cycles. This suggests that the reduced ruthenium derived from the second incorporation tent to aggregate at the surface of existing ruthenium particles. The typical TEM micrograph of Figure 6-21 clearly shows the presence of ruthenium nanoparticles outside of the hexagonal channels of the $HS(CH_2)_3SiO_{1.5}/9SiO_2$. No particles inside the pores are revealed.

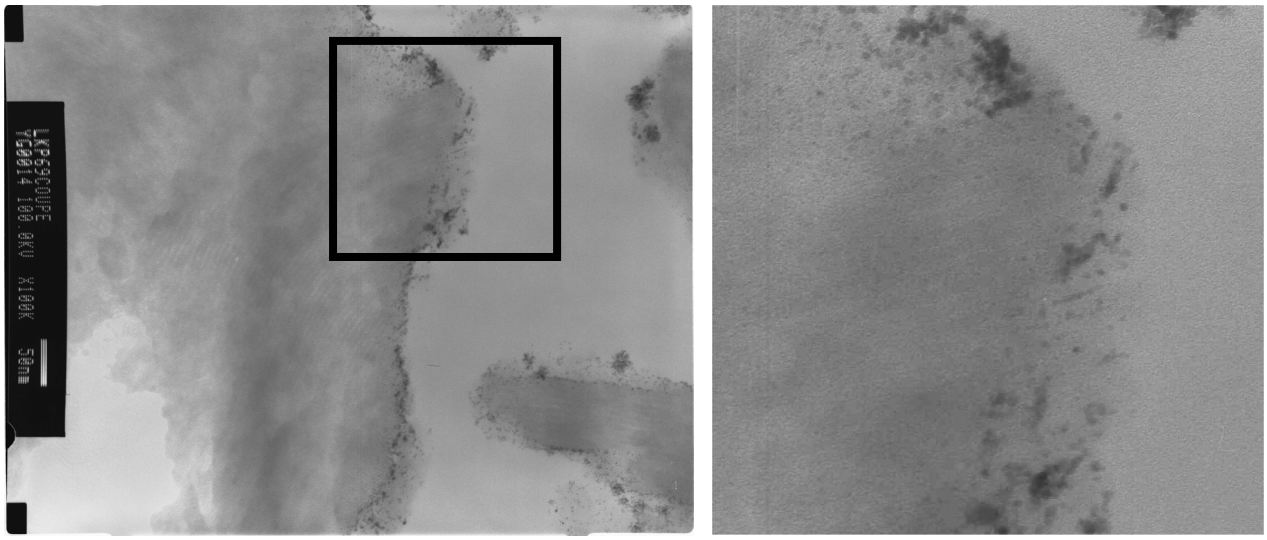

Figure 6-21: TEM micrographs and magnification of ruthenium particles incorporated in $HS(CH_2)_3SiO_{1.5}/9SiO_2$

XRD analysis (Figure 6-22) reveals that the material exhibits an intense diffraction peak, characteristic of crystalline ruthenium nanoparticles in a hcp structure a mean diameter of 2.0–2.5 nm. In addition, the overall pore structure was retained after functionalisation.

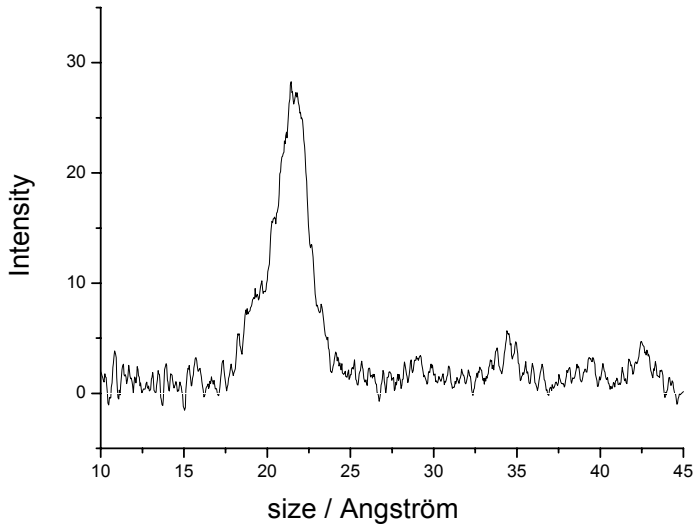

Figure 6-22: XRD measurements of ruthenium particles incorporated in $HS(CH_2)_3SiO_{1.5}/9SiO_2$

Upon treatment with a different functional group (-SH), the reduced ruthenium derived from secondary incorporation tend to agglomerate on the surface of existing ruthenium particles.

6.3.4 $HO_2C(CH_2)_3SiO_{1.5}/9SiO_2$ as template for ruthenium nanoparticles

When a mesoporous material functionalised with COOH groups was used for the organisation of ruthenium nanoparticles, the incorporation of the particles in the pores was not very regular. The pores of this material present a diameter 72 Å. Some particles form bigger agglomerates outside the material. Nevertheless, the presence of small particles inside the pores can be observed (Figure 6-23).

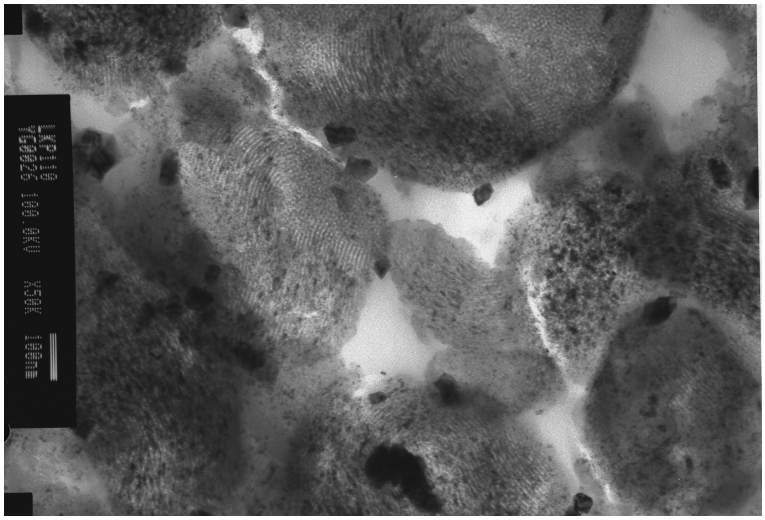

Figure 6-23: TEM micrograph of Ruthenium particles incorporated in $HO_2C(CH_2)_3SiO_{1.5}/9SiO_2$

The estimation of the particles size by eye was difficult due to the agglomeration of the particles. A mean size of 2.4 nm was discovered by XRD analysis (Figure 6-24)

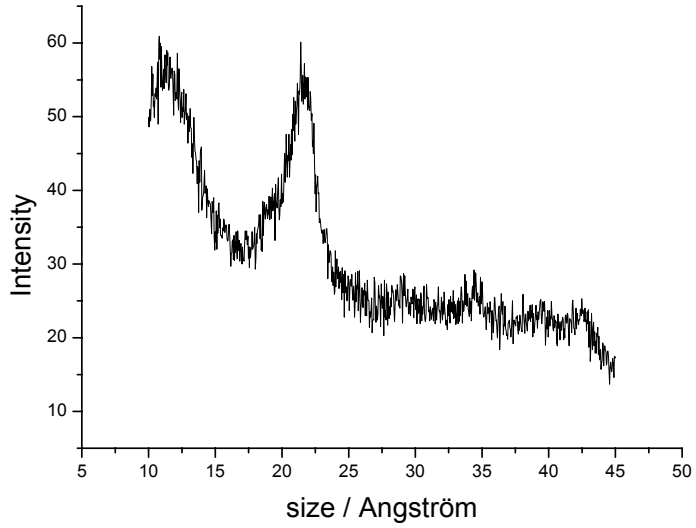

Figure 6-24: XRD measurements of ruthenium particles incorporated in $HO_2C(CH_2)_3SiO_{1.5}/9SiO_2$

6.3.5 $H_2N(CH_2)_3SiO_{1.5}/9SiO_2$ as template for ruthenium nanoparticles

A novel type of functionalised mesoporous silica was prepared containing -NH_2 groups. The pore size of this material is about 60 Å. In this case, ruthenium particles are clearly visible quasi-exclusively within the pore channels of the material. However, due to the "hyper-branched" morphology of this material, the accessibility to the pore channels seems to be limited. Indeed, a non homogeneous distribution of the nanoparticles within the material is obtained. The nanoparticles are mainly located in the border pore channels (Figure 6-25).

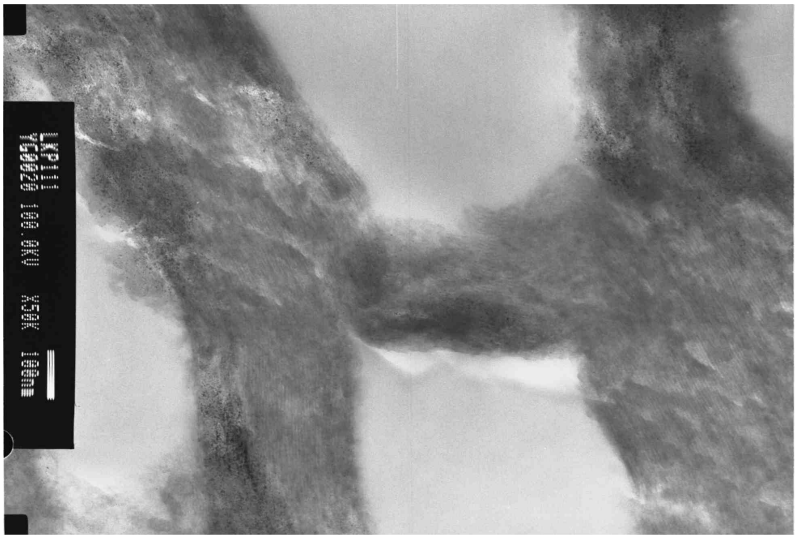

Figure 6-25: TEM micrograph of ruthenium particles incorporated in $H_2N(CH_2)_3SiO_{1.5}/9SiO_2$ after one impregnation/reduction cycle

Even after an additional impregnation/reduction cycle (Figure 6-26), the incorporation of the particles did not improve: agglomerated particles can be observed as clouds which are situated on top of the material.

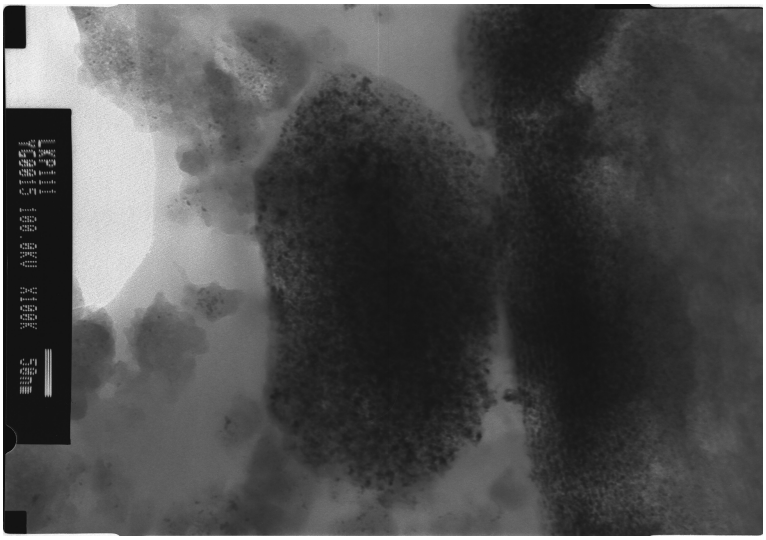

Figure 6-26: TEM micrograph of ruthenium particles incorporated in $H_2N(CH_2)_3SiO_{1.5}/9SiO_2$ after two impregnation/reduction cycles

In order to improve the incorporation of the ruthenium particles, a different functionalised silica was prepared.

6.3.6 $(CH_3CH_2O)_2P(=O)(CH_2)_3SiO_{1.5}/9SiO_2$ as template for Ru nanoparticles

Prior modification of the inner pore surface with Si-P groups was accomplished using a selective functionalisation method on the inner pore walls; therefore, the ruthenium nanoparticles can only form in the pore channels. The pore diameter of this material is estimated to be 52 Å. The specific surface area is 831 $m^2g^{-1}$and the volume of the pores is 1.15 cm^3g^{-1}.

TEM imagery permits direct observation of the morphology and distribution of ruthenium nanoparticles in the $(CH_3CH_2O)_2P(=O)(CH_2)_3SiO_{1.5}/9SiO_2$ composite. For only one cycle of impregnation, the presence of the particles inside the pores can be confirmed. Figure 6-28 clearly shows uniformly dispersed ruthenium nanoparticles in the hexagonal channels of $(CH_3CH_2O)_2P(=O)(CH_2)_3SiO_{1.5}/9SiO_2$. The particles are, on average, 2.0-3.0 nm in size and of regular shape. The metal particles are only found inside the channels of the mesoporous material.

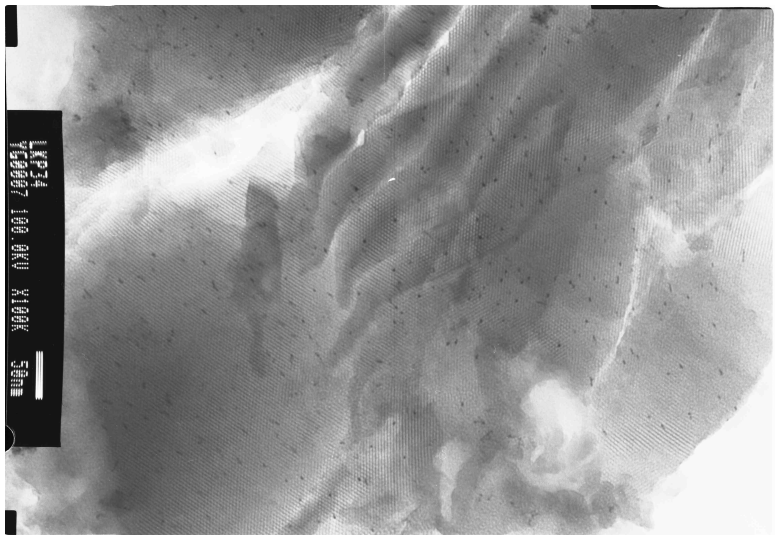

Figure 6-27: TEM micrograph of ruthenium particles incorporated in $(CH_3CH_2O)_2P(=O)(CH_2)_3SiO_{1.5}/9SiO_2$ after one impregnation/reduction cycle

After two impregnation/reduction cycles, the density of the metal in the pores clearly increased as can bee see from the TEM micrograph (Figure 6-28). A tendency to form elongated forms can be observed.

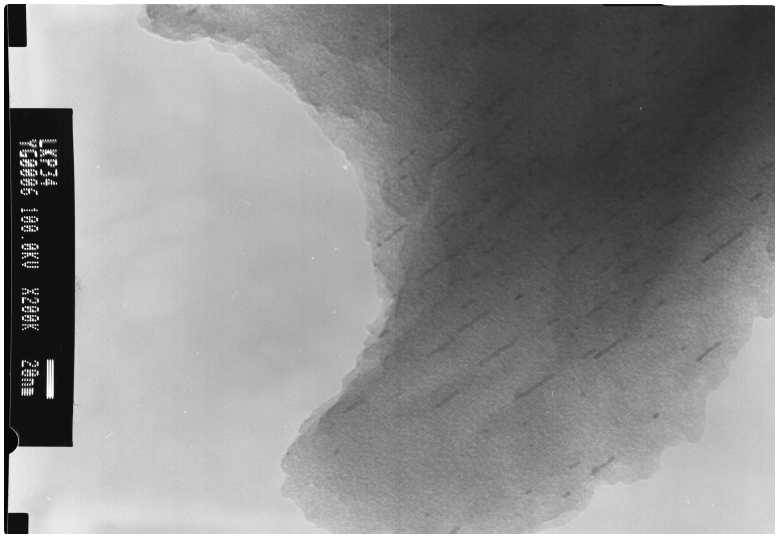

Figure 6-28: TEM micrograph of ruthenium particles incorporated in $(CH_3CH_2O)_2P(=O)(CH_2)_3SiO_{1.5}/9SiO_2$ after one impregnation/reduction cycle

The particles maintain the same size as those in SBA-15 (2.3 nm) and have a slightly higher particle density in the channels. The reduced ruthenium derived from the second incorporation tent to form individual small particles in the channels of $(CH_3CH_2O)_2P(=O)(CH_2)_3SiO_{1.5}/9SiO_2$. This demonstrates that the amount of metal loading as well as the morphology of Ru in host $(CH_3CH_2O)_2P(=O)(CH_2)_3SiO_{1.5}/9SiO_2$ can be rationally

favoured depending on the functional groups of the host and through repeating reduction cycles. When two impregnation/reduction cycles are completed, we could observe a progessive formation of Ru nanorods inside the pores of the material (Figure 6-29).

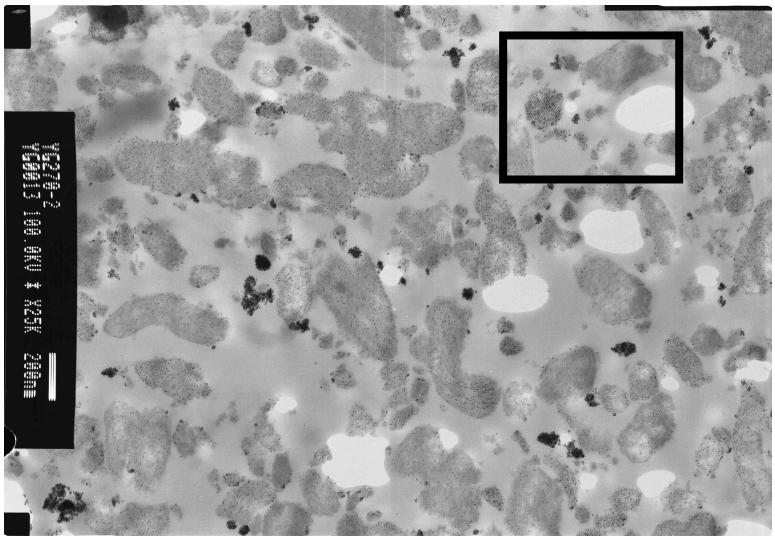

Figure 6-29: TEM micrograph of ruthenium particles incorporated in $(CH_3CH_2O)_2P(=O)(CH_2)_3SiO_{1.5}/9SiO_2$ after two impregnation/reduction cycles

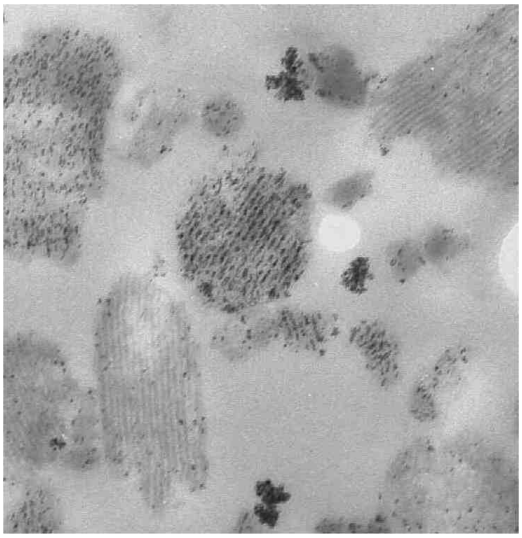

Figure 6-30: Enlargement of TEM micrograph of ruthenium particles incorporated in $(CH_3CH_2O)_2P(=O)(CH_2)_3SiO_{1.5}/9SiO_2$ after two impregnation/reduction cycles

The enlargement of the TEM micrograph provides further information on the ruthenium particles within the mesoporous silica framework channels. As seen in Figure 6-30, the regular pore structure consists of metallic nanowires within the channels of $(CH_3CH_2O)_2P(=O)(CH_2)_3SiO_{1.5}/9SiO_2$. The size of the particles in this material was investigated by XRD analysis (Figure 6-31) and a mean diameter of 2.4 nm was obtained.

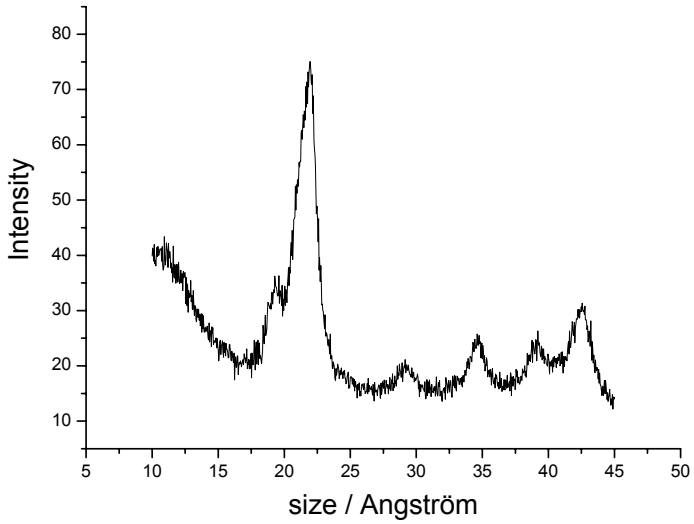

Figure 6-31: XRD measurements of ruthenium particles incorporated in $(CH_3CH_2O)_2P(=O)(CH_2)_3SiO_{1.5}/9SiO_2$

When the impregnation/reduction cycle is repeated, the density of the metal inside the pores of $(CH_3CH_2O)_2P(=O)(CH_2)_3SiO_{1.5}/9SiO_2$ clearly augmented.

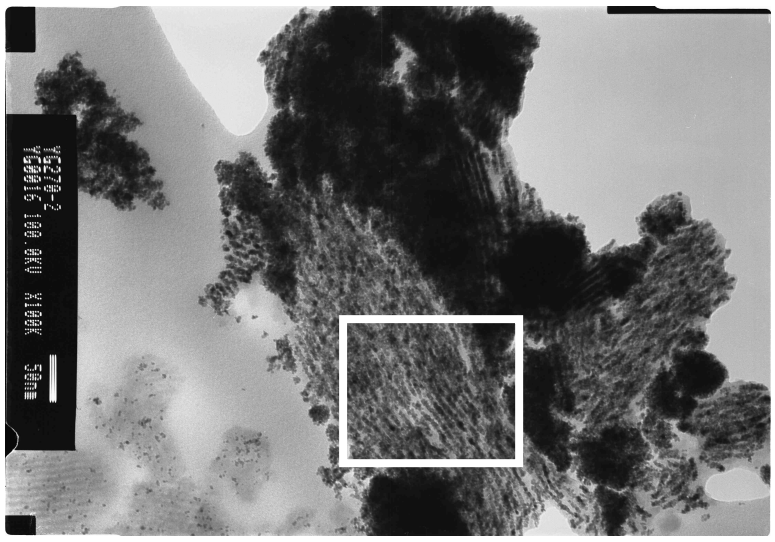

Figure 6-32: TEM micrograph of ruthenium particles incorporated in $(CH_3CH_2O)_2P(=O)(CH_2)_3SiO_{1.5}/9SiO_2$ after 3 impregnation/reduction cycles

The TEM micrograph (Figure 6-32) shows that the density of ruthenium particles in modified $(CH_3CH_2O)_2P(=O)(CH_2)_3SiO_{1.5}/9SiO_2$ silica increases. A significant improvement in the formation of nanowires is also evident. It is apparent from the TEM studies, that a much better incorporation of particles is obtained by repeated impregnation/reduction cycles and

surfactant modified silica which have a preference for the growth of ruthenium particles inside their pores. A growth of ruthenium nanowires inside the pores can be observed. The entrapped ruthenium particles are visible in an enlargement in Figure 6-33, which shows that the spatial distribution of the nanoparticles perpendicular to the channels is consistent with the pore spacing. It provides a direct proof of the presence of metallic nanowires within the channels of $(CH_3CH_2O)_2P(=O)(CH_2)_3SiO_{1.5}/9SiO_2$. The regular structure of the nanowires further demonstrates the superior performance of this functionalised silica material.

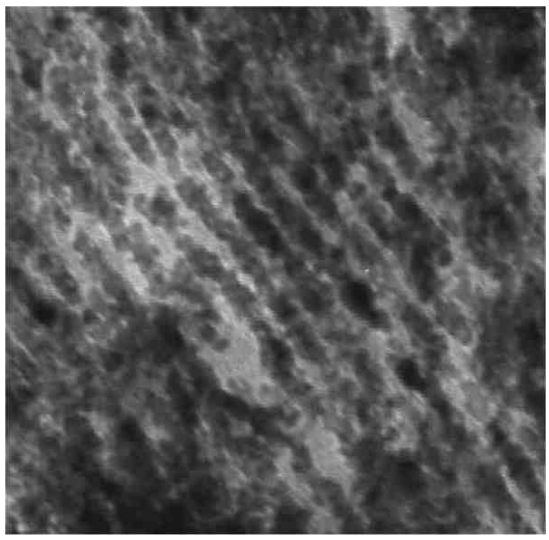

Figure 6-33: Enlargement of TEM micrograph of ruthenium particles incorporated in $(CH_3CH_2O)_2P(=O)(CH_2)_3SiO_{1.5}/9SiO_2$ after repeated impregnation/reduction cycles

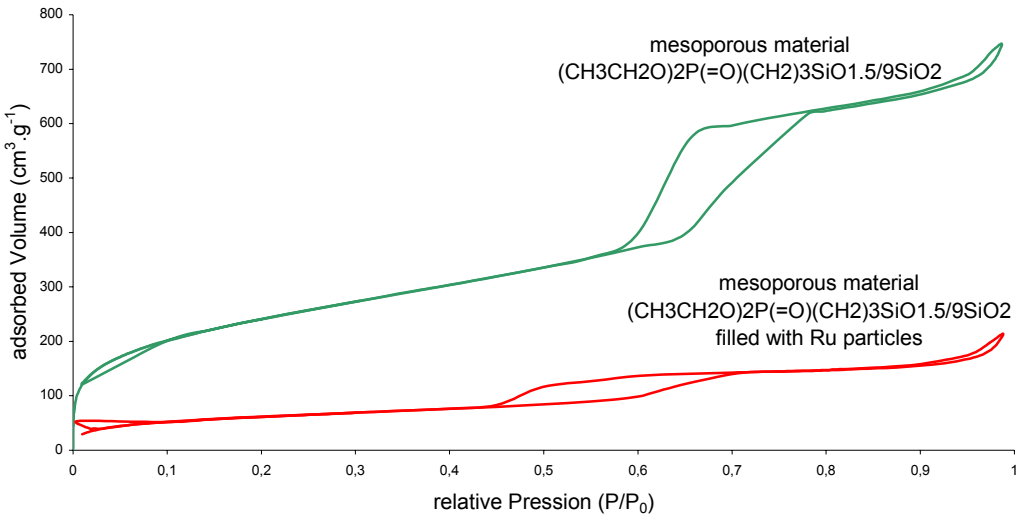

Figure 6-34: Isotherms of the mesoporous material $(CH_3CH_2O)_2P(=O)(CH_2)_3SiO_{1.5}/9SiO_2$ before and after filling with ruthenium nanoparticles

The adsorbed volume increases for the filled material decreased in comparison with the initial pore volume. The decrease of the adsorbed volume is in agreement with a smaller specific surface (Figure 6-34). The hysteresis shifts slightly to the left which is in accordance with a decrease of the pore size due to the incorporated Ru nanoparticles as shown in Figure 6-35.

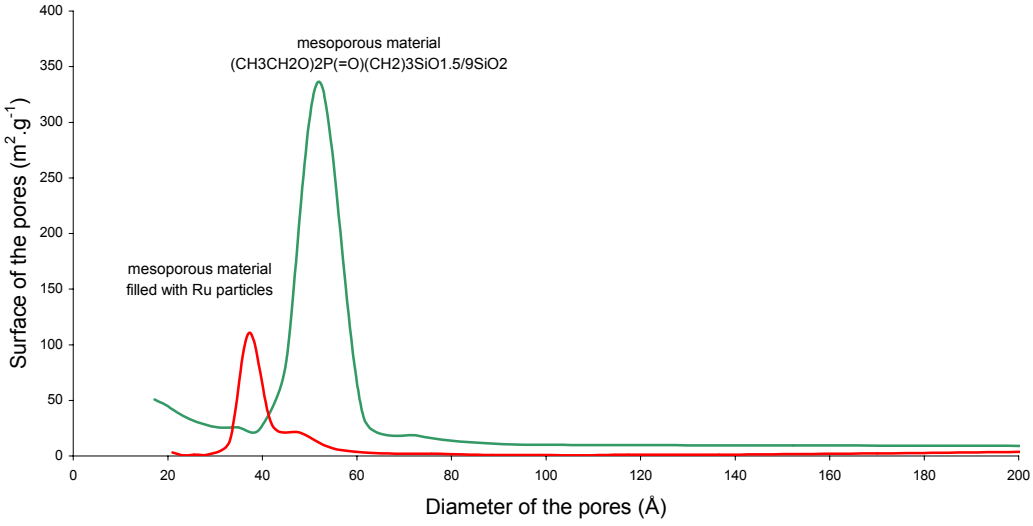

Figure 6-35: Influence of the incorporated Ru nanoparticles on the pore diameter of the silica

The material obtained, Ru / $(CH_3CH_2O)_2P(=O)(CH_2)_3SiO_{1.5}/9SiO_2$ was calcinated at two different temperatures (100 °C, 300 °C) and under either argon or under oxygen.

For the calcinations at 100 °C, some variation of the material could be observed. The aspect of the particles inside the pores of the material seem to change and the formation of agglomerates can be stated (Figure 6-36).

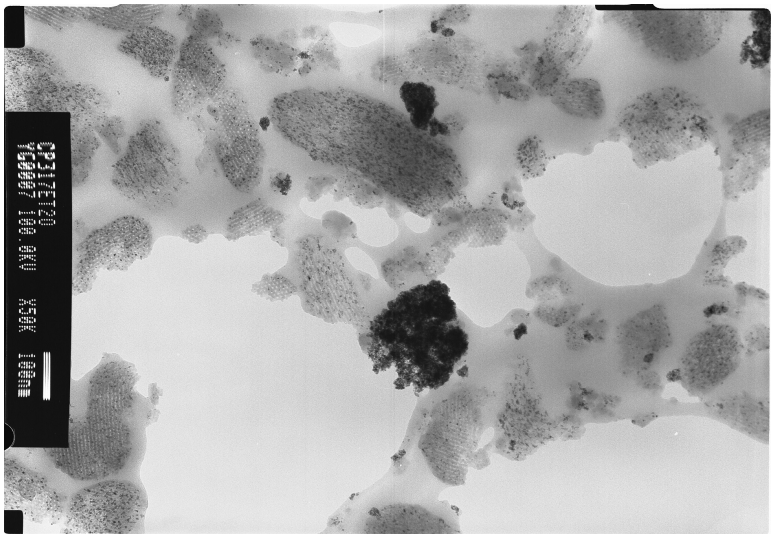

Figure 6-36: TEM micrograph of Ru / $(CH_3CH_2O)_2P(=O)(CH_2)_3SiO_{1.5}/9SiO_2$ after calcination at 100 °C under argon

If the temperature is increased to 300 °C, an even more obvious change is apparent. This different aspect is due to the destruction of the mesoporous system, which is obviously not stable at this high temperature. Therefore the organisation of the particles is not given any more (Figure 6-37).

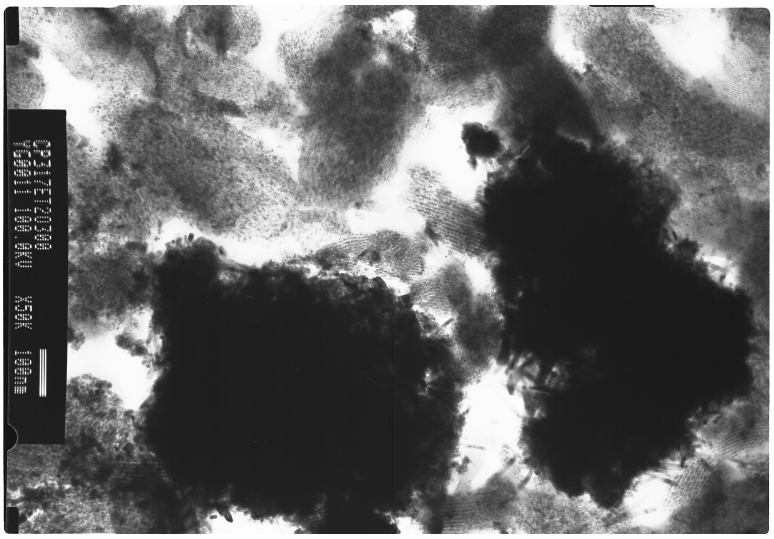

Figure 6-37: TEM micrograph of Ru / $(CH_3CH_2O)_2P(=O)(CH_2)_3SiO_{1.5}/9SiO_2$ after calcination at 300 °C under argon

The calcination under argon seems to lead to the formation of agglomerated ruthenium particles outside the pores. Surprisingly, a calcination under air does not lead to changes in the system. The material stays the same as can be seen from the TEM micrograph in Figure 6-38.

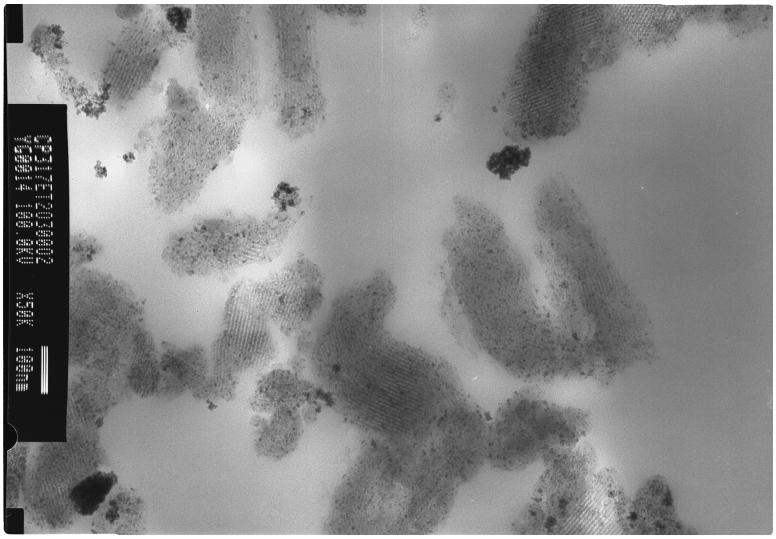

Figure 6-38: TEM micrograph of Ru / $(CH_3CH_2O)_2P(=O)(CH_2)_3SiO_{1.5}/9SiO_2$ after calcination at 300 °C under air

A formation of RuO_2 which could limit the coalescence of the particles was suggested. This could be verified by XRD analysis since the presence of a signal corresponding to RuO_2 was observed (Figure 6-39).

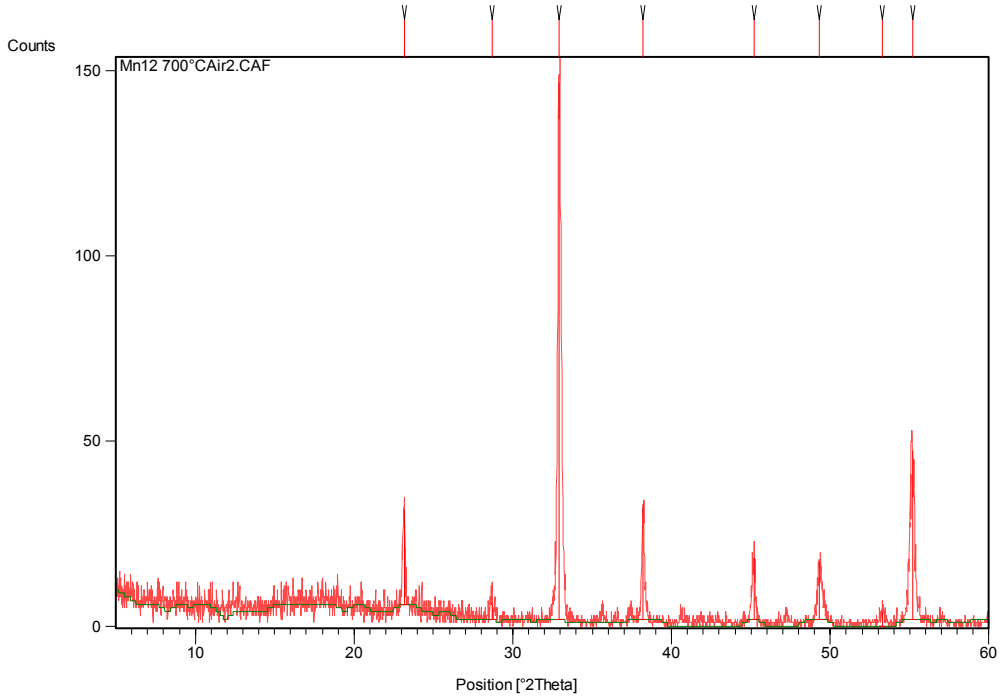

Figure 6-39: XRD measurements of Ru / $(CH_3CH_2O)_2P(=O)(CH_2)_3SiO_{1.5}/9SiO_2$ after calcination under air

For the incorporation of ruthenium nanoparticles inside the pores of the mesoporous material $CH_3CH_2O)_2P(=O)(CH_2)_3SiO_{1.5}/9SiO_2$ the formation of Ru nanowires could be observed in the channels of the silica. This shows that the modification of the surface is the key step for selective Ruthenium loading in the pore channels.

Another method for the organisation of the Ru particles inside mesoporous templates have been attempted. Therefore, we stabilised the particles with an organic molecule to perform a hydrolysis reaction on the molecule afterwards in order to form a mesoporous material around the particles.

6.3.7 $Ph_2N(CH_2)_{11}O(CH_2)_3Si(OEt)_3$ as stabilising agent for ruthenium particles

As a second approach for the incorporation of Ru nanoparticles inside of mesoporous silica, the organic molecule $Ph_2N(CH_2)_{11}O(CH_2)_3Si(OEt)_3$ was used in order to stabilise in a first step the ruthenium nanoparticules with this ligand. The molecule contains a group which is able to stabilise the Ru particles and a group which can then be polycondensed in order to

form the mesoporous silica around the particles. In a second step the hydrolysis of the (Si-$OEt)_3$ group of the molecule can be realised.

This ligand was added to a solution of the organometallic precursor Ru (COD)(COT) which was decomposed under the usual conditions as seen in Scheme 6-3.

$$Ru(COD)(COT) + Ph_2N(CH_2)_{11}O(CH_2)_3Si(OEt)_3 \xrightarrow[\text{3 bar } H_2,\ \text{r.t., 45 min.}]{\text{MeOH/THF}} [Ru^0]Ph_2N(CH_2)_{11}O(CH_2)_3Si(OEt)_3$$

Scheme 6-3: Stabilisation of Ru nanoparticles by $Ph_2N(CH_2)_{11}O(CH_2)_3Si(OEt)_3$

Figure 6-40 shows the aspect of ruthenium particles stabilised by 0.5 eq $Ph_2N(CH_2)_{11}O(CH_2)_3Si(OEt)_3$. All particles are of a homogenous size of 3 nm and are dispersed regularly on the microscopy grid. A localised self-organisation was observed.

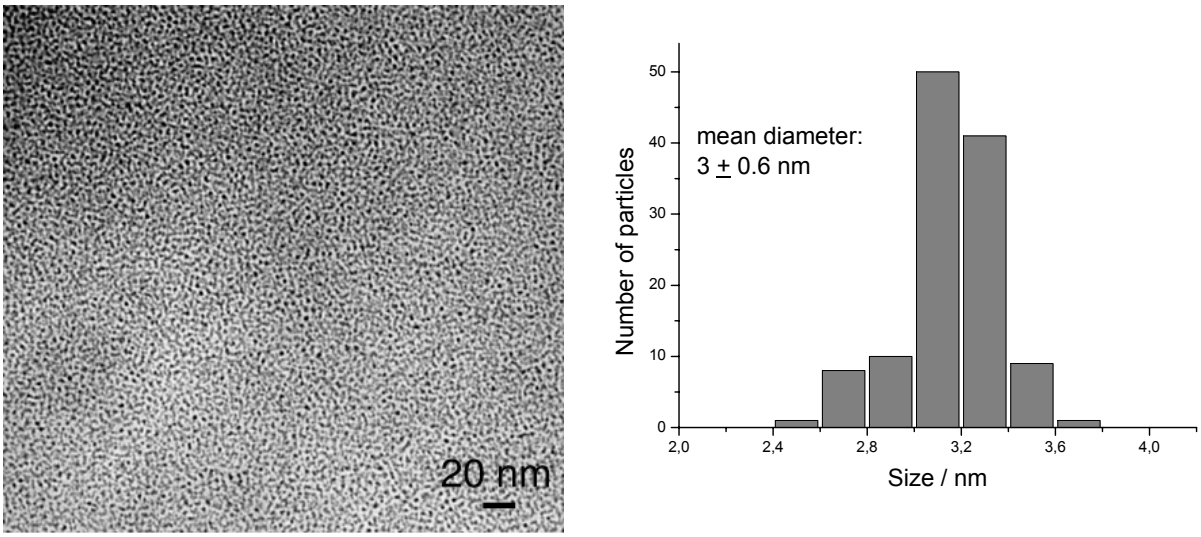

Figure 6-40: TEM micrograph and size histogram of ruthenium particles stabilised by 0.5 eq $Ph_2N(CH_2)_{11}O(CH_2)_3Si(OEt)_3$

To finalise, this solution was treated by sol-gel process and was followed by a calcination at 300 °C as shown in Scheme 6-4.

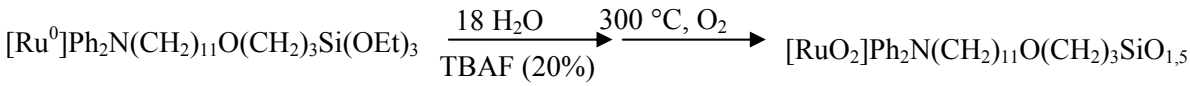

Scheme 6-4: Treatment of the Ru / $Ph_2N(CH_2)_{11}O(CH_2)_3Si(OEt)_3$ particles

After this treatment we obtained ruthenium particles inside the pores of the silica. The particles are regularly dispersed in the material and a beginning auto-organisation was observed as monitored in Figure 6-41.

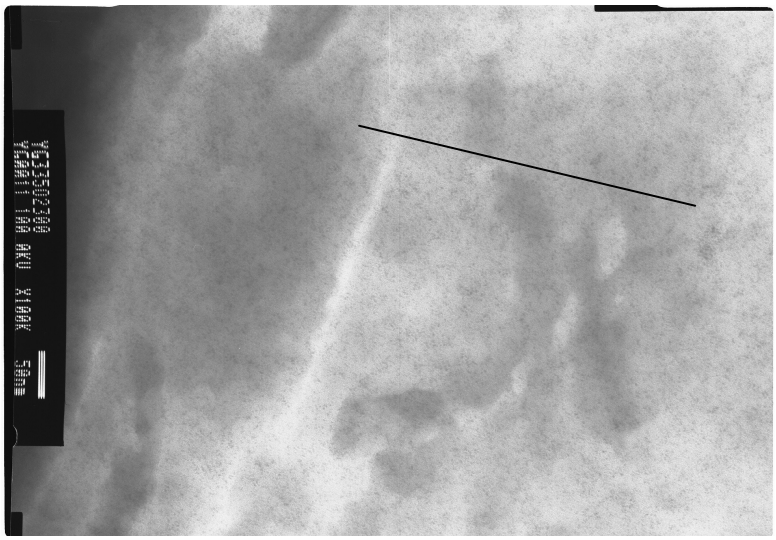

Figure 6-41: TEM micrograph of polymerised Ru / 0.5 eq $Ph_2N(CH_2)_{11}O(CH_2)_3Si(OEt)_3$

6.3.8 Conclusion

In conclusion, ruthenium nanoparticles have been synthesised within the pore channels of selectively modified mesoporous silica using an impregnation and in situ reduction process with repeating impregnation/reduction cycles. The materials have been functionalised with various groups, thus effectively avoiding the formation of large agglomerates of particles outside the channels.

Table 6-3 summarises the obtained results for the different mesoporous silica.

Table 6-3: Results for the organisation of Ruthenium nanoparticles in mesoporous materials

Mesoporous material	Pore size / Å	Cycles	Ru / %	C / %	H / %	Si / %	S / %	XRD/ Å
SBA-15	70	2	21.35	13.95	1.30	23.97	-	23
		3	27.70	13.89	1.45	27.94	-	
$HS(CH_2)_3SiO_{1.5}/9SiO_2$	45	2	10.62	14.47	2.59	25.97	3.05	20-25
		3	11.30	15.98	2.43	26.7	3.10	
$HO_2C(CH_2)_3SiO_{1.5}/9SiO_2$	72	1					-	
$H_2N(CH_2)_3SiO_{1.5}/9SiO_2$	60	1					-	24
$(CH_3CH_2O)_2P(=O)(CH_2)_3SiO_{1.5}/9SiO_2$	52	1	21.81	13.4	1.45	24.80	-	24
		2	22.46	11.79	1.89	28.21	-	
		3	31.62	14.3	2.71	26.43	-	

For SBA-15, the presence of the particles was observed both inside and outside of the pores. The mean size of the particles is 2.3 nm. The use of $HS(CH_2)_3SiO_{1.5}/9SiO_2$, $HO_2C(CH_2)_3SiO_{1.5}/9SiO_2$ and $H_2N(CH_2)_3SiO_{1.5}/9SiO_2$ did not lead to well organised particles inside the materials. These materials do not have the capability to incorporate nanoparticles in their pores. In the case of $HS(CH_2)_3SiO_{1.5}/9SiO_2$, the formation of particles (2.0-2.5 nm) could only be observed outside the pores. In contrast to that, the material $(CH_3CH_2O)_2P(=O)(CH_2)_3SiO_{1.5}/9SiO_2$ is able to organise the particles of 2.4 nm inside its pores. In addition, a formation of elongated agglomerates of particles could be observed. By increasing to three the number of impregnation and decomposition cycles, the formation of nanowires could be obtained in this case. Ruthenium nanoclusters were formed from Ru(COD)(COT) in the pore channels, by in situ reduction, with a concentration values of more than 20 % on average. A preferential growth of Ruthenium wires along the channels was also observed in TEM micrographs.

In this work, it is shown that surfactant-modified silica supports provide nanoreactors inside the silica structure for the preparation of uniformly dispersed Ruthenium nanoparticles in the supports. It is apparent from the TEM and XRD studies that a much better particle dispersion and smaller and more uniform particles are obtained on certain surfactant-modified silica than with the unmodified solid. The functionalised silica act as better supports for the nanoparticles through covalent linkage by the pendant organic functionality, thereby perfectly accommodating them inside the mesopores.

In addition, ruthenium nanoparticles have been stabilised by long chain tertiary amines ($Ph_2N(CH_2)_{11}O(CH_2)_3Si(OEt)_3$). The obtained particles are monodisperse in size and homogeneously separated in solution. These nanoparticles which are formed show a tendency to organise themselves which increases after gelification of the solution.

These materials could find potential applications in catalysis.

7 Catalysis

In this chapter, catalytic applications of ruthenium nanoparticles will be described. In the first part the enantioselective catalysis of asymmetric hydrogen transfer from iso-propanol by ruthenium particles stabilised with chiral ligands is described. The second part concerns the hydrogenation of 1,3-butadiene and the oxidation of carbon monoxide by Ru particles induced in mesoporous alumina membranes.

A novel kind of heterogeneous catalyst, consisting of alumina membranes, whose pores were lined with palladium nanoparticles, was generated in our group.[237] Its use to hydrogenate 1,3-butadiene in the gas phase at room temperature resulted in an increase in activity of about 60 %, compared to the same material in a grinded form. This effect must be traced back to the fact that the gases are forced through the pores and therefore have intense contact with the Pd particles. In a heterogeneous catalytic system, using traditional supports, large parts of the gaseous components pass the catalyst through the interspaces.

The filling of nanoporous alumina membranes of various pore widths with ruthenium nanoparticles synthesised from the organometallic complex Ru(COD)(COT) and their application in 1,3-butadiene hydrogenation and CO oxidation was studied. These catalytic materials were obtained using two different methods.

The first approach to fill the pores of the membranes involves the use of pre-formed colloidal solutions. Colloidal solutions of size controlled ruthenium nanoparticles can be prepared by decomposition of the organometallic precursor Ru(COD)(COT) under an H_2 atmosphere in a methanol/THF mixture or a pure alcohol as solvent and in the absence of further stabilisers.[102] Different particles sizes can be obtained depending on the reaction medium composition. These quasi-naked particles are then expected to display high activity in catalysis. Such Ru colloidal solutions were further used to fill membranes of various pore diameters which were selected depending on the particles size. These concentrated pre-prepared nanoparticles solutions were transferred into membranes of adequate pore sizes by vacuum induction.

This second route consisted of the decomposition of Ru(COD)(COT) under usual conditions (3 bar H_2; 45 min.) inside the pores using concentrated solutions and vacuum drying.

This method appears efficient for preparing homogenous materials for catalysis. Therefore, nanoparticles embedded in membranes of appropriate pore size were prepared and tested in the catalytic hydrogenation reaction of 1,3-butadiene and oxidation of CO. The catalytic reactions were carried out in a closed system where 1,3-butadiene and H_2 or CO were pumped through a 200 μm thick membrane, sealed in a glass tube.[237]

7.1 Application of ruthenium nanoparticles stabilised by chiral aminoalcohol and oxazoline ligands in enantioselective catalysis

Chiral oxazolines were developed in 1884 by Andreasch et al..[238] Their application in asymmetric catalysis is known since the 1990s.[239] Although Ru molecular systems are extensively used in homogenous catalysis, Ru colloids remain little investigated.[240] Nitrogen donor ligands such as chiral oxazolines, easily prepared from β-aminoalcohols,[241] are used as stabilising agents for ruthenium nanoparticles. The co-ordination chemistry of chiral oxazolines and aminoalcohols has been studied for their applications to different enantioselective catalytic processes,[242,243] such as Ru-catalysed reduction of aryl/alkyl ketones.[148,244] β-aminoalcohols were shown to be excellent chiral auxiliaries in Ru-catalysed asymmetric hydrogen transfer processes.[245]

The molecular complex $[Ru(p\text{-cymene})Cl_2]_2$ was used for asymmetric hydrogen transfer.[246] Concerning the molecular systems, the highest activities are observed using aminoalcohols.

The catalytic activity of ruthenium nanoparticles stabilised by chiral ligands was investigated in asymmetric reduction processes. Asymmetric hydrogen transfer from isopropanol to acetophenone was catalysed by Ru colloids. The Ru/oxazolines catalysts are less active than the aminoalcohol ones but lead to better enantioselectivities.

The main drawback from homogeneous catalysis is the difficult recovery of the catalyst. There are two important approaches which attempt to solve this problem: the use of biphasic systems or the heterogenisation of catalysts. The application of nanoparticles leads to properties different from those known for molecular systems. When considering the field of asymmetric catalysis, the only systems which so far display a selectivity comparable to that of molecular complexes associate cinchonidine to platinum particles, both in heterogeneous and colloidal catalysis.[247,248] The use of novel systems associating metal nanoparticles and organic

ligands for selective catalytic transformations is very attractive but subject to several requirements. In order to adjust the properties of such materials in catalysis[249,250,251] and to obtain reproducible catalytic activities, the particles must have a controlled size and surface composition. They must also be stable under the reaction conditions. In the last few years, the synthesis of such materials in our group was accomplished using an organometallic approach as described in chapter 5.3. This interest in organometallic precursors arises both from the possibilities of access to monodisperse particles of very small size (1-2 nm) and from their interesting surface co-ordination chemistry, as demonstrated for amine-stabilised Ruthenium nanoparticles.[34] The surface area of catalysts increases markedly with the decrease of the particles size. For example, small nanoparticles with a diameter of 1 nm have approximately 100% of atoms on their surface, while bigger nanoparticles with a diameter of 10 nm only have about 15% of atoms on their surface. When the surface area is larger, the catalytic activity is higher.

Oxazoline ligands have been used as chiral auxiliaries in homogenous catalysis[252] and, over the last 10 years, have been applied to asymmetric catalysis.[253,254,255,256,257,258]

The first results Preliminary results of the catalytic tests conducted on asymmetric hydrogen transfer of acetophenone using isopropanol as hydrogen source (Scheme 7-1) concerning the use of chiral ligands stabilised Ru particles previously described in chapter 5.3 as catalysts are described in this chapter. The reaction takes place in basic conditions in isopropanol as the solvent. The conversion and the enantiomeric excess were determined by gas chromatography using a chiral column.

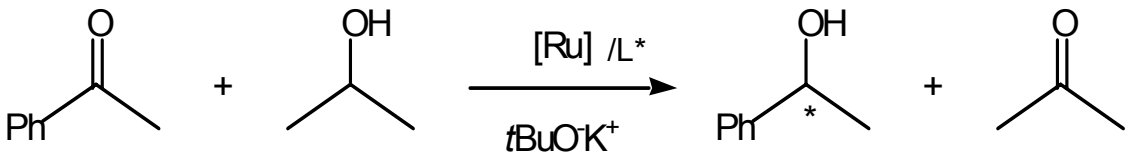

Scheme 7-1: Asymmetric hydrogen transfer of acetophenone using isopropanol catalysed by the stabilised Ru / L colloids*

This work has been carried out in collaboration with the Department of Inorganic Chemistry of the University of Barcelona in Spain, where the chiral ligands have been synthesised and the catalysis was performed. The chiral ligands used have previously been tested in molecular systems.[167,168,259,260,261,262,263] The catalytic tests are summarised in Table 7-1.

Table 7-1: Ru colloids-catalysed hydrogen transfer of acetophenone

Entry	Ru / L*		added ligand / eq	t / h	conversion / %	ee / %
1	1	$MoxNH_2Et$	0.2	12	58	0
2	1	$MoxNH_2Et$	1.2	12	64	0
3	1	$MoxNH_2Et$	2.2	12	10	11 (S)
4	2	$MoxNH_2iPr$	0.2	12	65	10 (R)
5	2	$MoxNH_2iPr$	1.2	12	15	10 (S)
6	2	$MoxNH_2iPr$	2.2	72	20	11 (S)
7	3	MoxOHEt	0.2	12	39	0
8	3	MoxOHEt	1.2	12	59	0
9	3	MoxOHEt	2.2	12	11	0
10	4	MoxOHiPr	0.2	12	85	0
11	4	MoxOHiPr	1.2	12	44	0
12	6	NH_2OH	0.2	12	77	0
13	6	NH_2OH	1.2	12	31	0
14	6	NH_2OH	2.2	12	2	14 (R)
15	7	NH_2OHiPr	2.2	12	5	nd
16	8	S,S-B	0.2	76	16	4 (R)
17	9	$Bisox(CH_2)_4Et$	0.2	12	53	0
18	9	$Bisox(CH_2)_4Et$	1.2	12	76	0
19	10	Bisox-SMe	0.2	12	98	0
20	10	Bisox-SMe	1.2	12	99	0
21	10	Bisox-SMe	2.2	12	56	5 (S)
22	11	S,S-G	0.2	48	62	5 (R)

In all cases, the asymmetric induction is very low. Blank tests demonstrated that no reaction is produced in L* absence. The presence of the ligand on the metallic surface is necessary to obtain active systems: systems without the ligand or in which the ligand is added during the catalysis do not display any activity (conversion after 72 hours: 9 %, ee: 0). For all nanocatalysts, the ligand concentration has an important impact on the reaction conversion. When an excess of ligand is added for catalysis the conversion decreases. But, higher ligand concentrations favour a modest but real and reproducible ee increase up to 14 %. This demonstrates the existence of an important interaction between colloidal particles and ligands. The colloids are recovered "unchanged" after catalysis which was corroborated by TEM spectroscopy (see for example Figure 7-1). The size of the particles remain unchanged, but their dispersion is different: they are more agglomerated after catalysis.

a) b)

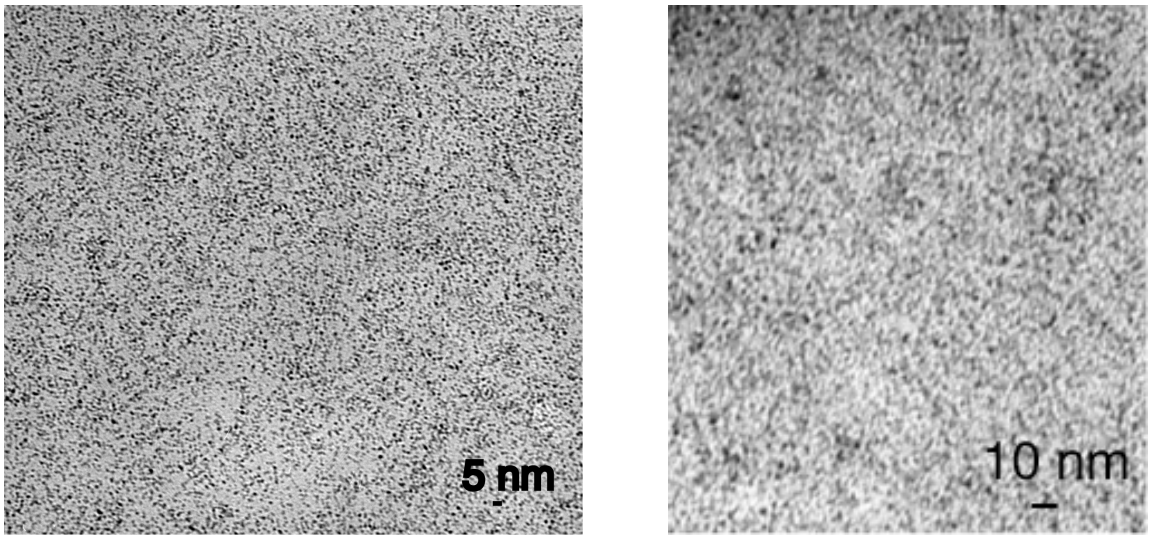

Figure 7-1 : TEM micrograph of Ru/MoxOH particles a) before and b) after catalysis

A very different behaviour between ruthenium complexes and colloids is observed: the colloids are more active, less selective than the molecular systems and very sensitive to temperature.

7.1.1 Conclusion

This is the first report to document the first synthesis of ruthenium nanoparticles stabilised by chiral ligands, namely aminoalcohols, alcohol- and amino-oxazolines. The surface co-ordination of the ligands leads to the stabilisation of the metal particles in solution as well as to a strong influence on their catalytic performances. Although the catalytic activities are not very good, these nanocatalysts are active in mild conditions and, in some cases, with oxazolines, more efficient but less selective than the corresponding molecular catalysts. The catalytic data are reviewed in Table 7-2.

Table 7-2: Molecular system catalysed hydrogen transfer of acetophenone with Ru

Entry	L	Ru/L	S/Ru	t (h)	Conversion(%)	ee (%)
1	$MoxNH_2Et$	1/2	20/1	24	20	43 (R)
2	$MoxNH_2iPr$	1/2	20/1	24	75	45 (S)
3	MoxOHiPr	1/2	20/1	72	1	nd
4	NH_2OH	1/1	20/1	0.75	90	10 (R)
5	NH_2OHiPr	1/1	20/1	0.75	92	32 (S)
6	S, S-B	1/2	20/1	72	92	25 (S)
7	Bisox-SMe	1/2	20/1	3	7	4 (S)
8	S, S,-G	1/2	20/1	48	62	29 (S)

The asymmetric hydrogen transfer from isopropanol to acetophenone was catalysed either by molecular systems (addition of ligands and with the pre-formed complexes on $[Ru(p\text{-cymene})Cl_2]_2$) or the Ru colloids described above (Table 7-1). Concerning the molecular systems, the highest activities are observed using Bisox-SMe. Colloids stabilised by aminoalcohols and oxazolines) are less active and selective than the corresponding molecular systems. However, Bisox-SMe (entries 19-21) are more active but less selective than the corresponding molecular catalysts. For nanocatalysts, the ligand concentration has an important impact on the reaction conversion. In all cases however, the asymmetric induction is very modest. The presence of the ligand on the metallic surface is necessary to give active systems. Furthermore, it is clear that higher ligand concentrations favour a modest but real and reproducible ee increase up to 14 %. This demonstrates the existence of an important interaction between colloidal particles and ligands.

This activity, different from that of colloids stabilised by oxazolines, and the very low enantiomeric excesses obtained compared to those of the molecular systems both suggest a fluxional behaviour of the ligands at the surface of ruthenium as recently observed for Ru / amine systems. This is also confirmed by the decrease in activity and increase in selectivity observed upon addition of excess ligand to the catalytic system. It is interesting to note the very modest but significant and reproducible ee associated with an increase of the oxazoline concentration in solution. The requirement is to design new ligands that are capable of binding to nanoparticles as well as performing target reactions.

When a pressure of 3 bar H_2 is added for the catalytic test with the Ru particles, an increase to nearly 100 % for the conversion can be observed, while no effect on the molecular system be stated. This suggest a high activity of the Ru nanoparticles in hydrogenation.

Catalytic reactions have also been carried out with ruthenium particles incorporated in mesoporous alumina membranes as will be described in the following section.

7.2 Catalytic hydrogenation of 1,3-butadiene by Ru nanoparticles inside mesoporous alumina membranes

It is known that heterogeneous catalysis only take place at the surface of the catalysts.[264] Metal nanoparticles possess a great number of surface atoms. The number of surface atoms rises when the size of the particles decreases. Naked ruthenium particles of adjustable size consist of a clean surface since no further stabilisers are used.[265] The synthesis method described in section 5.3 allows the preparation of ruthenium nanoparticles presenting several advantages:

- Size control
- Clean surface
- Highly porous surface

The real size control offers the possibility obtaining particles of various sizes which are giving then a ”panel” of potential catalytic materials. The high reactivity of these particles is demonstrated by their reaction with air: the particles are very air sensitive and burn in the open air. The active sites are then accessible. In addition, these particles present a porous aspect enhancing then the specific surface area which is important for the contact between reactivs in catalysis Such particles then present an interest as materials for catalysis.

Heterogeneous catalysis has been studied over the last 40 years.[266,267] Catalytic active systems need free co-ordination sites, consequently for heterogeneous catalysts only the surface atoms of the metal are reactive.[266] This makes an organisation in mesoporous systems appealing, rather than supporting metals to enlarge the contact area. Hydrogen on Pd, Pt and as well on Ru is dissociated on the metal surface and is therefore activated by the metal for

the hydrogenation of 1,3-butadiene.[268] Pd catalysts have been organised in alumina membranes and tested in heterogeneous catalysis.[237]

The Ru nanoparticles were organised inside the pores (see chapter 6) to increase the contact between the active surface sites on the catalyst and the gas for an increasing of the reactivity. Heterogeneous hydrogenation of 1,3–butadiene was chosen as a test reaction to characterise the reactivity of the Ru particles organised in Al_2O_3 membranes. The mechanism of the hydrogenation is illustrated in Figure 7-2.

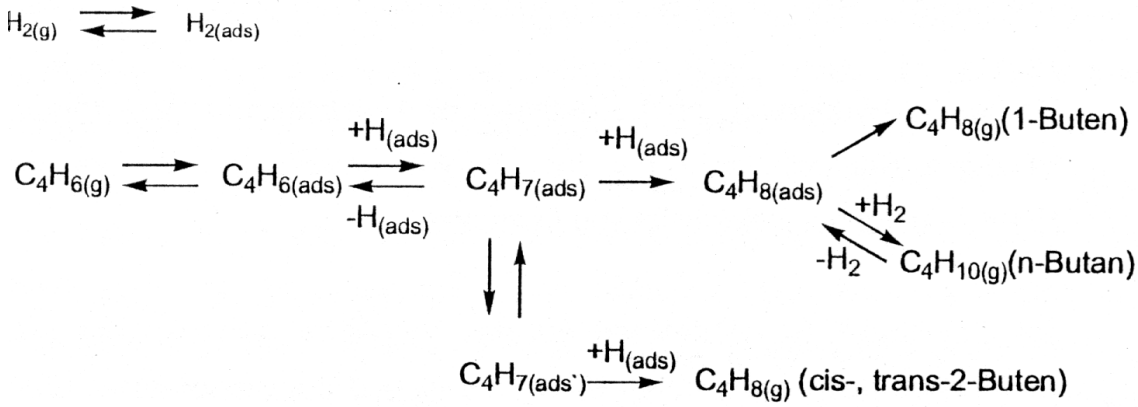

Figure 7-2: Mechanism of the hydrogenation of 1,3-butadiene[269]

Ruthenium nanoparticles included in alumina membranes have been prepared either by dihydrogen decomposition of the complex Ru(COD)(COT) to give pre-prepared colloidal solutions which were then used to fill the pores of nanoporous alumina membranes by vacuum introduction, or by *in situ* decomposition. These hybrid systems were tested in the hydrogenation of 1,3-butadiene and in the oxidation of carbon monoxide in the gas phase. The use of Ru loaded membranes resulted in considerably increased activities compared with grinded samples.

The catalytic reactions were conducted in a closed system where 1,3-butadiene and H_2 are pumped through a 200 μm thick membrane, sealed in a glass tube. The reaction products were analyzed by gas chromatography. The experimental set-up for the hydrogenation reactions is described in the experimental section.

As reported in chapter 6, the inclusion inside the channels of a membrane with a mean pore diameter of 21 nm using a solution of Ru(COD)(COT) in a mixture MeOH/THF 2.5/97.5

resulted in a loading of the pores with particles of 5 nm (Figure 7-3). This material has been used for catalytic hydrogenation of 1,3-butadiene in gas phase.

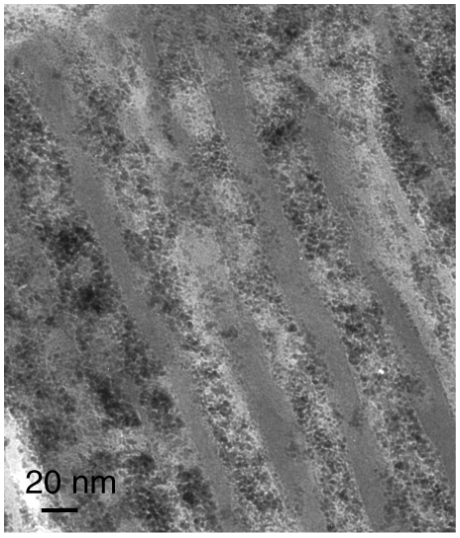

Figure 7-3: TEM image of Ru particles obtained from in situ decomposition of Ru(COD)(COT) in MeOH/THF 2.5/97.5 inside a channel of a 21 nm pores diameter alumina membrane (15 V)

With that material a very good conversion has already been obtained at room temperature. Figure 7-4 shows the course of the hydrogenation of 1,3-butadiene obtained at room temperature, using the catalytic material presented in Figure 7-3. After only 40 minutes a complete conversion of 1,3-butadiene to butane is achieved.

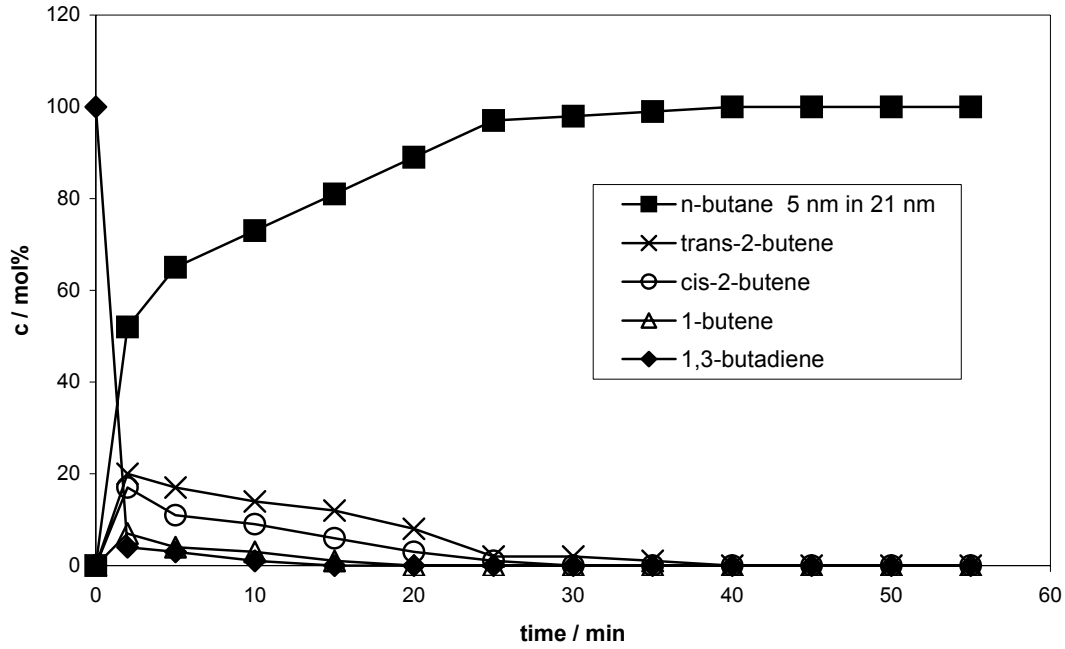

Figure 7-4: Course of hydrogenation of 1,3-butadiene at room temperature, using MeOH/THF 2.5/97.5 particles (3-6 nm) in 15 V Al_2O_3 membrane (21 nm)

Other particles sizes organised in Al_2O_3 membranes have also been tested. For example, Figure 7-5 shows the incorporation of Ru nanoparticles from a MeOH/THF 5/95 mixture inside the pores of a 20 V membrane. The aspect of the particles seems to be regular and they appear dense. An organisation in chains for the particles can be observed. Their mean diameter is evaluated at 17 nm.

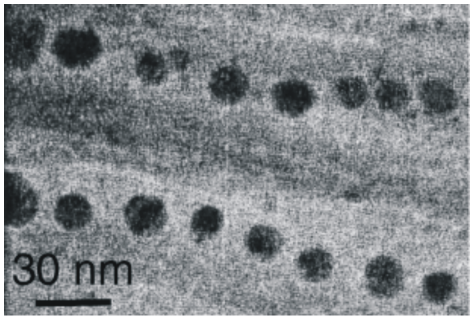

Figure 7-5: TEM image of Ru particles obtained from in situ decomposition of Ru(COD)(COT) in MeOH/THF 5/95 inside a channel of a 28 nm pores diameter alumina membrane (20 V)

With that catalyst, a conversion of 100 % was attained at room temperature after 60 minutes against a conversion of 100 % after only 40 minutes for the previous one. This can be explained by the larger size of the particles. Indeed, in the first case the mean size of the

particles is about 5 nm while in the second experiment the mean size is about 17 nm which indicates a decrease in the number of active sites in the second case.

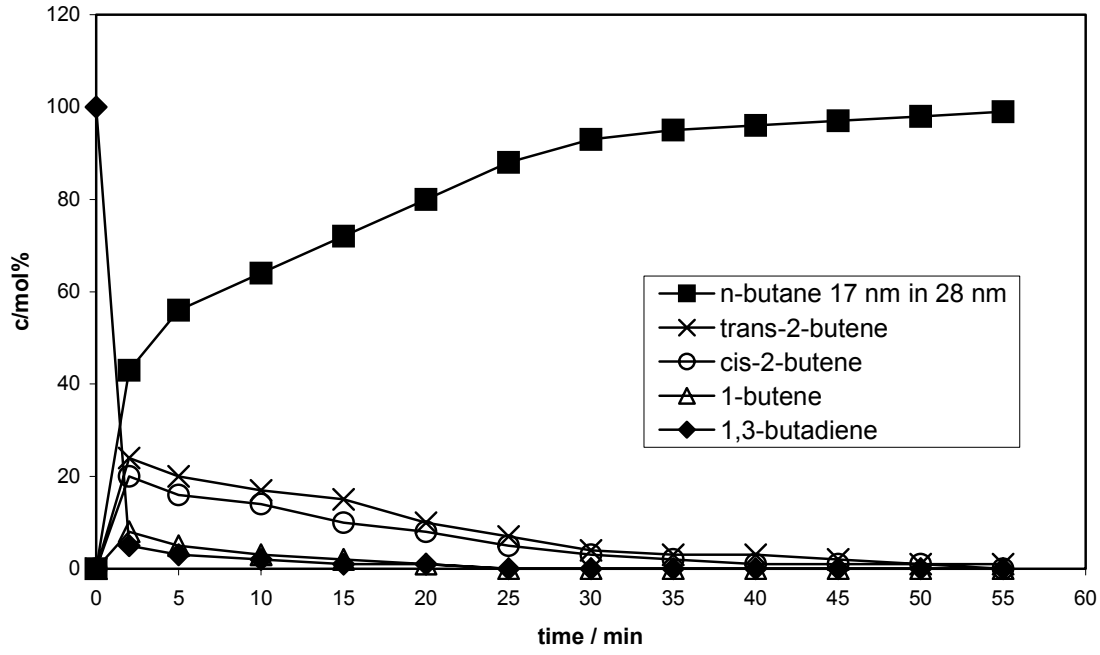

Figure 7-6: Course of hydrogenation of 1,3-butadiene at room temperature, using MeOH/THF 5/95 particles (16,7 nm) in 20 V Al_2O_3 membrane (28 nm)

This catalytic reaction has been studied for all the materials prepared by incorporation of Ru particles in Al_2O_3 membranes described in section 6.2. A correlation between the reactivity and their mean size could be defined: a decreasing of the activity of the particles has been observed with the increasing of their size.

Figure 7-7 a–c show three characteristic courses of hydrogenation with different particle sizes, representative of the eight different materials used in the performed catalytic reactions.

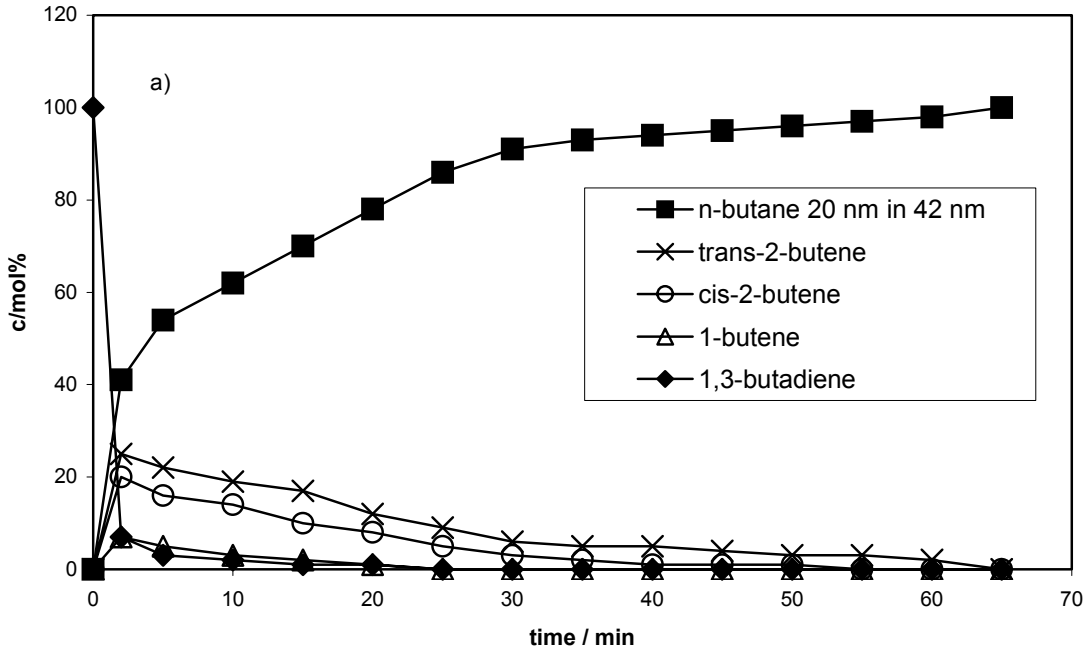
a)
c/mol%
time / min
n-butane 20 nm in 42 nm
trans-2-butene
cis-2-butene
1-butene
1,3-butadiene

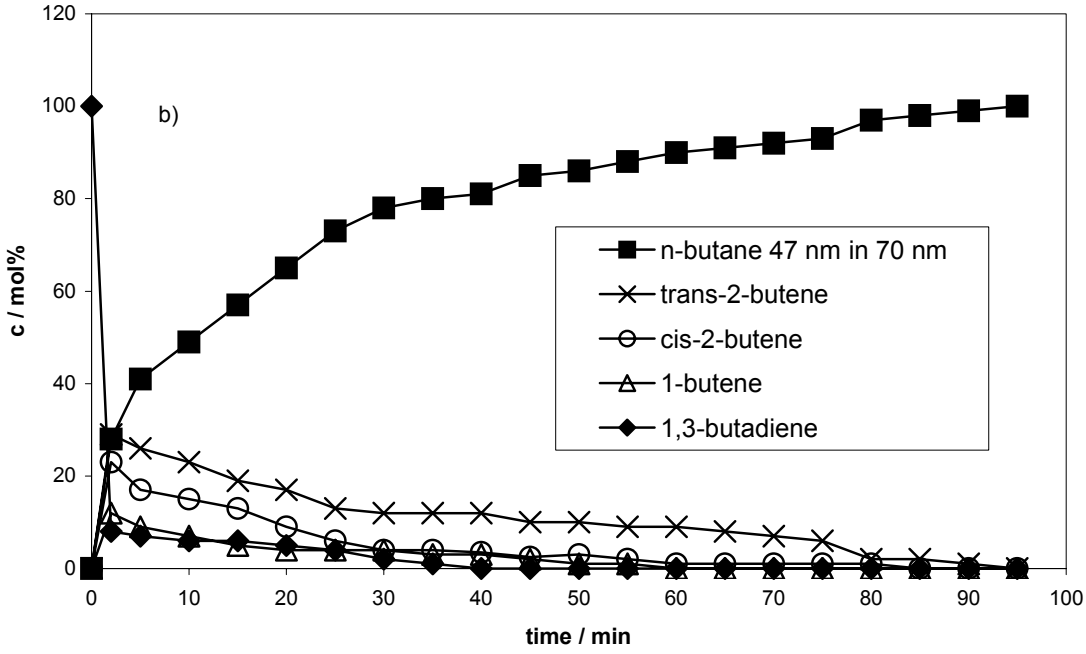
b)
c / mol%
time / min
n-butane 47 nm in 70 nm
trans-2-butene
cis-2-butene
1-butene
1,3-butadiene

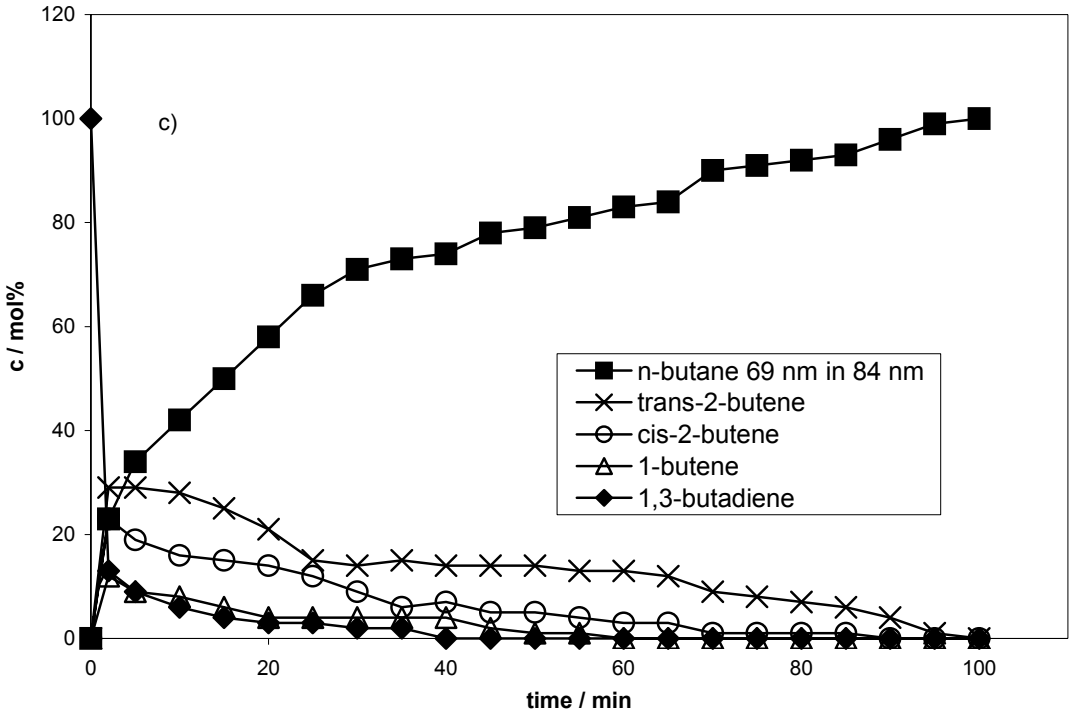

Figure 7-7: Course of hydrogenation of 1,3-butadiene at room temperature, using a) MeOH/THF 10/90 particles (19,8 nm) in 30V Al_2O_3 membrane (42 nm) b) MeOH/THF 50/50 particles (47 nm) in 50 V Al_2O_3 membrane (70 nm) and c) MeOH/THF 75/25 particles (69 nm) in 60 V Al_2O_3 membrane (84 nm)

7.2.1 Conclusion

Table 7-3 summarises the different performances of the different tested catalysts as a function of the particles size. The required time for a 100 % conversion is given for the catalytic reactions performed at room temperature.

Table 7-3: Relation between the particles size and their reactivity as a function of time

Particles size / nm	Pore diameter Al_2O_3/ nm	Time / min for 100 % conversion	T.O.F. / min^{-1}
5	21	40	325
17	28	60	317
20	42	65	311
24	42	76	302
34	56	84	296
47	70	97	287
69	84	102	281

Figure 7-8 summarises the catalytic results and shows the different time scales to reach full conversion according to the different catalytic systems consisting of nanoparticles incorporated into alumina membranes. As can easily be seen, the activity of the Ru nanoparticles decreases as their size increases. From the 100 % n-butane value after 40 minutes in the case with 3-6 nm particles, the activity continuously decreases to about 100 minutes for the 69 nm particles. The Turn over frequencies (T.O.F.)[270] have been calculated as follows:

$$TOF_i = \frac{\Delta n_i}{\Delta t \bullet n_{metal}}$$

with:

Δn_i = amount of formed product i

Δt = time interval

n_{metal} = amount of substance of catalyst

The best activity could be observed for the smallest particles in a 21 nm membrane with a T.O.F. of 325 min^{-1}. The activity decreases with the increasing particles sizes to a T.O.F. of 281 min^{-1} This trend could, of course, be expected since the smaller particles offer the more effective surface to the reactants. However, bearing in mind the purpose of this work, namely to study the importance of the structure of this kind of catalyst, it is of special interest to compare these results with those obtained when the same materials are used in a ground form instead of intact membranes. Similar catalytic reactions have been performed with ground materials containing after filling Ru nanoparticles with a mean diameter between 5 and 69 nm.

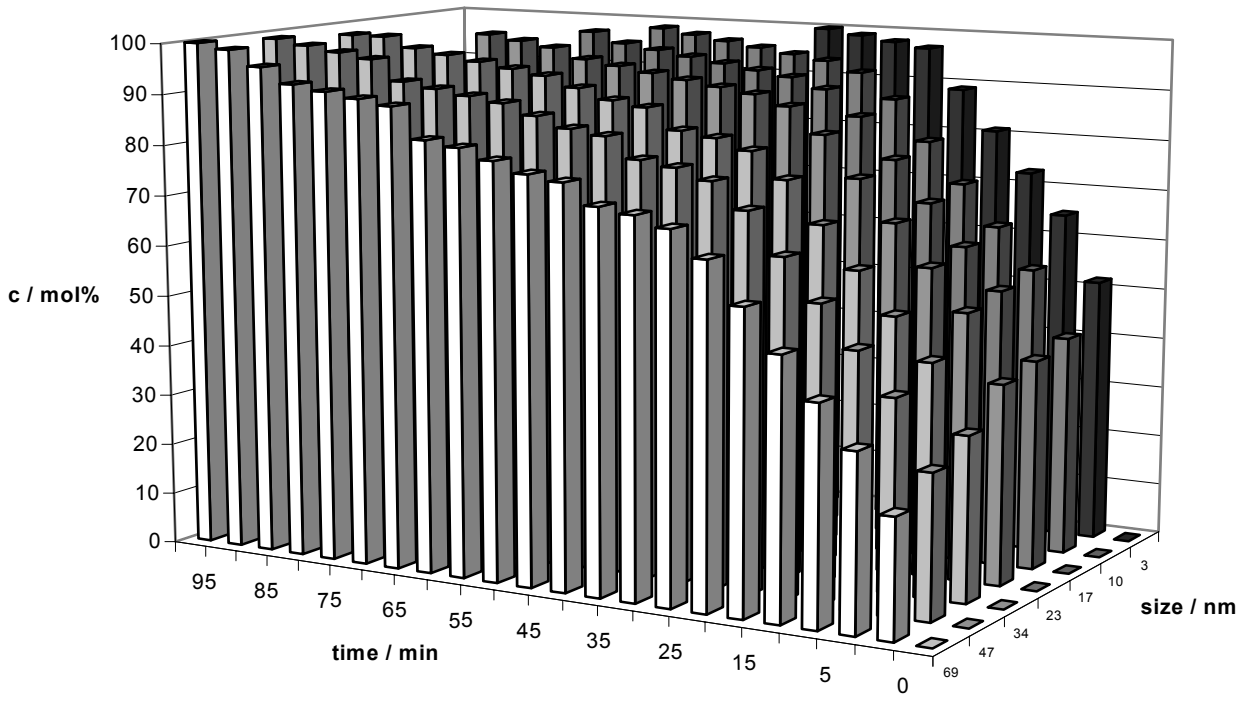

Figure 7-8: Survey of the conversion of hydrogenation of 1,3-butadiene into n-butane with Ru particles of various sizes in nanoporous alumina membranes

In the literature no ruthenium nanoparticles are mentioned as catalyst for hydrogenation of 1,3-butadiene. Nevertheless, the T.O.F. of 325 min^{-1} can be compared with catalysis on palladium particles. A T.O.F. of 296 min^{-1} is found for catalysis under the same conditions with Pd particles of 2.5 nm.[274]

Clearly, the same trend is true for the ground catalysts: as for the structured materials, the smaller particles reach full conversion before the larger ones (Figure 7-9). However, the delays in reaching the 100 % values are obviously longer. Even for the small particles, full conversion is only observed after 80-90 minutes whereas for the larger ones, at least 170 minutes are necessary. This difference of reactivity probably reflects the better diffusion of the reactants and products into intact membrane channels than in the ground forms.

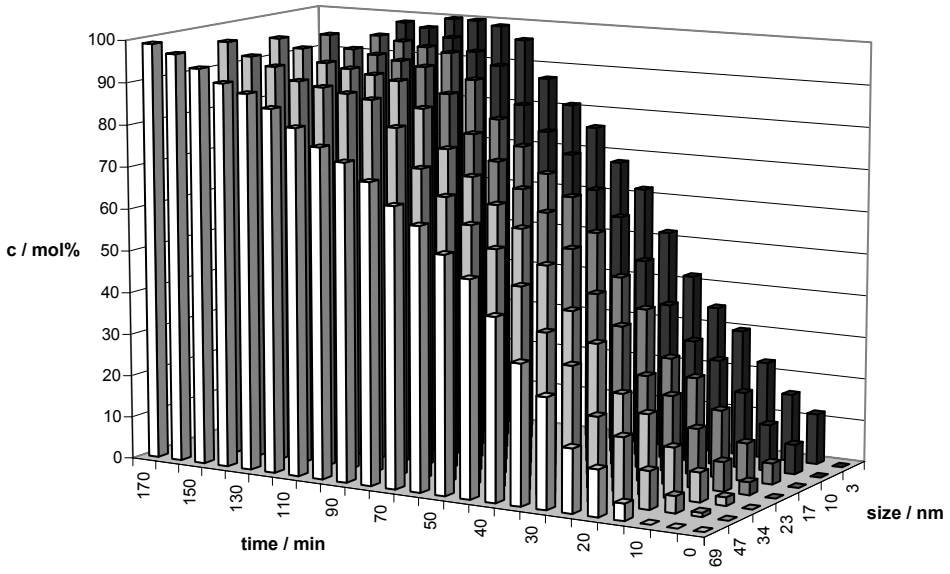

Figure 7-9: Survey of the conversion of hydrogenation of 1,3-butadiene into n-butane with Ru particles of various sizes in nanoporous alumina membranes in a ground form

Table 7-4: Survey of the conversion of hydrogenation of 1,3-butadiene with Ru particles of various sizes in nanoporous alumina membranes in a ground form.

Particles size / nm	Pore diameter Al_2O_3 / nm	Conversion after 55 min. / %	T.O.F. / min^{-1}
5	21	100	195
17	28	99	188
20	42	97	181
24	42	95	173
34	56	92	166
47	70	88	157
69	84	81	151

In conclusion, highly porous ruthenium nanoparticles incorporated in the pores of alumina membranes constitute good catalysts. This is due to the organisation of the particles in the mesoporous structure, consequently improving the contact area between the reactants.[271] The smaller the particles the higher is their catalytic reactivity in agreement with literature.[272,273] For the ground catalysts the gas is probably flowing through the gaps of the material and is not forced to pass via the small pores. Therefore the reaction is controlled by diffusion leading to a decreasing concentration of the reactants on the particles surface.[266]

In comparison with ligand stabilised clusters (e.g. $PdDDSiMe(OMe)_2$)[274] the activity of the naked particles is higher because of a higher occurrence of free surface atoms. These active sites are sterically less blocked than in the presence of protecting ligands.[274,275]

7.3 CO oxidation by Ru nanoparticles inside alumina membranes

CO is mostly found in the noxious fumes of industries, exhaust fumes and domestic fuel gases. This is due to the incomplete burning of combustibles. CO is very poisonous and leads to suffocation since it forms a stronger complex with the haemoglobin of blood than does oxygen and consequently inhibits its transfer.[276] Usually CO is removed from exhaust fumes by oxidation into CO_2 using platinum and palladium catalysts.[277,278] It is known that gold clusters are very efficient in this type of catalysis at low temperatures.[279,280] Since ruthenium is known as a good catalyst for CO oxidation this reaction was chosen to characterise the synthesised particles.

For the 1,3-butadiene hydrogenation we employed Ru particles synthesised in MeOH/THF mixtures which have mean diameters from 5 to 69 nm. The smallest particles were the most reactive catalysts. Therefore, the particles prepared for CO oxidation reaction are ruthenium particles synthesised in pure alcohols as these particles are much smaller than ruthenium particles synthesised in MeOH/THF mixtures. Nevertheless, a material prepared from a mixture MeOH/THF 2.5/97.5 containing particles of 5 nm has been compared to the particles synthesised in pure alcohols.

The synthesis of Ru/alcohol materials is presented in chapter 2. The different alcohols tested in this catalytic study were n-propanol, pentanol, heptanol and dodecanol. The characteristics of the particles synthesised in pure alcohols are summarized in Table 7-5.

Table 7-5: Ru nanoparticles synthesised in various alcohols

alcohol	Observations	Size / nm	Morphology
MeOH/THF	brown - black	5	porous
2.5/97.5	stable for 2 weeks		
Propan-1-ol	clear brown	4	aggregates
CH_3-CH_2-CH_2-OH	stable for 4 month		
Pentanol	clear brown	2-3	monocrystalline
CH_3-$(CH_2)_4$-OH	stable for several weeks		
Heptanol	very clear brown	3,1	monocrystalline
CH_3-$(CH_2)_6$-OH	stable for a year		
Dodecanol	brown	2.5	monocrystalline
CH_3-$(CH_2)_{11}$-OH	stable for over a year		

This synthesis method appeared to be a good method for the preparation of reactive metal particles since for the hydrogenation (see chapter 7.2) a higher reactivity for smaller particles was observed. Therefore, for the CO oxidation membrane samples have been prepared with the small particles formed by decomposition in pure alcohols.

7.3.1 Catalytic oxidation of CO by Ru nanoparticles in Al_2O_3 membranes

For the CO oxidation some samples were prepared from small particles obtained by *in situ* decomposition in pure alcohols in presence of the membranes as described above in chapter 2. For all particles a 15 V membrane with approximately 21 nm pores was used and the efficient *in situ* preparation was applied in all cases.

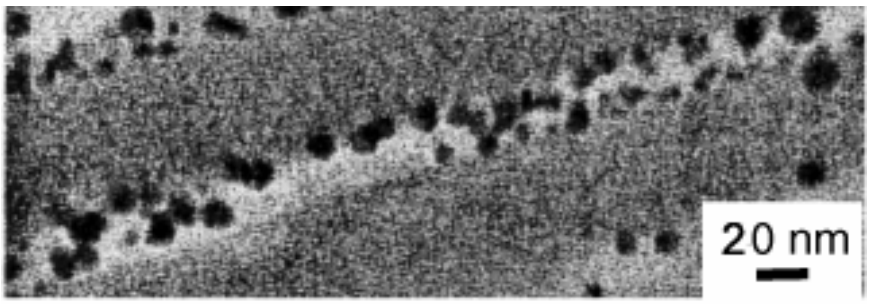

Figure 7-10: TEM image of 15 V membrane (21 nm pores) with Ru/propanol particles

Figure 7-10 shows an image of a 15 V membrane filled with Ru/propanol particles obtained by *in situ* decomposition in propanol. The tested particles preserve their characteristics as did the particles investigated in the colloidal solution. The pores of the membrane are uniformly filled with particles providing a good contact area between catalyst and the CO gas to be converted. Figure 7-11 shows the course of the CO oxidation conducted at 170 °C with this catalyst. A complete conversion to CO_2 is achieved after 1000 minutes.

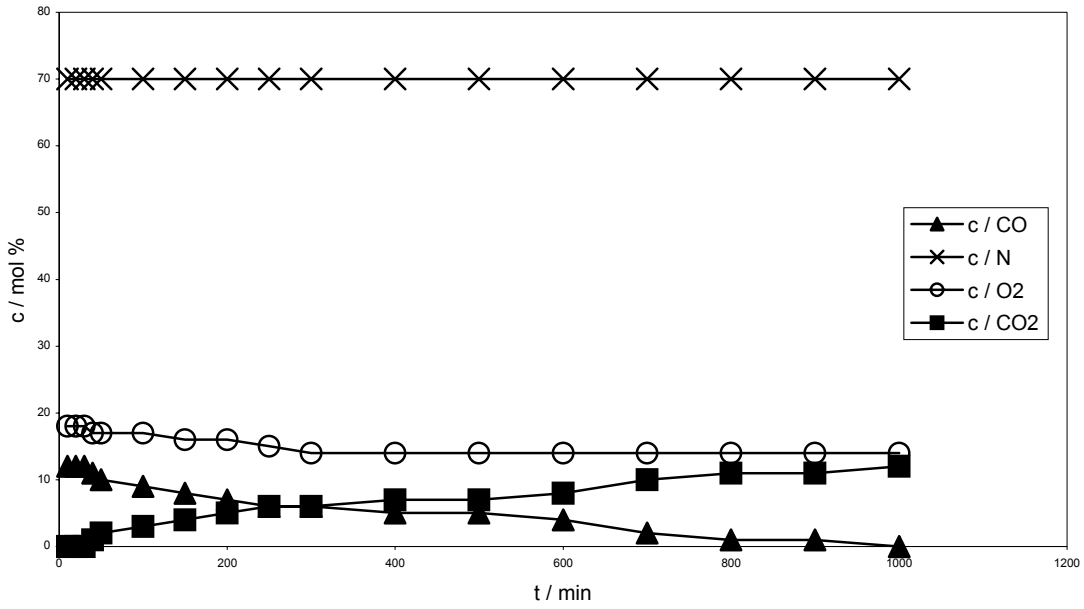

Figure 7-11: Course of oxidation of CO at 170 °C using Ru/propanol particles (4 nm) in 15 V Al_2O_3 membrane (~ 21 nm)

When a material was prepared from a solution in pentanol, an agglomerated state of the particles was confirmed (Figure 7-12). Nevertheless, the pores are uniformly filled and a catalytic test was performed on this material as seen in Figure 7-13. In this case a better conversion can be observed in accordance with the smaller particles size than for the precedent particles prepared using Ru/propanol.

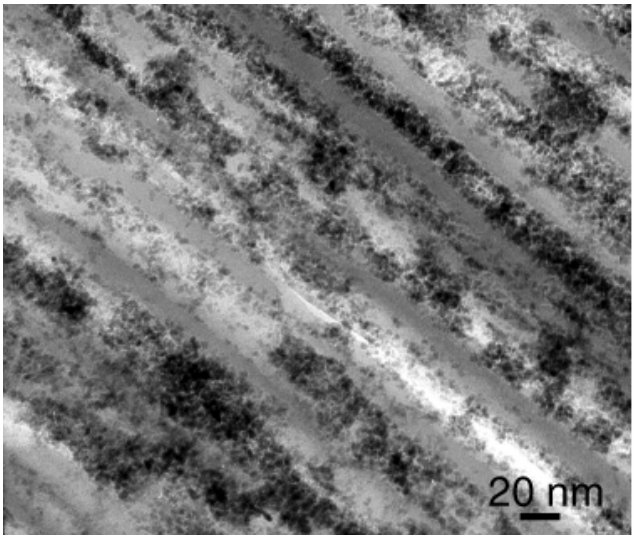

Figure 7-12: TEM image of 15 V membrane (21 nm pores) with Ru/pentanol particles

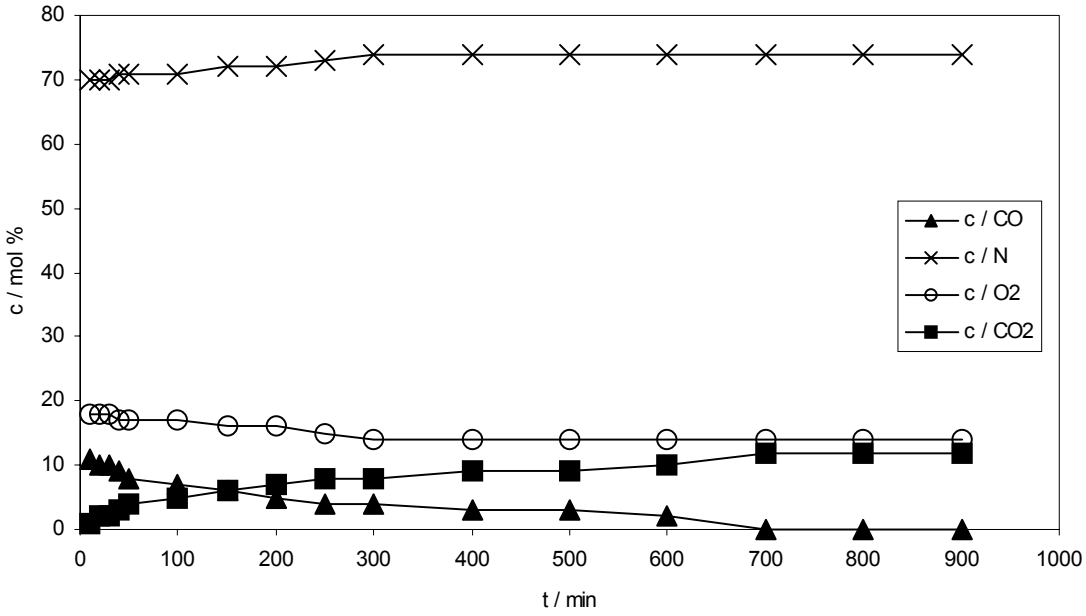

Figure 7-13: Course of oxidation of CO at 170 °C using Ru/pentanol particles (2-3 nm) in 15 V Al_2O_3 membrane (~ 21 nm)

The most well separated particles were obtained in pure heptanol. The incorporated particles remain well separated in the pores of the membrane and no clogging of the material was observed.

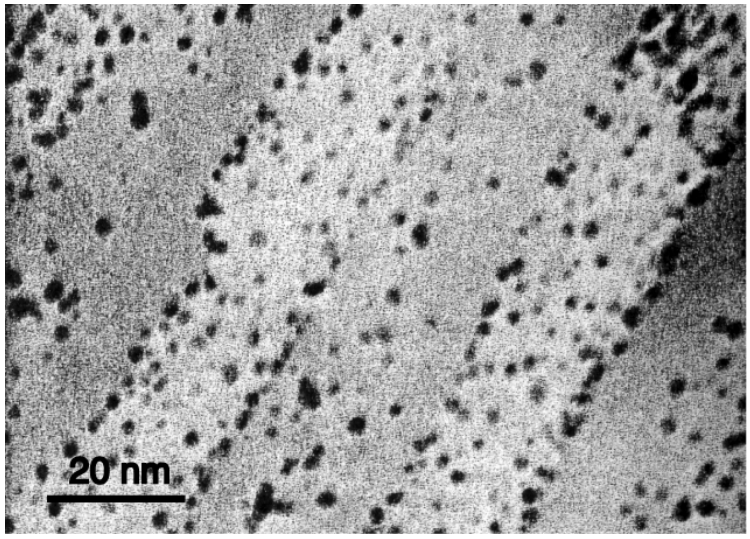

Figure 7-14: TEM image of 15 V membrane (21 nm pores) with Ru/heptanol particles

Indeed, in this case the obtained conversion rose to 100 % after only 600 minutes as can be seen in Figure 7-15.

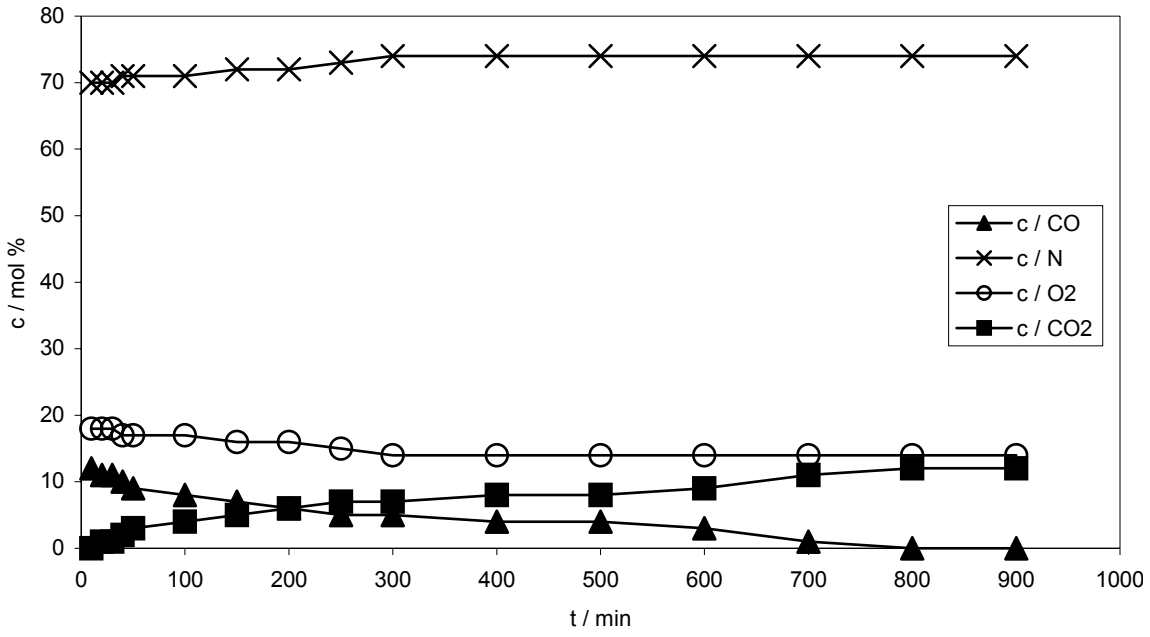

Figure 7-15: Course of oxidation of CO at 170 °C using Ru/heptanol particles (3 nm) in 15 V Al_2O_3 membrane (~ 21 nm)

The experiments presented are representative of the other tested systems. The observed trend is an increasing activity with the decreasing size of the catalyst as summarized in Table 7-6. Although no great difference between the systems can be observed, a trend is

still evident: a faster conversion is obtained for smaller and better dispersed particles incorporated in the Al_2O_3 membrane.

Table 7-6: Survey of the turnover rates of CO oxidation with Ru particles of various sizes in nanoporous alumina membranes

Catalyst	Size / nm	Conversion after 600 min. / %	T.O.F. / min^{-1}
MeOH/THF 2.5/97.5	3-6	94	1.67
Propanol	4	96	2.58
Pentanol	2-3	98	2.98
Heptanol	3	97	3.05
Dodecanol	2.5	99	3.17

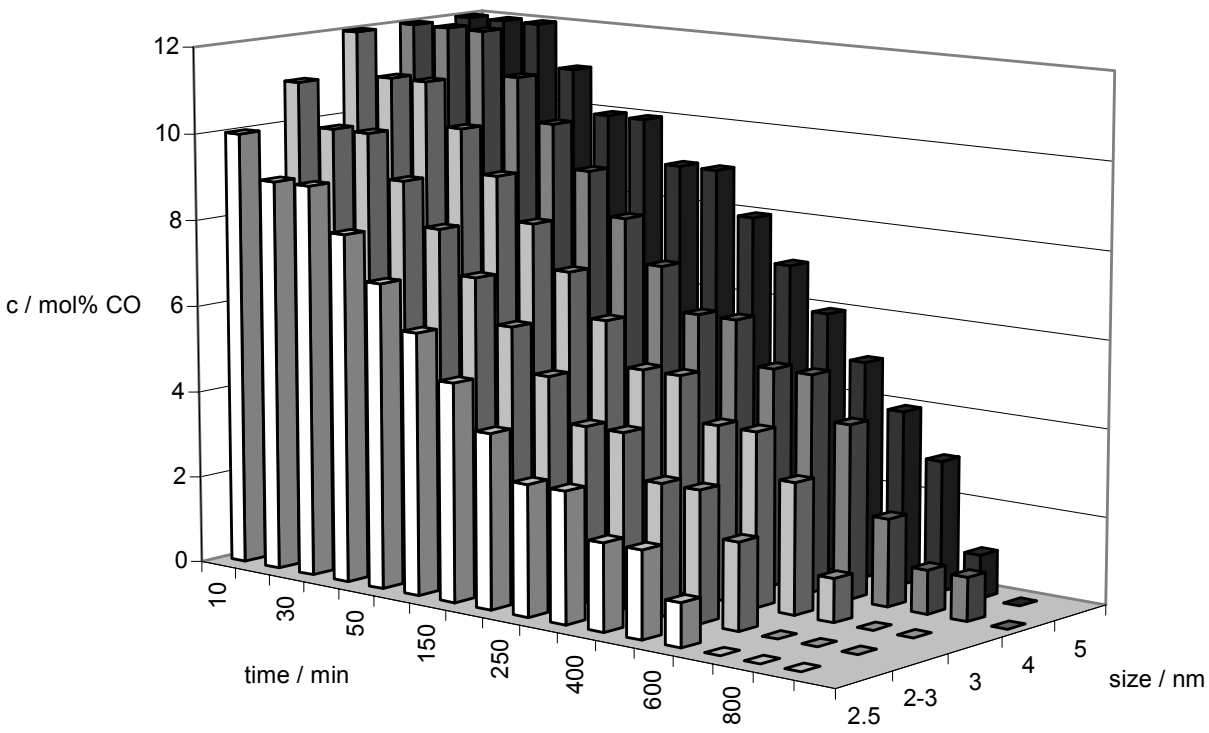

Figure 7-16: Comparison between the applied Ru particles sizes for the CO oxidation

The comparison (Figure 7-16) demonstrates that the trend for the activity is maintained: The smaller the particles the better is the obtained conversion. Due to the bigger surface area the reactivity of the smaller particles is higher.[281] The temperature of this reaction was 170 °C. Only very low activities could be observed at lower temperatures. The Turn-

over-Frequency for the smallest catalytic material synthesised in dodecanol (2.5 nm) is 3.17 min^{-1}. This is in the order of magnitude of the activity which was found for 1.4 nm gold cluster (3.21 min^{-1}).[274]

7.3.2 Conclusion for Ru nanoparticles organised in Al_2O_3 membranes

In conclusion, this work appears as a convincing proof for the efficiency of this type of catalytic systems consisting of nanoparticles included into nanoporous membranes for gas phase large scale catalytic applications. A tendency could be observed: the smaller the particles the higher is their catalytic activity due to the increased number of surface atoms. The organisation of the particles inside the porous Al_2O_3 enhances a better of the contact between the catalyst and the reactants. It can be assumed that a particularly attractive field of applications would be the catalytic transformation of unwanted gases present in trace quantities either in the atmosphere or as a result of certain chemical manufacturing processes into harmless compounds.

8 Conclusion

Size controlled ruthenium nanoparticles have been prepared by decomposition of the organometallic precursor Ru(COD)(COT) (COD = 1,5-cyclooctadiene, COT = 1,3,5-cyclooctatriene) under an H_2 atmosphere in organic solutions. The stabilisation of these nanoparticles has been carried out in the presence of either a pure alcohol or an alcohol/THF mixture, or organic ligands as further stabilisers. An organisation of the particles has also been realised using mesoporous alumina membranes and silica materials. The characterisation of the particles has been realised by different techniques both from organometallic or solid state chemistry such as electronic microscopy (TEM, HRTEM), X-ray diffraction (XRD), wide-angle X-ray scattering (WAXS) and photoelectron spectroscopy (XPS). Finally, some catalytic experiments have been performed.

When the particles are synthesised in pure alcohols, the colloidal solutions are stable for long periods of time, until more than one year for some of them. The TEM micrographs reveal the presence of sponge-like agglomerates formed from individual particles or of isolated and well dispersed monocrystalline particles depending upon the alcohol alkyl chain; long alkyl chains favouring the formation of monodisperse individual particles of small size. In all cases the size distributions are narrow. WAXS and XRD analyses indicate the exclusive presence of hcp ruthenium in these materials. The size of the agglomerates or of the particles can be controlled by adjusting the reaction temperature or the composition of the solvent mixture.

In the case of MeOH/THF mixtures, a linear correlation was established between the solvent composition and the size of the particles in the range 2-85 nm. This variability was attributed to the formation of a micro emulsion acting as a nanoreactor and resulting from the segregation of the cyclooctane formed in the reaction from the polar medium.

In the case of heptanol, the heptyl chain allows the medium to be homogeneous and therefore the particles remain well separated. ^{13}C and ^{1}H NMR studies evidence the weak co-ordination of heptanol on the surface of the particles and the presence of a fast exchange between free and coordinated ligands. The most interesting aspect of this study is the observation of dihydrogen evolution in the NMR tube. It is hence probably due to the dihydrogen desorption resulting from the formation of surface hydrides in the synthesis

conditions. This demonstrates the concomitant presence of both functional ligands and labile ligands at the surface of nanoparticles and therefore the possibility to develop a novel complex chemistry at the surface of metal nanoparticles using the traditional concepts of organometallic chemistry and monodisperse particles as "super-atoms".

The particles can also be stabilised by long chain amines or thiols to give after appropriate work-up colloids which can be obtained as powders and handled like organometallic compounds. Whereas the amine ligands exchange rapidly at the surface of the particles with free amines, the thiols oxidatively add to ruthenium and excess thiol leads to the reductive elimination of disulfides which are released into the solution and do not exchange with the ligands present at the surface of the particles. This may be the reason why the colloids adopt so different structures and super-structures, even though the alkyl chains are the same and the functional groups similar. The alkyl chains of the sulphur ligands will encircle the particle and interpenetrate with the alkyl chains of other ligands either free or located at the surface of other particles hence leading to the formation of superstructures. A slow catalytic coupling of thiols into disulfides which may be removed from the colloid surface was observed. The presence of some organisation of the amines in THF could allow the growth of ruthenium particles in the channel created in this way and hence explain the vermicular aspects of the colloids. Alternatively, the dynamics of the amines could also allow changes in the co-ordination sites at the surface of the particles and therefore, the preferred co-ordination of the amine along the growth axis of the hcp structure, perpendicular to the basal plane. In any case, the dynamics of the amine will favour the coalescence of initially formed spherical particles and therefore favour the formation of worm-like particles. This study demonstrates that the coupling of traditional techniques of characterisation of nanomaterials (HREM, WAXS) with simple techniques of organometallic chemistry may provide useful information on the chemical reactivity of the surface of the nanoparticles and shed light on elementary surface reaction steps such as substitution, oxidative addition and reductive elimination. Such a study may also help designing nanoparticles of defined shape and organisation at the microscopic level. The NMR studies evidence the processes of dynamic ligand exchange and catalytic coupling of thiols at the surface of metal nanoparticles, and the dynamics of coordinated ligands with the shape of the particles. As a whole, this experiment evidences a rare example of observation of a dynamic process at the surface of metal nanoparticles by solution NMR. The originality of the present system lies in the observation of both the spectra for coordinated ligands and those for the rapid exchange.

Ruthenium nanoparticles were stabilised by chiral ligands, namely aminoalcohols and amino-oxazolines. The surface co-ordination of the ligands leads to an excellent stabilisation of the metal particles in solution as well as to an influence on their catalytic performances. Although the catalytic activities are not very good, these nanocatalysts are active under mild conditions and, in some cases, with oxazolines, more efficient but less selective than the corresponding molecular catalysts. This activity and the very low enantiomeric excess obtained compared to those of the molecular systems both suggest a fluxional behaviour of the ligands at the surface of ruthenium as recently observed for amine/Ru systems. This is also confirmed by the decrease in activity and increase in selectivity observed upon addition of excess ligand to the catalytic system. It is interesting to note the very modest but significant and reproducible ee associated with an increase of the oxazoline concentration in solution.

Ruthenium nanoparticles included in alumina membranes have been prepared either by dihydrogen decomposition of the complex Ru(COD)(COT) to give pre-prepared colloidal solutions which were further used to fill the pores of nanoporous alumina membranes by vacuum introduction, or by *in situ* decomposition. These hybrid systems were tested in the hydrogenation of 1,3- butadiene and the CO oxidation in the gas phase. The use of Ru loaded membranes resulted in considerably increased activities compared with grinded samples. This work appears as a convincing proof for the efficiency of such catalytic systems consisting of nanoparticles included into nanoporous membranes for gas phase catalytic applications. A particularly attractive field of applications would be the catalytic transformation of unwanted gases present in trace quantities either in the atmosphere or as a result of some chemical productions into harmless compounds.

Ruthenium nanoparticles have been organised in mesoporous silica. We used different functionalised silica. The organisation of the particles inside these material was more or less successful depending on the functional group of the silica. In the case of a phosphonated material we obtained nanowires of Ruthenium inside the channels.

This work shows that the organometallic complex Ru(COD)(COT) is a very interesting precursor for the preparation of various nanoparticles whose size and surface state can be controlled. In addition, these particles are active in catalysis. At this date, not many works are available in the literature concerning ruthenium particles.

9 Inhaltsübersicht

Rutheniumnanopartikel wurden durch Wasserstoffzersetzung des Komplexes Ru(COD)(COT) (COD = 1,5-Cylcooctadien; COT = 1,3,5-Cyclooctatrien) zur Erzeugung kolloidaler Lösungen synthetisiert. Die Zersetzung findet unter milden Bedingungen, wie Raumtemperatur und unter 3 bar Wasserstoffdruck über 45 Minuten, statt. Die Synthese der Nanopartikel kann durch die Wahl des Lösemittels und eingesetzte Liganden beeinflusst werden.

Zunächst wurden Rutheniumnanopartikel in reinen Alkoholen (Methanol, n- und iso-Propanol, Pentanol, Heptanol, Dodecanol und Oleylalkohol) hergestellt. Die erhaltenen Kolloide zeigen unterschiedliche Größenverteilungen, Stabilitäten und Anordnungen der Partikel in der Lösung. Diese Faktoren hängen von der Länge der Kohlenstoffkette der eingesetzten Alkohole als Reaktionsmedium ab. In reinem Methanol beträgt der Durchmesser der Nanopartikel etwa 76 nm. In allen anderen längerkettigen Alkoholen wurde eine Größenverteilung der Partikel zwischen 2 und 5 nm festgestellt. Von einer Alkylkette mit fünf Kohlenstoffatomen (Pentanol) an aufwärts, konnten monokristalline Partikel beobachtet werden.

Da sehr große Partikel in reinem Methanol beobachtet wurden und die Stabilisierung in reinem Tetrahydrofuran (THF) nicht möglich war, wurden Mischungen aus diesen beiden Lösemitteln in Betracht gezogen. Lösemittelmischungen aus unterschiedlichen Verhältnissen von Methanol und THF führten zur Synthese von hochporösen Rutheniumnanopartikeln. Der Durchmesser dieser blumenkohlartigen Gebilde kann an Hand der Methanolkonzentration im Reaktionsgemisch reguliert werden. Bei einem Gehalt von 2.5 % Methanol wurden 3-6 nm große Nanopartikel erhalten, während bei einem Methanolgehalt von 90 % 85.9 nm große Kolloide beobachtet wurden. Daraus folgt ein linearer Zusammenhang zwischen der Methanolkonzentration in der Reaktionsmischung und der Teilchengröße, die mit Hilfe der Reaktionsmischung zwischen 3 und 86 nm gewählt werden kann. Der Grund für diese Anhängigkeit ist womöglich die Bildung von Nanoreaktoren bestehend, aus Cyclooktan im Inneren und einer Hülle aus Methanol die im THF stabilisiert wird. So kann man sich vorstellen, dass die Menge an Methanol, die Größe dieser Nanotropfen beeinflusst, in denen die Bildung der Kolloide stattfindet.

Das Phänomen der Stabilisierung der Kolloide durch reine Alkohole wurde am Beispiel von Heptanol besonders untersucht, da eine gute Verteilung der Partikel in Lösung, eine hohe Stabilität und monokristalline Kolloide erhalten wurden. Die Stabilisierung der 3 nm großen Kolloide wurde mit Hilfe von Infrarot und NMR Spektroskopie untersucht. Die Existenz von Heptanolmolekülen konnte an Hand von IR-Spektroskopie bestätigt werden. Mittels NMR-Spektroskopie konnte Heptanol an der Oberfläche der Partikel beobachtet werden, wobei ein verändertes Verhalten des Alkohol festgestellt wurde, was durch die Nähe zur Metalloberfläche zustande kommt. Im ^{1}H NMR-Spektrum deutet das Fehlen der Signale für die α–, β– and γ– Protonen der Alkylkette auf eine Bindung der Heptanolmoleküle mit der Metalloberfläche hin. Der Vergleich der ^{13}C NMR-Spektren von freiem Heptanol und der stabilisierten Kolloide deutet auf einen Austausch von freiem und gebundenem Heptanol hin. Eine interessante Beobachtung ist die Entwicklung von Wasserstoff im NMR-Röhrchen (4.8 ppm).

Nach der Erzeugung von sogenannten „nackten“ Clustern wurden Rutheniumnanopartikel mit organischen Liganden wie Thiolen, Aminen, chiralen Aminoalkoholen und Oxazolinen stabilisiert.

Unterschiedliche langkettige Thiole wurden zur Stabilisierung der Kolloide eingesetzt. Die erhaltenen Partikel waren in Abhängigkeit von dem benutzten Thiol zwischen 1 und 3 nm groß. IR Spektroskopie bestätigte die Gegenwart von Thiolmolekülen auf der Metalloberfläche. ^{1}H NMR-Experimente zeigten durch das Fehlen der α–, β– and γ– Protonen der Alkylkette eine Bindung mit der Rutheniumoberfläche. Weitere Experimente (^{1}H NMR und ^{13}C NMR) führten zur Beobachtung von Dithiolen, die an der Metalloberfläche gebildet wurden. Diese Reaktion wurde wahrscheinlich von den Rutheniumpartikeln katalysiert.

Bei der Stabilisierung mit unterschiedlich langkettigen Aminen konnten bis zu 3 nm große Partikel beobachtet werden. Neuartige Formen der Kolloide wurden erhalten. Die länglichen Partikel wurden mittels NMR Spektroskopie untersucht und ein dynamisches Verhalten der Liganden auf der Metalloberfläche wurde bestätigt. Nach den Beobachtungen sind die Aminmoleküle über die $–NH_2$ Gruppe mit der Metalloberfläche verbunden und die CH_3-Gruppe am anderen Ende der Alkylkette biegt sich ebenfalls auf die Oberfläche, um eine lockere Bindung einzugehen, die durch die Zugabe von einem Überschuss an freien Liganden

ersetzt wird. Die Existenz der Liganden sowie von Hydriden auf der Oberfläche der Metallpartikel konnte mittels Festkörper-NMR-Spektroskopie bewiesen werden.

Chirale Aminoalkohole und Oxazoline wurden zur Stabilisierung der Kolloide eingesetzt. Hierbei wurden verschiedene funktionale Gruppen angewendet und die erhaltenen Kolloide waren stabil in Lösung und zeigten verschiedene Aspekte. Diese neuen Materialien wurden in enantioselektiver Katalyse gestestet.

Kolloidale Lösungen, eingebettet in Aluminiummembranen, wurden benutzt, um die Poren durch Vakuum-Induktion zu befüllen. *In-situ*-Zersetzung des Komplexes Ru(COD)(COT) fand zur Organisation der Partikel innerhalb der Poren statt. Eine regelmäßige Befüllung der Poren wurde erreicht. Diese Hybridsysteme wurden bei der Hydrierung von 1,3-Butadien in der Gasphase getestet. Der Gebrauch der Ru-beladenen Membranen erbrachte eine deutlich gesteigerte Aktivität im Vergleich zu gepulverten Proben.

Rutheniumpartikel, stabilisiert mit chiralen Liganden, zeigten hohe Reaktivität beim asymmetrischen Wasserstofftransfer von iso-Propanol zu Acetophenon. Die beobachtete Enantioselektivität war jedoch sehr gering.

Die Organisation von Rutheniumnanopartikeln wurde in verschieden funktionalisierten Silikaten durchgeführt. Dabei wurde eine dreidimensionale Anordnung der Kolloide in den Kanälen der Silikate erreicht. In einer Phosphonat-funktionalisierten Matrix konnten Rutheniumnanodrähte erzeugt werden.

Eine andere Methode der Organisierung von Rutheniumnanopartikeln wurde durch die vorherige Stabilisierung mit langkettigen Aminen getestet. Dazu wurden die Liganden, die die Kolloide umgeben, anschließend polymerisiert und das Silikat wurde um die Partikel geformt, welche eine lineare Anordnung in den Poren erkennen ließen.

Zusammenfassend kann man sagen, dass der organometallische Komplex Ru(COD)(COT) zur Herstellung von Rutheniumnanopartikeln sehr geeignet ist und in Gegenwart von stabilisierenden Liganden zum Erhalt verschiedenster Kolloide führt. Die Größe und Oberflächenbeschaffenheit der Nanopartikel kann kontrolliert werden. Diese Nanopartikel sind reaktiv in katalytischen Reaktionen und können in mesoporösen Aluminiummembranen und funktionalisierten Silikaten angeordnet werden. Zu diesem Zeitpunkt sind nur sehr wenige Arbeiten in der Literatur bekannt, die Rutheniumnanopartikel betreffen.

10 Résumé de la thèse

Les nanoparticules métalliques suscitent un intérêt croissant ces dernières années en raison de leurs propriétés physiques ou chimiques particulières dues à leur état de la matière, intermédiaire entre l'état moléculaire et l'état métallique. Les travaux décrits dans ce manuscrit concernent l'élaboration de nanoparticules métalliques de ruthénium, matériaux potentiellement intéressants pour des applications dans le domaine de la catalyse, leur caractérisation et leur organisation dans des membranes d'alumine et des mésoporeux. Des résultas obtenus en catalyse sont également présentés.

La méthode de synthèse de nanoparticules de ruthénium suivie est basée sur la décomposition du précurseur organométallique Ru(COD)(COT) (Ruthenium-1,5-cyclooctadiène-1,3,5-cyclooctatriène) en solution dans un milieu organique et sous 3 bar de dihydrogène, à température ambiante. Cette méthode permet, de façon reproductible, un contrôle efficace de la taille, de la dispersion et de l'état de surface des espèces formées.

La stabilisation des nanoparticules de ruthénium a été réalisée par addition de ligands organiques, en particulier des alkylamines et des alkylthiols, l'utilisation de tels ligands offrant l'avantage de pouvoir moduler l'état de surface des particules, et donc leur propriétés. Une étude a été menée en variant la longueur de la chaîne alkyle du ligand et sa concentration dans le milieu afin de déterminer son influence sur la forme et l'organisation des particules. La stabilisation de nanoparticules de ruthénium par l'octanethiol et l'hexadécylamine a ainsi été étudiée, et il s'avère que la forme des particules varie en fonction du ligand: les particules sont sphériques avec le thiol et vermiculaires dans le cas de l'amine. De plus, tout en demeurant individuelles, ces particules ont tendance à se regrouper en agglomérats, dont la forme et les dimensions (disques, sphères ou cylindres) semblent dépendre de la quantité de ligand dans le milieu.

Les nanoparticules ainsi produites sont caractérisées par des méthodes de caractérisation qui relèvent aussi bien de la chimie moléculaire (IR, RMN,…) que de la chimie du solide (ATG-ATD, microscopie électronique, diffusion des rayons X aux grands angles,…). La RMN s'avère un outil très intéressant pour caractériser les ligands à la surface des particules car elle renseigne sur les interactions entre les ligands et la surface des particules. Les résultats obtenus mettent en évidence une réactivité des ligands à la surface des

particules différente suivant leur nature. Par exemple, dans le cas de l'amine, un échange entre ligands libres et ligands coordonnés a été observé. En présence d'un excès de thiol, la production catalytique de disulfure témoigne de la réactivité des particules. Par ailleurs, la présence de H_2 et D_2 à la surface des particules a été mise en évidence par des études en RMN à l'état solide et en solution. Ces espèces apparaissent donc comme des clusters géants à la surface desquels une véritable chimie organométallique de surface est envisageable.

Des oxazolines chirales ont également été utilisées comme agents stabilisants, et ont conduit à des particules de ruthénium de taille comprise entre 2 et 2.5 nm. Ces nouveaux colloïdes ont été testés en catalyse asymétrique, dans la réaction de transfert d'hydrogène de l'isopropanol vers l'acétophénone.

Enfin, les pores de membranes d'alumine et de matrices mésoporeuses ont été remplis à l'aide de nanoparticules et, dans le cas des membranes, ces matériaux on été testés en catalyse en phase gazeuse, pour les réactions d'hydrogénation du 1,3-butadiene en butane et d'oxydation du monoxyde de carbone en dioxyde de carbone.

11 Experimental

11.1 Listing of used chemical products

The used chemical products are mentioned hereafter in alphabetic order and with the precision of their provenance and purity. The solvents have been used immediately after distillation.

- 2-aminobutanol
- Argon (Argon U, Air liquide)
- 1,3-Butadiene
- Carbon monoxide (Air liquide)
- Chiral oxazolines : Collaboration G. Muller, University of Barcelona
- Cyclohexane (99 %, Aldrich)
- 1,5-Cyclooctadiene (99 %, Aldrich) : purified by filtration through an alumina column
- Cyclooctane (99 %, Aldrich)
- Dodecanol-1 (99 %, Aldrich)
- Dodecanethiol (99 %, Aldrich)
- Dihydrogen (99 %, Air liquide)
- Ethanol (99.5 %, SDS)
- Heptanol (99 %, SDS) : dried over Magnesium sulphate (Fluka) and distilled over magnesium (Aldrich) which was previously activated with iodine (Rectapur)
- Hexadecylamine (99 %, Fluka)
- Methanol (99 %, SDS) : dried over Magnesium sulphate (Fluka)and distilled over magnesium (Aldrich) which was previously activated with iodine (Rectapur)
- Octanethiol-1 (97 %, Aldrich)
- Octylamine-1 (98 %, Aldrich)

- Oleylalcohol (98 %, Aldrich)
- Membrane Al_2O_3 (Collaboration G. Schmid, UHG Essen)
- Pentane (99 %, SDS) : distilled over CaH_2
- Pentanol (99 %, Fluka) : dried over Magnesium sulphate (Fluka) and distilled over magnesium (Aldrich) which was previously activated with iodine (Rectapur)
- Propanol-1 (99 %, Aldrich) : dried over sodium carbonate (Rectapur), distilled over sodium (Merck)
- Propanol-2 (99,5 %, Riedel de Haen) : dried over sodium carbonate (Rectapur), distilled over sodium (Merck)
- $RuCl_3$, 3 H_2O (43,5 % Ru, Janssen)
- Silica mesoporous, (Collaboration Y. Guari, LCMOS-UM II, Montpellier)
- Tetrahydrofurane (99,5 %, SDS) : distilled over a mixture sodium (Merck) / benzophenone (Aldrich)
- Toluene (99 %, SDS), distilled over a mixture sodium (Merck) / benzophenone (Aldrich)
- Zinc (95 %, Merck)

All operations were carried out using standard Schlenk tube or Fischer-Porter bottle techniques under argon. All reagents were purchased from Aldrich, Merck or Janssen and most of the solvents from SDS, except pentanol and propanol-2 which were purchased from Fluka and Riedel de Haen, respectively. The solvents were distilled in nitrogen atmosphere just before use. THF was heated under reflux over sodium benzophenone, pentane over calcium hydride, methanol over magnesium after activation on iodine. The other alcohols (propanol-1, propanol-2 and pentanol) were dehydrated over magnesium sulphate before heating over magnesium after activation on iodine. All reagents and solvents were degassed under vacuum at the liquid nitrogen temperature by 3 vacuum/argon cycles.

11.2 Synthesis of Ru(COD)(COT)

Ruthenium-1,5-cyclooctadiene-1,3,5-cyclooctatriene was prepared according to a published procedure from $RuCl_3 \cdot 3H_2O$.[96,282] In a 250 mL flask 3g (11,5 mmol) of $RuCl_3 \cdot 3H_2O$ were dissolved in 30 ml methanol. 60 ml (490 mmol) of cyclooctadiene, previously purified by passing through an alumina column (10 cm), were added to the mixture. Finally, 5 g zinc were inserted and the mixture was heated under reflux at 90 °C for 3 hours. After complete cooling down, the mixture was decanted and the solution filtered from the precipitate which was washed three times with 20 ml of toluene. The solvent was evaporated until a dry product was obtained. The solid was extracted with pentane and filtered by an alumina column. The obtained yellow solution is concentrated to 10 mL and stored over night at –30 °C. Yellow crystals are obtained. It was purified by recrystallisation in pentane and the resulting highly sensitive yellow crystals were stored under argon at –30°C. Their purity was checked by elemental analysis and ^1H NMR spectroscopy. $RuCl_3 \cdot 3H_2O$ was purchased from Janssen.

Yield: 70 %
Microanalysis : theoretical : C 61 %, H 7 %, Ru 32 %
experimental : C 60,4 %, H 6,4 %, Ru 28 %

11.3 Characterisation of nanoparticles

The prepared colloids were characterised by microanalysis to determine the ratio between metal and ligand shell. Infrared spectroscopy (IR) provides information about the presence of ligand at the surface. The size and morphology of the particles is observed by transmission electron microscopy (TEM and HREM). Wide angle X-ray scattering (WAXS) and X-ray diffraction give more information about the size and the crystal structure of the particles.

11.3.1 TEM analysis

Specimen for TEM analysis were prepared by slow evaporation of a drop of the colloidal solutions deposited under argon onto holey carbon-covered copper grids. The TEM experiments were performed at the "Service Commun de Microscopie Electronique de l'Université Paul Sabatier" on a JEOL 200 CX-T electron microscope operating at 200kV or a Philips CM12 electron microscope operating at 120kV with respective point resolution of 4.5 and 5 Å. HREM observations were carried out with a JEOL JEM 2010 electron microscope working at 200 kV with a resolution point of 2.5 Å. The transmission electron microscopy was used as a standard tool of analysis to determine the mean size of the ruthenium particles. The size distributions were assembled through a manual analysis of enlarged micrographs by measuring at least 100 particles on a given grid in order to obtain a statistically size distribution and a mean diameter.

Preparation of the membrane samples for TEM analysis was realised by embedding of the membrane in Araldite CY 212 resin before sectioning by an Ultra Cut Microtom (Leica). The thickness of the samples varied from 50 to 100 nm. TEM images were obtained by using a Philips FEG-CM 200 instrument working at 200 kV accelerating voltage.

11.3.2 AFM measurements

AFM measurements have been effectuated in the Centre of Molecular and Macromolecular Studies, Polish Academy of Science in Lodz.

11.3.3 Microanalysis

Elemental analyses were performed at the "Services d'Analyses du CNRS" in the LCC for carbon, nitrogen, oxygen and hydrogen determinations and in Lyon for ruthenium determination and at the University of Essen.

11.3.4 X-ray powder diffraction (XRD analysis)

Data collection for XRD analysis was performed on small amounts of powder (obtained after drying) at ENSIACET at Toulouse University. XRD profiles of the particles were measured with Seifert XRD 3000 TT X-ray diffractometer with $Cu_{K\alpha}$ radiation. The

XRD diagram reveals the hcp structure of the ruthenium particles and their approximate size using the Scherrer equation.

11.3.5 WAXS analysis

The data collection for the wide-angle X-ray scattering was performed on small amounts of powder at the CEMES/CNRS, Toulouse. The powder was obtained after drying, sealed in 1.5-mm-diam Lindemann glass capillaries after filling in a glove-box. The measurements of the x-ray intensity scattered by the samples irradiated with graphite-mono chromatised molybdenum K_α (0.071069 nm) radiation were performed using a dedicated two-axis diffractometer. Time for data collection was typically 20 hours for a set of 457 measurements collected at room temperature in the range $0°<\theta<65°$ for equidistant s values ($s=4\pi(\sin\theta/\lambda)$†). The data were reduced in order to extract the structure-related component of WAXS, the so-called reduced intensity function, normalized to a number of atoms corresponding to the size of the particle, and Fourier transformed to allow for radial distribution function (RDF) analysis, using

$$F(r) = \frac{2r}{\pi}\int_{s_{min}}^{s_{max}} s.i(s).\sin(r.s).ds$$

where F(r) is actually a reduced RDF whose maximum for a given r value indicates that at least two atoms in an elementary volume are separated by the distance r. Analysis of the experimental data provided an approximate measurement of the metal-metal bond length and of the order extent inside the particles. To further investigate the structure, different models were defined in order to compute theoretical functions for intensity and radial distribution via the Debye formula:

$$i_D(s) = 2\sum_{i=1}^{N-1}\sum_{j=i+1}^{N} f_i(s).f_j(s).\frac{\sin(s.r_{ij})}{s.r_{ij}}.\exp(-b_{ij}.s^2)$$

where N is the total number of atoms in the model, f_i the atomic scattering factor for atom i, r_{ij} the distance between atoms i and j and b_{ij} a dispersion factor affecting the i-j interaction). Best values for the parameters defining the models were estimated from the agreement reached between experimental and computed RDF, both normalized to one atom, but also between the related reduced intensity functions.

11.3.6 IR analysis

Infra red analysis have been performed on a Perkin Elmer Spectrometer GX (FT-IR System). The sample of the colloids have been prepared as KBr pellets.

11.3.7 NMR experiments

The solution NMR experiments have been performed on a Bruker (250 MHz or 400 MHz) spectrometer.

Solid state and gas phase NMR has been realised at the Free University of Berlin in Germany. The solid state NMR experiments are performed on a Pulse-Fourier-NMR spectrometers: a Varian Infinity Plus operating at a field of 14.09 T (599.97 MHz for ^{1}H). The spectrometer uses an Oxford wide bore (89 mm) super conducting magnets. On the spectrometer, Chemagnetics probes are used: a 5 mm HXY probe of T3 type. The powdered samples are glass sealed in an insert placed in the centre of zirconium oxide rotors with end caps usually made of Teflon. Magic angle adjustment is performed either with the 79Br FID of potassium bromide or with the ^{2}H FID of deuterated polystyrene.

The gas phase spectra were acquired on a Bruker AMX500 spectrometer with a field of 11.75 Tesla and resonance frequencies of 500.13 MHz for ^{1}H and 76.66 for ^{2}H. The samples were glass sealed in 5 mm NMR tubes.

The calculated spectra have been simulated with ACD HNMR Predictor und CNMR Predictor of the Advanced Chemistry Development Inc.

11.4 Synthesis of ruthenium nanoparticles from Ru(COD)(COT)

11.4.1 General Synthesis of ruthenium particles in a pure solvent

The decomposition reaction of Ru(COD)(COT) (20 mg; 63.5 mmol) dissolved under argon in 20 mL of the chosen solvents was carried out at room temperature under 3 bar H_2 in a closed pressure bottle with vigorous magnetic stirring for 45 min. When THF, cyclooctane or pentane were used as solvents the initial yellow solution darkened immediately and a black solid precipitated. When the reaction was performed in a pure alcohol, the initial yellow

solution darkened in a few minutes to become brown and remained unchanged and stable under argon atmosphere for at least several days. Addition of pentane or cyclooctane then gave a black precipitate made up of particles.

11.4.2 General Synthesis of ruthenium particles in a solvent mixture composition

Ru(COD)(COT) (20 mg; 63.5 mmol) was dissolved under argon in a total volume of 20 mL of a MeOH/THF mixture in a closed pressure bottle. Different MeOH/THF mixtures in which the volume ratio MeOH/THF was comprised between 2.5/97.5 to 90/10 were tested. After pressurization at room temperature under 3 bar of H_2, the initial yellow solution turned dark brown in a few minutes. The vigorous magnetic stirring and the H_2 pressure were maintained for 45 minutes. After that period of time, the hydrogen pressure was eliminated, and a drop of each colloidal solution was deposited under argon on a holey carbon-covered copper grid for microscopy analysis. The different products could then be isolated by evaporation to dryness, or precipitation by addition of cyclooctane or cyclohexane, filtration and drying under vacuum.

11.4.3 General Synthesis of Ru particles with thiols and amines

150 mg (0.476 mmol) of Ru(COD)(COT) were introduced in a Fischer-Porter bottle and left in vacuum during 30 minutes. 125 mL of THF degassed by freeze-pump cycles were then added. The resulting yellow solution was cooled at 193 K after which a solution of the chosen quantity of ligand in 25 mL THF was introduced in the flask. The bottle was pressurized under 3 bar dihydrogen and the solution allowed to warm slowly to room temperature. After 20 hours, an homogeneous brown solution is obtained. After elimination of excess dihydrogen, approx. 3 mL of the solution were passed under argon over a small alumina column. The absence of colour of the filtrate indicates the full decomposition of the precursor. The volume of the solution was then reduced to approx. 15 mL, 50 mL pentane were added and the resulting mixture cooled to 193 K at which temperature a brown precipitate formed. It was filtered, washed with pentane and dried in vacuum.

11.5 Synthesis of ruthenium particles with aminoalcohol and oxazoline ligands

Ruthenium colloids were prepared following a procedure similar to that previously described in 11.4.3 but using asymmetric ligands as stabilisers. In a typical experiment Ru(COD)(COT) is dissolved in a Fischer-Porter bottle at 193 K in a THF solution containing 0.2 eq of the appropriate ligand L* (1-11). The used ligands have previously been prepared in the Department of Inorganic Chemistry, Barcelona in the group of G. Muller. The resulting yellow solution is then exposed to a dihydrogen atmosphere (3 bar), allowed to warm to room temperature and left to react for 24 hours under vigorous stirring. The colloids obtained in this way are purified by precipitation upon addition of pentane, filtration and drying in vacuum. The particles were isolated as dark brown powders and dissolved in THF or isopropanol. In all cases, the particles were found to be stable with time and did not show any sign of decomposition. These new colloids were characterised by IR spectroscopy, TEM (Transmission Electron Spectroscopy) and WAXS (Wide Angle X-Ray Scattering) analysis.

Listing of the used ligands

- (R)-(+)-2-aminobutanol
- (S)-2-amino-3-methyl-1-butanol (L-Valinol)
- 2-(4'R)-(4'-ethyl-3',4'-dihydrooxazol-2'-yl)-aniline
- 2-(4'S)-(4'-isopropyl-3',4'-dihydrooxazol-2'-yl)-aniline
- 2-(4'R)-(4'-ethyl-3',4'-dihydrooxazol-2'-yl)-phenol
- 2-(4'S)-(4'-isopropyl-3',4'-dihydrooxazol-2'-yl)-phenol
- 2-(3'S, 4'S)-(3'-phenyl-4'-hydroxymethyl-3',4'-dihydrooxazol-2'-yl)-toluene
- 1,2-bis[(4'S)-(4'-isopropyl-3',4'-dihydrooxazol-2'-yl)]ethane
- 1,4-bis[(4'R)-(4'-ethyl-3,4-dihydrooxazol-2'-yl)]butane
- 2,2'-bis[(4'S)-[4'-(2-methylthio)propyl-3',3'-diphenyl-3',4'-dihydrooxazol-2'-yl]]
- 1,2-bis[(4'S)-(4'isopropyl-3',4'-dihydrooxazoly-2'-yl)]benzene

11.5.1 MoxNH$_2$Et: (4R)-2-(4'-ethyl-3',4'-dihydrooxazol-2'-yl)aniline

IR (NaCl) ν: 3472, 3293, 2962, 1639 (**C=N**), 1492, 1260, 1069, 756 cm^{-1}.

^{1}H NMR (250 MHz, $CDCl_3$, 298 K) δ: 1.02 (pt, *J* = 7.2 Hz, 3H, **4'b**), 1.65 (m, 2H, **4'a**), 4.32 (m, 1H, **4'**), 3.93 (pt, *J* = 8.5 Hz, 1H, **3'**), 4.38 (pt, *J* = 9.4 Hz, 1H, **3'**), 6.12 (bs, 2H), 6.68 (ptd, *J* = 9.4 Hz, *J* = 1.2 Hz, 1H, CH), 6.69 (pdd, *J* = 9.8 Hz, *J* =1.0 Hz, 1H, CH), 7.21 (ptd, *J* = 9.8 Hz, *J* = 2.2 Hz, 1H, CH), 7.69 (pdd, *J* =9.7 Hz, *J* =2.0 Hz, 1H, CH) ppm.

^{13}C NMR (50 MHz, $CDCl_3$, 298 K) δ: 8.2 (**4'b**), 26.9 (**4'a**), 66.1 (**4'**), 69.4 (**3'**), 129.5 (C, Ph), 127.5 (C, Ph), 113.5 (C, Ph), 113.8 (C, Ph), 129.8 (C, Ph), 127,5 (C, Ph), 164.5 (**C**=N) ppm.

11.5.2 MoxNH$_2$iPr: (4'S)-2-(4'-isopropyl-3',4'-dihydrooxazol-2'-yl)aniline

IR (KBr) ν: 3395 (N-H), 3261 (N-H), 1640 (C=N), 1255 (C-O) cm $^{-1}$.

^{1}H NMR ($CDCl_3$, 250 MHz; multiplicity, coupling constants in Hz, and relative integration in parentheses): 7.67 (pdd; 8.8, 1.6; 1H); 7.19 (pt; 7.4; 1H); 6.69 (m; 2H); 6.13 (bs; 2H); 4.32 (ppd; 8.6, 7; 1H); 4.11 (m; 1H); 4.00 (t; 7.3; 1H); 1.81 (m; 1H); 1.03 (d; 6.8; 3H); 0.93 (d; 6.8; 3H) ppm.

^{13}C NMR ($CDCl_3$, 50 MHz): 163.4, 148.5, 131.8, 129.5, 115.9, 115.5, 109.1, 72.9, 68.7, 33.2, 19.1, 18.6 ppm.

Microanalysis: C, 70.29; H, 8.02; N, 14.74. Calc. For $C_{12}H_{16}N_2O$: C, 70.58; H, 7.84; N, 13.72 %.

11.5.3 MoxOHEt: 2-[(4'S)-(4'-ethyl-3',4'-dihidrooxazol-2'-il)]-phenol

IR (NaCl) ν: 3993 (OH), 3068, 2962, 1643 (C=N) cm^{-1}.

^{1}H NMR (200 MHz, $CDCl_3$, 298 K) δ: 0.99 (t, *J* = 7.5 Hz, 3H, 4'b), 1.69 (m, 1H, 4'a), 1.66 (m, 1H, 4'a), 4.25 (m, 1H, 4'), 3.99 (pt, *J* = 7.8 Hz, 1H, 3'), 4.42 (dd, *J* = 9.5 Hz, *J* = 8.5 Hz, 1H, 3'), 6.99 (ptd, *J* = 8.0 Hz, *J* = 1 Hz, 1H, CH), 7.34 (ddd, *J* = 8.0 Hz, *J* =7.5 Hz, *J* =2.0

Hz, 1H, CH), 6.84 (ptd, *J* = 7.5 Hz, *J* = 1.5 Hz, 1H, CH), 7.63 (dd, *J* =8.0 Hz, *J* =2.0 Hz, 1H, CH), 12.3 (bs, 1H, OH) ppm.

^{13}C NMR (50 MHz, $CDCl_3$, 298 K) δ: 10.0 (4'b), 28.7 (4'a), 66.7 (4'), 71.4 (3'), 116.5 (C, Ph), 118.4 (C, Ph), 127.9 (C, Ph), 133.8 (C, Ph), 132.1 (C, Ph), 159,8 (C, Ph), 164.9 (C=N) ppm.

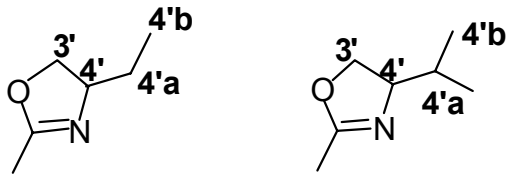

11.5.4 Bisox(CH_2)$_4$Et:1,4-bis[(4'R)-(4'-etil-3',4'-dihidrooxazol-2'-il)]butane

IR (NaCl) $\bar{\nu}$: 2966, 2932, 2878, 2874, 1666 (**C=N**), 1462, 1259, 803 cm^{-1}.

11.6 Alumina membranes

The porous alumina membranes were prepared by anodic oxidation of plates of pure aluminium (99.999 % purity) which were used as the anode material. Several steps are necessary for the synthesis of the alumina membranes. The metal surface is first degreased and cleaned from old oxide residues by immersing in a solution of 12 g K_2CrO_7 in 250 mL 10% H_3PO_4 at 90 °C for 10 minutes. Afterwards, the metal plates are electrically polished for cleaning in a bath consisting of 1100 mL conc. H_3PO_4 and 700 mL conc. H_2SO_4. The polishing was achieved after 10 min at 90 °C. The voltage for the anodic oxidation that will be performed later will be chosen in function of the voltage applied during the electronic polishing.[283]

In a third step, the porous alumina membrane was formed by an electrochemical process. For the galvanic anodic oxidation the aluminium is used as the anode, and it is anodised for 24 hours at 0 °C. Lead served as the cathode as shown in Figure 11-1.

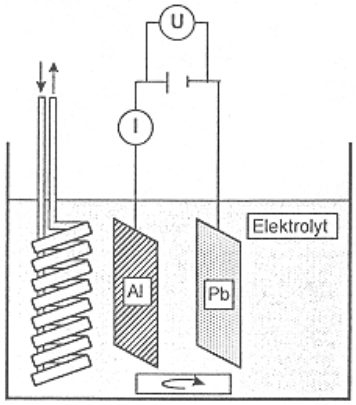

Figure 11-1: Anodic oxidation of aluminium

The type of the electrolyte was selected in accordance with the desired pore size: the electrolyte solution used depends on the voltage of the anodization which influences the mean diameter of the resulting pores as shown in Table 11-1.

Table 11-1: Applied anodising voltages and the resulting pore sizes

Anodising voltage / V	Electrolyte	Intensity / mA•cm^{-2}	Pore diameter / nm
15	10 % H_2SO_4	0.2 – 1.7	~ 21
20	10 % H_2SO_4	0.2 – 1.7	~ 28
30	5 % H_2SO_4	1.7 – 6.5	~ 42
40	4 % Oxalic acid	3.1 – 5.2	~ 56
50	2.5 % Oxalic acid	1.5 – 3.5	~ 70
60	1 % Oxalic acid	1.6 – 3.5	~ 84
80	0.5 % Oxalic acid	1.4 – 4.8	~ 112

Voltages of 15 – 80 V were applied at 0°C, depending on the required pore size. The reaction time depends on the film thickness needed. The membrane was removed by reduction of the voltage.[178] The voltage reduction was achieved in 5 % steps down to 6 V and then in 0.3 V steps. The membrane was removed by dipping into a solution of 12.5 % H_2SO_4 and 3 % oxalic acid for 2.5 hours. The colourless membranes were purified beforehand by 3 vacuum/argon cycles before use.

11.7 Incorporation of Ru nanoparticles in the pores of alumina membranes

The filling of the membranes with particles was accomplished by three different methods. All operations were carried out using standard Schlenk tube or Fischer-Porter bottle techniques under argon.

11.7.1 Filling by filtration

The first method consisted of using the membrane as a filter and passing the colloidal solution via the pores of the nanoporous material. The colour of the membrane obtained changed to a light brown.

11.7.2 Vacuum filling

For the second method (filling by vacuum induction), a colloidal solution was prepared under the conditions described in chapter 3: Different MeOH/THF mixtures were used, in which the volume ratio MeOH/THF was comprised between 2.5/97.5 to 90/10. In a second step, the membrane was introduced in a chosen particle solution for impregnation during 24 hours without stirring at room temperature. After that time the solvent was evaporated under vacuum. The colour of the membranes changed from transparent to brown after the reaction.

11.7.3 Decomposition in situ

The third method (*in situ* decomposition) corresponds to the impregnation of the membrane with a concentrated solution of the Ru(COD)(COT) precursor (200 mg, in 5 mL MeOH/THF mixture) for at least 24 h under argon. The *in situ* decomposition of this complex inside the vacuum dried membrane was then carried out at room temperature under 3 bar H_2 in a closed pressure bottle for 45 min. The membrane then displayed a dark brown or even black colouring. All the samples resulting from the impregnation experiments were analysed by TEM after embedding in a resin matrix. Their Ru content was determined by microanalysis.

11.8 Preparation of Ruthenium-mesoporous material

The mesoporous material (150 mg of the solid) was previously degassed for 48 hours under vacuum at 180 °C to eliminate all the oxygen in the pores. The solid was covered by a very concentrated solution of the precursor Ru(COD)(COT) (200 mg (0.634 mmol) in 10 mL THF, distilled and degassed). After stirring for 24 hours the solvent was partially evaporated (5 mL) and the mixture was pressurized for 24 hours with 3 bar dihydrogen at room temperature. At the end of the decomposition the solution was filtered and the solid dried under vacuum for 24 hours. For the impregnation with the precursor and the decomposition of the mesoporous material with a thiol function the temperature was lowered to -80 °C to avoid a reaction between the Ru(COD)(COT) and the functional groups before the addition of H_2.

The material was characterised by TEM, XRD and microanalysis.

The mesoporous silica materials have been synthesised in the LCMOS-UM II of the University of Montpellier in collaboration with the group of R. Corriu.

- SBA-15 (70 Å)
- $HS(CH_2)_3SiO_{1.5}/9SiO_2$ (45 Å)
- $HO_2C(CH2)_3SiO_{1.5}/9SiO_2$ (72 Å)
- $H_2N(CH2)_3SiO_{1.5}/9SiO_2$ (60 Å)
- $(CH_3CH_2O)_2P(=O)(CH_2)_3SiO_{1.5}/9SiO_2$ (52 Å)

11.9 Catalysis

11.9.1 Reaction conditions of the asymmetric hydrogen transfer from isopropanol with chiral amino alcohols and oxazoline ligands stabilised ruthenium nanoparticles

This catalytic tests have been performed in the group of G. Muller in the Department of Inorganic Chemistry at the University of Barcelona in Spain.

0.12 mmol acetophenone (2 mL of dissolution 0.06 M in isopropanol) and 0.024 mmol *t*-BuOK (2 mL of dissolution 0.012 M in isopropanol) were mixed with $6 \cdot 10^{-3}$ mmol of Ru catalyst. The conversion of substrate was determined by GC and the enantiomeric excess was determined by GC using a chiral column. For the catalytic system $6 \cdot 10^{-3}$ mmol Ru (based on starting [Ru(COD)(COT)] complex) were added to $1.5 \cdot 10^{-3}$ mmol of free oxazoline ligand.

11.9.2 Hydrogenation of 1,3-butadiene

This part of the work has been carried out in the Department of Inorganic Chemistry at the University of Essen under the direction of Professor G. Schmid.

Catalytic tests of butadiene hydrogenation have been carried out in a special reactor made of Duran glassware. The reactor was flushed beforehand with N_2. Blank tests consisting of the use of the empty reactor, and the use of two different pore sizes and no impregnated membranes were made. The starting materials were mixed before they were pumped to the

reactor with a membrane pump N010ST.16E (KNF Neuberger). The velocity was controlled by a gas flow meter from Bailey/Fischer/Porter. The temperature was checked by a heating system from Horst Laborgeräte GmbH. The membrane was fixed on a special holder and the gas mixture was pumped through. The obtained products were constantly extracted with a gas-proof syringe and analysed by gas chromatography on a Shimadzu GC – 8A chromatograph equipped with a Sebaconnitril / Oxidipropionacid column. The analyses have been performed at 40 °C under nitrogen as gas vector. The reaction temperature was held constantly at 25 °C by a thermo element from Rössel Messtechnik. The gas flow rate amounted 160 mL per minute.

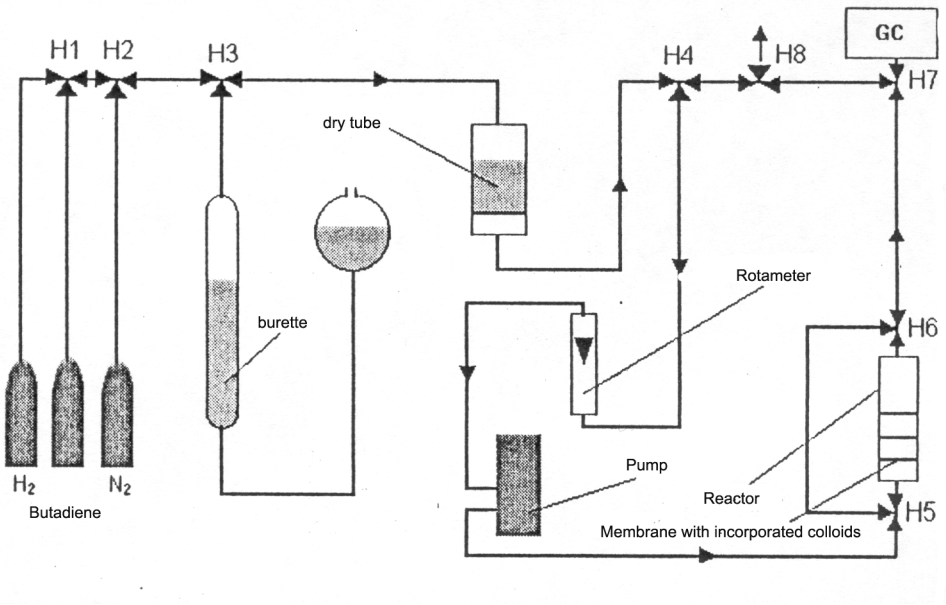

Figure 11-2: Scheme of the used reactor for catalysis with Ru particles in Al_2O_3 membranes

Before the reaction the whole reactor was flushed with N_2, used as an inert gas. The starting materials were mixed in the burette in the required quantities and they were introduced into the reactor by opening valves H 3, H 4 and H 8. The membrane was fixed in the reactor as shown in Figure 11-3.

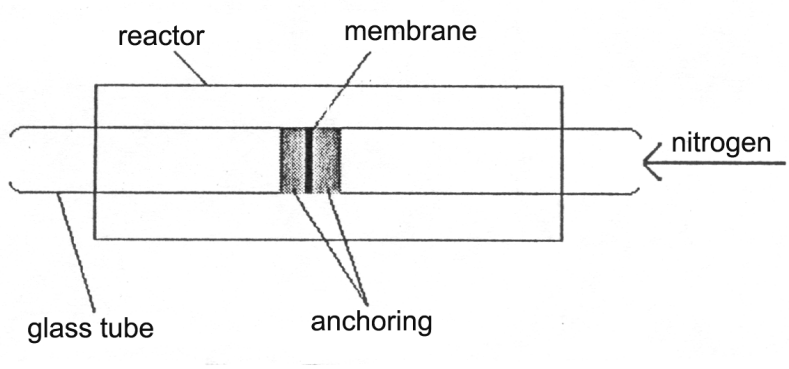

Figure 11-3: Scheme of the anchoring of the membrane in the reactor

11.9.3 CO Oxidation

For the CO Oxidation the same procedure was applied as for the 1,3-butadiene hydrogenation (see 11.9.2). The flow rate was 160 mL per minute and the reaction temperature was constant at 170 °C.

Abbreviations

AFM: Atomic Force Microscopy

COD: 1,5-cyclooctadiene

COT: 1,5,7-cyclooctatriene

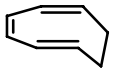

GC: Gas Chromatography

HDA: Hexadecylamine

IR: Infra Red Spectroscopy

NMR: Nuclear Magnetic Resonance

PVP: Polyvinylpyrrolidone

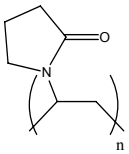

TEM: Transmission Electron Microscopy

THF: Tetrahydrofurane

TBAF: Tetrabutylammonium fluorine

WAXS: Wide Angle X-Ray Scattering

XRD: X-Ray Diffraction

Lebenslauf

Persönliche Angaben

Name	Katrin PELZER
Adresse	Sundernholz 78, 45134 Essen
Telefon	+49(0)201/441457
E-Mail	katrinpelzer@gmx.net
Familienstand	ledig
Staatsangehörigkeit	deutsch
Geburtsdatum und -ort	23. Februar 1975 in Essen

Schulbildung

1981 – 1985	Grundschule Stiftsschule in Essen-Stadtwald
1985 – 1994	Gymnasium Marienschule in Essen-Werden
Mai 1994	Abitur mit den Leistungsfächern **Chemie** und **Mathematik** sowie den Grundfächern Deutsch und Erdkunde, **Note: 2,1**

Studium

10.1994 – 03.2000	Studium der Chemie (DII) an der Universität GH Essen
SS 1996	**Vordiplom** Chemie (DII), Universität GH Essen, **Note: gut**
SS 1998	**Auslandssemester (Erasmus) an der Universität Huddersfield**, **England:** *„Synthesis and Application of Oligosaccarides“* und *„Determination of Chlorine in Organic Waste Water“*
WS 1999/2000	**Diplomarbeit** der Universität Essen in Zusammenarbeit mit dem Laboratoire de Chimie de Coordination CNRS und an der Universität Paul Sabatier in Toulouse, Frankreich: *„Synthesis and Organisation of Ruthenium Nanoparticles“* **Abschluss: Diplom-Chemikerin, Note: sehr gut**
2000	Meeting „CLUPOS“, Universität Canterbury, England Vortrag der bisherigen Forschungsergebnisse
Juli – August 2000	**Berufspraktikum IAESTE in Lissabon, Adubos de Portugal Portugal**: *„Control of the water-cooling system of an ammonia and urea plant”*

Promotion

seit November 2000 Anfertigung der **Promotion** „Doctorat co-tutelle“ zwischen der Universität Essen unter der Leitung von Prof. Dr. Günter Schmid und am Laboratoire de Chimie de Coordination CNRS der Universität Paul Sabatier in Toulouse, Frankreich unter der Leitung von Dr. Bruno Chaudret.

Titel der Arbeit: *„Synthesis of nano-sized ruthenium particles: Stabilisation without any further Stabiliser, Ligands Stabilisation and organisation in Al_2O_3 Membranes and mesoporous materials“*

Professionelle Weiterbildung

2001 **Forschungsaufenthalt,** am Institut für Anorganische Chemie, Universität Barcelona (3 Wochen) in der Arbeitsgruppe von Prof. Dr. G. Muller

Thema: *"Catalytic tests of metal nanoparticles stabilised with chiral oxazoline ligands on hydrogen transfer"*

2001 **Forschungsaufenthalt,** an der Universität Lund, Schweden (2 Wochen), in der Arbeitsgruppe von Prof. Dr. G. J.O. Bovin

Thema: *"Study of frozen solutions of ruthenium particles with CRYO Microscopy"*

2002 **Forschungsaufenthalt,** am Institut für Anorganische Chemie, Universität Barcelona (4 Wochen) in der Arbeitsgruppe von Prof. Dr. G. Muller

Thema: *"Catalytic tests of metal nanoparticles stabilised with chiral oxazoline and aminoalcohols ligands on hydrogenation of ethylpyruvate transfer*

2003 **Forschungsaufenthalt,** am Institut für Anorganische Chemie, Freie Universität Berlin, (4 Wochen), in der Arbeitsgruppe von Prof. Dr. H.-H. Limbach

Thema: *"Solid State NMR evidence for mobile surface Hydrides on Ru Nanoparticles"*

Publications

1. *"Ligand-Stabilised Ruthenium Nanoparticles : Synthesis, Organisation and Dynamics"*, Katrin Pelzer, Cheng Pan, Karine Philippot, Bruno Chaudret, *J. Am. Chem. Soc.*, **2001**, 123, 7584-7593.

2. *"Synthesis of size controlled ruthenium nanoparticles induced by an appropriate choice of the solvent composition"*, Katrin Pelzer, Olivia Vidoni, Karine Philippot, Bruno Chaudret., *Adv. Funct. Mat.*, **2003**, 13 (2), 118.

3. *"Ruthenium Nanoparticles in Nanoporous Alumina: Generation, Characterisation and Catalytic Properties"*, Katrin Pelzer, Karine Philippot, Bruno Chaudret, W. Meyer-Zaika, Günter Schmid, *Z. Anorg. Allg. Chem.*, **2003**, 629, 1217.

4. *"In-situ XRD study of the structural evolution of ruthenium nanoparticles of various sizes and shapes during oxidative and reductive treatments"*, Katrin Pelzer, Karine Philippot, Bruno Chaudret, Fabrice Dassenoy, Walter Vogel, *J. Phys. Chem. B*., submitted.

5. *"Stabilisation of ruthenium nanoparticles by chiral aminoalcohol and Oxazoline ligands and their application in catalysis"*, Susanna Jansat, Katrin Pelzer, Karine Philippot, Bruno Chaudret, Montserrat Gomez, Guillermo Muller, in preparation.

6. *"Evidence for Surface Hydrides and Weak Metal-Alcohol Interactions in Monodisperse Heptanol Stabilised Ruthenium Nanoparticles"*, Katrin Pelzer, Karine Philippot, Bruno Chaudret, *Z. Phys. Chem.*, 217, **2003**.

7. *"First Direct NMR Evidences for the Presence of Mobile Surface Hydrides on Ruthenium Nanoparticles"*, Tal Pery, Katrin Pelzer, Gert Buntkowski, Karine Philippot, Hans-Heinrich Limbach and Bruno Chaudret, *Angew. Chem.*, in preparation.

8. *"CO-Oxidation by Ruthenium Nanoparticles in Nanoporous Alumina"*, Katrin Pelzer, Karine Philippot, Bruno Chaudret, Günter Schmid, in preparation.

9. *"Organisation of Ruthenium Nanoparticles in mesoporous functionalised silica"*, Katrin Pelzer, Karine Philippot, Yannick Guari, Robert Corriu, Bruno Chaudret, *Adv. Funct. Mater.*, in preparation.

10. *"NMR Study of Ru Nanoparticles stabilised by Organosilane Fragments"*, B. Laleu, F. Lefebre, J. P. Candy, K. Pelzer, K. Philippot, B. Chaudret, J. M. Basset, *Chem. Comm.,* in press.

12 Bibliography

[1] G. Schmid, *Chem. Rev.*, **1992**, *92*, 1709.

[2] G. Schmid Ed., Cluster and Colloids, From Theory to Application, *VCH Weihnheim*, **1994**.

[3] L. N. Lewis, *Chem. Rev*. **1993**, *93*, 2693.

[4] M. M. Maye, Y. Lou, C.-J. Zhong, *Langmuir*, **2000**, *16*, 7520.

[5] M. D. Musick, C. D. Keating, M. H. Keefe, M. J. Natan, *Chem. Mater.*, **1997**, *9*, 1499.

[6] L. M. Liz-Marzan, P. Mulvaney, *New J. Chem*., **1998**, 1285.

[7] K.A. Easom, K.J. Klabunde, C.M. Sorensen, G.C. Hadjipanayis, *Polyhedron*, **1994**, 13, 1197.

[8] N. Toshima Y. Yonesawa., *N. J. Chem*., **1998**, 1179.

[9] W. Yu, M. Liu, H. Liu, X. Ma, Z. Liu, *Journal of Colloid and Interface Science,* **1998***, 208,* 439.

[10] H. Bönnemann, G. Braun, W. Brijoux, A. Schulze Tilling, K. Seevogel, K. Siepen, *J. Organomet. Chem.* **1996**, *520*, 143.

[11] Schön, G.; Simon, U. *Colloid Polym. Sci.,* **1995**, *273*, 101.

[12] Colvin, V.L.; Schlamp, M.P.; Alivisatos, A.P., *Nature*, **1994**, *370*, 354.

[13] Alivisatos, A.P., *Science*, **1996**, *271*, 933.

[14] C. Nayral, E. Viala, P. Fau, F. Senocq, J.-C. Jumas, A. Maisonnat, B. Chaudret*, Chem. Eur. J*., **2000**, *6*, 4082.

[15] T. Ould Ely, C. Amiens, B. Chaudret, E. Snoeck, M. Verelst, M. Respaud, J.-M. Broto, C*hem. Mater*., **1999**, *11*, 526.

[16] Fendler, J.H. *Chem. Mater*., **1996**, *8*, 1616.

[17] Wang, Z.L. *Adv. Mater.*, **1998**, *10*, 13.

[18] Colvin, V.L.; Schlamp, M.P.; Alivisatos, A.P. *Nature*, **1994**, *370*, 354.

[19] Rao, C.N.R.; Kulkarni, G.U.; Thomas, P.J.; Edwards, P.P. *Chem. Soc. Rev*., **2000**, *29*, 27.

[20] T. Sawitowski, *Dissertation*, UGH Essen, **1999**.

[21] M. Kröll, *Dissertation*, UGH Essen, **2000**.

[22] A. Roucoux. J. Schultz, H. Patin, *Chem. Rev*., **2002**.

[23] K. S. Birdy, *Handbook of Surface and Colloid Chemistry,* Ed. K. S. Birdy, CRC Press.

[24] S. Roginsky, A. Schalnikoff, *Kolloid Z.*, **1927**, 43, 67.

[25] U. Kolb, S. A. Quaiser, M. Winter, M. T. Reetz, *Chem. Mater*., **1996**, 8, 1889.

[26] M.T. Reetz, S.A Quaiser, *Angew. Chem. Int. Ed.,* **1995**, 34, 2241.

[27] K.S. Suslick, J.W. Goodale, P.F. Schubert, *J. Am. Chem. Soc.*, **1981**, 103, 7342.

[28] K. S.Suslick, J.D. Goodale, H.H. Wang, P.F Schubert, *J. Am. Chem. Soc.*, **1983**, 105, 5781.

[29] H. Bönnemann, W. Brijoux, R. Brinkmann, E. Dinjus, T. Jouβen, B. Korall, *Angew. Chem. Int. Ed.*, **1991**, 10, 1312.

[30] M. Faraday, Phil. *Trans. Royal Soc*., **1857**, 147, 145.

[31] D.H. Napper, *J. Colloid Interface Science*, **1977**, 58, 390.

[32] D. De Caro, J.S. Bradley, *Langmuir*, **1997**, 13, 3067.

[33] J.S. Bradley, E.W. Hill, C. Klein, B. Chaudret, A. Duteil, *Chem. Mater*., **1993**, 5, 254.

[34] C. Pan, K. Pelzer, K. Philippot, B. Chaudret, F. Dassenoy, P. Lecante, M-J. Casanove, *J. Am. Chem. Soc.*, **2001**, 123, 7584-7593.

[35] Pan, C.; Dassenoy, F.; Casanove, M.-J.; Philippot, K.; Amiens, C.; Lecante, P.; Mosset, A.; Chaudret, B. *J.Phys.Chem.B*, **1999**, *103*, 10098.

[36] Rodriguez, A.; Amiens, C.; Chaudret, B.; Casanove, M.-J.; Lecante, P.; Bradley, J.S. *Chem. Mater.*, **1996**, *8*, 1978.

[37] Naka, K.; Yaguchi, M.; Chujo, Y. *Chem. Mater.*, **1999**, *11*, 849.

[38] Shenton, W.; Pum, D.; Sleytr U.B.; Mann, S. *Nature*, **1997**, *389*, 585.

[39] Cassagneau, T.; Mallouk, T.E.; Fendler, J.H. *J. Am. Chem. Soc.*, **1998**, *120*, 7848.

[40] Yonezawa, T.; Tominaga, T.; Richard, D. *J. Chem. Soc. Dalton Trans.* **1996**, 783.

[41] Sato, T.; Brown, D.; Johnson, B.F.G. *J. Chem. Soc. Chem. Commun.* **1997**, 1007.

[42] Gomez, S.; Philippot, K.; Colliere, V. ; Chaudret, B. ; Senocq, F. ; Lecante, P. *J. Chem. Soc. Chem. Commun.* **2000**, 1945.

[43] Terrill, R.H.; Postlethwaite, T.A.; Chen, C.-H.; Poon, C.-D.; Terzis, A.; Chen, A.;Hutchison, J.E.; Clark, M.R.; Wignall, G.; Londono, J.D.; Superfine, R.; Falvo, M.; Johnson, Jr., C.S.; Samulski, E.T.; Murray, R.W. *J. Am. Chem. Soc.* **1995**, *117*, 12537.

[44] V. P. Menton, C. R. Martin, *Anal. Chem.,* **1995**, 67, 1920.

[45] J. C. Hulteen, C. R. Martin, J. Mater. Chem., **1997**, 7, 7, 1075.

[46] D. Routkevitch, A. A. Tager, *IEEE Transaction on Electron Devices*, **1996**, 43, 10, 1646.

[47] K. Schwarz, M. Eppele, *Chem-A Europeen Journal*, **1998**, 10, 1898.

[48] M. Antoniette, B. Berton, *Adv, Mater.,* **1998**, 10, 2, 154.

[49] C. L. Bowles, A. Malek, G. A. Ozin, *Chemical Vapor Deposition*, **1996**, 2, 3, 97.

[50] G. E. Thomson, G. C. Wood, *Treatise on Material Science and Technology*, **1983**, 23, 205.

[51] H. Zhou, M. Zhu, *J. Mater. Chem*., **2003**, 13, 1115.

[52] D. Zhao, Q. Huo. D. Feng, *Science*, **1998**, 279, 548.

[53] P. Braunstein, L. A. Oro, P. R. Raithby, *Wiley-VCH Weinheim*, **1999**.

[54] Monika, Bäumle, *Dissertation*, UGH Essen, **2000**.

[55] M. Zhao, M. Crooks, *Angew. Chem*., **1999**, 95, 706.

[56] L. Erades, *Thèse Université Paul Sabatier*, Toulouse, **2003**.

[57] D.R. Lide, (ed.), CRC Handbook of Chemistry and Physics 1999-2000 : *A Ready-Reference Book of Chemical and Physical Data (CRC Handbook of Chemistry and Physics*, CRC Press, Boca Raton, Florida, USA, 79th edition, **1998**.

[58] P. Pyykkö, Z. Naturforsch., **1992**, 47a, 189.

[59] www.webelemtents.com

[60] P. Claus, A. Brückener, C. Mohr, H. Hofmeister, *J. Am. Chem. Soc*., **2000**, 122,11430.

[61] U. A. Paulus, U. Endruschat, G. J. Feldmeyer, T. J. Schmidt, H. Bonnemann, R. J. Behm, *J. Catal*., **2002**, 195, 383.

[62] R. A. Salkar, P. Jeevanandam, S. T. Aruna, Y. Koltypin, A. Gedanken, *J. Mater. Chem*., **1999**, 9, 1333.

[63] A. Martino, S. A. Yamanaka, J. S. Kawola, D. Loy, *Chem. Mater*., **1997**, 9,423.

[64] T. Li, J. Moon, A. A. Morrone, J. J. Mecholsky, D. R. Talham, J. H. Adair, *Langmuir,* **1999**, 15, 4328.

[65] K. V. Sarathy, G. U. Kulkarni, C. N. R. Rao, *Chem. Comm*., **1997**, 537.

[66] Sun, S.; Murray, C.B.; Weller, D.; Folks, L.; Moser, A. *Science,* **2000**, *287*, 1989.

[67] Vidoni, O.; Philippot, K.; Amiens, C.; Chaudret, B.; Balmes, O.; Malm, J.-O.; Bovin, J.-O. ; Senocq, F. ; Casanove, M.-J. *Angew. Chem. Int. Ed.* **1999**, *38*, 3736.

[68] M. Respaud, J.-M. Broto, H. Rakoto, A. R. Fert, L. Thomas, B. Barbara, M. Verelst, E. Snoeck, P. Lecante, A. Mosset, J. Osuna, T. Ould Ely, C. Amiens, B. Chaudret*, Phys. Rev. B*, **1998**, *57*, 2925.

[69] Schmid, G.; Maihack, V.; Lantermann, F.; Peschel, S. *J. Chem. Soc. Dalton Trans.* **1996**, 589.

[70] Schmid, G.; Bäumle, M.; Geerkens, M.; Heim, I.; Osemann, C.; Sawitowski, T. *Chem. Soc. Rev.* **1999**, 179.

[71] Fink, J.; Kiely, CC.J.; Bethell, D.; Schiffrin, D.J. *Chem. Mater.*, **1998**, *10*, 922.

[72] Chen, S.; Murray, R.W. *Langmuir*, **1999**, *15*, 682.

[73] Chechick, V.; Crooks, R.M. *Langmuir*, **1999**, *15*, 6364.

[74] Lin, X.M.; Wang, G.M.; Sorensen, C.M.; Klabunde, K.J. *J. Phys. Chem. B*, **1999**, *103*, 5488.

[75] Taleb, A.; Petit, C.; Pileni, M.-P. *J. Phys. Chem. B*, **1998**, *102*, 2215.

[76] Yee, C.K. ; Jordan, R.; Ulman, A.; White, H.; King, A.; Rafailovitch, M.; Sokolov, J. *Langmuir*, **1999**, *15*, 3486.

[77] K. S. Suslick, *Science*, **1990**, 247, 1439.

[78] T. Hyeon, M. Fang, K. S. Suslick, *J. Am. Chem. Soc*., **1996**, 118, 5492.

[79] K. S. Suslick, S. J. Doktycz, *J. Am. Chem. Soc*., **1989**, 111, 2342.

[80] K. S. Suslick, S. B. Choe, A. A. Cichowlas, M. W. Grinstaff, *Nature*, **1991**, 353, 414.

[81] K. Okitsu, H. Bandow, Y. Maeda, *Chem. Mater*., **1996**, 8, 315.

[82] K. S. Suslick, J. D. Goodale, H. H. Wang, P. F. Schubert, *J. Am. Chem. Soc*., **1981**, 103, 7342.

[83] D. de Caro, B. Chaudret, *Chem. Mater.*, 8, **1996**, 1987.

[84] X. Cao, Y. Coltipin, G. Kataby, R. Prozorov, A. Gedanken, *Journal of Materials Research*, **1995**, 10, 2952.

[85] Kataby, A. Ulman, R. Prozorov, A. Gedanken, *Langmuir*, **1998**, 14, 1512.

[86] N. Arul Dhas, H. Cohen, A. Gedanken, *Journal of Physical Chemistry B*, **1997**, 101, 6834.

[87] J.S Bradley, *Clusters and Colloids*, G. Schmid, **1994**, Ed G Schmid VCH Weinheim, ch 6, 459.

[88] H. Bönnemann, R. Brinkmann, P. Neiteler, *Appl. Organomet. Chem.*, **1994,** 8, 361.

[89] J.S. Bradley, E.W. Hill, C. Klein, B. Chaudret, A. Duteil, *Chem. Mater*., **1993**, 5, 254.

[90] F. Dassenoy, K. Philippot, T. Ould Ely, C. Amiens, P. Lecante, E. Snoeck, A. Mosset, M.J. Casanove, B. Chaudret, *New Journal of Chemistry*, **1998**, 704.

[91] W. Yu, M. Liu, H. Liu, X. Ma, Z. Liu, *Journal of Colloid and Interface Science,* **1998***, 208,* 439.

[92] S. Gao, J. Zhang, Y.-F. Zhu, C.-M. Che, *New J. Chem*., **2000**, *24*, 739.

[93] Liu, M.; Yu, W.; Liu, H. *J. Mol. Catal. A* **1999**, *138*, 295.

[94] Bönnemann, H.; Brijoux, W.; Brinkmann, R.; Fretzen, R.; Jounsen, T.; Köppler, R.; Neiteler, P.; Richter, J. *J. Mol. Catal.* **1994**, *86*, 129.

[95] Lewis, L.N.; Lewis, L. *Chem. Mater.* **1989**, *1*, 106.

[96] Pertuci, P.; Vituli, G., *Inorganic Synthesis* **1983**, *22*, 178.

[97] Ould Ely, T.; Pan, C.; Amiens, C.; Chaudret B.; Dassenoy, F.; Lecante, P.; Casanove, M.-J.; Mosset, A.; Respaud, M.; Broto, J.M., *J. Phys. Chem. B*, **2000**, 104, 695.

[98] J. S. Bradley, E. W. Hill, C. Klein, B. Chaudret, A. Duteil, *Chem. Mat.,* **1993**, 5, 254.

[99] A. Duteil, *Thèse de l'Université Paul Sabatier*, Toulouse, France, **1992**.

[100] K. Pelzer, *Diplomarbeit*, UGH Essen, **2000**.

[101] Aldrich, FT-Infra Red Spectra, Ed.3.

[102] K. Pelzer, O. Vidoni, K. Philippot, B. Chaudret, *Adv. Funct. Mat.,* **2003**, 13, 118.

[103] T. Ould Ely, *Thèse de l'Université Paul Sabatier*, Toulouse, France, **1998**.

[104] N. Cordente, M. Respaud F. Senocq, M.-J. Casanove, C. Amiens, B. Chaudret*, Nano Letters*, **2001,** *1*, 10, 565.

[105] J.S. Bradley, J.M. Millar, E.W. Hill, S. Behal, B. Chaudret, A. Duteil, *Faraday Discuss .Chem. Soc*. **1991**, 92, 255.

[106] I. V. Yudanov, R. Sahnoun, K.M. Neyman, N. Rösch, J. Hoffmann, S. Schauermann, V. Johánek, H. Unterhalt, G. Rupprechter, J. Libuda, H.-J. Freund, *J. Phys. Chem. B* **2003**, 107, 255.

[107] D. de Caro, J.S. Bradley, *New J. Chem*., **1998**, 1267.

[108] Badia, A.; Gao, W.; Singh, S.; Demers, L.; Cuccia, L.; Reven, L. *Langmuir*, **1996**, *12*, 1262.

[109] Badia, A.; Cuccia, L.; Demers, L.; Morin, F.; Lennox, R.B. *J. Am. Chem. Soc.* **1997**, *119*, 2682.

[110] Hostetler, M.J.; Wingate, J.E.; Zhong, C.-J.; Harris, J.E.; Vachet, R.W.; Clark, M.R.; Londono, J.D.; Green, S.J.; Stokes, J.J.; Wignall, G.D.; Glish, G.L.; Porter, M.D.; Evans, N.D.; Murray, R.W., *Langmuir*, **1998**, *14*, 17.

[111] J. Kubota, K. Aika, *J. Chem. Soc., Chem. Commun*., **1992**, 661.

[112] K. Christmann, *Mol. Phys*., **1998**, 66, 1.

[113] K. Christmann, *Surf. Sci. Rep*., **1998**, 9, 1.

[114] B. Moreno, S. Sabo-Etienne, B. Chaudret, A. Rodriguez, F. Jalon, S. Trofimenko, *J. Am. Chem. Soc,* **1995**, 117, 7441.

[115] A. Ozaki, K. Aika, *Catalysis-Science and Technology*, J. R. Anderson, M Boudart, Springer Verlag, Berlin, **1981**, vol. 1, 87.

[116] Chechick, V.; Crooks, R.M. *Langmuir*, **1999**, *15*, 6364.

[117] Shenton, W.; Pum, D.; Sleytr U.B.; Mann, S. *Nature*, **1997**, *389*, 585.

[118] Cassagneau, T.; Mallouk, T.E.; Fendler, J.H. *J. Am. Chem. Soc.*, **1998**, *120*, 7848.

[119] Fink, J.; Kiely, CC.J.; Bethell, D.; Schiffrin, D.J. *Chem. Mater.*, **1998**, *10*, 922.

[120] Chen, S.; Murray, R.W. *Langmuir*, **1999**, *15*, 682.

[121] Lin, X.M.; Wang, G.M.; Sorensen, C.M.; Klabunde, K.J. *J. Phys. Chem. B*, **1999**, *103*,5488.

[122] Naka, K.; Yaguchi, M. ; Chujo, Y. *Chem. Mater.*, **1999**, *11*, 849.

[123] Ohara, P.C.; Heath, J.R.; Gelbart, W.M. *Angew. Chem. Int. Ed.* **1997**, *36*, 1078.

[124] Korgel, B.A.; Fitzmaurice, D. *Adv. Mater.* **1998**, *10*, 661.

[125] Petit, C.; Taleb, A.; Pileni, M.-P. *J. Phys. Chem. B*, **1999**, *103*, 1805.

[126] Sato, T.; Brown, D.; Johnson, B.F.G. *J. Chem. Soc. Chem. Commun.* **1997**, 1007.

[127] Sun, S.; Murray, C.B.; Weller, D.; Folks, L.; Moser, A. *Science,* **2000**, *287*, 1989.

[128] K.J. Klabunde, G. Cardenas-Trivino, *Active Metals : Preparation, Characterisation, Applications*, (Ed A. Fürstner), VCH Weinheim, **1996**, 237-277.

[129] P. J. Thomas, G. U. Kulkarni, C. N. R. Rao, *J. Phys. Chem. B*, **2000**, 104, 8138-8144.

[130] C. Larpent, H. Patin, *J. Mol. Catal*.. **1988**, 44, 191-195.

[131] Jr. Porter, L. A., L. Ji, S. L. Westcott, M. Graupe, R. S. Czernuszewicz, N. J. Halas, T. R. Lee, *Langmuir*, **1998**, 14, 7378.

[132] F. Titan, J. Klabunde, *New. J. Chem*., **1998**, 22, 1275.

[133] T. Yonezawa, K. Yasui, N. Kimizuka, *Langmuir*, **2001**, 17, 271.

[134] Schmid, G.; Meyer-Zaika, W.; Pugin, R.; Sawitowski, T.; Majoral, J.-P.; Caminade, A.-M.; Turrin C.-O. *Chem. Eur. J.,* **2000**, *6*, 1693.

[135] Bradley, J.S.; Millar, J.; Hill, E.W. *J. Am. Chem. Soc.* **1991**, 113, 4016.

[136] Schmid, G.; Giebel, U.; Huster, W.; Schwenk, A. *Inorg. Chim. Acta,* **1984**, 85, 97.

[137] Schmid, G. *Structure and Bonding* **1985**, 62, 51.

[138] L. G. de Jongh, *Physics and Chemistry of Metal Cluster Compounds*, Kluwer, Dordrecht, **1994.**

[139] *Nanotechnology*, *Molecularly Designed Materials*; (Eds Chow G-M and Gonsalves K.E.); A.C.S. Symposium Series 622: Science and Engineering, Inc., 20-24 August 1995, American Chemical Society, Washington, DC **1996.**

[140] Personal communication.

[141] Schmid, G.; Meyer-Zaika, W.; Pugin, R.; Sawitowski, T.; Majoral, J.-P.; Caminade, A.-M.; Turrin C.-O. *Chem. Eur. J.,* **2000**, *6*, 1693.

[142] Tanev, P.T.; Pinnavaia, T.J. *Science,* **1996**, *271*, 1267.

[143] Ulagaappan, N.; Battaram, N.; Rraju, V.N.; Rao, C.N.R. *J. Chem. Soc. Chem. Commun.* **1996**, 2243.

[144] J. U. Köhler, J. S. Bradley, *Langmuir*, **1998**, 14, 2730.

[145] M. Peer, J. C. de Jong, M. Kiefer, T. Langer, H. Rieck, H; Schell, P. Sennhenn, J. Sprinz, H. Steinhagen, B. Wiese, G. Helmchen, *Tetrahedron*, **1996**, 52*,* 7547.

[146] Y. Jiang, Q. Jiang, X. Zhang, *J. Am. Chem. Soc.*, **1998**, 120, 3817.

[147] T. Langer, G. Helmchen, *Tetrahedron Lett.,* **1996**, 37, 1381.

[148] Q. Jiang, D. van Plew, S. Murtuza, X. Zhang, *Tetrahedron Lett.,* **1996**, 37, 797.

[149] A. Duteil, R. Quéau, B. Chaudret, *Chem. Mat.* **1993**, 5, 341.

[150] J. D. Aiken III, R. G. Finke, *J. Mol. Catal.*, Chemical **1999**, 145,1.

[151] A. K. Gosh, P. Mathivanan, J. Cappiello, *Tetrahedron: Asymmetry* **1998**, 9, 1.

[152] G. Helmchen, A. Pfaltz, *Acc. Chem. Res*., 33, **2000**, 33, 6.

[153] Liu, M.; Yu, W.; Liu, H. *J. Mol. Catal. A* **1999**, *138*, 295.

[154] Lewis, L .N. ; Lewis, L. *Chem. Mater.* **1989**, *1*, 106.

[155] C. Bolm, K. Weikhardt, M. Zehnder, T. Rauff, *Chem. Ber.,* 124, **1991**, 1173.

[156] M. Reuman, A. I. Meyers, *Tetrahedron*, 1985, **41***,* 837;

[157] M. Peer, J. C. de Jong, M. Kiefer, T. Langer, H. Rieck, H; Schell, P. Sennhenn, J. Sprinz, H. Steinhagen, B. Wiese, G. Helmchen, *Tetrahedron*, 1996, **52***,* 7547.

[158] M. Gómez, G. Muller, M. Rocamora, *Coord. Chem. Rev*., 1999, **193-195**, 769.

[159] Y. Jiang, Q. Jiang, X. Zhang, *J. Am. Chem. Soc.*, 1998, **120**, 3817.

[160] T. Langer, G. Helmchen, *Tetrahedron Lett.,* 1996, **37**, 1381.

[161] Q. Jiang, D. van Plew, S. Murtuza, X. Zhang, *Tetrahedron Lett.,* 1996, **37**, 797.

[162] R. Noyori, S. Hashiguchi, *Acc. Chem. Res.,* 1997, **30**, 97.

[163] J. Takehara, S. Hashiguchi, A. Fujii, I. Shin-ichi, T. Ikariya, R. Noyori, *Chem. Commun.*, 1996, 233.

[164] M. Palmer, T. Walsgrove, M. Wills, *J. Org. Chem*., 1997, **62**, 5226.

[165] D. G. I. Petra, P. C. J. Kamer, P. W. N. M. van Leeuwen, K. Goubitz, A. M. van Loon, J. G. de Vries, H. E. Schoemaker, *Eur. J. Inorg.Chem.,* 1999, 2335.

[166] K. Everaere, A. Mortreux, M. Bulliard, J. Brussee, A. van der Gen, G. Nowogrocki, J-F. Carpentier, *Eur. J. Org. Chem.,* 2001, 275.

[167] M. Gomez, S. Jansat, G. Muller, M. A. Maetsro, J. Mahia, *Organometallics*, 21, **2002**, 1077.

[168] M. Gomez, S. Jansat, G. Muller, M. C. Bonnet, J. Breusard, M.Lemaire, *J. Organomet. Chem.,* 659, **2002**, 186.

[169] M. Gomez, S. Jansat, G. Muller, M. A. Maetsro, J. Mahia, M. Font-Bardia, X. Solans, *J. Chem. Soc.,* Dalton Trans., **2001,** 1432.

[170] M. J. McKennon, A. I. Meyers, K. Drauz and M. Schwarm, *J. Org. Chem.,* 58, **1993**, 3568.

[171] J. Kubota, K. Aika, *J. Chem. Soc., Chem. Commun*., **1992**, 661.

[172] Y. Sakamoto, M, Kaneda, O. Teraski, D. Zhao, J. M. Kim, G. D. Stucky, H. J. Shin, R. Ryoo, *Nature*, 408, **2000**, 449.

[173] Q. Huo, D. I. Margolese, G. D. Stucky, *Chem. Mater.,* 8, **1996**, 1147.

[174] J. Y. Ying, C. P. Mehnert, M. S: Wong, *Angew. Chem. Int. Ed.,* **1999**, 38, 56.

[175] M. E: Dabis, *Nature* **2002**, 417, 813.

[176] T. Sawitowski, , Y. Miguel, A. Heilmann, G. Schmid, *Adv. Funct. Mater.* **2001**,11, 235.

[177] T. Kyotani, L. Tsai, A. Tomita, *Chem. Comm.* **1997**, 701.

[178] G. Hornyak. M. Kröll, R. Pugin, T. Sawitowski, G. Schmid, J.O. Bovin, G. Karsson, H. Hofmeister, S. Hopfe, *Chem. Eur. J.* **1997**, 3, 1951.

[179] J. W. Diggle, T. C. Downie, C. W. Goulding, *Chem. Rev.* **1969**, *69*, 365.

[180] J. P. O'Sullivan, G. C. Wood, *Proc. R. Soc.* London 1970, *317*, 511.

[181] G. E. Thompson, G. C. Wood, *Sci. Technol.* **1983**, *23*, 205.

[182] G. E. Thompson, R. C. Furneaux, G. C. Wood, J. A. Richardson, J. S. Goode, *Nature,* **1978**, *272*, 433.

[183] T. Sawitowski, *Diplomarbeit, Univ. GH Essen*, **1996**.

[184] C. Martin, Membrane-Based Synthesis of Nanomaterials, *Chemistry of Materials*, 8, 1739, **1996**.

[185] T. Sawitowski, Y. Miguel, A. Heilmann, G. Schmid, *Adv. Funct. Mater*. **2001**, 11, 435.

[186] G. Schmid, *J. Mater. Chem*. **2002**, 12, 1231.

[187] P. M. Paulus, F. Luis, M. Kröll, G. Schmid, L. J. de Jongh, *J. Magn. Mater*, **2000**, 224, 180.

[188] A. Heilmann, P. Jutzi, A. Klipp, U. Kreibig, R. Neuendorf, Th. Sawitowski, G. Schmid, *Adv. Mater*. **1998**, 10, 398.

[189] J. W. Diggle, T. C. Downie, C. W. Goulding, *Chem. Rev*. **1969**, 69, 365.

[190] G. E. Thompson, R. C. Furneaux, G. C. Wood, J. A. Richardson, J. S. Goode, *Nature*, **1978**, 272, 433.

[191] G. E. Thompson, G. C. Wood, *Sci. Technol*. **1983**, 23, 205.

[192] M. M. Lohrengel, *Mater. Sci. Eng*. **1993**, 17, 202.

[193] J. P. O'Sullivan, G. C. Wood, *Proc. R. Soc*. London **1970**, 317, 511.

[194] O. Jessenesky, F. Müller, U. Gösele, *Appl. Phys. Lett*., **1998**, 72/10, 1173.

[195] K. Wefers, C. Misra, *Alcoa Laboratories*, **1987**.

[196] J. C. Hulteen, C.R. Martin, *J. Mater. Chem*., **1997**, 7, 1075.

[197] P. Braunstein, H.-P. Kormann, W. Meyer-Zaika, R. Pugin, G. Schmid, *Chem. Eur. J*., **2000**, 6/24, 4637.

[198] G. A. Ozin, Nanochemistry: Synthesis in Diminishing Dimensions, *Adv. Mater*. **1992**, 10, 612.

[199] T. Sato, D. G: Hasko, H. Ahmed, J. Vac. Sci. Technol., 1997, 15, 45.

[200] C.M. Zelenski, G. L. Hormyak, P. K. Dorhout, *Nanostructured Materials*, 9, 173, **1997**.

[201] P. Hoyer, H. Masuda, *Journal of Material Science*, 15, 1228, **1996**.

[202] D. AlMawlawi, C. Coombs, *Journal of Applied Physics*, 70/8, 4421, **1991**.

[203] E. Riedel, *Anorganische Chemie*, de Gruyter, Berlin, 3.Aufl., **1994**.

[204] V. P. Parkhutik, V. I. Shershulsky, *Appl. Phys*., **1992**, 25, 1258.

[205] T. Sawitowski, *Diplomarbeit*, Univ. GH Essen, **1996**.

[206] J. W. Diggle, T. C. Downie, C. W. Goulding, *Chemical Review*, 69, 7497, **1992**.

[207] C. A. Foss Jr., G. L. Hornyak, J. A. Stockert, C. R. Martin, *J. Phys. Chem*., **1994**, 98, 2963.

[208] C. A. Foss Jr., G. L. Hornyak, J. A. Stockert, C. R. Martin, *Adv. Mater*., **1993**, 5, 135.

[209] C. A. Foss Jr., G. L. Hornyak, J. A. Stockert, C. R. Martin, *J. Phys. Chem.*, **1992**, 96, 7497.

[210] V. P. Parkhutik, V. I. Shershulsky, *Appl. Phys*., **1992**, 25, 1258.

[211] R. C. Furneaux, W. R. Rigby, A. P. Davidson, *Nature*, **1989**, 332.147.

[212] G. L. Hornyak, S. Peschel, T. Sawitowski, G. Schmid, *Micron*, **1998**, 4, 183.

[213] G. Neubert, *Phys. i. u. Zeit*, **1988**, 4, 112.

[214] D. Sarid, V. Elings, *J. Vac. Sci. Technol*., **1991**, B9 (2), 431.

[215] T. Hanaoka, A. Heilmann, P. Jutzi, A. Klipp, H.-P. Kormann, U. Kreibig, M. Kröll, R.Neuendorf, T. Sawitowski, G. Schmid, *Applied Organometallic Chemistry*, 12, 367, **1998**.

[216] V. P. Menon, C. R. Martin, *Analyt. Chem*., **1995**, 67, 1920.

[217] S. Kawai, I. Ishiguro, *J. Electrochem. Soc.,* Electrochem. Sci. Technol., **1976**, 123, 1047.

[218] L. C. A. van der Oetelaar, O. W. Nooji, S. Oerlemans, *J. Phys. Chem*., **1998**, 102, 3445.

[219] K. Pelzer, O. Vidoni, K. Philippot, B. Chaudret, *Adv. Funct. Mat*,. **2003**, 13, 118.

[220] K. Pelzer, Karine Philippot, B. Chaudret, W. Meyer-Zaika, G. Schmid, *Z. Allg. Anorg. Chem*, **2003**, 629, 7,8, 1223.

[221] Khushalani, D.; Hasenzahl, S.; Mann, S. *J. Nanosci. Nanotechnol.* **2001**, *1(2)*, 129.

[222] Breitscheidel, B.; Zieder, J.; Schubert, U. *Chem. Mater.* **1991**, *3*, 559.

[223] Kresge, C. T.; Leonowicz, M. E.; Roth, W. J.; Vartuli, J. C.; Beck, J. S. *Nature* **1992**, *359*, 710.

[224] Mulukutla, R. S.; Asakura, K.; Namba, S.; Iwasawa, Y. *Chem. Commun.* **1998**, 1425.

[225] Fröba, M.; Köhn, R.; Bouffaud, G.; Richard, O.; van Tendeloo, G. *Chem. Mater.* **1999**, *11*, 2858.

[226] Fukuoka, A.; Osada, M.; Shido, T.; Inagaki, S.; Fukushima, Y.; Ichikawa, M. *Inorg. Chim. Acta.* **1999**, *294*, 281.

[227] Yuan, Z. Y.; Liu, S. Q.; Chen, T. H.; Wang, J. Z.; Li, H. X. *Chem. Commun.* **1995**, 973.

[228] Schweyer, F.; Braunstein, P.; Estournès, C.; Guille, J.; Kessler, H.; Paillaud, H.-L.; Rosé, J. *Chem. Commun.* **2000**, 1271.

[229] MacLachlan, M. J.; Ginzburg, M.; Coombs, N.; Raju, N. P.; Greedan, J. E.; Ozin, G. A.; Manners, I. *J. Am. Chem. Soc.* **2000**, *122*, 3878.

[230] Guari, Y.; Thieuleux, C.; Mehdi, A; Reyé, C.; Corriu, R. J. P.; Gomez-Gallardo, S.; Philippot, K.; Chaudret, B.; Dutartre, R. *Chem. Commun.* **2001**, 1374.

[231] Soulantica, K.; Maisonnat, A.; Fromen, M.-C.; Casanove, M.-J.; Lecante, P.; Chaudret, B. *Angew. Chem. Int. Ed.* **2001**, *40*, 448.

[232] X. Feng, G. E. Frywell, L.-Q. Wang, A. Y. Kim, J. Liu, K. M. Kemner, *Science*, 276, **1997**, 923.

[233] K. Moller, T. Bein, *Chem. Mater*., 10, **1998**, 2950.

[234] D. Zhao, J. Feng, Q. Huo, N. Melosh, G. H. Frederickson, B. F. Chmelka, G. D. Stucky, *Science*, **1998**, 279, 548.

[235] Q. Huo, D. I. Margolese, U. Ciesla, P. Feng, T. E. Gler, P. Sieger, R. Leon, P. M. Petroff, F. Schuth, G. D. Stucky, *Nature*, **1994**, 368, 317.

[236] G. Fagherazzi, A. Benedetti, G. Deganello, D. Duca, A. Martorana, G. Spoto, *J. Catal.*, **1994**, 150, 117.

[237] G. Schmid, H.-P. Kormann, *J. Mol. Catal. A* **2003**, in press.

[238] R. Andreasch, *Monatsh. Chem*., **5** (1884) 33.

[239] A. Pfaltz, *Acc. Chem. Res*., **26** (1993) 339.

[240] Liu, M.; Yu, W.; Liu, H. *J. Mol. Catal. A* **1999**, *138*, 295.

[241] M. Reuman, A. I. Meyers, *Tetrahedron*, **1985**, 41*,* 837.

[242] M. Gómez, G. Muller, M. Rocamora, *Coord. Chem. Rev*., **1999**, 193-195, 769.

[243] A. K. Ghosh, P. Mathivanan, J. Cappiello, *Tetrahedron: Asymmetry,* **1998**, 9, 1.

[244] R. Noyori, S. Hashiguchi, *Acc. Chem. Res.,* **1997**, 30, 97.

[245] G. I. Petra, P. C. J. Kamer, P. W. N. M. van Leeuwen, K. Goubitz, A. M. van Loon, J. G. de Vries, H. E. Schoemaker, *Eur. J. Inorg. Chem.,* **1999**, 2335.

[246] S. Jansat, Tesi Doctoral, University of Barcelona, **2001**.

[247] H. Bönnemann, G.A. Braun, *Chem. Eur. J*., **1997**, 3, 1200.

[248] J. U. Köhler, J. S. Bradley, *Langmuir*, **1998**, 14, 2730.

[249] L.N. Lewis, *Chem. Rev*., **1993**, 93, 2693.

[250] J.D. Aiken III, R. G. Finke, *J. Mol. Catal. A*, **1999**, 145, 1.

[251] M. A. El-Sayed, *Acc. Chem. Res*., **2001**, 257.

[252] R. Andreasch, *Monatsh. Chem*., **5** (1884) 33.

[253] A. Pfaltz, *Acc. Chem. Res*., **26** (1993) 339.

[254] J-C. Clinet, E. Dunach, M. Gomez, G. Muller, S. Olivero, D. Panyella, M. Rocamora, *Organometallics*, 16, **1997**, 5900-5908.

[255] M. Gomez, S. Jansat, G.Muller, D. Panyella, P. W. N. M. van Leeuwen, P. C. J. Kamer, K. Goubitz, and J. Fraanje, *Organometallics*, 18, **1999**, 4970-4981.

[256] Josep Maria Canal, Montserrat Gomez, Francisco Jimenez, Merce Rocamora, Guillermo Muller, Elisabet Dunach, Delphine Franco, Alicia Jimenez, and F. H. Cano, *Organometallics*, 19, **2000**, 966-978.

[257] G. Helmchen; A. Pfaltz, Acc.Chem.Res., 33 (2000) 336.

[258] A. Pfaltz, *Acc. Chem. Res*., 26, **1993**, 339.

[259] J. Canal, M. Gomez, D. Franco, G. Muller, F. Jimenez, M. Rocamora, A. Jiminez, E. Dunach, F. H. Cano, *Organometallics*, **2000**, 19. 966.

[260] M. Gomez, S. Jansat, G. Muller, G. Noguera, H. Teruel, V. Moliner, E. Cerrada, M. Hursthouse, *Eur. J. Inorg. Chem*., **2001**, 1071-1076.

[261] M. Gomez, S. Jansat, G. Muller, M. A. Maestro, J. Maha, *Organometallics*, 21, **2002**,1077-1087.

[262] M. Gomez, S. Jansat, G. Muller, M. C. Bonnet, J. A. J. Breuzard, M. Lemaire, *J. Organomet. Chem*., 659, **2002**, 186-195.

[263] M. A. Perics, C. Puigjaner, A. Riera, A. Vidal-Ferran, M. Gomez, F. Jimenez, G. Muller, M. Rocamora, *Chem. Eur. J.*, 8, **2002**, 4164-4178.

[264] B. C. Gates, *Chem. Rev*. **1995**, 95, 511.

[265] G. A. Ozin, S. A. Mitchell, *Angew. Chem.,* **1983**, 95, 706.

[266] W. F. Maier, *Angew. Chem*., **1989**, 101, 135.

[267] E. F. Meyer, R: L. Burwell, *J. Am. Chem. Soc.,* **1963**, 85, 2881.

[268] B. Poelsema, L. S. Braun, K. Lenz, L. K. Verheij, G. Cosma, *Surf. Sci*, **1986**, 171, 395.

[269] C. M. Pradier, Y. Berthier, *J. Catal*., **1984**, 89,362.

[270] M. Boudart, *Chem. Rev.,* **1995**, 95,661.

[271] S. Emde, *Dissertation*, Univ. GH Essen, **1995**.

[272] M. Boudart, *J. Mol. Catal*., **1985**, 30, 27.

[273] J. G. Ulan, W. F. Maier, *J. Org. Chem*., **1987**, 52, 3132.

[274] H. P. Kormann, *Dissertation*, Univ. GH Essen, **2001**.

[275] V. Maihack, *Dissertation*, Univ. GH Essen, **1996**.

[276] A. F. Hollemann, E. Wiberg, *Lehrbuch der Anorganischen Chemie*, Walter de Gruyter, Berlin, **1985**.

[277] E. Koberstein, *Chem. i. u. Zeit*, **1984**, 18, 37.

[278] K. C. Taylor, *Catalytic Science Technology*, Springer Verlag, Berlin, **1984**.

[279] M. Haruta, S. Tsubota, T. Kobayashi, H. Kageyama, M. J. Genet, B. Delmon, *J. Catal*., **1993**, 144, 175.

[280] M. Haruta, S. Tsubota, T. Kobayashi, S. Ueda, *Surf. Sci. Catal.,* **1993**, 75, 2657.

[281] L. N. Lewis, *Chem. Rev.*, **1993**, 93, 2693-2730.

[282] P. Pertuci, G. Vitulli, Dalton, **1980**, 1961-1964.

[283] T. Sawitowski, *Dissertation*, UGH Essen, **1999**.